Investigating the role of *BRAF*^{V600E} in the serrated neoplastic pathway of colorectal cancer

Thesis submitted for the degree of

Doctor of Philosophy

At the University of Leicester

By

Kimberley Rhianne Snell (M.Sc University of Leicester)

Department of Biochemistry

University of Leicester

September 2012

Abstract

Investigating the role of *Braf*^{V600E} in the serrated neoplastic pathway

of colorectal cancer

Kimberley Snell

Over 40 missense mutations in the *BRAF* gene have been identified in human cancers. Of these, 90% harbour the *BRAF*^{V600E} mutation, which results in a constitutively active protein with a 500-fold kinase activity compared to wildtype. This is the most common genetic mutation in melanoma, however it is also found in a subset of colorectal cancers, which progress through the serrated neoplastic pathway.

This study was set out to investigate the role of *BRAF*^{V600E} in serrated lesions of Colorectal cancer, using a mouse model that expresses this mutation in the cells of the mouse GI tract. Expression of the *Braf*^{V600E} gene is under the control of Cre recombinase, which is controlled at the transcriptional and post-transcriptional levels. This form of regulated expression, mimics the sporadic onset of human serrated CRCs.

After 3 days of *Braf*^{V600E} expression, the number of cells in the crypt increased up to ~200 cells per crypt compared to the controls. However this was not sustained and at ~1wk p.i. oncogene-induced-senescence (OIS) occurred. This was in association with elevated expression levels of *p16*^{INK4a} and *p15*^{INK4b} TSGs. At around 12wks p.i. OIS was evaded with the growth of serrated adenomas in a small number of mice. These were devoid of p16^{INK4a} expression. Analysis of the CpG island in exon 1α of the gene revealed elevated levels of methylation in the tumours. In support of this, levels of the DNA methyltransferases Dnmt3b and the histone methylase Ezh2 were highly expressed in the tumours. The Ezh2 is known to target the *p16*^{INKa} gene locus, suggesting a role for methylation in the inactivation of this gene as a mechanism for malignant progression.

These results provide strong evidence that *BRAF*^{V600E} has an oncogenic role in the early stages of serrated CRC and furthermore, as suggested in equivalent human lesions, inactivation of TSGs through targeted methylation is associated with this mutation in CRC development.

Acknowledgements and dedication

Abbreviations

ARF	Alternative reading frame
APC	Adenomatous polyposis coli
βNF	Beta-napthoflavone
CDK	cyclin dependent kinase
cDNA	complimentary deoxyribonucleic acid
CHIP	chromatin immuno-precipitation
CIMP	CpG island methylator phenotype
CRC	colorectal cancer
DNA	deoxyribonucleic acid
E2F	E2 promoter binding factor
EGF	epidermal growth factor
ERK	extracellular signal-regulated kinase
EtOH	ethanol
GDP	guanosine diphosphate
G Protein	guanine nucleotide-binding protein
GTP	guanosine triphosphate
JNK	c-Jun N-terminal kinase
kDa	kilodalton(s)
LI	large intestine
LSL	Lox-stop-Lox
MAPK	mitogen-activated protein kinase
MAPKK	mitogen-activated protein kinase kinase
MAPKKK	mitogen-activated protein kinase kinase kinase
MEF	mouse embryo fibroblast
min	minute(s)
mRNA	messenger ribonucleic acid

IV

OIS	Oncogene-induced-senescence
PCR	polymerase chain reaction
PcG	Polycomb group
p.i.	post-Braf^{V600E} induction
PRC	Polycomb repressor complex
EGFR	epidermal growth factor
qPCR	quantitative real time polymerase chain reaction
RAF	rapidly accelerated fibrocarcinoma
RAS	rat sarcoma
Rb	retinoblastoma protein
RBD	RAS binding domain
RNA	ribonucleic acid
RNAi	RNA interference
S	synthesis
SI	small intestine
sec	second(s)
siRNA	small interfering RNA
SOS	son of sevenless
TGF-β	transforming growth factor-β
TM	tamoxifen
TSG	tumour suppressor gene
v/v	volume/volume
VEGF	vascular endothelial growth factor
wk(s)	weeks
WT	Wildtype
w/v	weight/volume
V600E	*Braf*^{V600E} mutation

Contents

Introduction

1.1 Cell signalling

1.1.1 Mitogen activated protein kinase (MAPK) cascades

Mitogen activated protein kinase (MAPK) signalling cascades relay signals from extracellular stimuli in order to activate intracellular processes. In mammals, there are four key MAPK cascades that regulate key cellular processes (Figure 1.1). These signalling pathways are activated at the cell membrane by multiple stimuli including hormones, cytokines, growth factors and environmental stressors, which bind and activate membrane-bound receptors (Avruch et al., 2001). The signal is translocated down a triple-tiered hierarchy of kinases; the first being a mitogen activated protein kinase kinase kinase (MAPKKK), which activates a dual-specificity mitogen activated protein kinase kinase (MAPKK) and lastly the activation of a mitogen activated protein kinase (MAPK) (Kyriakis et al., 1992). At each tier, activation of the effector MAPK protein occurs through phosphorylation. The MAPKKK phosphorylates serine-threonine residues on the MAPKK, which then phosphorylates threonine/tyrosine residues on a MAPK (Derijard et al., 1994). Active MAPK proteins then phosphorylate target kinases on serine/proline and threonine/proline residues in the cytoplasm and nucleus, as well as directly targeting transcription factors (Yang et al., 2003; Marais et al., 1993; Treisman, R. 1999).

Figure 1.1 Diagram to show the various the Mitogen activated protein kinase (MAPK) cascades. In mammals there are four main MAPK casades, which are triggered by mitogens, growth factors and environmental stressors. The signal is relayed from an activated RTK at the plasma membrane, to a G coupled protein and down a triple-tiered phosphorylation cascade; MAPKKK to a MAPKK and lastly a MAPK.
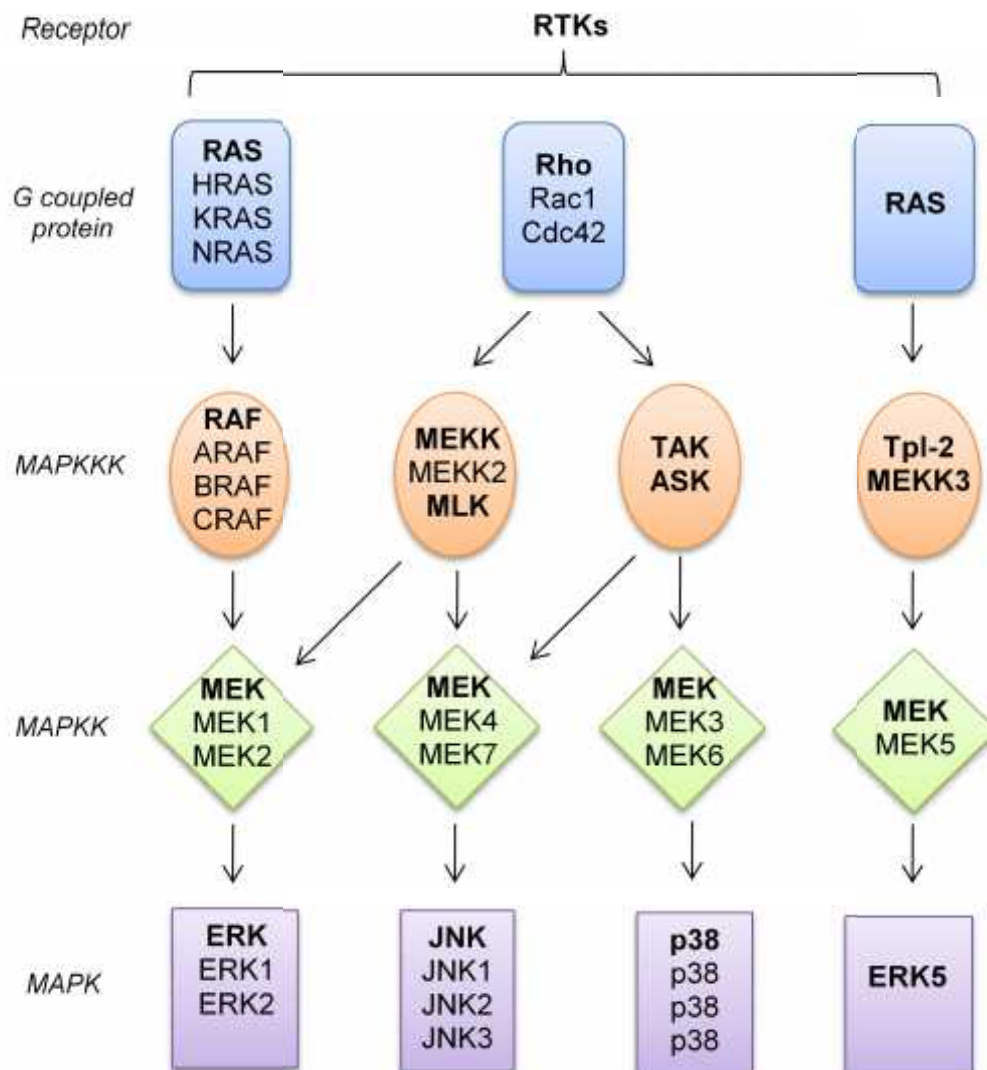
There are four main MAPKs; extracellular related kinase (ERK), c-Jun N-terminal kinase (JNK), p38 and ERK5, these are activated by specific MAPKK/MAPKKK proteins, although there is some degree of crosstalk between the MAPK pathways. Classification of each MAPK pathway is dependable on the specific MAPK activated i.e. ERK or JNK and also by which protein kinases most often interact with one another. Furthermore, activation of each MAPK pathway is associated with different types of stimuli and there is a high level of crosstalk between the cascades, at each level of activation. The best characterised cascade is by the G coupled protein RAS, this leads to ERK activation and regulation of many important cellular activities. This will be discussed in the next section.

The JNK pathway is initiated more favourably by cytokines, pro-inflammatory and external stressors such as interleukin molecules and less often growth factors (Xie et al., 2000; Pearson et al., 2001). These bind receptors which activate the Rho family of GTPase proteins such as Rac1 and Cdc42 (Kolch et al., 2000). There are three isoforms of JNK 1, 2 and 3. These are effectors of MEK4 and 7, which in turn are activated by phosphorylation by MAPKKK such as; MEKK1, 2, 3 and 4, mixed lineage kinase (MLK) and transforming growth factor-β- activating kinase (TAK) (Pearson et al., 2001).

The p38 MAPKs are activated in response to stress and pro-inflammatory stimuli, which initiate the MAPK cascade at the cell membrane as described for JNK (above). There are four variants of p38; α, β, γ and δ. These are

activated by MEK3 and 6, which are initially phosphorylated by upstream protein kinases such as the TAK and apoptosis signalling kinase (ASK) (Wang et al., 1996; Hutchison et al., 1998; Chen et al., 1999).

The ERK5 pathways are activated by specific stimuli such as serum and the epidermal (EGF) growth factor and its activation appears to be cell type dependant (Kato et al., 1997; 1998). Activation of ERK5 occurs via MEK5 phosphorylation which is downstream of MEKK3 and the Cot proto-oncogene product, Tpl-2 (Wang et al., 1997).

1.1.2 RAS-activated MAPK cascade

The MAPK cascade leading to ERK activation is one of the best characterised of the MAPK pathways and is activated at the plasma membrane by active RAS (Figure 1.2). Initially, mitogens and growth factors bind to membrane bound receptor tyrosine kinases, typically growth factor receptors such as the epidermal growth factor receptor (EGFR) and vascular endothelial growth factor receptor (VEGF). On mitogen activation, tyrosine residues on their cytosolic regions become auto-phosphorylated leading to the recruitment and activation of the guanine nucleotide-exchange-factor protein son of sevenless (SOS) and growth factor receptor-bound protein-2 (Grb2) (Lowenstein et al., 1992; Li et al., 1993). These function as interim proteins to relay the signal downstream from the active RTK, through binding and activation of RAS, from a GDP to a GTP active state (Clark et al., 1985). RAS induces a phosphorylation cascade by recruiting RAF proteins to the cell membrane, where they become phosphorylated on specific tyrosine and serine residues

4

Figure 1.2 The RAS activated Mitogen activated protein kinase (MAPK) cascade. In mammals this is activated at the plasma membrane by mitogen binding to a membrane-bound receptor tyrosine kinase (RTK). On stimulation the RTK becomes autophosphorylated, which in-turn actives the recruitment of GRB and SOS proteins. These bind and activate RAS, at the plasma membrane from a GDP to a GTP active state. RAS-GTP then stimulates a triple-tiered MAPK phosphorylation cascade from RAF-MEK-ERK. ERK activates substrates in the cytoplasm and nucleus, which includes gene transcription.
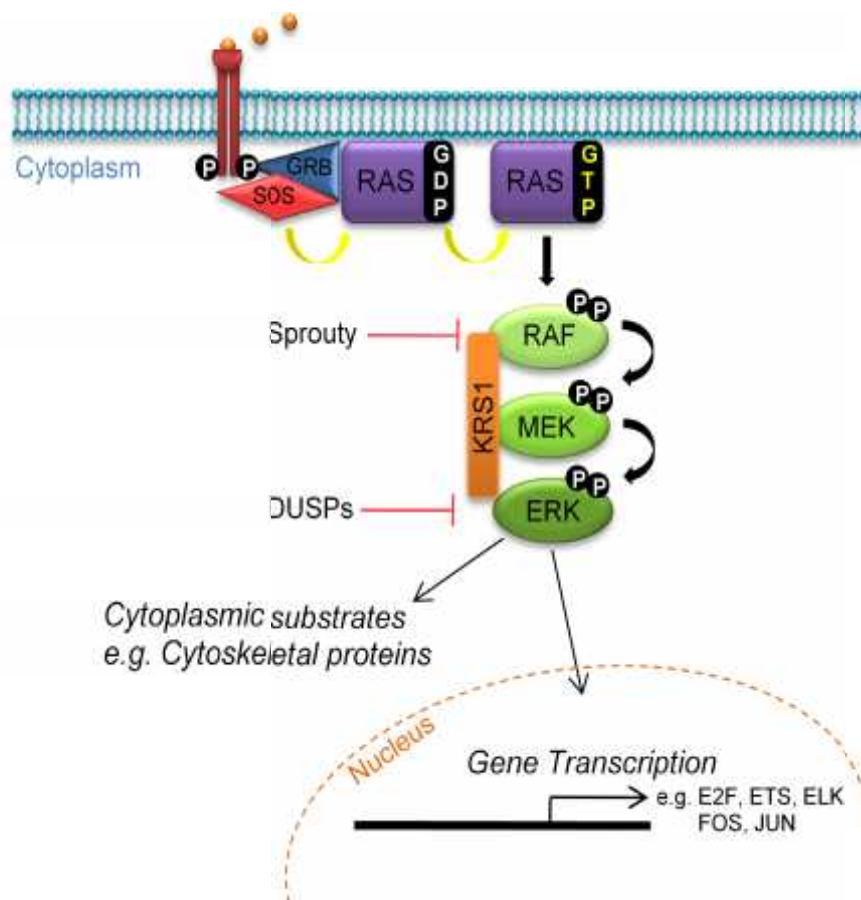
(Vojtek et al., 1993; Marais et al., 1997). RAF then phosphorylates MEK, which phosphorylates ERK. The interactions between the RAF/MEK/ERK proteins also requires the kinase suppressor of Ras (KSR1) scaffolding protein (Razidlo et al., 2004). Phospho–ERK (ppERK) has many substrates in the cytoplasm including skeletal proteins and negative regulators of the MAPK cascades, such as DUSPs and Sprouty. ERK also has targets in the nucleus, of which gene transcription factors are a major target, including c-myc and c-fos. ERK activity leads to activation of important cellular processes, such as proliferation, growth, survival and in contrast, apoptosis and senescence (Erhardt et al., 1999; Pearson et al., 2001; Zhu et al., 1998).

1.1.3 The three RAF isoforms

The first *RAF* gene to be isolated was *vraf* from the 3611-MSV murine retrovirus, which was then identified as a cellular homologue of CRAF (Rapp et al., 1983; Bonner et al., 1984; 1985). Following this, *v-mil*, another *RAF* gene, was isolated from the Mill-Hill No.2 virus, whose sequence homology was found to match the human *ARAF* gene (Sutrave et al., 1984; Huleihel et al., 1986).

The mammalian *RAF* gene encodes three isoforms known as; ARAF, CRAF (RAF-1) and BRAF (Wellbrock et al., 2004). These function as serine/ threonine kinases in the ERK-activated MAPK cascade. The human RAF proteins contain three highly conserved regions CR1, CR2 and CR3 (Figure 1.3). The CR1 region harbours the RAS-binding domain (RBD), this allows RAS-guanine-5'-triphosphate (GTP) binding and is required for RAF

Figure 1.3 Protein structures of the three RAF homologues. There are three RAF homologues ARAF, CRAF and BRAF, each share 3 highly conserved regions CR1, CR2 and CR3. These contain phosphorylation residues that are important in regulation and activation of the RAF kinases. The N-terminus contains CR1 and CR2, which harbours the RAS-binding domain (RBD) and cytosine rich domain (CRD) and a key phosphorylation site that is constitutively phosphorylated. The CR3 harbours the kinase domain, this contains the N-region that has two phosphorylation residues required for kinase activation. Although these are not conserved in BRAF, which instead has two adjacent aspartate amino acids (D) that give this region a negative charge. The activation segment (AS) contains two threonine residues, which are also required for RAF activation.
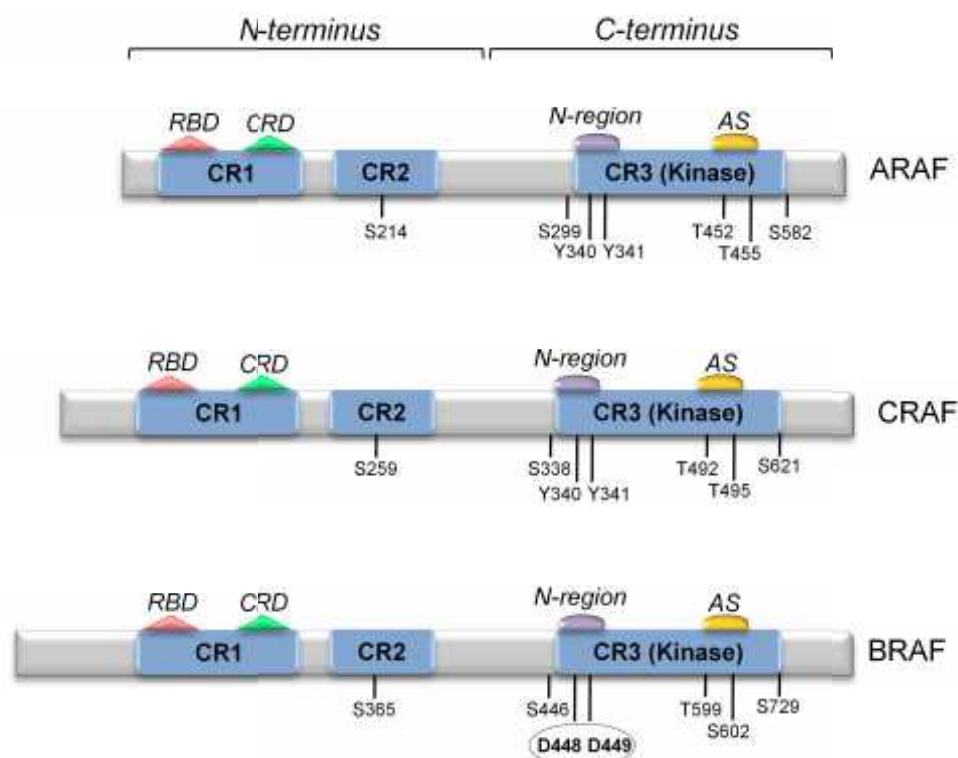
recruitment to the plasma membrane and activation. CR1 also contains the cysteine-rich domain (CRD), which is important for RAS binding stabilisation (Avruch et al., 2001). The CR2 region harbours a key regulatory serine (S) residue that is constitutively phosphorylated and binds the 14-3-3 scaffold protein, when RAF is inactive (Light et al., 2004). The CR1 and CR2 reside in the 'negative regulatory terminal' (N-terminal) of the protein, named because of the regulatory roles of the CR1 and CR2 regions that hold the RAF protein in an inactive state. The CR3 region is in the catalytic segment (C-terminal) and harbours the kinase domain. Within this domain are key phosphorylation sites for activation of the protein function and for functional MEK activation.

Although the RAF proteins are highly conserved in the CR1, 2 and 3 region, there are differences in their regulation and activation. This is partly due to the fact that outside the conserved regions their amino acid sequences vary. This is evident when comparing their molecular weights; ARAF is the smallest at 68kDa, followed by CRAF, which is 72kDa and differential splicing of exons (8b and 9b) in the *BRAF* gene results in protein products between 72-100kDa (Hmitou et al., 2007). The three RAF isoforms are expressed ubiquitously in all human and mouse tissues. However, expression of ARAF is greater in urogenital tissue and BRAF is the predominant isoform in neuronal tissues (Storm et al., 1990; Barnier et al., 1995). Homologous knockout of *Craf* and *Braf* in mice proves embryonic lethal, whereas *Araf* mice only survive after birth up to 21 days. This suggests they have individual roles in development and as such have non-redundant functions (Wojnowski et al., 1997; Huser et al., 2001; Pritchard et al., 1996).

1.1.4 Regulation differences and activation of RAF proteins

The RAF functional differences can also be explained by the regulation of their catalytic domains. The activation of ARAF mimics that on CRAF, however BRAF requires less phosphorylation events.

In-active RAF proteins are situated in the cytoplasm, they have two conserved serine phosphorylation residues, which in BRAF these are S365 at the beginning of the CR2 domain and S729 at the end of the C-terminus (Figure 1.3). When RAF is inactive these are phosphorylated and the scaffold protein 14-3-3 resides between the two serine sites (Hekman et al., 2004). This interaction holds the protein in a closed conformation. Activated RAS-GTP binds to in-active RAF and recruits it to the membrane where it undergoes several activation steps (Marais et al., 1997). It is thought that the protein phosphatase 2A (PP2A) removes the serine phosphorylation from the CR2 region (Abraham et al., 2000; Ory et al., 2003). Following this CRAF and ARAF require phosphorylation on residues in two regions of the kinase domain (Mason et al., 1999). The first region is known as the 'negative-regulatory region' (N-region) where a serine and two tyrosine (Y) residues are phosphorylated (King et al., 1998; Fabian et al., 1993). The region known as the 'activation segment' harbours the serine and threonine phosphorylation residues (Chong et al., 2001). However, this is not the case for BRAF, which only requires phosphorylation of S602 and T599 in the activation segment (Zhang and Guan, 2000). The phosphorylation sites required for activation of CRAF/ARAF in the N-regions are replaced with a constitutively phosphorylated

S446 and two aspartic acid residues, which inhibit the negative regulatory effects the N-terminal has over the catalytic domain (Brummer et al., 2006).

BRAF has been found to have a higher basal kinase activity than CRAF and ARAF (Marais et al., 1996; Mason et al., 1999). This is thought to be because the negatively charged N-region provides BRAF with a 'primed' catalytic domain, which is in an open conformation and is more acceptable to MEK binding and activation.

1.1.5 BRAF mutations occur in multiple human cancers

In 2002, a study identified mutations in the *BRAF* gene in multiple human cancers (Davis et al., 2002). The highest proportion was in Melanoma (66%) and to a lower extent in; ovarian, colon, papillary thyroid and breast cancers. This study identified 43 somatic missense mutations in the *BRAF* gene (Figure 1.4). Interestingly, the majority of cancers (80%) expressed a mutant gene with a nucleotide switch of thymidine (T) to adenosine (A) at nucleotide 1796. This causes an amino acid change of valine to glutamic acid in residue 600, known as BRAF^{V600E}. The V600E mutation resides in the activation segment, in between the two key phosphorylation sites. The *BRAF^{V600E}* mutation was identified in 92% of melanomas, suggesting this is an important oncogene in this form of cancer.

At the present time, mutations in *BRAF* are acquired in 30-60% of melanomas, 30-50% of thyroid cancers, 30% of ovarian cancers and 5-20% colorectal

Figure 1.4 The majority of mutations in the BRAF gene in human cancers are located in the kinase domain of the protein. Over 40 mutations in BRAF have been identified in human cancers. These have been found to reside in the glycine-rich P-loop and the activation segment. A hydrophobic interactions between these two regions is thought to hold the BRAF protein in an inactive state. Mutations in these regions are thought to disrupt this interaction resulting in a constitutively active protein. Adapted from Wellbrock et al., 2004.
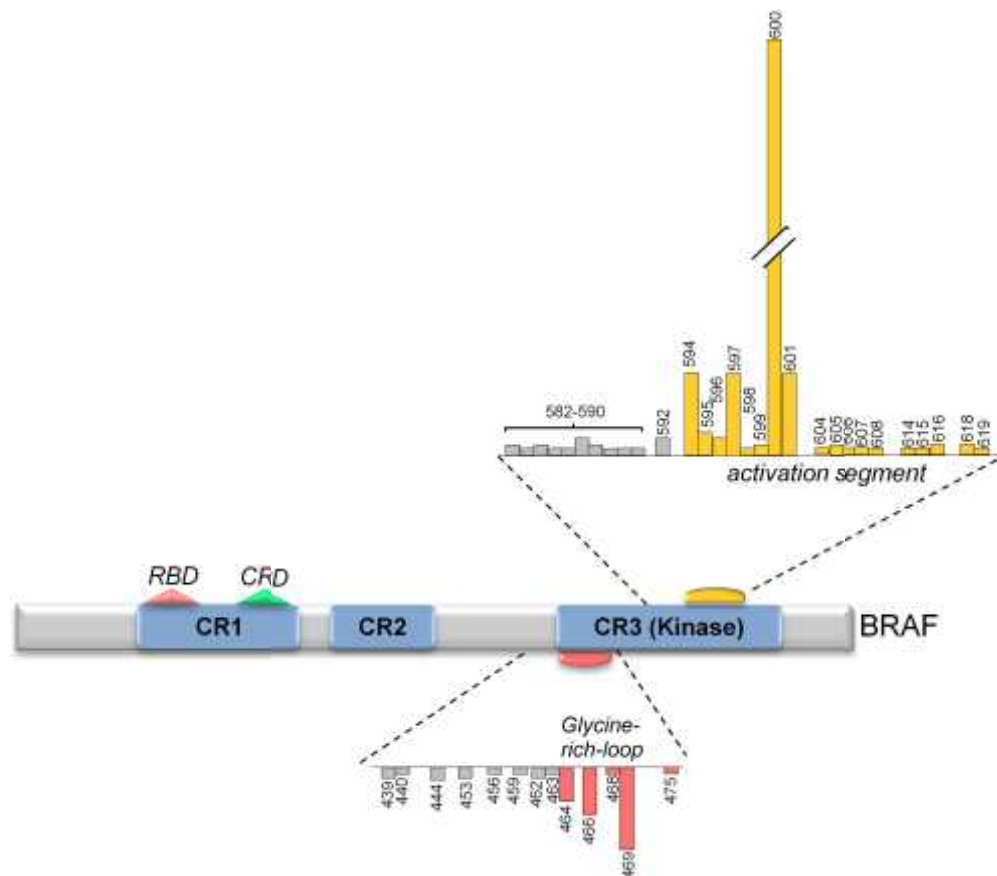
cancers, with only 1-3% in other cancers (Wellbrock et al., 2004). Of these, ~90% exhibit the single T-A switch at position 1796 encoding $BRAF^{V600E}$.

The reasons for this can be explained in the structure of the BRAF/BRAF^{V600E} protein. It was found that when the protein is in an inactive state, it is folded and allows for hydrophobic interaction to be formed between the residues G463-V470 of the N-region, known as the glycine-rich P loop and G596-V599 of the kinase domain, known as the activation loop (Wan et al., 2004). Interestingly, nearly all of the known *BRAF* mutations are located in these regions (Davies et al., 2002). The $BRAF^{V600E}$ mutation therefore interrupts the regulatory hydrophobic interaction of the glycine-rich loop and activation loop. This mutation also sits directly between the key S598 and T602 phosphorylation residues and therefore acts as a phospho-mimetic (Figure 1.5). Both of these aspects provide BRAF^{V600E} with its oncogenic capabilities.

Not all of the BRAF mutants identified in cancers, have elevated kinase activity to the extent of BRAF^{V600E}, such mutants are known as having intermediate activity and are located in the P-loop and activation-loop (Wan et al., 2004). Furthermore striking is that three of the BRAF mutants also identified were found to have impaired catalytic activity, however they were still able to active MEK/ERK. In the same study, it was shown that these mutants are able to activate CRAF *in vivo*, subsequently leading to ERK activation. Following this it has now been shown that impaired BRAF mutants can activate CRAF most likely through heterodimerisation (Garnett et al., 2005).

Figure 1.5 The *BRAF^V600E* mutation results in a constitutively active BRAF protein. The kinase domain of BRAF requires phosphorylation on two residues T599 and S602. The *BRAF^V600E* mutation resides in between these residues and is thought to mimic these phosphorylation events, resulting in a constitutively active kinase domain.
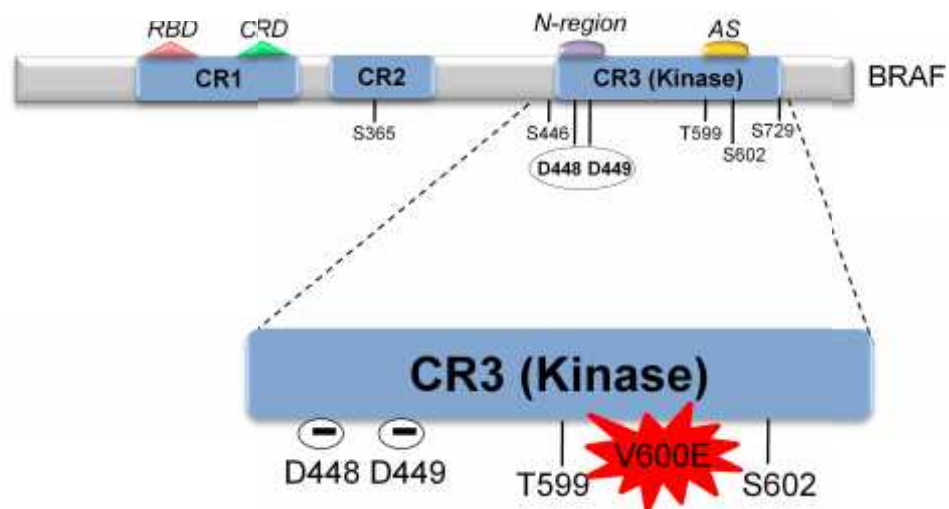
1.1.6 BRAF is an oncogene unlike CRAF and ARAF

$BRAF^{V600E}$ is the most frequent mutation in melanomas. Significant to this, BRAF mutations have been identified in 80% of melanoma precursor lesions, known as 'nevi' (Pollock et al., 2003). This is thought to be because it is involved in a key ERK signalling cascade in melanocytes (Busca et al., 2000). $BRAF^{V600E}$ has been shown to up-regulate ERK activation in melanocytes and transform these cells in vitro (Sharma et al., 2005; Wellbrock et al., 2004).

To date, mutations in CRAF are very rare in cancers and none have been described in the ARAF gene. This is most likely due to the differences between the catalytic activation. As mentioned before, the catalytic domain in BRAF is already partly primed in the N-region therefore any activating mutations in the activation segment would be efficient enough to fully activate BRAF. This is supported by the fact that CRAF kinase activity does not increase when it exhibits BRAF activating mutations (Emuss et al., 2005).

1.2. Colorectal cancer

1.2.1. Synopsis of Colorectal Carcinogenesis (CRC)

Colorectal carcinogenesis (CRC) is a disease that affects the large bowel, which is made up of the colon and the rectum. In the UK it is the third most common cancer in both men and women, with 41,142 cases diagnosed in 2009 and just under half of these proved fatal (16,013) (Cancer research UK, 2009). CRC is the second cause of cancer related deaths in the UK. The disease occurs more predominantly on the left-hand side of colon with two-thirds of cases identified in the colon and one-third in the rectum. It is an age related

disease with ~80% occurring in the over 60s and occurs in both men and women similarly (12:10 ratio).

On a worldwide scale, in 2008 CRC was the third and second most common cancer in men and women respectively and 1.24 million new cases were diagnosed (Cancer research UK, 2009). The majority were in developed western countries in comparison to the undeveloped.

1.2.2 Familial/Inherited CRC

Around 15-20% of CRC cases are familial (hereditary) due to a single inherited germline mutation (Kinzler and Vogelstein, 1996). There are two main genetic diseases; the familial adenomatous polyposis (FAP) and the hereditary non-polyposis colorectal cancer (HNPCC) involved in familial CRC. Both are inherited in autosomal dominant patterns.

FAP results from the loss of the adenomatous polyposis coli (*APC)* gene either though point mutations or chromosome 5q21 aberrations, where *APC* is located (Bodmer et al., 1987). APC is a key tumour suppressor in the Wnt signalling pathway, which is the major signalling pathway in the intestinal epithelium. APC regulates the level of nuclear β–catenin, whose activities provides the cell with pro-growth and survival signals (Sparks et al., 1998). Most mutations in *APC* result in a truncated and therefore inactive protein, which is unable to function as an inhibitor of β–catenin (Miyaki et al., 1994). Excessive signalling through the Wnt pathway is a key component in the early stages of most CRCs.

Individuals with FAP, develop multiple large intestinal polyps, which are precursor lesions to adenomas (Kinzler and Vogelstein, 1996).

HNPCC is five times more common than FAP (Ahnen et al., 1991). In this disorder mutations in the DNA mismatch repair (MMR) genes are most often acquired, particularly in the MutL homolog 1 and 2 (*hMLH1* and *hMLH2)* genes. This leads to genetic instability through DNA frame-shifts in non-encoding and encoding regions, such as TSGs (Iino et al., 2000). Possible targets are the insulin-like growth factor receptor (IGFR) and tumour growth factor β (TGF-β) (Souza et al., 1996; Markowitz et al., 1995).

1.2.3. The traditional adenoma to carcinoma pathway to CRC

As well as being an inherited/familial disease, ~80% of CRC cases occur sporadically. Traditionally, sporadic CRC was thought to progress through a typical subset of histopathological changes known as the adenoma to carcinoma sequence (Figure 1.6) (Fearon and Vogelstein, 1990). This is characterised by distinct genetic aberrations generally through the activation of oncogenes and the inactivation of tumour suppressor genes (TSG).

Not surprisingly, the most common initiating mutations are in the *APC* gene, which is mutated in 60% of sporadic CRCs (Jass JR, 2002). Due to either point mutations of the gene or through chromosome 5q allelic losses (similar to FAP). The *RAS* mutation, in particular *KRAS* of the MAPK pathway, is associated with the growth of adenomas in 35%-42% of CRCs (Leslie et al., 2002). Subsequently, allelic losses on chromosome 17p and 18q, resulting in *Tp53* and

Figure 1.6 Diagram to show the multiples stages in the progression of the traditional adenoma to carcinoma sequence of CRC. Mutations in the *APC* gene are the initiating factors the adenoma to carcinoma pathway. Progression of early lesions to adenomas, occurs through acquisition of proto-oncogenes, in particular the *KRAS* mutation. Malignant progression to carcinomas occurs through mutations in key TSGs, most commonly *Tp53*. Adapted from Rizk and Barker et al., 2012.
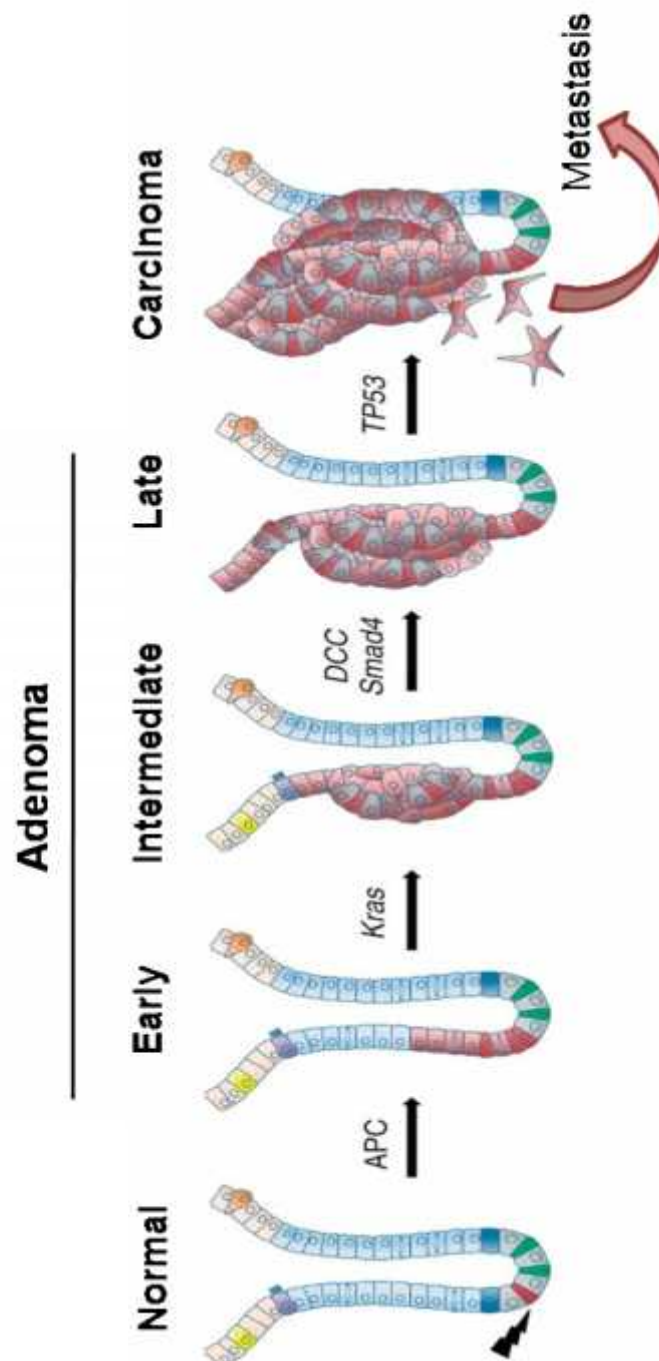
deleted in colorectal cancer (DCC/SMAD4), are related to advanced malignancy because they are only found in late stage adenomas and carcinomas (Takayama et al., 2006; Vogelstein et al., 1988). Since chromosomal gene losses are important in all stages of this pathway, it is also described as the chromosomal instability (CIN) pathway.

1.2.4. The serrated neoplastic pathway of CRC

An alternative pathway to CRC was first proposed by Longacre and Fenoglio-Preiser (1990), who described a subset of hyperplastic polyps and adenomas as 'serrated', which were morphologically different compared to the equivalent traditional CRC lesions. In this study, they identified lesions of increasing malignancy as having serrated and mucinous crypt epithelium. For many years the idea of a serrated neoplastic pathway, was highly controversial because hyperplastic polyps of the adenoma to carcinoma sequence were not thought to possess malignant potential (Hawkins et al., 2002). The serrated pathway provided a morphological link between polyps, adenomas and carcinomas.

Since its first discovery, multiple lesions have been characterised in this pathway (Jass et al., 2007). The earliest lesions are known as 'aberrant crypt foci' (ACF). These lesions are precursors to polyps and their histology represents the beginnings of crypt hyperplasia. Similar to the CIN pathway, 'hyperplastic polyps' are also identified in this pathway, but this pathway has alternative polyp subtypes; first being the hyperplastic polyp, but there is also the admixed polyp, which has a mixed morphology between a polyp and

adenoma. The there are two alternative adenomas described for this lesion the sessile serrated and traditional.

Over the last 10 years, research has provided support for this pathway of CRC, through the identification of specific biological features, which are exclusive from the traditional pathway. The most surprising discovery was that mutations in the *APC* gene are not the initiating factor, nor do they have a strong mutation rate in this pathway, at any level (Konishi et al., 2004). Similarly *p53* mutations are also very rare in serrated CRCs (Sawyer et al., 2002). Instead, mutations in *BRAF* are thought to be the key instigators and in this pathway, which are not found in the traditional pathway (Kambara et al., 2004). The *KRAS* mutation is also found in a sub-set of serrated lesions, although not to the same extent as in the traditional pathway (Rosenberg,. 2007). Interestingly, *BRAF* and *KRAS* mutations are mutually exclusive in this pathway, suggesting they initiate alternative pathways but have equivalent roles. The characterisation of these pathways is increasingly complicated, but it appears to evolve around the microsatellite stability (MS) of DNA. The method to distinguish these is down to the mutation and methylation of a subset of markers, usually MMR genes, TSG and MSI markers including; hMLH1, MGMT, MINT1, MINT2, p16 and BAT25 and BAT26 (O'Brian et al., 2004).

Studies have provided evidence for two distinct pathways in serrated CRC (Reviewed in Noffsinger, 2009) (Figure 1.7). The first is initiated by mutant *BRAF,* most often by the specific $BRAF^{V600E}$ mutation. As well as $BRAF^{V600E}$, lesions also exhibit a high level of microsatellite instability (MSI-H) and

Figure 1.7. The multiple stages in the progression of serrated neoplastic pathway of CRC. The serrated pathway is an alternative pathway to CRC. Furthermore, this pathway is thought to progress through two alternative genetic routes. The first is initiated by oncogenic mutations in BRAF and its progression is in association with mutations in MMR genes and CIMP-H and MSI. The alternative pathway has not yet been fully determined but it is classified as being activated by the KRAS mutations and is associated with inactivation of TSGs and MSS.
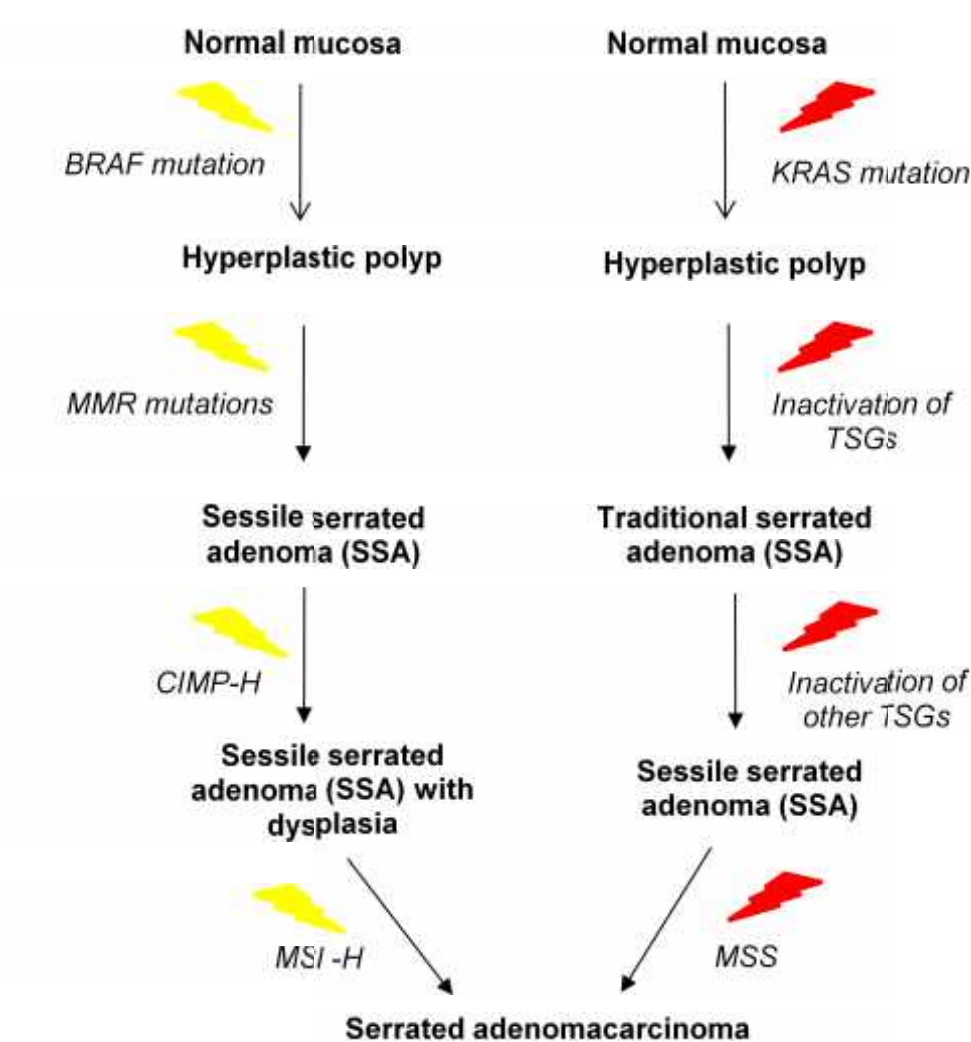
mutations in DNA mis-match repair genes (MMR), commonly the human mutL homologue 1 and 2 (hMLH1 and hMLH2) (Issa, 2004; Koinuma et al., 2004). Another key contributor to this pathway is substantial hypermethylation of CpG islands (CIMP-H), in a subset of identified genes such as tumour suppressor and DNA repair genes (Toyota et al., 1999; Weisenberger et al., 2006). Although the exact sequence of events has not been established, it is hypothesised that hypermethylation of MMR genes induces MSI-H, resulting in DNA frame-shifts in coding regions, leading to the loss of TSGs (Moran et al., 2012). These biological features are more commonly associated with hyperplastic polyps and sessile serrated adenomas.

The KRAS mutation is also associated with hyperplastic polyps and traditional serrated adenomas. These lesions exhibit a biologically different make-up compared to the BRAF expressing sub-type. Generally they are microsatellite low (MSI-L) or stable (MSS) and harbour mutations in unidentified TSGs and DNA repairs genes (Oliveira et al., 2007).

1.3. Composition of the mouse digestive system

There are no differences between the structure and epithelium of the human and mouse small and large intestines. The following descriptions of these GI tract organs are analogous to both species.

1.3.1 Morphology of the small and large intestines

The digestive system is made up of the stomach, small intestine (SI) and large intestine (LI). The small intestine is the middle section of the gut, which

connects the stomach to the large intestine. It is composed of three sections; the section nearest to the stomach is called the duodenum, followed by the jejunum and lastly the ileum which joins onto the colon. The large intestine is made up of the colon and rectum. The epithelium of the intestine is part of the mucosal layer, this sits on the submucosa and is underneath the muscle layer, known as the muscularis externa (Figure 1.8A).

1.3.2 The epithelium of the small and large intestines

The epithelium of the small intestine contains two structures; crypts and villi. The large intestine does not contain villi, only crypt structures. The crypts are at the base of the intestine, attached to the mucosa (Figure 1.8B). The crypt contains the epithelial stem cells and as such controls the cell population of the crypt and villi. At the base of the crypts resides the paneth cells, these are the only cell to migrate to the base of the crypt and have an anti-microbial role (Sancho et al., 2004). The crypt stem cells are located between the paneth cells and produce daughter progenitor cells known as transit amplifying (TA) cells, which migrate upwards whilst continuing to proliferate and differentiate until they reach the crypt-villus axis. Differentiated cells in the crypt are the endothelial cells and goblet cells, which produce mucin. Both these cell types are found in the villi, as well as enterocytes that have an absorptive function and endocrine cells which secrete hormones (Hocker and Wiedenmann, 1998). Cells in the crypt and villi are replenished every ~3-5 days. Once cell reach the tip of the villi they are lost through apoptosis.

Figure 1.8 Morphology of the mouse small intestine. The small intestine is made up of crypt and villi structures. The crypts lie on the mucosa and contain four different cell types; stem, paneth, goblet and endothelial. Stem cell progenitors make up the transit amplifying population, which are constantly dividing/differentiating and moving up the crypt into the villi. The villi also have endothelial and goblet cells, as well as enterocrine and enterocytes.
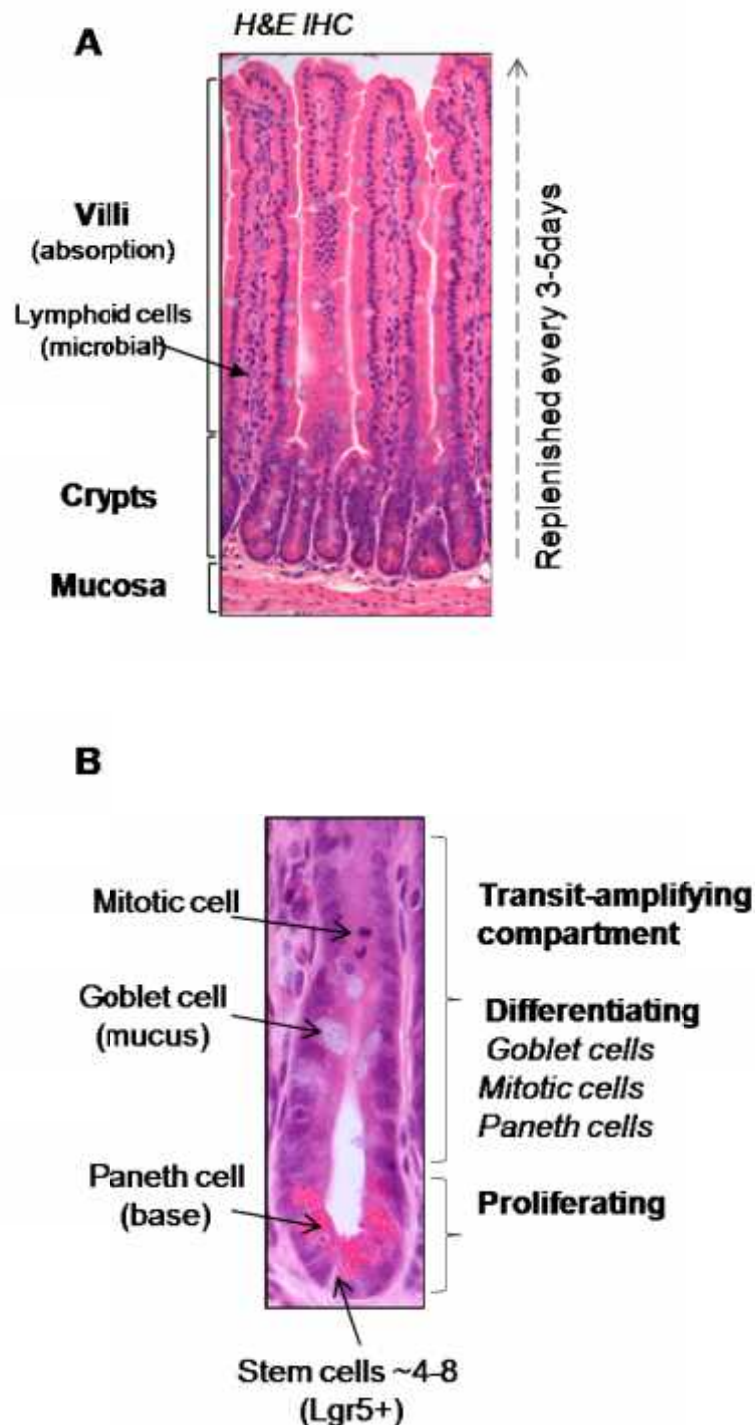
1.4. Alternative mouse models of colorectal cancers

The Wnt signalling pathway is an essential signalling pathway in the crypts of the intestinal epithelium (Ireland et al., 2004). As previously discussed, it is the APC tumour suppressor protein that has been established as a key early mutational target in both familial and sporadic CRC. A number of mouse strains have been developed that express various truncated Apc proteins these are known as $Apc^{min/+}$ mice (Fodde et al., 1994; Samson et al., 2004). These Apc mutant strains develop multiple polyps and/or various staged malignant lesions throughout the whole intestinal epithelium. In addition, $Apc^{min/+}$ mice have been cross bred to strains carrying a mutation in the Wnt target gene Myc and both $p53$ and $Smad4$ which are mutated in late stage CRC (Sansom et al., 2007; Reed et al., 2008; Takaku et al., 1998). Loss of Myc suppressed the effects of the $Apc^{min/+}$ mutation, surprisingly mutation of $p53$ did not have a noted effect on tumourigenic progression either. Whereas loss of $SMAD4$ expression significantly induced the malignant potential of $Apc^{min/+}$ mice.

1.5. Mouse model for conditional expression of $Braf^{V600E}$ in the gut

The $Braf^{V600E}$ mouse model used in this project was developed at the University of Leicester prior to the start of this study and is described in this section (Mercer et al., 2005) (Figure 1.9).

The Braf gene is located on chromosome 7 and has 18 exons. The T-A mutation of $BRAF^{V600E}$ occurs in exon 15. Targeting vectors were designed to contain a left and right arm, corresponding to the DNA sequences surrounding exon 14 and 15 of wildtype Braf. The right arm contains exon 15 with the T-A

Figure 1.9 Generation of a conditional 'knockin' mouse model that expresses the *Braf*^{V600E} mutation. A vector containing a Lox-stop-Lox (LSL) cassette containing loxP sequences, a minigene (MG) encoding wildtype exons 15-18, downstream of an exon 15 with the T-A transversion and two polyadenylation (PA) sites, was inserted into the mouse germline. Expression of Braf^{V60XE} is dependent on loss of the LSL cassette between the LoxP sites, to induce expression of exon 15 with the T-A transversion. This was performed by Cre recombinase.
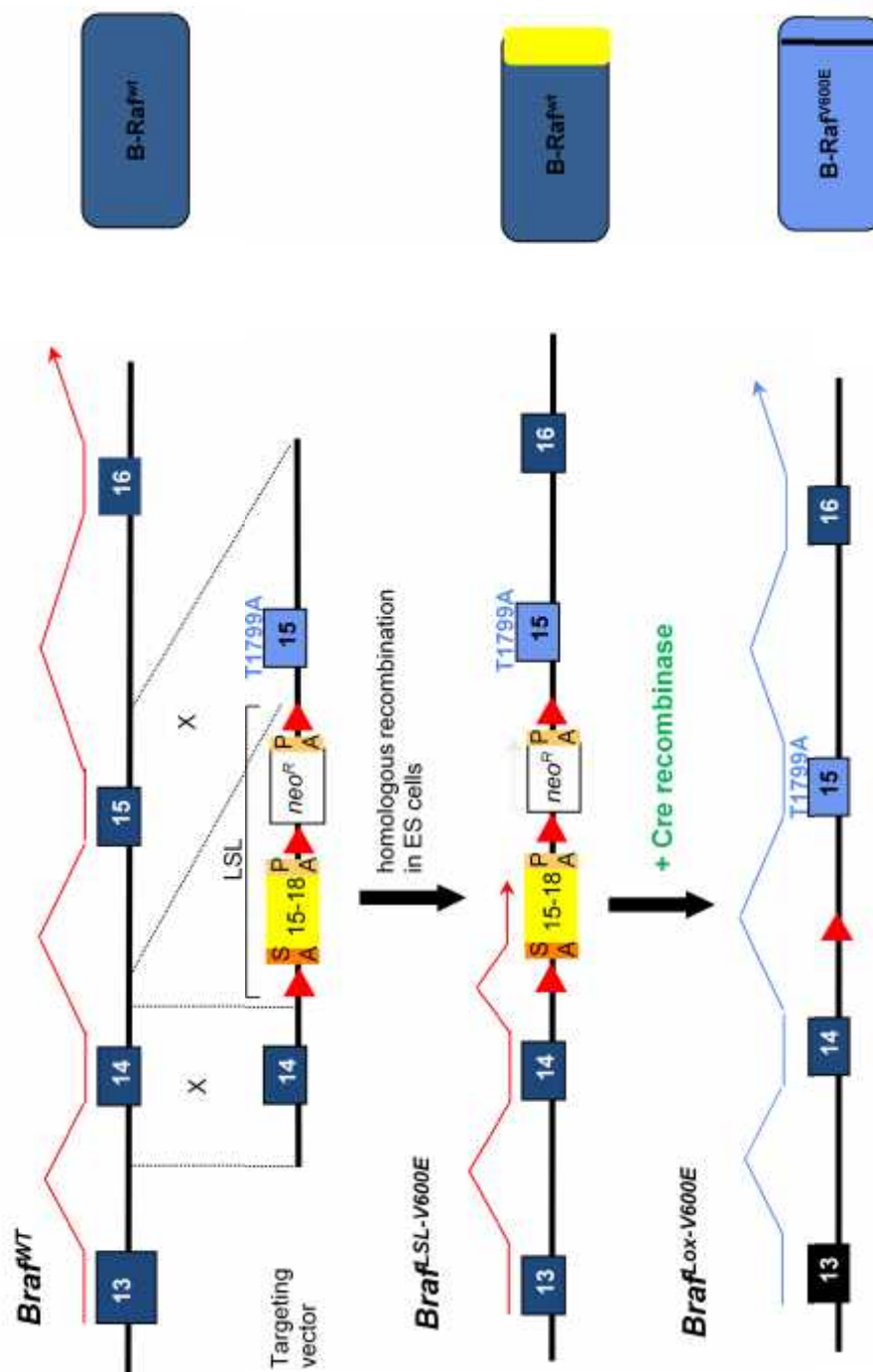
transversion. In between the right and left arm is a Lox-stop-Lox (LSL) cassette containing three loxP sequences, a minigene (MG) encoding wildtype exons 15-18 and two poly-adenylation (PA) sites. Insertion of this vector into ES cells, results in homologous recombination and integration of the LSL-allele into the mouse germline, but only on one allele and expression of wildtype Braf. This phenotype can be distinguished using PCR primers with sequences in the LSL, these mice are termed as Braf^{LSL}. Using this system expression of Braf^{V600E} is dependent on loss of the LSL cassette between the LoxP sites, to induce expression of exon 15 with the T-A transversion. This is generally performed by a Cre recombinase.

In order to express *Braf^{V600E}* conditionally, so to mimic that of sporadic CRC, the Ah*Cre*ER^{T} *Cre recombinase* strain was used in this mouse model (Kemp et al., 2004). Cre expression is under the control of the p450 cytochrome promoter, (*Cyp1a1*), which targets it to the cells of the gastrointestinal tract. This model allows dual controlled expression of *Cre recombinase* at the transcriptional and post-transcriptional level. In the first instance, beta-napthoflavone (β-NF) induces expression of a Cre fusion protein, consisting of Cre bound to a mutated estrogen receptor (CreER), which is responsive to Tamoxifen only (Figure 1.10). CreER resides in the cytoplasm, upon Tamoxifen stimulation CreER translocates to the nucleus where it induces homologous recombination of the LSL and transcription of Braf encoding the exon 15 with the T-A transversion (*Braf$^{LOX-V600E}$*) (Figure 1.11).

Figure 1.10 Transcriptional regulation of Cre recombinase using the AhCreER^T mouse model. Cre expression is under the control of the p450 cytochrome promoter, Cyp1a1, which targets it to the cells of the gastrointestinal tract. Transcription of *Cre recombinase* is activated by beta-napthoflavone (β-NF), which induces expression of a Cre fusion protein, consisting of Cre bound to a mutated estrogen receptor (CreER).
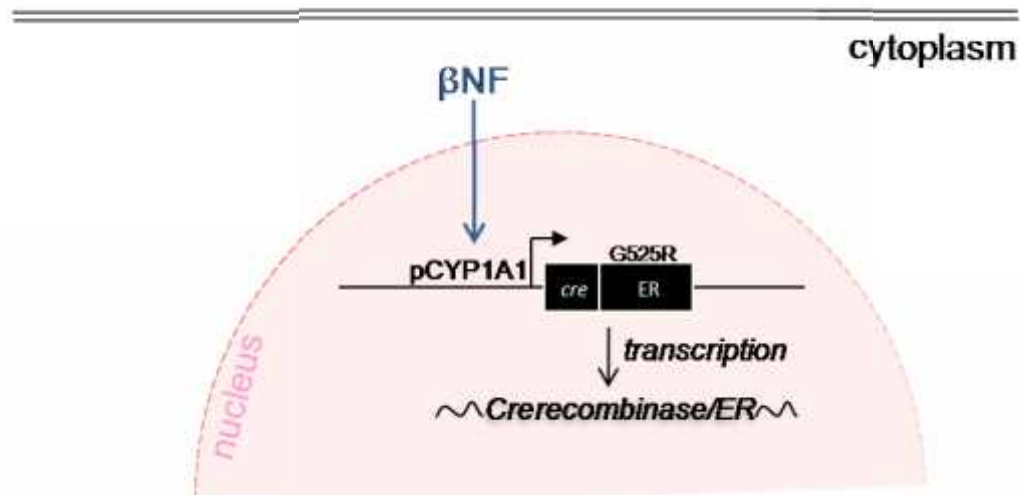
In the present study $Braf^{Lox-V600E}$ mice were crossed to mice expressing Ah*Cre*ER^{T}. Three phenotypes were analysed in this study, from the propective litters of this cross (Figure 1.12). The experimental phenotype analysed was the $Braf^{V600E/WT}/AhCreER^{T/0}$, which is denoted as VE in this study. There were two controls analysed for comparison. The first was wildtype for *Braf* ($Braf^{WT}$) denoted as WT, this phenotype was treated with both carrier oils (sunflower and corn). The second control was $Braf^{WT}/AhCreER^{T/0}$ denoted as Cre, this was treated with both βNF and TM.

To analyse the effects of $Braf^{V600E}$ in the mouse gut, mice small intestines (SI) were analysed over an experimental time course of $Braf^{V600E}$ expression from 1 day up to 12wks.

1.6. Project Aims

$Braf^{V600E}$ has been implicated as an initiating mutation in the serrated neoplastic pathway of CRC. Studies on this mutation had only been *in vitro,* up until a mouse model for CRC was developed, which expresses $Braf^{V600E}$ to mimic the onset of sporadic lesions which harbour this mutation.

The aims of this project were to analyse the intestinal epithelium in the presence of $Braf^{V600E}$ to confirm this as a key initiating factor in the development of serrated CRC. This project was also devised to analyse the morphological and molecular changes in the gut in the presence of excessive Braf^{V600E}-MAPK signalling in crypt cells. MAPK signalling through activated ERK stimulates multiple cellular processes. For this reason, analysis was directed at

Figure 1.12 *Braf*^V600E^ **mouse model for CRC.** Mice expressing the allele *Braf*^lox V600E^ were crossed to AhCreER^I^ mice. Three phenotypes were analysed in this study. The experimental phenotype is that *Braf*^V600E/WT^, which express Braf^V600E^ upon Cre recombination. The two controls analysed for comparison were; mice wildtype for *Braf* (*Braf*^WT^), treated with both carrier oils (sunflower and corn) and *Braf*^WT^/AhCreER^I/0^ treated with both βNF and TM.
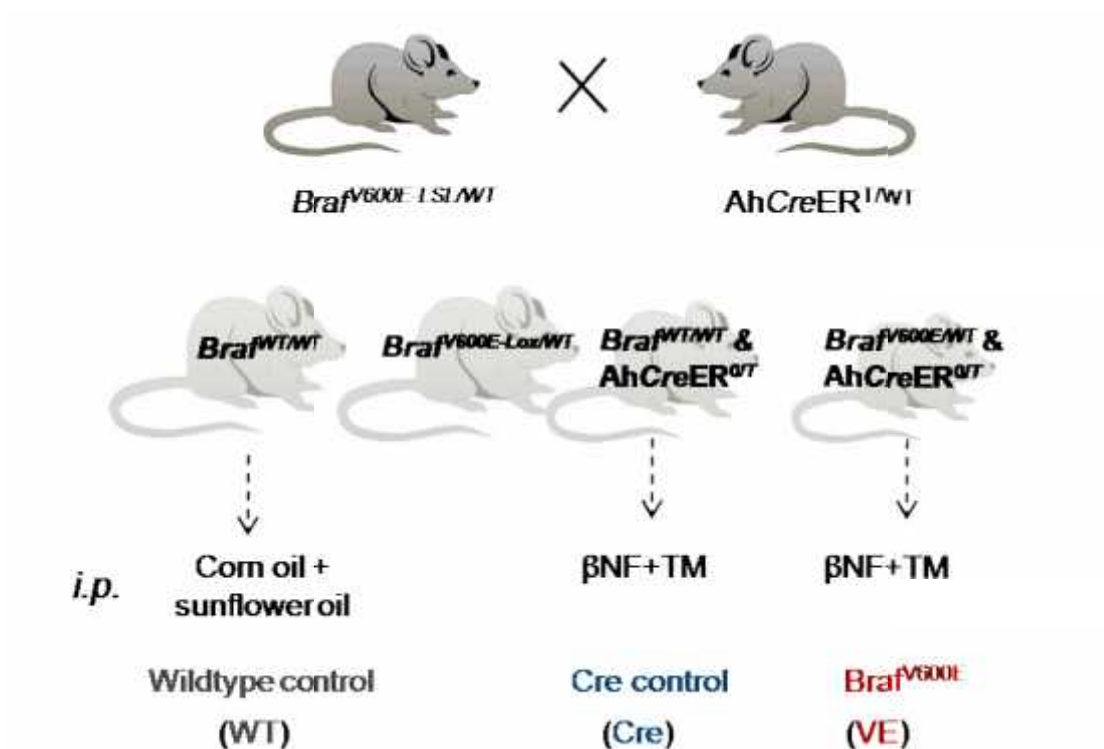
determining possible changes in 1) proliferation, 2) apoptosis and 3) senescence.   In serrated CRCs, the presence of the acquired *BRAF^(V600E)* mutation is associated with CIMP-H and because of this link methylation was also investigated in this model.

2. Materials and Methods

2.1 Molecular Biology

Unless stated otherwise all chemicals and reagents were supplied by Fisher Scientific. All water used in experiments was from a milliQ system and kept in sterile universal tubes.

2.1.1 Polymerase chain reaction (PCR) primer design

Primers for genomic DNA amplification were designed using Primer3 version 0.4.0 (http:frodo.wi.mit.edu/). They were synthesised by Invitrogen and reconstituted at 200pmol in dH$_2$O. Primer stocks were diluted 1:10 and 1µl of each stock was used to gain a working concentration of 1pmol/µl. All primer sequences are stated in Table 2.1.

2.1.2 Polymerase chain reaction components

For genotyping and other general PCR reactions ReddyMix PCR Master Mix (Thermo Scientific) (16µl) was used with 1pmol/µl of each primer (2µl). Between 10pg-1µg (2µl) of DNA was added to make a total reaction volume of 20µl. PCR products were electrophoresed on a 1.8% [w/v] agarose gel (as stated in *2.1.5*).

2.1.3 Sensitive polymerase chain reaction components (PCR)

PCR techniques that required a more sensitive approach to DNA amplification such as bisulphite converted DNA amplification and sequencing used alternative enzyme amplification reaction mixes, based around either Platinum *Taq* (Invitrogen) or KOD Hot Start DNA polymerases (Novagen) using conditions

Table 2.1 Sequences of primer used for PCR

Technique	Ref. (Lab-OCP)	Gene target	Sequence 5'-3'	Annealing temp (℃)
PCR Genotyping	125	*V600E Braf*	GCCCAGGCTCTTTATGAGAA	60
	137	*V600E Braf*	GCTTGGCTGGACGTAAACTC	60
	143	*V600E Braf*	AGTCAATCATCCACAGAGACCT	60
	361	*Cre recomb.* (F)	GCCTGGTCTGGACACAGTCC	57
	362	*Cre recomb.* (R)	GGTTCAGCATCCAACAAGGC	57
RT-PCR/ Q-PCR	422	*Calnexin* (F)	CTGGCAGTCAAGATGAGGAAG	59
	423	*Calnexin* (R)	AAGGTACACCAGGCCCTCTC	59
	230	*Dnmt3b*	CCCGGTACTTCTGGGGTAAC	55
	230 2	*Dnmt3b*	ACACGTCCGTGTAGTGAGCA	55
	231	*Dnmt3b*	CTTCAAGCGTACTGGGATCG	55
	231 2	*Dnmt3b*	TCCCGCCATAGCTATTTGTC	55
	232	*Dnmt3b*	GGAGAGTCACTGGAGGACCA	55
	232 2	*Dnmt3b*	GGCAAACAGGTGTCTGATGA	55
	386	*Dnmt3a (F)*	TCCCGGGGCCGACTGCGA	61
	387	*Dnmt3a2 (F)*	AGGGGCTGCACCTGGCCTT	61
	388	*Dnmt3a/2 (R)*	TCCCCCACACCAGCTCTCC	61
	322	*Jmjd3 (F)*	AGTCCATTGTGCCCATGATT	59
	323	*Jmjd3 (R)*	GCAGTAGTAGGCAGGCTCGT	59
	726	*Ezh2 (F)*	ACTGCTGGCACCGTCTGATG	51.8
	727	*Ezh2 (R)*	TCCTGAGAAATAATCTCCCCACAG	51.8
	348	*p15 (F)*	AGATCCCAACGCCCTGAA	59
	349	*p15 (R)*	GACAAGCGTGTCCAGGAAG	59
	560	*p16 (F)*	GTGTGCATGACGTGCGGG	59
	561	*p16 (R)*	GCAGTTCGSSTCTGCACCGTAG	59
	227	*p19 (F)*	AGTACAGCAGCGGGAGCATG	61
	259	*p19 (R)*	TCGCAGTTCGAATCTGCACC	61
Cdkn2a gene Sequencing (non-bisulphite)	306	*p16* exon 1 (F)	CGATCCTTTAGCGCTGTTTC	56
	307	*p16* exon 1 (R)	GATGGGACACTCCTTGCCTA	56
	317	*p16* exon 1 *seq*	CCTGAATCGGGGTACGACCG	n/a
	308	*p16* exon 2 (F)	GGCCGTGATCCCTCTACTTT	56
	309	*p16* exon 2 (R)	GGGTGGGTAAAATGGGAACT	56
	319	*p16* exon 2 *seq*	TATGGGTGTCCATGTTCTCA	n/a
	310	*p16* exon 3 (F)	GCCACCTAGAGAGCCTAGCA	n/a
	311	*p16* exon 3 (R)	TGAGAGTTTGGGGACAGAGG	n/a
	321	*p16* exon 3 *seq*	AAAGCATTTCTATGCTAAAA	n/a
	374	*p16* promo 1 (F)	TTGTTGGGATCTCAGCTTGG	60
	375	*p16* promo 1 (R)	GAAACAGCGCTAAAGGATCG	60
	376	*p16* promo 2 (F)	GGGCTGTCCGATCCTTTAG	63.9
	377	*p16* promo 2 (R)	GCCCTGGCCAGTCTGTCT	63.9
	378	*p16* promo 3 (F)	ATCTGGAGCAGCATGGAGTC	60
	379	*p16* promo 3 (R)	GATGGGAGAAACAAGACTTCTCA	60
Cdkn2a Bisulphite PCR /sequencing	293	*p16* exon 1α (F)	AGGAGGGATTTATTGGTTATA	61
	294 (s)	*p16* exon 1α (R)	AAATAAAAAAAACAAAACTTCTCAAAAATA	61
	364	*p16* exon 1α (F)	TAGGAGTAGAGTGTGGTTTTTTTTT	54.6
	365 (s)	*p16* exon 1α (R)	AAACACTCCTTACCTACCTAAATC	54.6
	510	*p16* promo 1 (F)	TTTAGTATTGGTAATTTTGTTTAAAG	58.6
	511 (s)	*p16* promo 1 (R)	AACAATCTACTTATAAAATATTTCTATTTT	58.6
	477	*p16* promo 2 (F)	TGGTATTTTTTAAAATGAGTTGTTTGA	51.8
	478 (s)	*p16* promo 2 (R)	CCCATACCTAATCACCCTTTAAC	51.8
	512	*p16* promo 2 (F) 2	TTTTATAGTTGTGTATAGAATTTTAGTATT	50.7
	513	*p16* promo 2 (R) 2	TATATCATCTTTTATTCAAAAAAAA	50.7
	479	*p16* promo 3 (F)	GTGTTAAAGGGTGATTAGGTATGG	55.9
	480	*p16* promo 3 (R)	CCTCCTTCCTTCCTCTAAAAATAATATA	55.9
	292 (s)	*p16* promo 3 (s)	CCACACTCTACTCCTAACCTAACTC	N/A
	519	*p16* promo 5 (F)	CCACACTCTACTCCTAACCTAACTC	61.1
	516 (s)	*p16* promo 5 (R)	TTGAATTTTGTATTTTTTTTTGTAGTT	61.1
	380	*p19* exon 1β (F)	GGTTTTTGGTTATTGTGAGGATTTA	61.1
	381 (s)	*p19* exon 1β (R)	AACCTTTCCTACCTAATCCAAAATT	61.1
	508	Cdkn2a Exon 2	GTTGGGTGTTTTTTTGTGTTT	61.1
	509 (2)	*Cdkn2a* Exon 2	TTTAAATTACTTCTTCTTTTTTCTAAATATC	61.1

recommended by manufacturers' guidelines, with the addition of 10% DMSO per reaction.

2.1.4 PCR cycling conditions

All PCR reactions were covered with a drop of mineral oil to prevent evaporation. Reactions were incubated in G-Storm™ PCR machines under the following conditions:

1. Initial denature: 95°C, 5 min

2. 35 cycles of:
   a. 95°C, 30 sec
   b. X°C, 30 sec or 1 min
   c. 72°C, 1 min per Kb product size

3. Extension: 72°C, 10 min

The annealing temperature denoted by X is dependent on the primer pair used (Table 2.1), this was determined using an initial temperature gradient.

2.1.5 Agarose gel preparation

Agarose (Roche) was melted in 1X TAE buffer (0.4M Tris base, 0.5M EDTA, pH7.7) to obtain a 1.8% [w/v] agarose gel. Gels were electrophoresed in 1X TAE at 100 V and samples were run against 5µg of 1Kb Plus DNA ladder™ (Invitrogen) to determine product size. DNA visualisation was achieved by adding 1µg/ml of ethidium bromide to the gel mix prior to pouring, which allowed DNA detection under a BioRad (transilluminator) gel documentation system. Reactions amplified in 2.1.3 were run with 5x loading dye composed of 30% [v/v] glycerol (Fisher) and 0.5% [w/v] Orange G.

2.1.6. PCR product purification

PCR reactions were purified using the QIAquick Gel Extraction kit (Qiagen) following the manufacturers' guidelines. Alternatively, when a PCR product was absent or of a low concentration, a second round of PCR amplification was performed. Briefly, the band (product) was excised from the gel using a scalpel and purified using the QIAquick Gel Extraction kit (Qiagen) as per protocol for product 'gel extraction'. The PCR was then repeated using the original primer sets using conditions stated in *2.1.4*.

2.1.7 RNA extraction from mouse whole small intestinal tissue

Approximately ~1cm of whole small intestine was removed and cut into smaller pieces and stored in RNA later (Invitrogen) at −20°C. When required, tissue samples for RNA isolation were weighed at 30mg and processed using an RNAeasy kit (Qiagen), following the manufacturers' guidelines for 'animal tissue RNA extraction' using the homogenisation technique.

Samples were processed on a 2100 Bioanalyser electrophoresis system to determine the 28s/18s composition and the RNA integrity number (RIN). RNA samples with a RIN above 7 were considered intact and suitable for further techniques. The concentration of RNA samples were analysed using 1 l of pure RNA on an Agilent Nanodrop, concentrations (ng/l) were automatically calculated based on the A260.

2.1.8 Reverse transcriptase polymerase chain reaction (RT-PCR)

For semi-quantitative and quantitative PCR amplifications RNA was converted to complementary (cDNA) using Superscript III (Invitrogen) kit. 500ng of RNA was converted using the protocol suggested by the manufacturer. Reaction volumes were made up to 20µl with milliQ dH_2O, resulting in standardisation of all RNA samples to a final concentration of 25ng. PCR analysis on cDNA for semi-quantitative gene expression was performed using ReddyMix PCR Master Mix (ABgene) using conditions stated in *2.1.4.*

2.1.9. Quantitative real-time PCR (qRT-PCR)

Two methods for quantitative real time PCR were used for analysis. The majority of genes were analysed using iQ^{TM} SYBR Green Supermix, whereas analysis of $p16^{INK4a}$ expression levels were determined using the Universal ProbeLibrary (Roche).

The iQ^{TM} SYBR Green Supermix method used RNA/cDNA made from 2.1.7/8. Total reaction volumes were 25µl and were composed of; 12.5µl of SYBR green, 0.4µl (300nm) of each primer, 11.7µl H_2O. Primers used are as stated in *Table 2.1*. Samples were run on a Roche lightcycler qPCR machine using the following protocol:

1. Denature: 95°C for 5 mins
2. Annealing: 35 cycles of: 95°C for 30 secs, 60°C for 30 secs, 1 min per Kb product size
3. Extension: 72°C for 10 mins

qRT-PCR analysis was performed using the 'Comparative' C_T method. Each sample was set up in quadruplet for both the gene of interest 'target' and the 'reference' gene, which was *Calnexin*. For each sample a C_T value was calculated, which describes the cycle number when the amplified DNA reaches an exponential threshold limit. The C_T values for each gene/sample were averaged. Then for each sample the averaged C_T 'reference' value was subtracted from the average C_T 'target' value, giving the ΔC_T value. Next, the experimental samples were normalised to the chosen 'calibrator' being the 'wildtype' in these experiments. Firstly, the wildtype was subtracted from itself to give $\Delta\Delta C_T$ and then each experimental ΔC_T value was subtracted from the wild type ΔC_T to give $2^{-\Delta\Delta C_T}$. The standard deviation was also calculated for each sample.

2.1.10 p16^INK4a qRT-PCR by the Universal ProbeLibrary (UPL)

cDNA was synthesised from RNA using the Superscript VILO™ cDNA synthesis kit (Invitrogen), using the manufacturers' instructions.

qPCRs were run using specific probes, identified using the Roche Universal Probe Library (UPL) ProbeFinder version 2.45 for mouse. Probes #7 and #106 were used for *p16^INK4a* and *Calnexin*, respectively. Primer sequences where calculated based on the probe sequences by the UPL ProbeFinder software. Reactions for both genes were set up using; 5µl Lightcycler master mix (Roche), 0.2µl probe, 2µl (8.3ng) cDNA, and 2.4µl dH_2O per sample.

Samples were set up in quadruplet in 96 well plates and processed at 60°C using the same PCR cycling conditions as in *2.1.9.* Sample analysis was also performed as stated in *2.1.9.*

2.1.11 Enzyme restriction digestion of DNA

Restriction enzymes were supplied by New England Biolabs. Enzyme restriction sites for AvaI (1x), BstUI (1x), HhaI (2x) and HpaII (4x) were identified in the 1kb promoter region of the $p16^{INK4a}$ gene. First round digestion on 25µg/ml DNA was performed using EcoRI (2 units), 1x concentration of restriction enzyme buffer, 2.5mM spermidine, reaction volumes were then made up to 300µl using Tris EDTA buffer (10mM Tris pH8 and 1mM EDTA) and incubated overnight at 37°C. EcoRI enzyme (2 units) was added to each sample and incubated at 37°C for 6hrs. Each sample was split into five eppendorfs and subjected to second enzyme digestion using AvaI, HhaI, HpaII or BstUI using appropriate buffer conditions at 37°C overnight.

Samples were precipitated using the solution containing; 0.1x [w/v] 3M sodium acetate, 2x 100% [v/v] EtOH and 0.01x [v/v] Carrier RNA (Qiagen). Samples were centrifuged at 4°C for 25 min, the supernatant was removed and pellets were washed in 2x volumes of 70% [v/v] EtOH. This was removed and pellets were left to dry prior to re-suspension in TE buffer (as before).

DNA was used in PCR reactions as stated in 2.1.2, using primers to amplify the region surrounding the 4 restriction digest sites (AvaI, BstUI, HhaI and HpaII). F-

2.1.12 Bisulphite DNA conversion and amplification

Bisulphite conversion was performed using the EZ DNA Methylation-gold kit (Zymo Research) using the manufacturers' guidelines. 500ng of DNA extracted in *2.4.4* was converted under the following conditions; 98°C for 10mins, 64°C for 2.5 hrs and then stored at 4°C. Converted DNA (2µl) was then used in Taq

polymerase PCR reactions (as stated in *2.1.3/4).* Samples were purified and re-amplified if required (as in *2.1.6).*

2.1.13 Bisulphite sequencing

Sequencing reactions were performed by the Protein, Nucleic Acid Chemistry Laboratory (PNACL) at the University of Leicester. Each reaction required; 8µl of 3-6ng/µl Bisulphite converted DNA (200-500bp length), 4µl of 1pmol/µl primer and 8µl of BigDye terminator. Primer sequences used for sequencing are denoted by an * in Table 2.1.

2.2 Chromatin histone immunoprecipitation (CHIP)

CHIP was performed at the London Research Institute at Lincoln Inn Fields under the supervision of Dr. Tomas Racek from the laboratory of Dr. Gordon Peters. CHIP was performed on wild type, cre control, 3 day, 1,2 and 6 weeks small intestine samples.

2.2.1 Preparation of tissue and crossing-linking for CHIP processing

Cells from the epithelial layer of the small intestine were removed as stated in *2.4.4.* to gain cell pellets. Cells pellets were washed in 1x PBS and re-centrifuged at 2700g and the PBS was removed. Cells were cross-linked in 1% [v/v] formaldehyde for 15 min at room temperature. The reaction was stopped by the addition of 125mM glycine to and samples were rotated for 10 min at room temperature. Cells were pelleted by centrifugation at 2000g for 5 min at 4°C and snap frozen in liquid nitrogen before being stored at –80°C.

2.2.2 Cell lysis and sonication

Cell pellets were thawed on ice and resuspended in PBS. They were centrifuged at 2000g for 5 min at 4°C. The PBS was aspirated and the pellets were resuspended in 300µl -1ml CHIP buffer (150mM NaCL, 50mM Tris-HCL (pH7.5), 5mM EDTA, 0.5% [v/v] NP-40, 1.0% [v/v] Triton X-100 and 2x Complete-EDTA tablets (Roche)). Samples were snap frozen 3x in liquid nitrogen and left to thaw on ice. Sonication was performed using a Bioruptor (Diagenode) for a total of 25 mins (30sec on/ 30 secs off). Samples were centrifuged at 12000g for 10 min at 4°C to gain protein/chromatin supernatants. Protein concentration was measured using a Bradford assay at A595. Each reaction contained; 1µl sample, 200µl Coomasie blue, 99µl 1x PBS, 700µl dH_2O and values were compared against a bovine serum albumin (BSA) standard curve.

For each sample, 10% of the total volume of chromatin was taken prior to immunoprecipitation (IP) and stored at –80°C as a control for total chromatin 'input'.

2.2.3 Immunoprecipitation and DNA isolation

Immunoprecipitations were set up using antibodies for H3K23me3 (Millipore 07-449), Ring1b (gift from Koseki), Ezh2 (polyclonal, Active motif 39901), Ezh2 (monoclonal, Active motif 39875) IgG mouse (ABcam, ab18413) and IgG rabbit (ABcam, ab246540) using 5µg of antibody per reaction. Sample chromatin concentrations were standardised by altering input volume. Total volumes were made up to 700µl with CHIP buffer (as above) and samples were incubated, rotating overnight at 4°C. 30µl per sample of either Protein A-agarose (rabbit) or protein G-agarose beads (mouse) (both Thermo Scientific (Pierce)) were washed

in 1ml CHIP buffer before Ab -bound- chromatin was transferred to the corresponding species bead slurry and incubated at 4°C, rotating for 2 hrs. Next, samples were centrifuged at 4°C for 3 min at 3000 rpm and the supernatant was removed. Bead pellets were then washed 3x in CHIP buffer and 2x in TE buffer, centrifuging at 2000g for 1 min at 4°C each time. After removal of the last TE buffer wash, 200µl of fresh elution buffer (1M [w/v] $NaHCO_3$, 10% [w/v] SDS, 1M [w/v] DTT) and dH_2O) was added to the beads and samples were vortexed for 15 min at room temperature. Samples were centrifuged at 1500g for 3 min at room temperature and the supernatants were kept. This was repeated and both supernatants (per sample) were combined and kept at room temperature.

At this stage the 10% input chromatin was thawed and combined with elution buffer (as above) and the total volume was made up to 400µl. Both the control and immunoprecipitated samples were treated with 20µl of 4M NaCl, vortexed and incubated overnight at 65°C (reverse cross-linking). DNA was further isolated by incubating chromatin samples for 2 hrs at 45°C in; 5M EDTA (pH8), 1M Tris (pH6.5), 2µl (20mg/ml) Proteinase K (Roche) and 4µl (10mg/ml) RNase A (DNase-free) (ABcam).

Chromatin IP's were added to 200µl of Phenol/Chloroform/IsoAmylAlcohol. Samples were then vortexed, centrifuged for 10 min at 10000 rpm and the water-phase (containing DNA) was removed. DNA was precipitated by the addition of 96% EtOH, 3M NaOAc and 1µl of glycogen (20mg/ml) and incubated for 30 min at –80°C. After incubation samples were centrifuged at 13200 rpm for 30 min at 4°C, washed with 70% ethanol and re-centrifuged at 13200 rpm for 15 min. All

traces of ethanol were removed and pellets were left to dry before being resuspended in 100µl H_2O.

2.2.4 CHIP analysis by qRT-PCR

PCR reactions were set up in 96 well plates and each sample was run in duplicate with the exception of sampled used for H3k27me3, which were run in quadruplet. Each reaction contained; 4µl of DNA, 12.5µl of SYBR green, 2µl each primer and 6.5µl dH_2O. All samples were amplified using 5 sets of primers stated in Table 2.2. Primers were specific for regions of the *Cdkn2a/b* locus encoding $p15^{INK4b}$, $p19^{ARF}$ and $p16^{INK4a}$. All primers worked at an annealing temperature of 60°C using 40 cycles.

Cdkn2a location	Forward primer 5'-3'	Reverse primers 5'-3'
$p15^{INK4b}$ exon 2	CTTCTTTTCCCCTCAGGTCA	TCGTGCACAGGTCTGGTAAG
$p19^{INK4b}$ exon 1β	CTCCCTTTGCTACCCCTGAGAG	TTACTTATTTCGCTCCCATCCAC
$p16^{INK4b}$ exon 1α	GATGGAGCCCGGACTACAGAAG	CTGTTTCAACGCCCAGCTCTC
$p16^{INK4b}$ exon 1α	CAAAAGTTACCCGACTGCAGATG	GAACTCTTTCGGTCGTACCCC
$p16^{INK4b}$ exon 2	TTCCCAGGAGCTGAAATTCCAG	AAAAATTCCCAACACCCACTTG

Table 2.2 CHIP primer sequences

For each time point PCRs were set up using each primer set for chromatin samples from IgG, INPUT and the antibody of interest. The Ct values for each sample were calculated (see *2.1.9*) and the duplicates were averaged. The average % of expression of the mock IgG control or mark/protein of interest (i.e. H3k27me3, Ezh2) was then calculated by first abstracting the INPUT to give a normalised value X and then using the formula 2^{-X}.

2.3 Western blot analysis

2.3.1 Preparation of protein lysates from frozen SI

On removal of the small intestine a sample of tissue was taken, washed in PBS and snap frozen in liquid nitrogen. This was then ground in a chilled mortar and pestle until a fine powder was obtained. 200-500 l of SDS lysis buffer (2% [w/v] SDS, 10% [v/v] glycerol, 50mM Tris pH6.8) was added and samples were briefly boiled.

2.3.2 Protein quantification of SI lysates

Protein concentrations were calculated against a Bovine serum albumin (BSA) standard curve of concentrations; 0, 2, 4, 8, 16 g/ l. 1 l of sample lysate was added to 1ml of Coomasie blue, these were left to stand for 10 min. Concentrations were measured at absorbance (A)595. These were compared to absorbance values of known BSA and concentrations were estimated. 5% Loading dye (bromophenol blue and β-mercaptoethanol) was then added to the remaining lysate and boiled for a further 5-10 mins and was then stored at -80ºC.

2.3.3 SDS-polyacrylamide gel electrophoresis (SDS-PAGE)

Depending on the size of the protein of interest, either 6% or 8% SDS-PAGE gels were used with a 5% stacking gel using constituents described in Table 2.3. Gels were electrophoresed in 1.5mm glass plates in 1x SDS-PAGE running buffer (25mM Tris, 192mM Glycine, 1% [w/v] SDS). 20 g of each lysate was loaded and electrophoresed on gels at 100 volts for ~2hrs. 5 l of prestained protein ladder (Fermentas PageRuler™) was used as a molecular weight marker.

Table 2.3 SDS-PAGE gel components

Gels for westerns			
	8% resolving	**6% resolving**	**5% stacking**
Components	**Volume (ml)**		
H_20	2.7	3.2	2.06
30% acrylamide	2.13	1.6	0.5
1M Tris pH8.8	3	3	0.375
10% [w/v] SDS	0.08	0.08	0.03
10% [v/v] APS	0.08	0.08	0.03
TEMED	0.0048	0.006	0.003

2.3.4 Semi-dry western transfer

Two 3mm thick pieces of card and a nitrocellulose membrane (Whatman PROTRAN) (6mm length x 8mm width) were soaked in 1x transfer buffer (48mM Tris, 39mM glycine, 1.3% [w/v] SDS, 20% methanol, 70ml dH_20). These were then placed in a -blot Trans SD semi-dry transfer cell (BioRad), with the nitrocellulose in between the two pieces of card. The SDS-PAGE gel was then sandwiched between the nitrocellulose membrane and the upper piece of card. The plate was set to transfer at 10 volts for 1hr.

2.3.5 Antibody treatment

After transfer the nitrocellulose membranes were stained with ponceau to check protein transfer, this was removed with brief washes of dH_20 and TBST (10mM Tris, 0.1% [v/v] Tween-20, 150mM NaCl). Non-specific proteins were blocked in 5% [w/v] milk TBST (as before) for 1hr at room temperature. The blot was cut in half and incubated in primary antibody diluted in 5% [w/v] milk (Table 2.4) rocking

at 4°C overnight. Blots were then washed 3x 5 min in TBST before being incubated in the appropriate secondary antibody; either rabbit or mouse (Sigma), diluted in 5% [w/v] milk at 1:3500, rocking for 1hr at room temperature. Subsequently, the membranes were washed again in 3x washes of TBST and then protein-antibody complexes were visualised first by soaking the blot in Supersignal West Pico Chemiluminescent Substrate kit (Pierce) added at a 1:1 ratio for 1 min at room temperature. The blot was wrapped in Saranwrap, placed into a cassette and developed on a photographic film (Fuji) in a dark room at room temperature.

Table 2.4 Details of primary and secondary antibodies used for western blot analysis

1° Ab	2° Antibody species	Dilution/Dilutant	Manufacturer
Dnmt3b	Mouse	1:166 / 5% milk PBS	Imgenex (IMG184A)
Ezh2	Mouse	1:25 / 5% milk TBST	BD Transduction labs (612666)
ERK2	Mouse	1:1000/ 5% milk PBS	Santa cruz (sc-154)

2.4. Mouse breeding and Cre recombinase induction

2.4.1 Breeding and genotyping

Mice heterozygously expressing either the *Braf*$^{LSL-V600E}$ or Ah*Cre*ER^{T} alleles were crossed to gain litter mates expressing both alleles. Mice were genotyped using DNA from an ear snip. Tissue was digested in 0.05M NaOH for 15 min at 95°C, followed by neutralisation through the addition of 1M Tris pH7.5. DNA was stored at 4°C.

2.4.2 Activation of Cre recombinase by Tamoxifen and β-napthoflavone

Recombination of the *Braf*$^{LSL-V600E}$ allele was achieved by Cre recombinase whose activity was dually regulated by β-napthoflavone and Tamoxifen. Briefly, β-napthoflavone (Sigma) was dissolved in pre-heated corn oil at 80mg/ml by incubating at 100°C with continuous vortexing. Tamoxifen (Sigma) was prepared in sunflower oil at 100mg/ml and incubated at 65°C for 1hr. Prior to use both prepared drugs were stored at –20°C. Injections of both drugs were given in the abdomen of mice between 7-12 weeks old, who had been genotyped as being either double heterozygotes or singly heterozygous for Ah*Cre*ER^T. β-napthoflavone was boiled and kept hot in a flask prior to injection. Tamoxifen was briefly warmed prior to use. A 200µl (8mg/ml) i.p. injection of β-napthoflavone was initially given. Twenty four hours later a second 200µl i.p of β-napthoflavone was given and a 200µl (10mg/ml) i.p of Tamoxifen. Mice genotyped for wild type BRAF (*BRAF*^{WT}) were given the same doses of pure oil without drug. After 3 days, 1, 2, 6 and 10 weeks post-i.p the small intestines were harvested for investigation.

2.4.3 Genotyping for ^{V600E}BRAF

Post-harvesting, genotyping was performed directly on small intestine tissue (as stated in 2.4.1) to reveal recombination of the *Braf*$^{LSL-V600E}$ allele. Two separate initial PCRs were performed on DNA extracted from an ear tissue to reveal mice with the *Braf*$^{LSL-V600E}$ allele (Primers 125&137) and/or Cre recombinase allele (Primers 360&361). Mice heterozygous for both were alleles were subjected to drug induced recombination (as stated in 2.4.2). Small intestines were harvested at designated time points and DNA was extracted from the duodenum. A third

PCR was performed to determine positive recombination and *Braf*^{V600E} expression (Primers 125&143).   Small intestines from the following three genotypes were analysed in this study; *BRAF*^{WT} (*Wild type*), AhCreER$^{T+/0}$ / *Braf*^{WT} (*Cre* control) and AhCreER$^{T+/0}$ /*Braf*$^{LSL-V600E/+}$ (*Braf*^{V600E} experimental).

2.4.4 Separation of the mouse SI epithelial layer and DNA isolation

The small intestine was removed from the top of the duodenum to the caecum and cut into three equal pieces. It was then inverted over 3x 2mm wooden rods and shaken in an incubator twice in two changes of 10mM EDTA in Hanks Balanced Salt Solution (HBSS) (Gibco) at 37°C for 15 min each time. Solutions from both incubations were centrifuged at 2700g for 15 min at 4°C to gain cell pellets. Cell pellets were then processed using the Wizard SV Genomic DNA Purification System (Promega) using the manufacturer's instructions. Additionally, 20mg/ml Proteinase K (Roche) and 4mg/ml Ribonuclease A protein (active) (Abcam) were also used per sample digestion. DNA was purified in 100µl nuclease-free water (Promega) and stored at 4°C. DNA concentrations were quantified using a spectrometer A260 value in dilutions of 1:50 or 1:25.

2.5 Histology

2.5.1 Harvesting of tissue and fixation

The whole small intestine from the stomach to the caecum was removed and washed in 1x PBS (137mM NaCl, 2.7mM KCl, 1.5mM KH$_2$PO$_4$, 8.1mM Na$_2$HPO$_4$). Each small intestine was 'swiss rolled' with the duodenum (stomach end) in the middle and transferred to 10x volume of 4% [w/v] paraformaldehyde (PFA) and

left submerged overnight on a rotator at room temperature. The tissue was then placed in 70% [v/v] EtOH and stored at 4°C.

2.5.2 Wax embedding and sectioning of small intestine tissue

Swiss rolled small intestines were placed in numbered cassettes and impregnated in paraffin wax (by Susan Giblett of University of Leicester). These were left to solidify at room temperature. Prior to use, blocks were cooled to 4°C and then sectioned using a microtome (Leica RM2135). Sections were transferred onto subbed slides and placed to dry in racks in a 37°C oven overnight.

2.5.3 Subbing of glass slides for tissue mounting

Glass slides (Raymond Lamb) were soaked in 5% [v/v] Decon overnight at room temperature. Slides were then washed in hot running water for 30 min followed by 5x, 5 min washes in milliQ H_2O, before being dried in a 60°C oven overnight. Dried slides were then put through 2 min washes of; 2% [v/v] 3-aminopropyltriethoxysilane in acetone (8mls in 400ml), 2x pure acetone washes, followed by 2x washes milliQ H_2O. Slides were then dried overnight in a 60°C oven.

2.5.4 Immunohistochemical analysis

Dewaxing and rehydration of sections were performed prior to each immunohistochemical procedure. Slides were incubated twice in xylene for 10 min each followed by 2x 100% EtOH for 10 min each. Slides were then placed in 2% [v/v] hydrogen peroxide in methanol for 15 min to block endogenous

peroxidases. Antigen retrieval was performed by boiling slides for 20 min in 10mM tri-sodium citrate buffer (10mM sodium citrate in dH_20 - pH6 with acetic acid), in a pre-headed pressure cooker. Slides (in buffer) were left to cool for 15 min and washed in distilled water then in 1x PBS. Tissue sections were circled with a hydrophobic PAP pen (ABcam) prior to incubation in either 10% goat or 4% swine serum diluted in 1x PBS for 1hr. Samples were then incubated in specific primary antibody, diluted as stated in Table 2.5 in the appropriate serum (Table 2.5) depending on the species of primary antibody, overnight at 4°C. Slides were then washed in 3x 10 min washes in 1x PBS before being incubated in secondary antibody (Dakocytomation (DAKO)) diluted 1:500 in serum/PBS solution as before, for 2 hrs at room temperature. Slides were washed in 3 changes of 1x PBS for 5 mins. Sections were then incubated in tertiary antibody Streptavidin-HRP (DAKO) for 30 min and then washed 3x in 1x PBS for 5 min each. Next samples were incubated in DAB Peroxide substrate kit (Vector laboratories) in dH_2O as per manufacturers guidelines, for up to 10 mins until colour developed and washed briefly in dH_2O. Samples were then rehydrated in 70% EtOH for 5 mins, 90% EtOH for 5 mins, 2x 100% EtOH for 10 mins each. Following by 2 changes of xylene for 10 mins each. Slides were then mounted with coverslips and DPX mounting medium (low viscosity) (Raymond lamb).

Haematoxylin and eosin staining was performed on serial sections using a Shandon Varistain by Jenny Edwards of the MRC unit Leicester.

1° Ab	Species	Dilution	2° Ab species	Serum	Manufacturer
Dec1	Rabbit	1:100	Swine α-rabbit	Swine	Sigma (S8443)
Dnmt3b	Mouse	1:100	Goat α-mouse	Goat (PBST)	Imgenex (IMG184A)
Ezh2	Mouse	1:25	Goat α-mouse	Goat	BD Transduction labs (612666)
Jmjd3	Rabbit	1:100	Swine α-rabbit	Swine	Abcam (ab3811)
ppERK	Rabbit	1:100	Swine α-rabbit	Swine	Cell signalling (9101)
Phospho Histone H3	Rabbit	1:100	Swine α-rabbit	Swine	Cell signalling (9701)
5-methylcytosine	Mouse	1:200	Goat α-mouse	Goat	AbDSerotec (AHP1826Z)

Table. 2.7 Details of primary and secondary antibodies used in immunohistochemistry

2.5.5 Morphometric crypt and villi analysis

Crypt and villi cell number analysis was performed using H&E stained serial sections. For each sample the numbers of columnar cells were counted in 50 crypts and villi under light microscopy. Only crypts that were both attached to the inner muscle layer and had paneth cells correctly situated at the base of the crypt were counted, as these were thought to be in the correct plane of section. For each sample the number of goblet, paneth and mitotic cells were counted (Figure 2.1).

Figure 2.1 Representation of crypt and villus structures. Diagram showing the small intestine crypt and villi structures and a haematoxylin and eosin (H&E) stained section of a crypt. For analysis the cell labelled within each structure were counted.
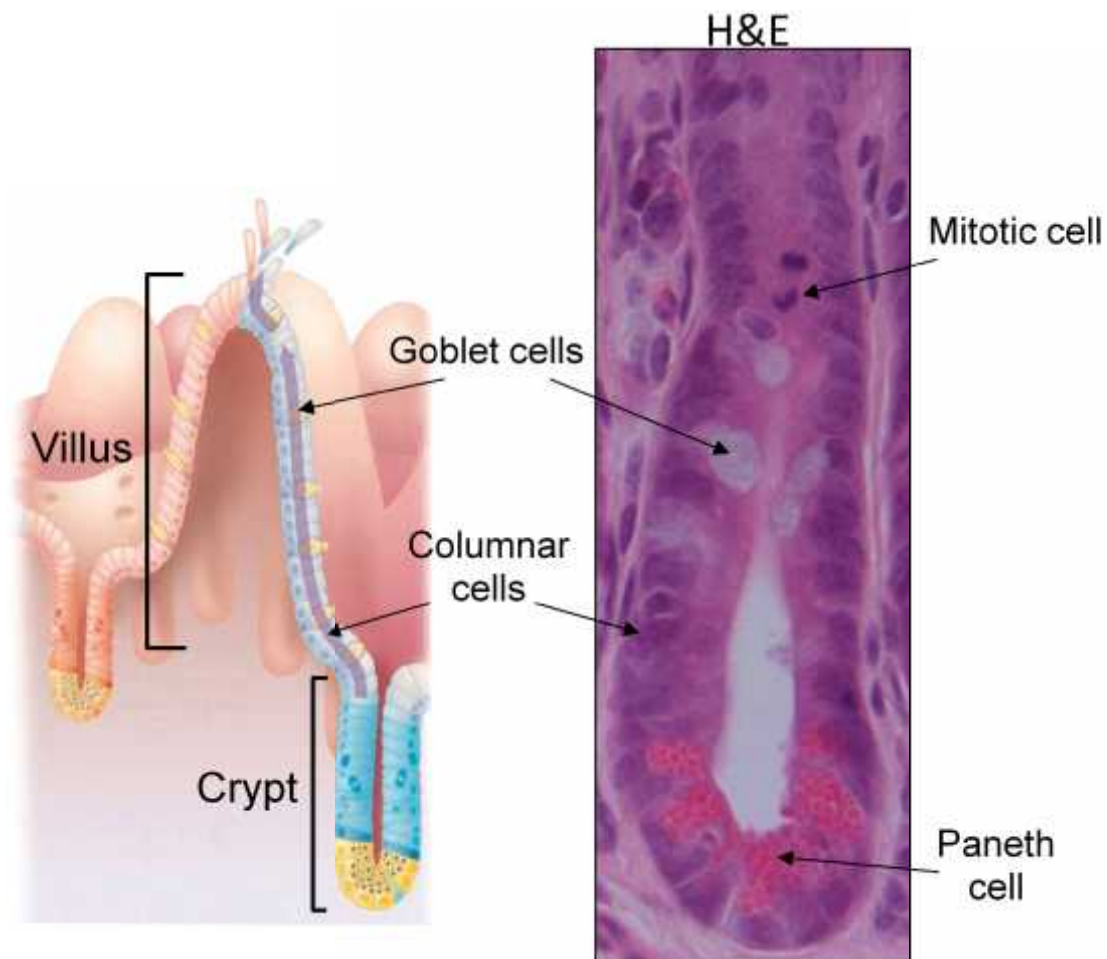
3. Characterising the phenotypic effects of Braf^{V600E} in the jejunum

3.1 Introduction

3.1.1 Cre-mediated Braf^{V600E} expression in the crypt epithelium

To investingate the role of *BRAF*^{V600E} in serrated CRC, a mouse model that spatially and conditionally expressed *Braf*^{V600E} was developed under the control of Cre recombinase activity (Mercer et al., 2005). The *Cre* strain 'Ah*Cre*ER^{T}' was used to induce *Cre* expression in the mouse SI because the Cre *recombinase* is targeted to the cells of the crypt epithelium. This is because it is under the control of the Cyp1a1 (Ah) promoter, which is expressed across the whole gastrointestinal epithelium (Kemp et al*.,* 2004)*.* Cre recombinase expression results in activation of recombination and expression of *Braf*^{V600E} in the transit amplifying and stem cells of the crypts. Expression of *Cre* is mediated by Tamoxifen (TM) and β-napthoflavone (βNF) which allows the controlled, sporadic expression of *Braf*^{V600E}.

3.1.2 Preliminary data from the Braf^{V600E} expressing ileum

Preliminary investigations had been carried out on the *Braf*^{V600E} mouse SI, prior to this study. Data was specifically collected from the ileum of the *Braf*^{V600E} mouse SI (Carragher et al., 2010). It was found that *Braf*^{V600E} expression in the epithelium of the ileum induced crypt hyperplasia after 3 days post induction (p.i.). This was associated with Mek-dependent activation of Erk and increased proliferation but no changes in apoptosis. In addition to this, cross talk was identified between the Braf^{V600E} activated MAPK cascade and with the key

survival signalling 'Wnt' pathway, through increased localisation of β-catenin in crypt cell nuclei. As with Erk, this was also found to be Mek-dependent.

Initially, the ileum was originally chosen to investigate because it was the closest region to the colon, where human lesions develop. For unknown reasons, in mouse models, genetic manipulation of genes involved in human colorectal cancers e.g. APC, leads to development of tumours in the SI rather than the LI (Samson et al., 2004).

In this study analysis was performed on the mouse SI. The SI has three distinct regions; the duodenum, which is closest to the stomach followed by the jejunum and then the ileum that is adjacent to the colon (Figure 3.2A). Previous studies using the Ah*Cre*ER^T strain have shown that Cre-mediated recombination is highest nearest to stomach rather than the colon, the reason for this is not known but it is thought dietary digestion could play a role (Kemp et al., 2004). In addition to this, the expression of the Cre recombinase is mosaic throughout the whole intestinal epithelium. Therefore, *Braf*^{V600E} was indirectly expected to be expressed in a mosaic pattern. The mosaicism obtained makes phenotypic changes more difficult to determine. For this reason it was felt to be important to analyse another area of the gut and so the middle section of the gut the jejunum was analysed here.

3.2 Aims

To investigate the morphological/molecular changes in the epithelium of the jejunum section of the small intestine in response to induced *Braf*^V600E expression, over the time course of 3 days to 10 wks p.i.

3.3 Results

3.3.1 PCR analysis to determine mouse genotype

As described in the Introduction, breedings were set up using mice heterozygous for *Braf*^+/LSL-V600E and mice heterozygous for Ah*Cre*ER^T/0 in order to obtain double heterozygous mice. Litters were genotyped by PCR using primers for the *Cre* gene, which produced a single band at 300bp (data not shown). Litters were also genotyped for the presence of the *Braf*^LSL-V600E allele using primer 125 (A) that anneals to exon 14 of *Braf*^WT and primer 137 (C) that anneals to exon 15 of the Lox-Stop-Lox (LSL) cassette on the mini-gene (Figure 3.1A). DNA heterozygous for the *Braf*^LSL-V600E produced a smaller band (150bp) as well as the WT band (450bp) (Figure 3.1B). Mice that carried both Ah*Cre*ER^T and *Braf*^LSL-V600E alleles were subjected to drug induction to induce Cre-mediated recombination of the LSL-cassette and allow *Braf*^V600E.expression. Post-induction, DNA was made directly from the SI and a PCR for Cre recombination was performed using primers 125 (A) and 147 (B). Primer 147 (B) anneals to exon 15 containing the T1799A nucleotide substitution. Positive recombination produced a band at 518bp corresponding to the Lox-V600E allele and the *Braf*^WT 450bp band (Figure 3.1C). Recombination and subsequently *Braf*^V600E expression, was shown to occur throughout the whole length of the small intestine and slightly higher levels were detected in the

Figure 3.1 Genotyping PCR for determining Cre-mediated recombination of the *Braf*^{LSL-V600E} allele. (A) Primers were designed to exploit the presence or absence of the Lox-Stop-Lox cassette (black arrows represent Lox-P sequences) and the expression of exon 15 with the T<A nucleotide transversion. Primers A+B confirm the presence of either *Braf*^{WT} or *Braf*^{OX V600E} alleles. Primers A+C confirm the presence of the *Braf*^{SL V600E} allele. Alternative band sizes are produced depending on the genotype. (B) PCR genotyping to identify the presence of a *Braf*^{SL V600E} allele in mice heterozygous for this allele, at 150bp. Genotyping from *Braf*^{/+} and *Braf*^{/+LSL V600E} mice are shown. (C) Shown is a PCR using DNA isolated from a mouse that expressed both allele; *Braf*^{SL V600E} and AhCreER^T were treated with β-napthoflavone (βNF) and Tamoxifen (TM) for 6wks. Positive Cre recombination is shown by the presence of a 518bp band above the *Braf*^{WT} band, indicating the *Braf*^{OX V600E} allele. M = 1Kb marker.
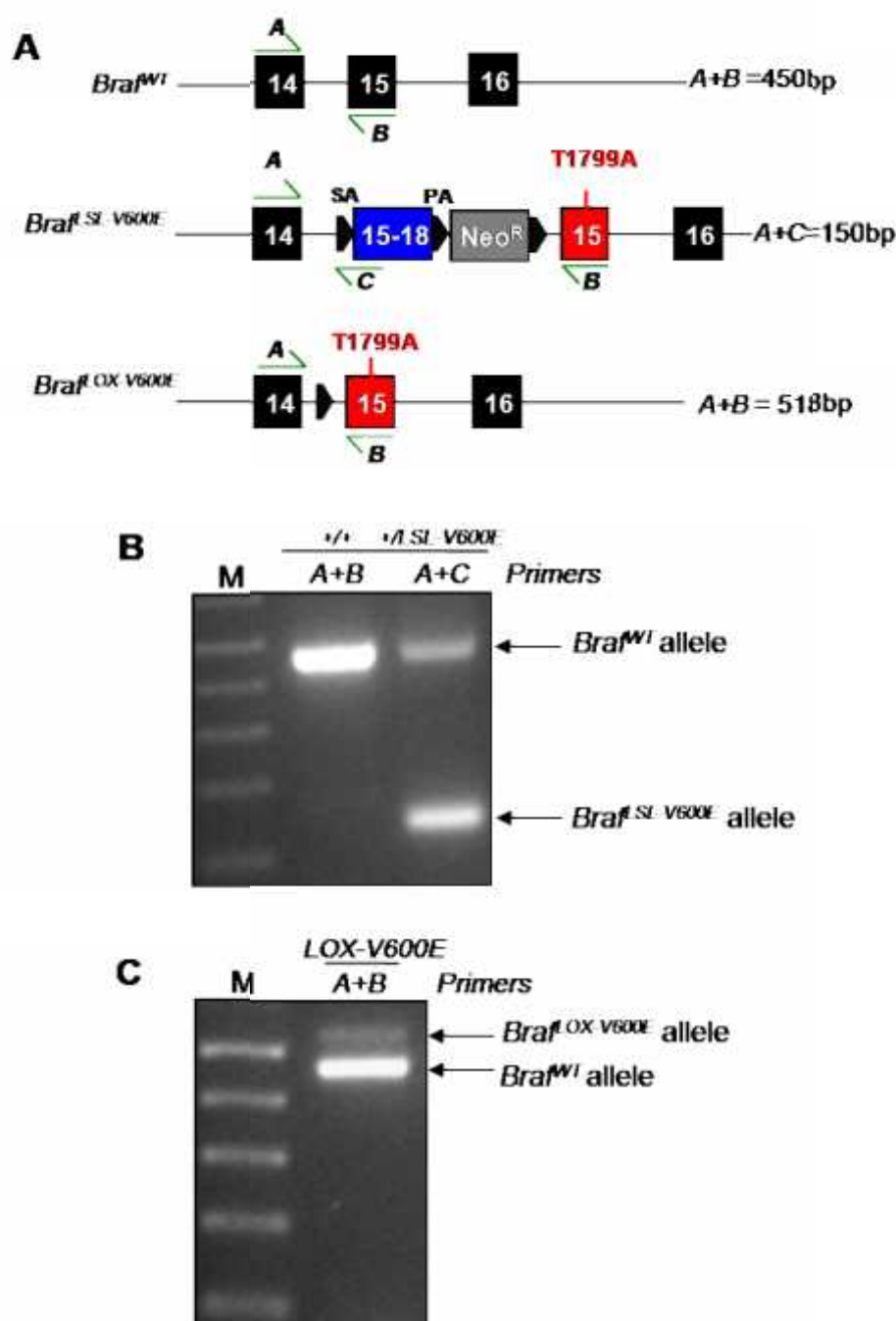
duodenum (Figure 3.2B). All *Braf*^{V600E} expressing mice, over the time course analysed in this study were confirmed as having recombined SI using the above PCR assay.

3.3.2 Morphometric analysis of the Braf^{V600E}-expressing jejunum crypts

In other cell systems, activation of the MEK/ERK pathway by BRAF^{V600E} is known to induce cell proliferation. To investigate this in the gut, crypt cell number was investigated post-*Braf*^{V600E} induction over the time course of 3 days to 10 wks p.i. Two controls were analysed alongside the *Braf*^{V600E}-expressing time course; wildtype (WT) and Cre recombinase that had been induced with βNF and TM (Cre) between 3 days-10 wks. For both control and experimental time points, 3 alternative mice were analysed. For each mouse, the number of cells in 50 crypts was counted, which was equal to a total of 150 crypts for each control/time point. Only one sample for each of the 1 and 2 day Braf^{V600E} samples were available and therefore only 50 crypts were counted in these cases.

Crypts are presented in a 2-dimensional (2-D) format on H&E sections and because of this not all visible crypts are in the correct plane and, if counted, could distort the total value for crypt cell number. Therefore only crypts were counted if they were full crypts, directly in contact with the sub mucosa and had visible Paneth cells (Figure 3.3).

Figure 3.2 Braf^{V600E} is expressed throughout the whole of the mouse SI following AhCreER^T-mediated recombination. (A) Representation of the mouse SI. Dissected SI was cut from the start of the caecum to the end of the duodenum and then segmented into 6 sections, 1-6 as indicated. (B) A Cre recombination PCR on DNA isolated from each section of SI from a 6wk VE-expressing mouse using primers A and B. Each section showed positive recombination to generate the *Braf*$^{flOX\ V600E}$ allele throughout the full length of the SI.
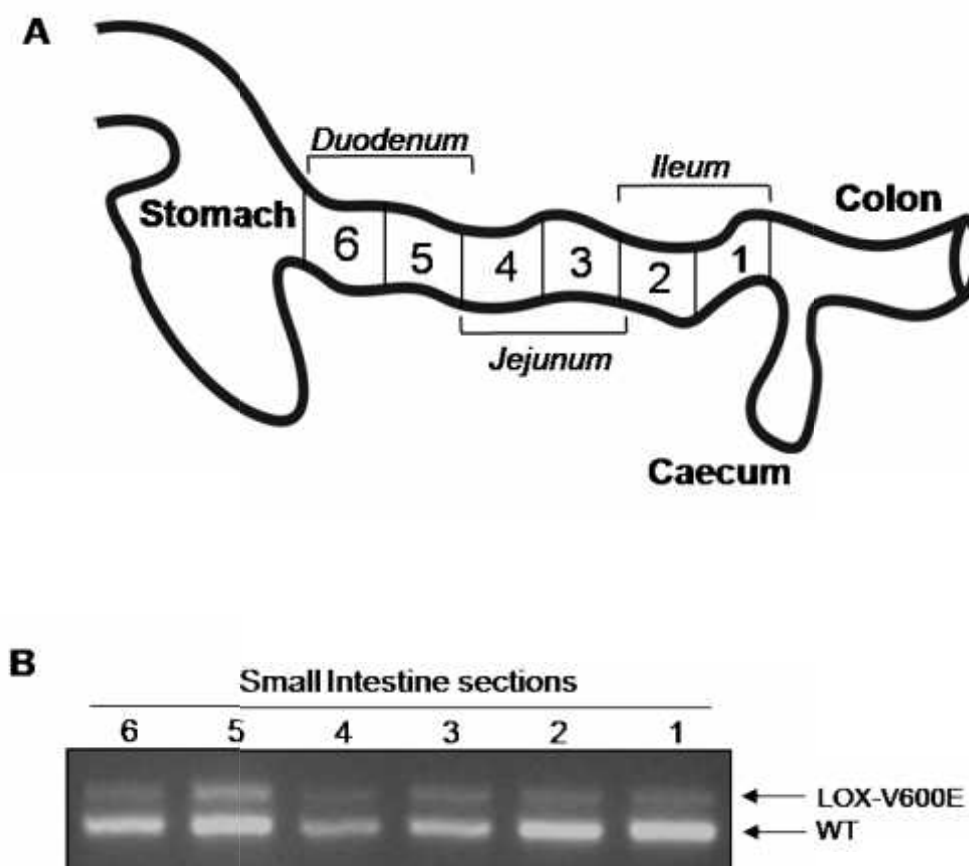
Figure 3.3   Method of morphometric analysis for counting the number of crypt columnar cells. For each crypt the number of columnar cells was counted from the base upwards to the top where the cells expand into the villi. Crypts were only included in the analysis on the basis that they were in the correct plane; this means they were full crypts that were directly attached to the sub mucosa and had visible Paneth cells (as indicated).

H&E

Visible Paneth cells

Attached to the submucosa
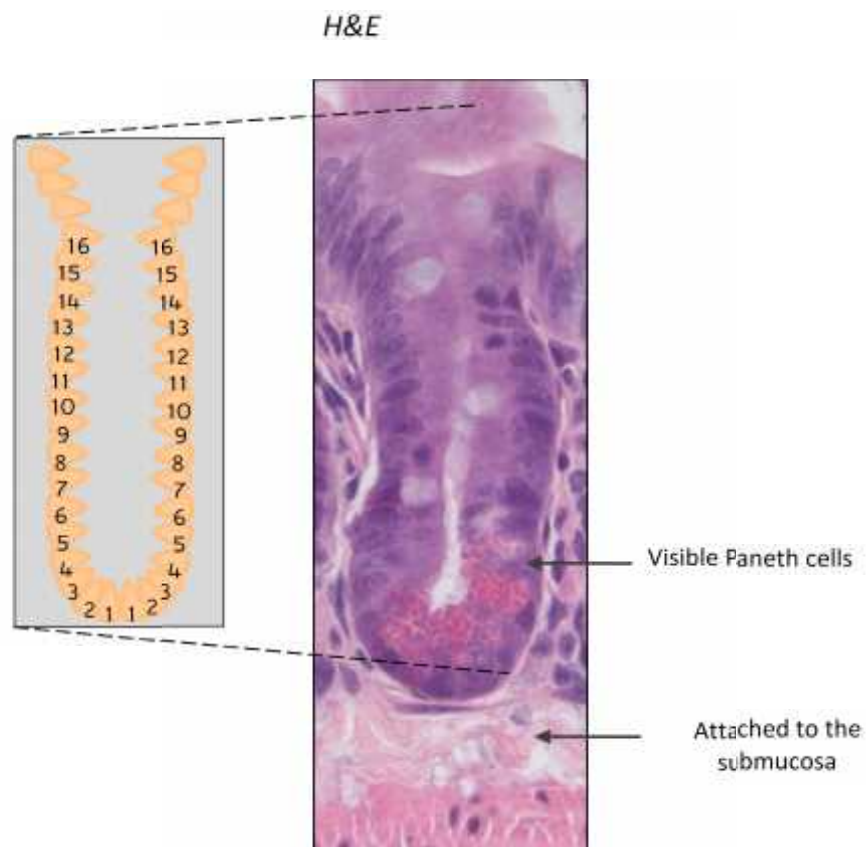
3.3.3 Crypt and villi cell numbers increase at 3 days post Braf^{V600E}-induction

In a 2-D crypt, the mean number of cells in the WT and Cre controls was found to be 37 and 44 respectively. Interestingly, the Cre value is significantly higher than the WT samples ($P<0.001$). This suggests Cre has a possible effect on inducing proliferation of the crypt cells. For this reason all statistical differences where compared to the Cre data. At 1 and 2 days post-induction the mean number of cells/crypt in the VE samples remained fairly stable at 41 and 45, respectively (Figure 3.4), which were similar to the controls. However, at 3 days post-induction the mean number of cells in the crypts of the VE samples increased to 49 (Figure 3.5). A typical crypt has a circumference of 16 cells and so this equates to an increase of up to 190 cells per 3-D crypt structure. In relation to this, the crypts were visibly longer in the 3 day VE samples compared to the controls (Figure 3.5B). These results indicate that the recombination and expression of Braf^{V600E} followed by activation of its downstream effectors and subsequent pathways, is manifested within 3 days in the crypt cells but not within 2 days. The increase in cell number may not be as significant as expected because it is relative to the level of Cre recombination. Not every crypt expresses Braf^{V600E} and so the effect of Braf^{V600E} is masked and it is the greater number of outliers, which have a high number of cells that represent the Braf^{V600E} expressing crypts.

The number of cells in the villi of the jejunum was also counted from 130 intact villi of 3 mice for each control/time point. At 3 days post-VE induction the number of cells per villus did not increase when compared to the controls (Figure 3.6A). However, at 1 wk post VE-induction there was a statistically

Figure 3.4 Crypt cell numbers are not elevated in the jejunum at 1 & 2 days post-[V600E]***Braf* induction.** Frequency graph counts of the number of cells per crypt for WT (n=150) Cre (n=150) and a 1 day VE (n=50) (A) and 2 day VE (n=50) (B). Mean values for each genotype are shown. Only one of each sample (n=1) was analysed and therefore statistical differences could not be compared to the controls.
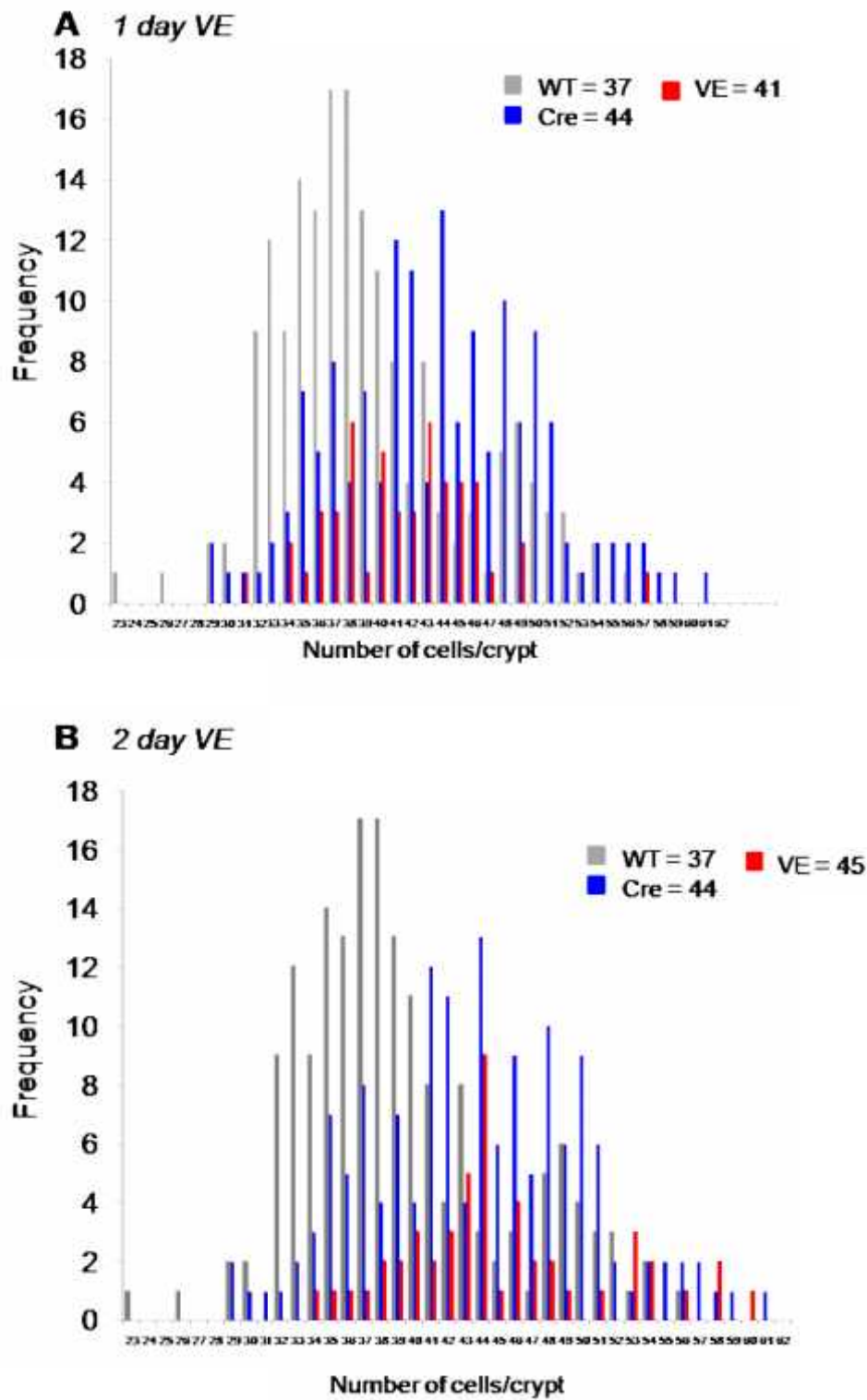
Figure 3.5 *Braf*[V600E] induces hyperplasia in the jejunum at 3 days post induction. (A) Frequency bar graph for the number of cells per 150 crypts in WT, Cre and 3day VE sample. The 3day VE has more cells per crypt on average than both control samples. Mean values for each genotype are shown and P values were calculated using an unpaired t-test. A statistical difference was observed between the Cre and 3day VE (P<0.005) (B) H&E stained sections of mouse jejunum from WT and 3 day VE samples. The length of crypts are increased compared to the WT, shown by the arrows. H&E scale bar = 100µm
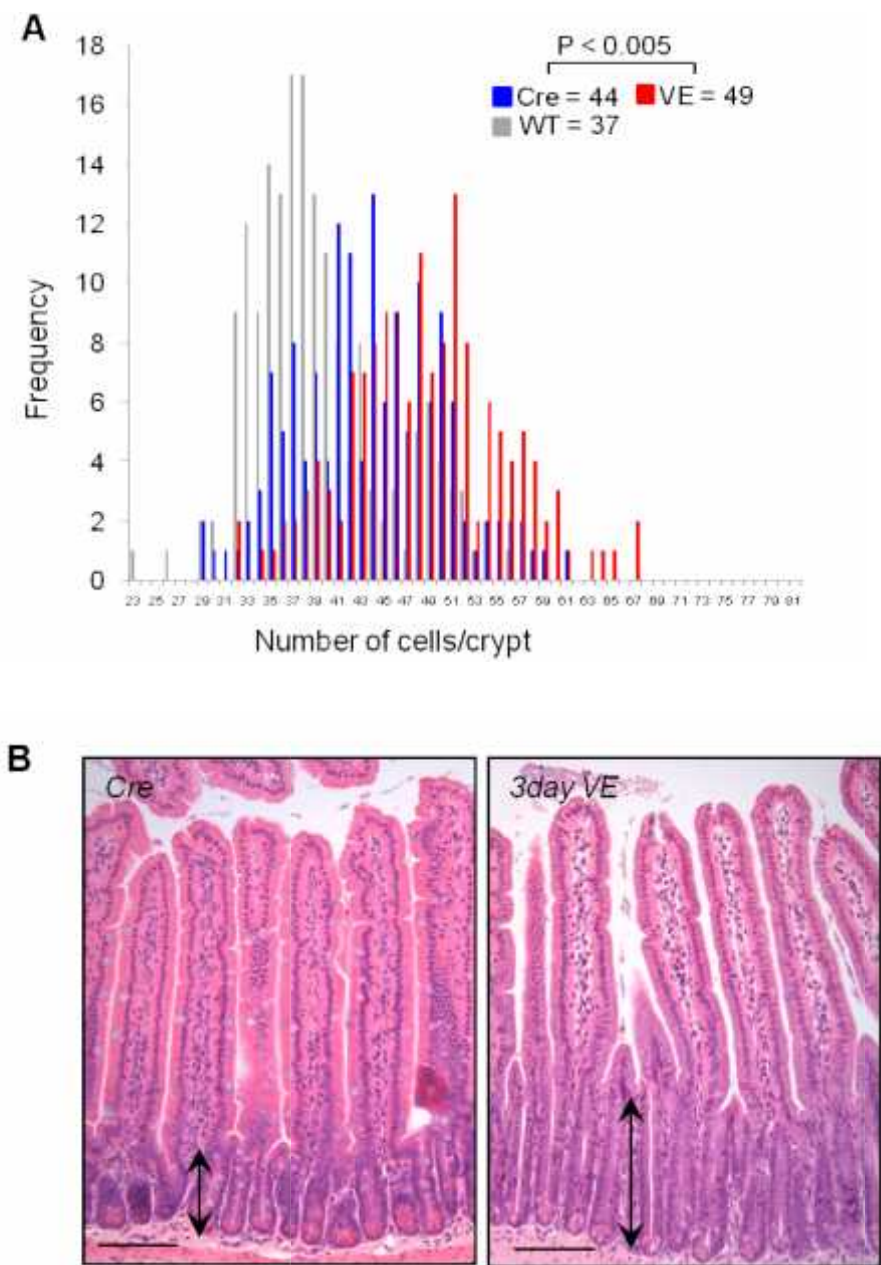
Figure 3.6 *Braf*[V600E] expression increases the number of cells in the villi of the jejunum at 1wk post-induction. (A) Frequency bar graph for the number of cells in 130 villi in WT, Cre and 3day VE samples. The mean values for each genotype are shown and the P value was calculated using an unpaired t-test. The number of cells remained stable in the 3 day genotype compared to the controls. (B) Frequency bar graph for the number of cells in 130 villi in WT, Cre and a 1wk VE sample. At 1wk post –induction the average number of cells per villi increased to a statistically higher number of 153 compared to the Cre control of 139. The 1wk VE genotype also had a large number of outliers, the highest being 236 cells compared to 190 in the Cre control.
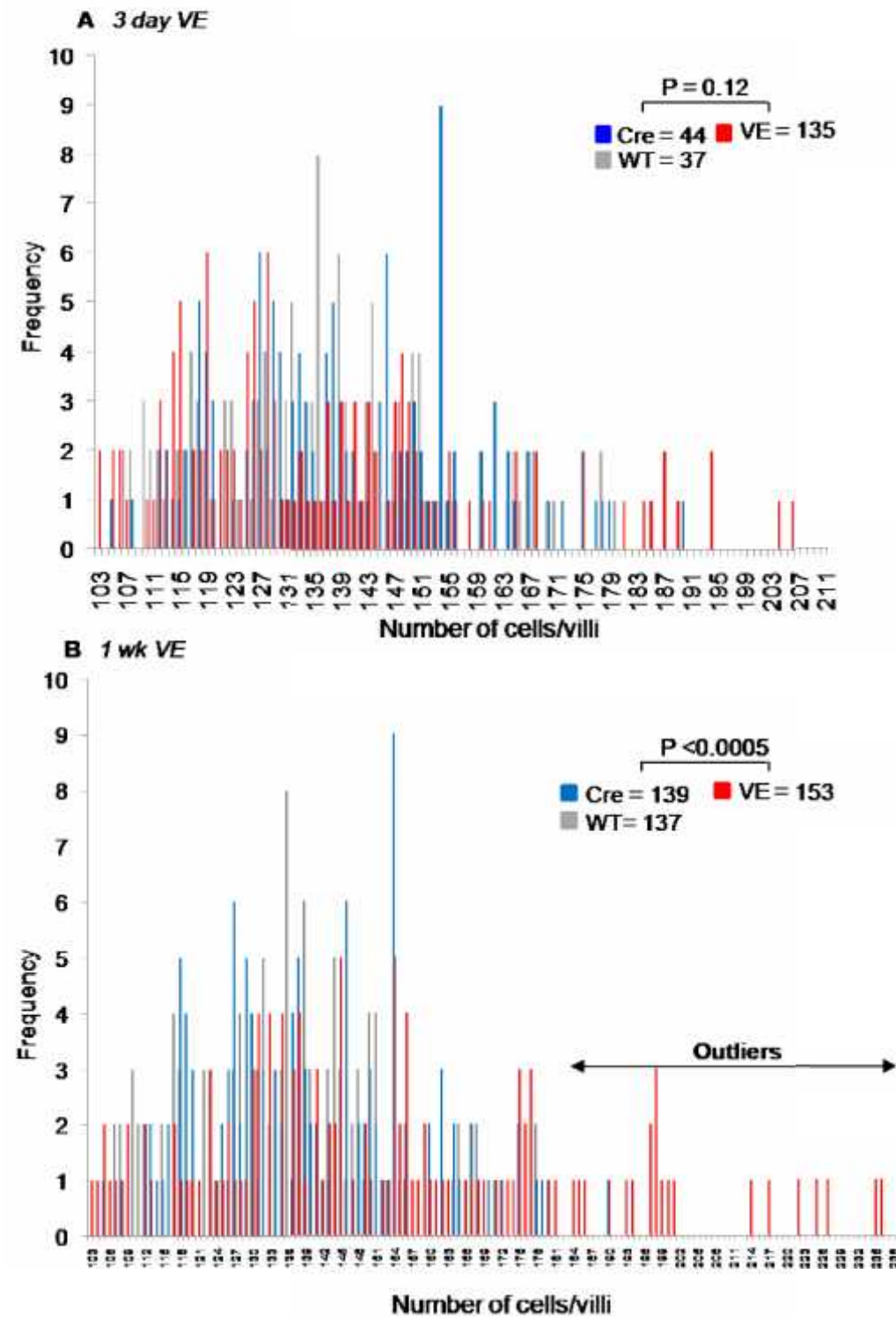
significant increase in the average number of cells from 139 (Cre) to 152 (1 wk VE) (P<0.0005) (Figure 3.6B). Also evident was the large number of outliers in the VE samples with the highest being 236 cells per villus in the 1 wk VE, compared to 180 for the Cre control.

3.3.4 *Braf*^V600E^ -expressing villi show a serrated appearance

Visible histological changes were evident between the controls and experimental samples. As previously shown in Figure (3.2), excessive proliferation in the 3 day VE samples resulted in visibly longer crypts compared to the controls. In addition to this, villi developed a 'serrated' epithelium and appeared wider and almost 'ballooned' in shape (Figure 3.7). This occurred from as early as 1 wk p.i. and was still evident at 10 wk p.i.

3.3.5 Elevated mitosis is associated with increased cell number

The level of mitosis was investigated using immunohistochemistry for the mark of phosphorylation of serine 10 of histone H3 (P-H3). Phosphorylation of this residue occurs during late G2 phase/mitosis and so anti-P-H3 antibodies can be used to identify cells in mitosis and therefore indicate proliferating cells. Immunohistochemistry for P-H3 was performed on jejunum sections from both control genotypes and 3 day and 1 wk VE treated samples (Figure 3.8A). The average number of positively stained (brown) P-H3 cells per 75 crypts was counted from 3 mice for each genotype/sample (Figure 3.8B). The difference between the average number of P-H3 positive cells in the Cre control and VE samples were not statistically significantly different (3 day; P<0.41 and 1 wk,

Figure 3.7 The Braf^V600E^ jejunum epithelium appears serrated. H & E stained sections of the jejunum from WT, Cre and a 10wk VE sample. The 10wk VE has obvious serrated villi compared to the controls, which appear neat and unified. Scale bars WT=200µm, Cre=100µm and 10wks=100µm.
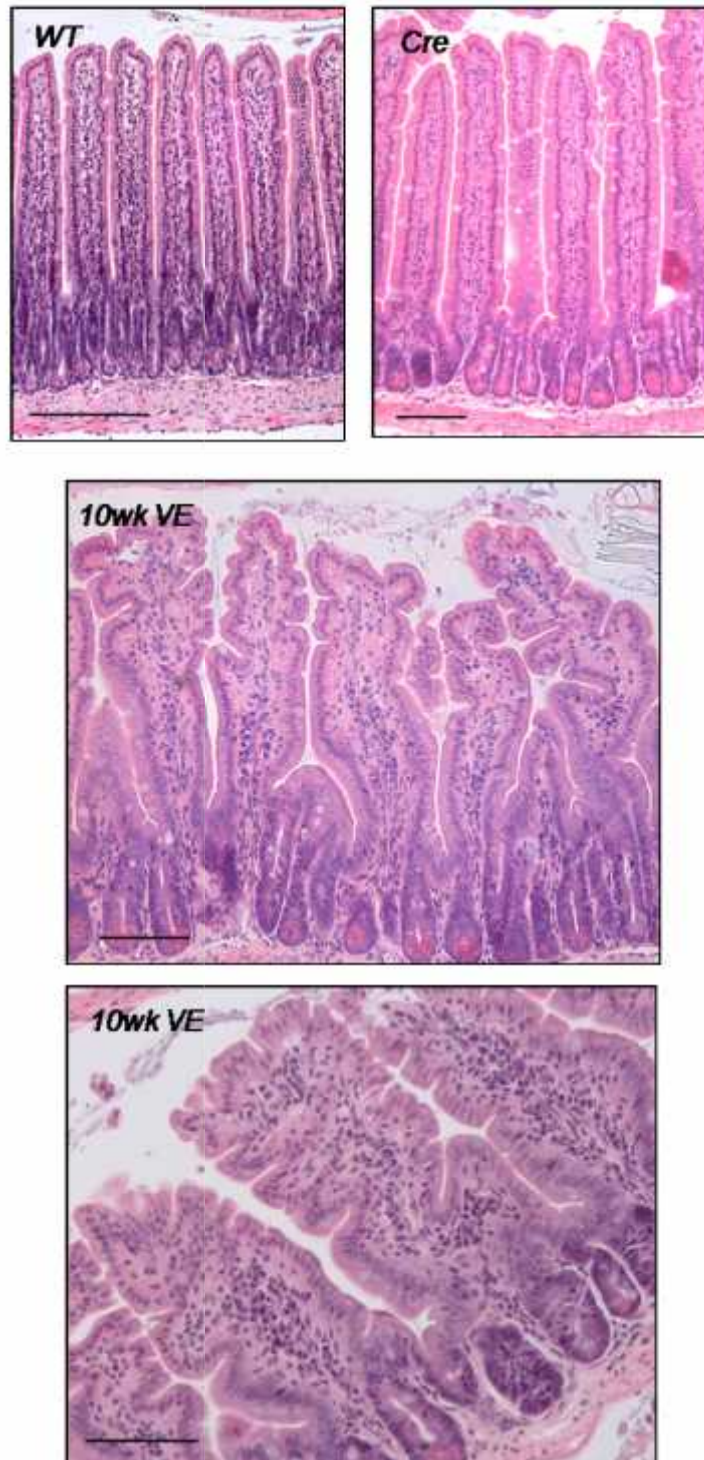
Figure 3.8 Early crypt hyperplasia is associated with increased mitosis. (A) Phospho-Histone H3 IHC on WT, Cre, 3day and 1wk VE SI jejunum sections. The brown stained cells represent those in mitosis. There was an increased number of positively stained cells in mitosis in the 3day and 1wk VE samples compared to both controls. An expanded view of a typical crypt is shown on the right of the main IHC sections. Sections were counterstained with haematoxylin. Scale bars = 250µm. **(B)** Graph to show the average number of mitotic cells in both controls, 3day and 1wk VE samples. Using Phospho-H3 stained sections under light microscopy, the number of positively stained cells were counted for 3 samples (25 crypts each) for each time point and averaged. Bars indicate mean and error bars indicate standard deviation. Although there is a trend to more mitotic cells in both the VE samples compared to the controls, the values were not statistically significant; 3day (P=0.32-0.41) and 1wk (P=0.26-0.33).
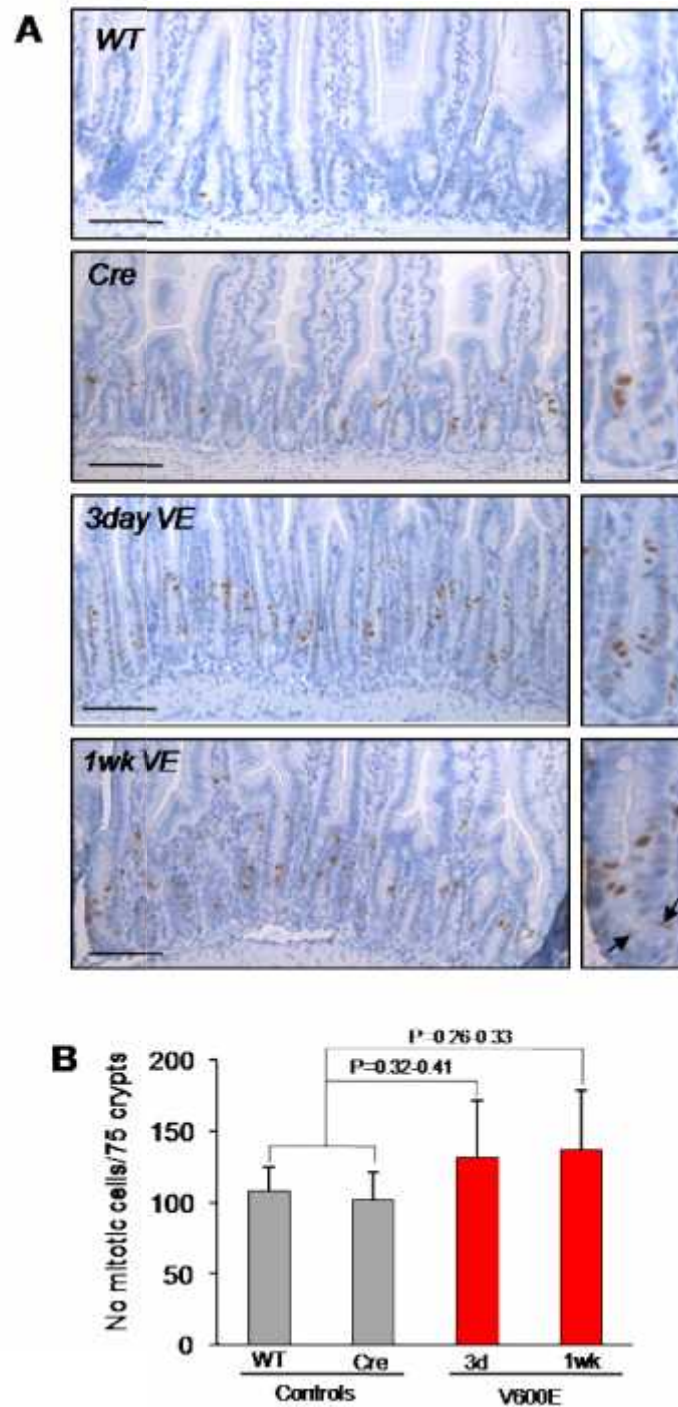
P<0.33), although there was a trend towards more positive cells in both the VE samples.

3.3.6 Increased crypt cell number is associated with elevated Erk signalling

The phosphorylation of the downstream Braf effector Erk was also investigated, which was expected to increase as a result of excessive signalling through the MAPK pathway. Sections from a WT and 1 wk VE jejunum SI were stained with an anti-ppErk using immunohistochemistry (Figure 3.9). A greater number of cells stained positively (brown) for ppErk in the crypts of the 1 wk VE section compared to the WT samples.

3.3.7 Crypt hyperplasia is not sustained in the *Braf*^{V600E} expressing crypts

The number of cells in the crypts of 1, 2, 6 and 10 weeks *Braf*^{V600E}-expressing jejunum was also investigated (as stated in 3.3.2). The number of cells remained elevated but did not increase further at 1 and 2 weeks post-induction with 47 cells counted per 2-D crypt on average for both 1 and 2 week samples (Figure 3.10). This equates to on average up to ~160 more cells per crypt than the Cre control, which is a statistically significant increase (P<0.005). However, at 6 weeks post-*Braf*^{V600E} expression the number of cells in the crypts was reduced to the same numbers as the Cre samples (44 per 2-D crypt) (Figure 3.11). Interestingly, in the 10 wk VE samples the number of cells increased slightly to 45, which equates to ~16 more cells per crypt on average (P=0.05). It is possible proliferation is regained at 10 wks p.i. as discussed in later chapters.

Figure 3.9 Elevated MAPK signalling in the crypt cells following Braf^{V600E} expression. ppErk IHC of the SI jejunum sections from a WT and 1wk VE sample. ppErk levels are high in the 1wk VE with particularly strong staining in the crypt cell nuclei. Both IHC sections were counterstained with haematoxylin. Scale bars = 50μm.
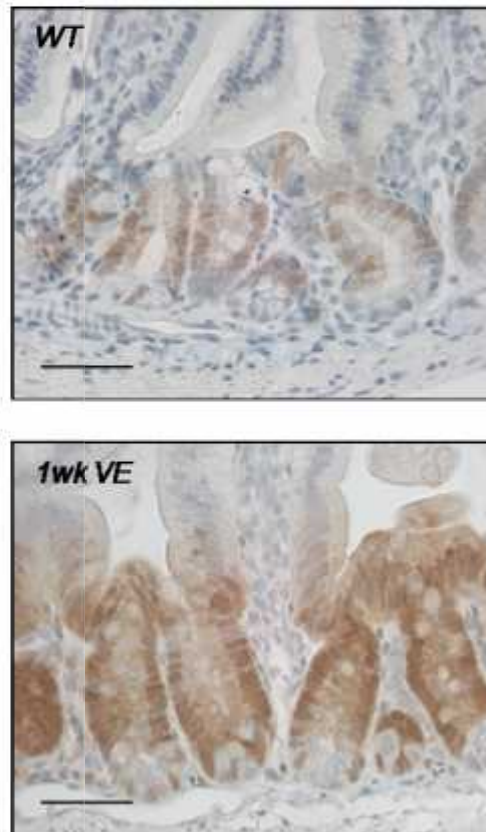
Figure 3.10 Crypt cell hyperplasia remains stable at 1wk and 2wks-post $Braf^{V600E}$ **induction.** Frequency graph counts of the number of cells per 150 crypts for WT, Cre, 1wk VE (A) and 2wk VE (B) samples. The mean values for each genotype are shown and the P values were calculated using an unpaired t test. These show positive significant differences between the Cre and VE samples ($P=0.005$).
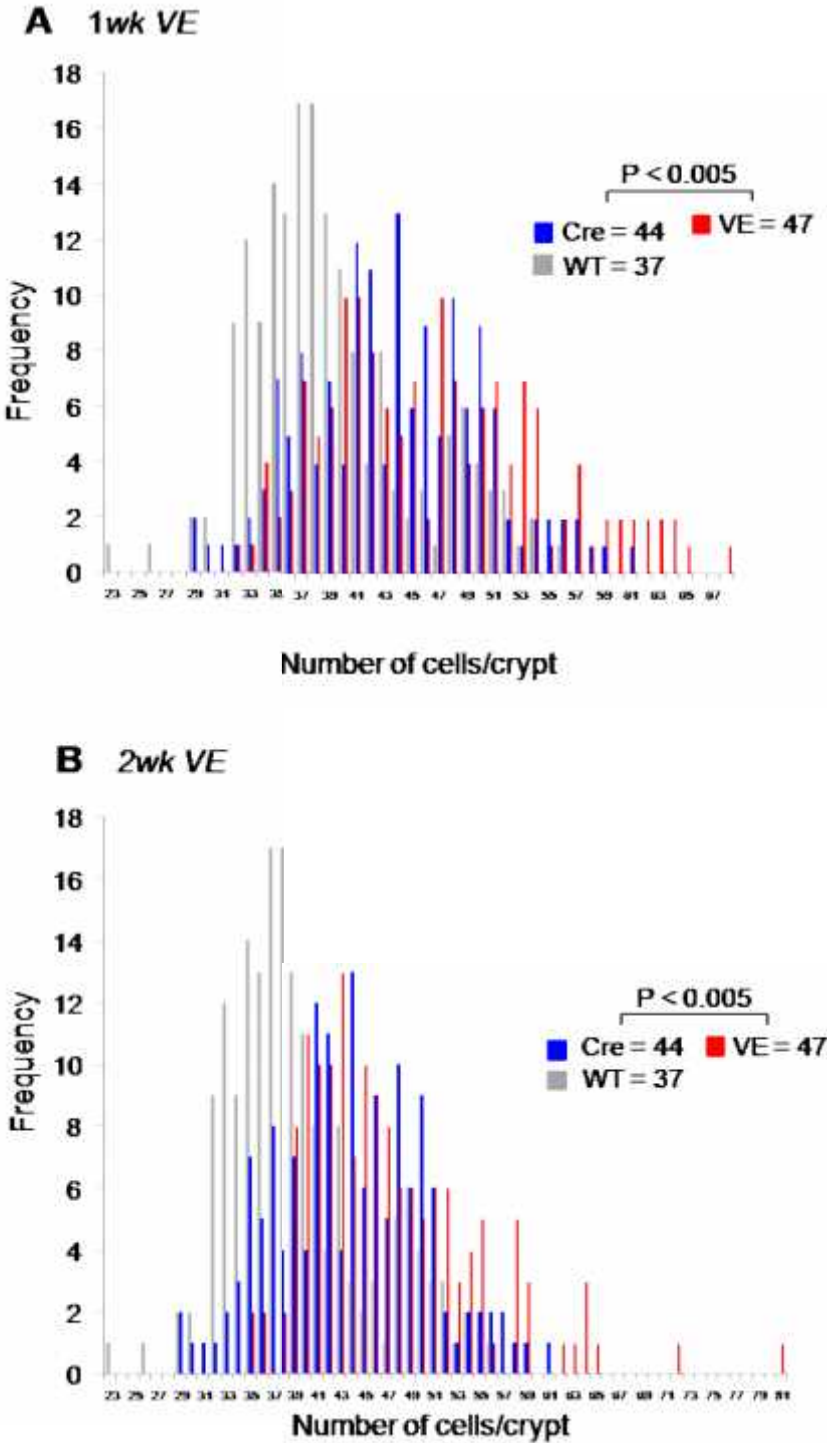
Figure 3.11 Crypt cell number homeostasis is regained at 6 and 10 weeks post- ***Braf*^V600E** **induction.** Frequency graph for the number of cells per 150 crypts of WT, Cre, 6wk VE (A) and 10 wk VE (B) samples. Mean values for each genotype are shown and P values were calculated using an unpaired t test. There was no statistical difference between the Cre control and the 6wkVE sample (P=1) but, at 10wks, a significant difference was calculated (P<0.05).
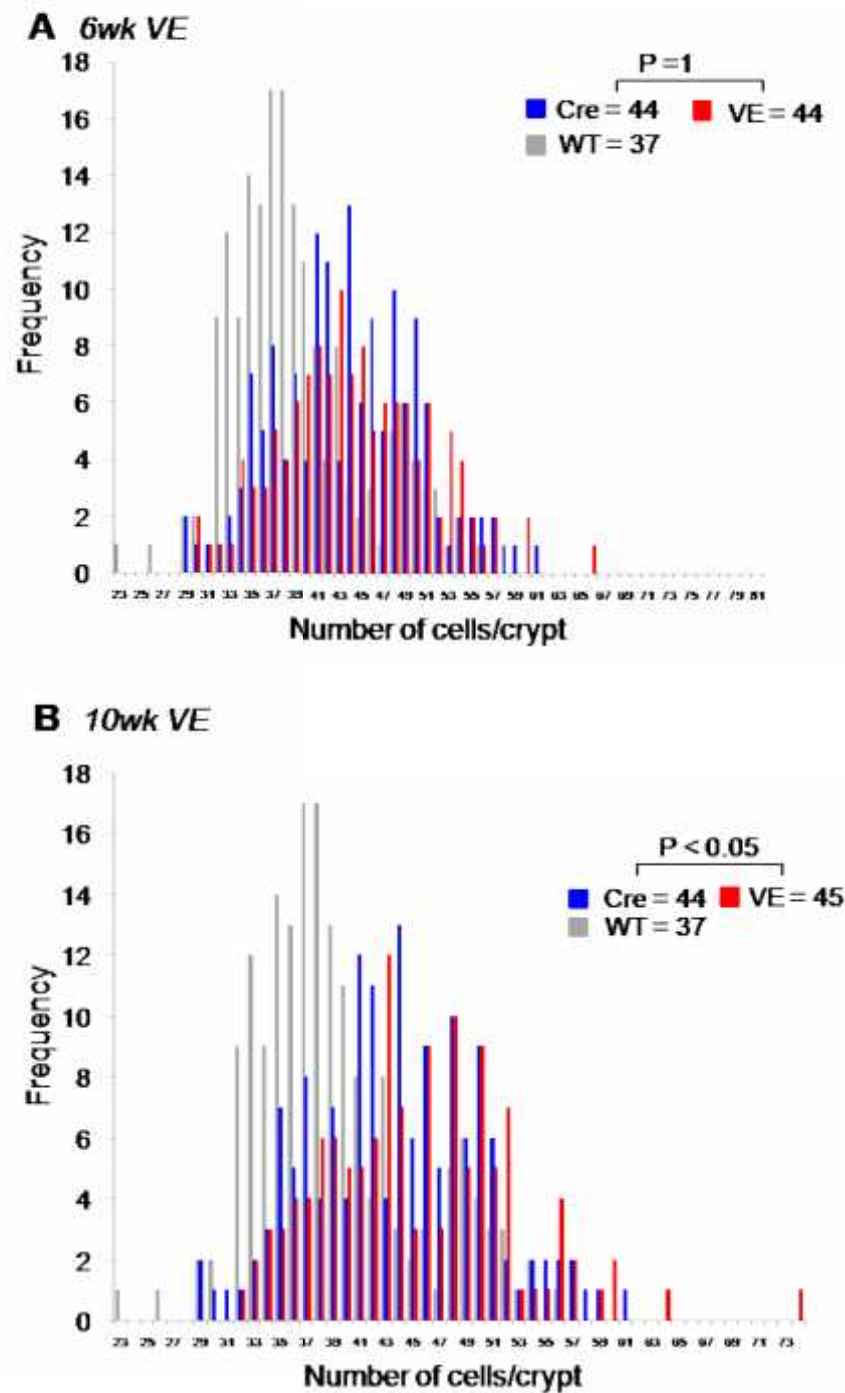
3.3.8 Erk phosphorylation is lost after 6 wks post-Braf^{V600E} induction

The levels of phospho-Erk were determined at 6 and 10 wks post-VE expression to identify whether reduced MAPK signalling coincided with the fact that crypt cell numbers did not increase further at these time points. Sections of the *Braf*^{V600E}-expressing jejunum at 6 and 10 wks p.i. were stained for phospho-Erk using IHC (Figure 3.12). Phospho-Erk staining was extremely low in both time points compared to the 1 wk VE samples. This suggests signalling upstream of Erk from Braf^{V600E}/Mek is not sustained at these time points.

3.3.9 Apoptosis levels remain stable post-Braf^{V600E} expression

Expression of hyperactivated Raf proteins has been shown to induce apoptosis in mouse haematopoietic cells (Hoyle et al., 2000 and Chang et al., 2001). Apart from increased proliferation, changes in apoptosis could also affect crypt cell number. Apoptotic cells were distinguished by a number of histological characteristics such as rounded shape, reduced size, high eosinophilic proportion to nucleus, nuclear condensation and loss of cell to cell attachments. A typical small intestine crypt with two labelled apoptotic cells is shown in Figure 3.13. The number of apoptotic cells was determined for each control and experimental time point by light microscopy using H&E sections. The average number of apoptotic cells were counted from 3 alternative mice for each sample (n=3), which were converted to a percentage number per crypt (Figure 3.13B). The number of apoptotic cells was not found to be significantly altered from 1wk to 11 wks+ post VE-expression in comparison to the controls. However, at 3 days post-VE expression the number of apoptotic cells was significantly higher than the WT (P=0.02) but 'not quite' significantly higher than the Cre control

Figure 3.12 Loss of MAPK activation. ppErk IHC was performed on WT, 1wk, 6wk and 10wk VE samples and sections were counterstained with haematoxylin. The levels of ppErk in the crypts of the SI are reduced from 6wks post-*Braf*^V600E^ induction compared to the 1wk VE sample. Scale bar = 50µm.
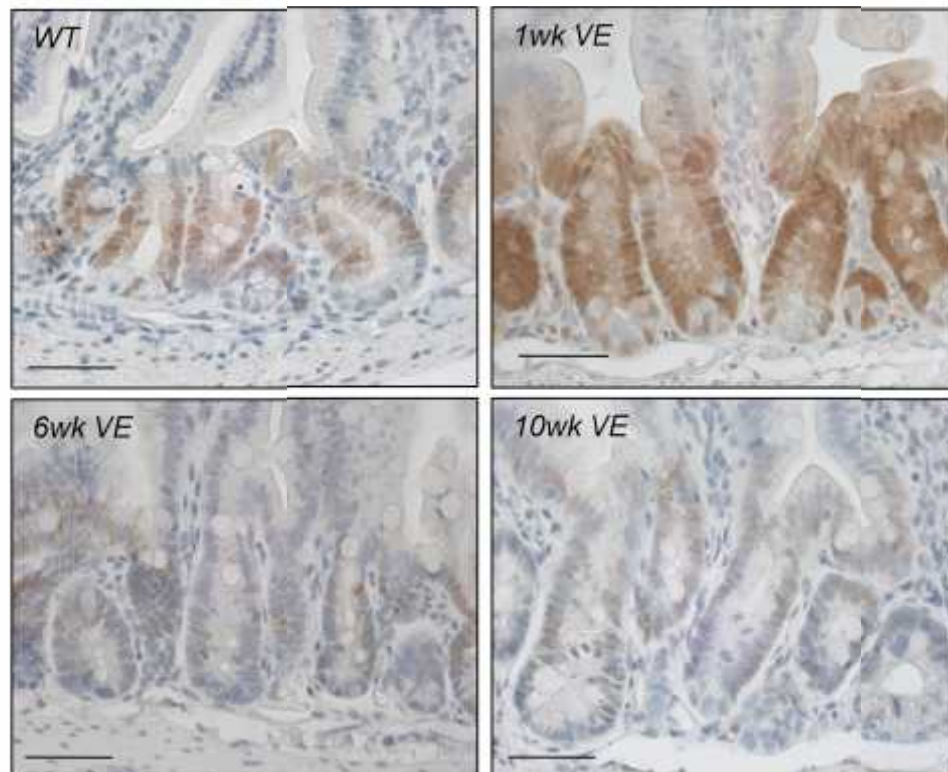
Figure 3.13 Quantification of apoptosis levels following *Braf*^{V600E} expression. (A) H&E stained section of a mouse SI crypt with two visible apoptotic cells indicated by the arrows. (B) Bar graph representing the % of apoptotic cells for WT, Cre and the *Braf*^{V600E}-expressing samples over a time course from 3 days-11wk+ post induction. Using H&E stained sections the number of apoptotic cells was counted under light microscopy, using 3 samples for each time point (n=3). The percentage of apoptotic cells was calculated per total number of cells for each sample and then the values were averaged. The 10+wks bar represents the combination of 11, 12, and 15 wk samples. Error bars represent standard deviation. There were no statistically significant differences between the controls and 1wk-11wk+ experimental samples. The 3day VE had a significantly higher number of apoptotic cells than the WT samples (P=0.02) but the levels were 'not quite' statistically higher than Cre samples (P=0.06).
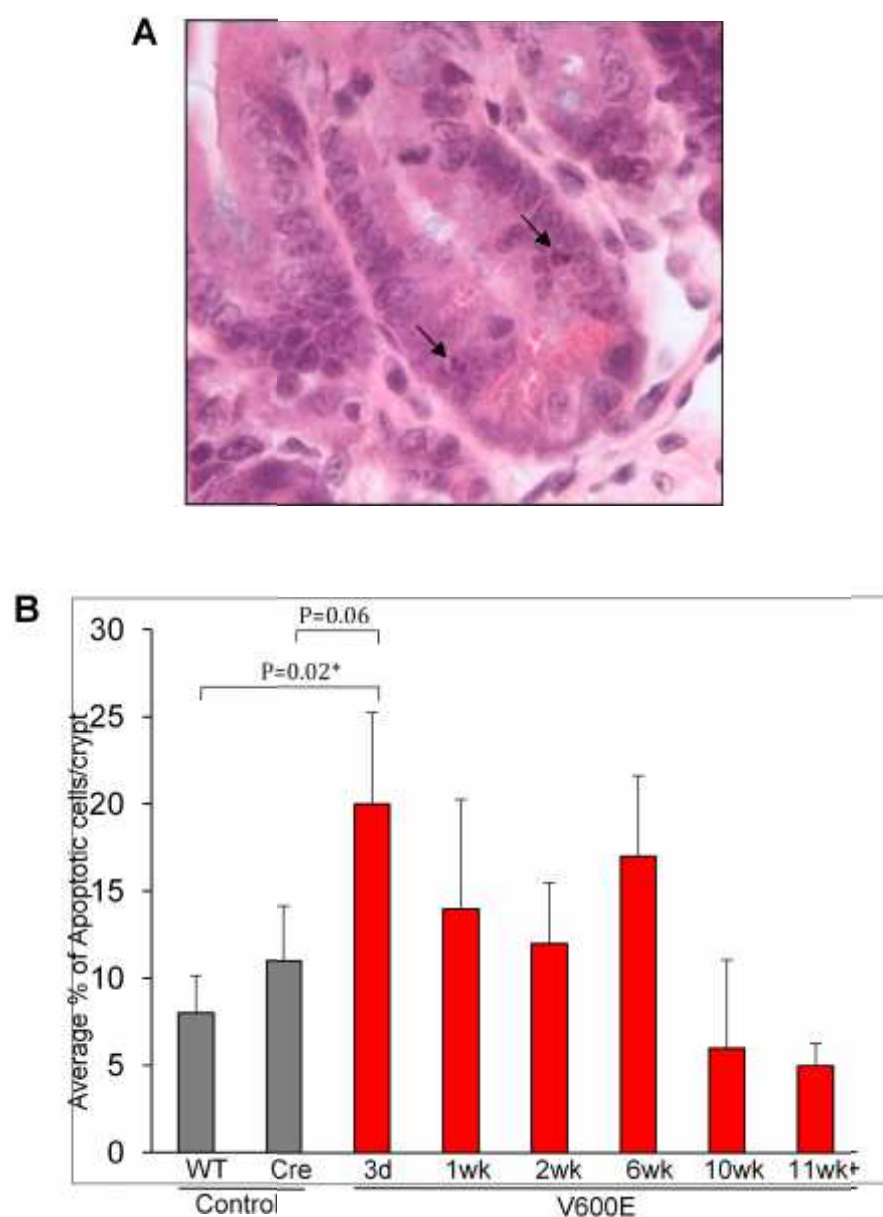
(P=0.06). Therefore, any observed effect may be related to Cre expression rather than Braf^V600E.

3.4 Discussion

In this mouse model, Cre-mediated *Braf*^V600E expression occurred throughout the whole length of the small intestine (stomach to caecum). Throughout the intestinal epithelium complete recombination was not observed with this Ah*Cre*ER^T transgenic line but instead a mosaic level of Cre recombination was observed (Fig 3.2). Using the Cre reporter strain *ROSA26,* the level of Ah*Cre*ER^T recombination in the small intestine of mice expressing *Braf*^V600E was identified as being up to 70% (Carragher et al., 2010). The Ah*Cre*ER^T transgene is expressed in a gradient from the duodenum to the ileum and is expressed at low levels in the colon (Kemp et al., 2004). This is important when interpreting changes in the intestinal epithelium because the crypts are mosaic in their expression of *Braf*^V600E, therefore experimental tissue has a combination of wildtype and mutant cells. As such the effect of Braf^V600E is partially masked and this maybe a contributing factor as to why large differences in crypt/villi cell number and mitosis between control and experimental samples were not observed. Positive Cre recombination was seen across the whole *Braf*^V600E-expressing time course from 3 days to 10 wks and beyond. In addition, recombination was seen throughout the SI and slightly higher levels were seen in the duodenum as expected as this is the nearest section to the stomach.

This chapter has provided evidence to support previous data obtained from the ileum. *Braf*^V600E has the ability to induce hyperproliferation of crypt epithelial

cells, which occurs after 3 days post-expression. The Cre recombinase control also had an increased number of cells compared to the pure wildtype suggesting it might create some damage in the intestine, which can affect crypt cell number. Crypt cell number in the VE samples did not increase at 1 and 2 days p.i. compared to the controls, suggesting ~2-3 days is the time frame needed for Cre-mediated Braf^V600E^ expression and cellular activity to take place. In addition to increased cell number at 3 days post *Braf*^V600E^-expression, the length of the crypts also increased, which is expected. The level of proliferation was sustained for up to 2 wks and was associated with phosphorylation /activation of the key downstream effector Erk. The level of mitosis in the crypts was also increased at 3 days and 1 wk post-induction. As a consequence the number of cells in the villi was also elevated at 1 wk post-induction due to the increase in crypt cell number at 3 days p.i. This corresponded with serrations seen in the villi as early as in the 1 wk post-VE expression and the epithelium remained serrated up to 10 wks p.i. Serrations in the villi of the ileum was also observed (Carragher et al., 2010). In human serrated CRC the serrated appearance is thought to be associated with increased cell number and an inhibition of apoptosis (Tateyama et al., 2002), although the data presented in this Chapter indicates elevated cell proliferation is the key factor rather than down-regulated apoptosis

It was observed that the initial burst of proliferation was not sustained because after 1 to 2 weeks of *Braf*^V600E^-expression the average number of crypt cells remained stable and was not further increased. In addition, after 6 wks p.i. crypt cell numbers returned to baseline levels. This was also associated with the

73

absence of phosphorylation and activation of Erk at late time points. These results suggest crypt homeostasis is re-adjusted in the presence of the *Braf*^{V600E} oncogene activity. One explanation for this is that the excessive MAPK signalling from *Braf*^{V600E} to Erk is inhibited after the initial proliferative stage. Previous studies have shown there are two types of negative regulators of the MAPK cascade that are rapidly activated in response to oncogenic MAPK signalling (Zhang et al, 2010). These are Sproutys that inactivate Raf proteins and the dual specificity phosphatases (DUSPs), which dephosphorylate Erk in both the cytoplasm and nucleus. High levels of DUSPs 4 & 6 have been identified in cells with mutant KRAS and constitutively activated Erk (Bild et al., 2005). The activation of a negative feedback loop would explain the loss of phospho-Erk at the later time points in response to up-regulated DUSPs and Sproutys. Interestingly the 10 wk VE samples showed a slightly elevated level of crypt cell number compared to the Cre control indicating that pro-proliferative signals may be re-activated.

The Cre recombined *Braf*^{LOX-V600E} bands were present in all samples over the time course, including the 2 wks and 6 wks time points. This suggests crypt stem cells are recombined and express Braf^{V600E} because cells are replenished in the mouse crypts every 3-5 days. Ah*Cre*ER^T has previously been shown to recombine in Transit Amplifying (TA) cells and data presented here would suggest recombination has occurred both in TA and stem cells, which would result in a continued supply of crypt TA cells expressing Braf^{V600E}.

The MAPK pathway has been linked to both the suppression and activation of

apoptosis and so changes in apoptosis in response to VE were investigated here. However, the level of apoptosis in the VE-crypts was stable over the time course, in comparison to the controls. Therefore, changes in apoptosis cannot account for the increase in cell number, this is most likely due to the increased proliferation observed.

In conclusion, expression of Braf^{V600E} in the jejunum results in early crypt hyperplasia and is associated with elevated MAPK signalling. However, this is not sustained and post ~2wks expression the excessive signalling through *Braf*^{V600E} is lost. These results mimic the previous results obtained from investigating *Braf*^{V600E} in the mouse ileum (Carragher et al., 2010). In the previous study the effects of inhibiting the Erk cascade using the MEK inhibitor PD184352 were investigated and showed that crypt hyperplasia in the ileum could be reversed. This showed a direct role for the Erk cascade in the phenotype. Due to time constraints, the effect of PD184352 on the jejunum was not investigated.

4. Investigation of *Braf*^V600E^-induced senescence in the mouse small intestine

4.1 Introduction

4.1.1 Senescence is a state of permanent cell cycle arrest

Senescence is a form of irreversible cell cycle arrest. It was first described in 1961, through culturing of human foetal cells (Hayflick and Moorhead, 1961). It was determined that cultured cells could only divide by a limited number of cumulative population doublings (CPD), depending on the species. This phenomenon is known as 'replicative senescence'. One of the theories behind what causes senescence is the natural shortening of telomeres on the tips of chromosomes. Telomeres are repeated DNA sequences (TTAGGG) that are gradually lost during each cell replication and different cell types have alternative telomere lengths (Moyzis et al., 1988; Bodnar et al., 1988). Following this, another form of senescence was defined and is known as premature or stress-induced senescence that is induced by various environmental stresses. These include low oxygen levels known as hypoxia, and oncogenic signalling, which is known as oncogene-induced-senescence (OIS).

Oncogenes are defined as molecules that have the ability to induce excessive cellular functions to promote tumourigenesis. Oncogenes result from the acquisition of mutations that induce cellular hyperproliferation. They can be classified into multiple groups, these include; growth factors and growth factor receptors, signal transducers, transcription factors, chromatin remodelers and cell cycle regulators.

Mounting evidence suggests senescence occurs through mechanisms that are activated in response to DNA damage (Bartkova et al., 2006). DNA damage can be caused by chemical compounds, radiation and also through de-regulation of reactive oxygen species (ROS). These factors lead to lesions in DNA that include single or double strand breaks (SSB/DSB), which alter the structure and function of DNA. These types of lesions activate multiple proteins and signalling pathways which together are known as the DNA damage response (DDR). These pathways result in either DNA damage repair or activation of senescence and apoptosis depending on the type of DNA damage.

Two key signalling pathways activated by DDRs are those associated with *p53* and the *p16*^{INK4a} genes (Figure 4.1). These pathways have direct effects on the cell cycle by inducing senescence (cell cycle arrest) at the G1-S phase and in addition p53 can induce apoptosis, a form of programmed cell-death.

The *p53* gene is the most well characterised TSG in humans. It is activated by the deactivation of its inhibitor Mdm2, by p14^{ARF} or p19^{ARF} in mice. p53 directly binds to the DNA of its target genes and stimulates transcription of proteins involved in cell cycle arrest and senescence, in particular *p21*^{CIP1}. p21^{CIP1} inactivates Cyclin-E/Cyclin Dependent Kinase 2 (Cdk2) complexes resulting in S-phase cell cycle arrest. The alternative, but also well defined pathway to senescence is through activation of the p16^{INK4a} pathway. p16^{INK4a} inhibits the Cyclin D and Cyclin dependent kinases 4 and 6 (Cdk4 & 6) complexes resulting in activation of the Retinoblastoma (Rb) protein and cell cycle arrest at S-phase (Serrano, Hannon &

Figure 4.1 *p16^INK4a^* and *p19^ARF^* activate senescence through alternative signalling pathways. A cell grows and divides through 4 stages of the cell cycle. During the G1 phase cells grow and this is prior to S phase where DNA is replicated. At G1 phase cells can also enter G0 and become dormant/senescent. Cell cycle check points exist during G1 phase to ensure dysfunctional cells do not continue further into the cycle and divide. Multiple cell cycle inhibitory pathways are activated to induce cell cycle arrest. This is thought to occur in response to DNA double strand breaks (DSB). One pathway occurs through activation of *p16^INK4a^* that inhibits cyclin dependent kinases (CDK) 4/6, which results in dephosphorylation of the retinoblastoma (Rb) that inhibits S phase entry. The second pathway is activated through p19^ARF^ that inhibits the Mdm2 protein, which results in p53 induced cell cycle arrest also at G1/S phase entry. Both pathways cause cell entry to G0 but, in addition, p53 can induce apoptosis.
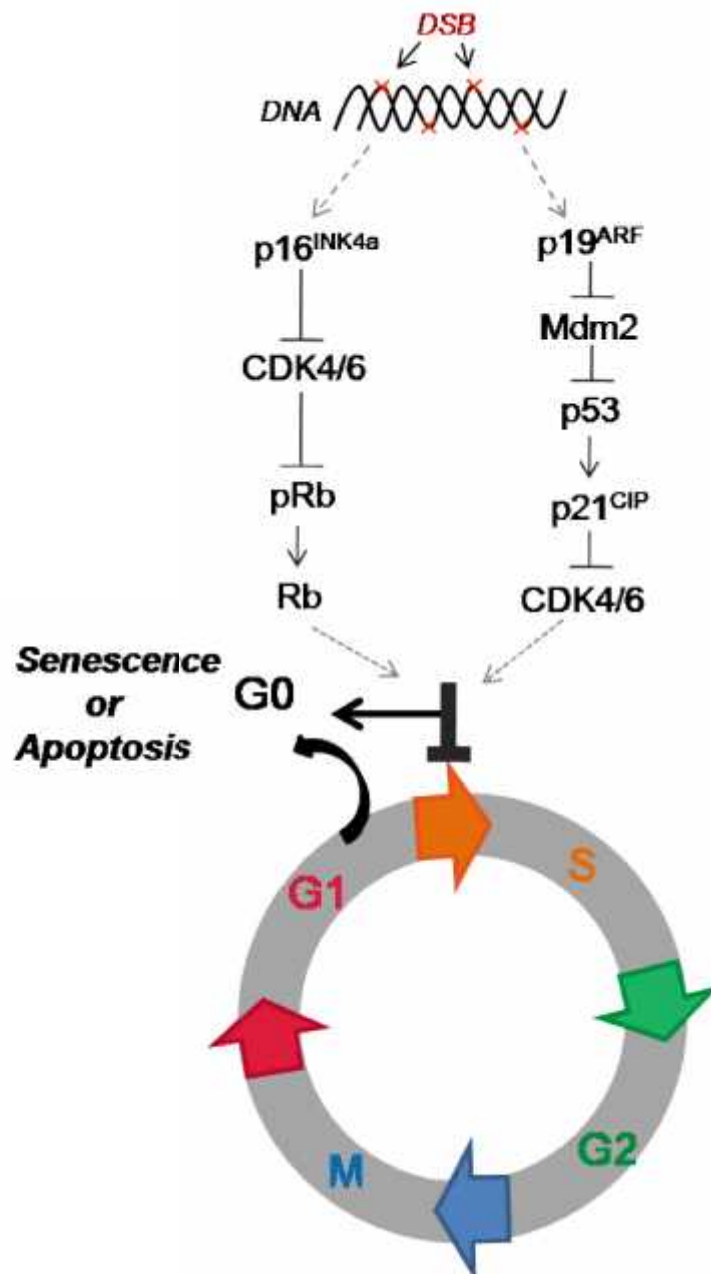
Beach, 1993).

4.1.2 Three transcripts are transcribed from splicing at the Cdkn2a/b loci

The *Cdkn2a* locus is located on the reverse strand of chromosome 4 in the mouse and encodes two alternatively spliced transcripts named *p16*[INK4a] and *p19*[ARF]. *p16*[INK4a] is encoded from three exons; exon 1α, 2 and 3 (Serrano et al., 1993). *p19*[ARF] is encoded by part of exon 2 but is transcribed from an alternative first exon, 1β that is 20kb upstream of exon 1α and is transcribed from an alternative open reading frame (ARF) (Figure 4.2). *p19*[ARF] encodes a protein whose function is unrelated to that of p16[INK4a], although they both negatively regulate cell cycle progression. Upstream of the *Cdkn2a* locus resides the *Cdkn2b* gene, which is comprised of two exons and encodes the *p15*[INK4b] transcript. The *p15*[INK4b] gene encodes a protein with a similar function to that of p16[INK4a] as cyclin dependent kinase (CDK) 4 and 6 inhibitors (Ortega et al., 2002).

4.1.3 Models of Braf[V600E]-induced senescence

The constitutive level of signalling through the MAPK pathway will determine the cellular response. Oncogenic signalling through the MAPK cascade, by Ras in particular, has previously been shown in cultured cells to induce cell transformation followed by a lack of tumourigenic progression, classified as senescence (Serrano et al., 1997). Over recent years, mouse models have been developed to investigate this phenomenon in various tissue types, to determine if this is an artefact of culturing or in fact a physiological mechanism to inhibit tumour development.

Figure 4.2 The Cdkn2a and Cdkn2b gene loci encode three tumour suppressor genes. (A) The *Cdkn2a* locus is comprised of the *p19^ARF^* and *p16^INK4a^* genes and the transcripts for the two genes are produced by differential splicing. Upstream, the *Cdkn2b* locus encodes the *p15^INK4b^* gene. (B) Amino acid sequences for all three TSGs, as coded by the colour box. Orange – *p15^INK4b^*, Green – *p19^ARF^* and Blue *p16^INK4a^*. All three genes function as tumour suppressors that inhibit the cell cycle. *p16^INK4a^* and *p15^INK4b^* encode proteins with a similar amino acid sequence and as such have similar functions. However, although *p19^ARF^* shares part of the sequence of exon 2 with *p16^INK4a^* it has an alternative amino acid sequence and function. The bold letter indicate homology in the amino acid sequences.

A

p15^INK4b^   p19^ARF^   p16^INK4a^

B

p15^INK4b^
MLGGSSDAGLATAAARGQVETVRQLLEAGADPNALNRFGRRPIQVMMMMGSAQVAELLLL
HGAEPNCADPATLTRPVHDAAREGFLDTLVVLHRAGARLDVCDAWGRLPVDLAEEQGHR
DIARYLHAATGD

p16^INK4a^
MESAADRLARAAAQGRVHDVRALLEAGVSPNAPNSFGRTPIQVMMMMGNVHVAALLLNYG
ADSNCEDPTTFSRPVHDAAREGFLDTLVVLHGSGARLDVRDAWGRLPLDLAQERGHQDIV
RYLRSAGCSLCSAGWSLCTAGNVAQTDGHSFSSSTPRALELRGQSQEQS

p19^ARF^
MGRRFLVTVRIQRAGRPLQERVFLVKFVRSRRPRTASCALAFVNMLLRLERILRRGPHRNP
GPGDDDGQRSRSSSSAQLRCRFELRGPHYLLPPGARRSAGRLPGHAGGAARVRGSAGCA
RCLGSPAARLGPRAGTSRHRAIFAFRWVLFVFRWVVFVYRWERRPDRRA

One of the most well characterised models of senescence is in melanoma, whereby human skin nevi are thought to represent benign senescent lesions. Melanocytic nevi predominantly express the *BRAF*^{V600E} mutation and it is thought to be the initiating mutation in their development (Pollock et al., 2003; Wellbrock et al., 2004). Strikingly, melanocytes can remain in proliferative arrest for decades without any malignant progression and this was hypothesised to reflect oncogene-induced-senescence (OIS). Indeed, the ectopic expression of *BRAF*^{V600E} in human melanocytes has been shown to induce initial proliferative transformation followed by cell cycle arrest, which was in association with p16^{INK4a} expression. Furthermore, a mouse model was developed to express (Cre-mediated) *Braf*^{V600E} in melanocytes from the endogenous *Braf* gene mice expressing *Braf*^{V600E} developed multiple melanocytic nevi that were reminiscent in histology of the human equivalent nevi (Dhomen. et al., 2009). Most of these nevi did not progress to melanoma; instead the epithelium showed signs of senescence, with a lack of expression of proliferative markers and positive expression of the senescence-associated (SA) β-galactosidase, a marker of senescence. p16^{INK4a} expression was found to be upregulated in *Braf*^{V600E} expressing nevi. Interestingly, several Braf^{V600E}-expressing mice developed melanoma but on further investigation using *p16*^{INK4a} 'null' mice (co-expressing *Braf*^{V600E}) it was shown that this was not, as expected, dependent on the loss of p16^{INK4a} expression. *p16*^{INK4a} null mice still developed nevi without melanoma development and in addition *p16*^{INK4a} was also expressed in a number of melanomas. This mimics the role of *p16*^{INK4a} in humans, because in human melanomas ~50% of familial melanomas exhibit deletions or mutations in the *p16*^{INK4a}/*p19*^{ARF} locus but

still develop nevi (Orlow et al., 2007).

In a similar study where *Braf*^{V600E} was conditionally expressed in mouse lung tissue, mice developed multiple lung adenomas (Dankort et al., 2007). Further progression to adenocarcinoma stage was only detected in 2 out of 57 mice. On analysis, the stable adenomas were found to express two key markers of senescence p19^{ARF} and Dec1. Their epithelium also showed a low level of proliferation. When the Braf^{V600E} expressing mice were crossed to a mouse strain null (homozygous) for *p16*^{INK4a}*/p19*^{ARF}, the lungs from 2 out of 4 mice exhibited adenocarcinoma development. In this model, Braf^{V600E} was able to induce adenomas followed by senescence with a possible role of *p16*^{INK4a}*/p19*^{ARF} although like with melanoma, carcinoma growth was not solely dependable on *p16*^{INK4a}*/p19*^{ARF} expression.

Similarly to melanoma and lung cancers, a role for OIS has been defined in colorectal cancer (CRC). It is thought that early benign colon lesions, known as hyperplastic polyps, mimic that of human melanocytic nevi. This is particularly evident for a subset of polyps that are part of the serrated neoplastic pathway. These lesions most often harbour mutations in both the key MAPK signalling proteins, *BRAF*^{V600E} and *RAS* and these have both been linked to OIS (Minoo and Jass 2006). In association with this it was initially suggested that *p16*^{INK4a} had a role in human CRC when it was found to be expressed in early stage neoplastic regions of the human colon and also in some later stage transformed lesions of the colon (Dai et al., 2000). An *in vivo* study revealed that loss of *p16*^{INK4a} in mice carrying a

mutation in the *Apc* gene, a key TSG gene involved in CRC, resulted in the growth of intestinal tumours (Gibson et al., 2005). One of the most recent studies specifically identified p16[INK4a] upregulated expression in human *BRAF*[V600E]-expressing polyps and early stage adenomas (Kriegl et al., 2011).

These models provide strong evidence that excessive signalling through MAPK-activated proteins can induce OIS as a mechanism to halt malignant transformation by inactivating one or more TSGs. It would appear that the TSG involved i.e. *p16*[INK4a] or *p19*[ARF] is dependent on the tissue type. In the case of *Braf*[V600E]-expressing cancers, the findings suggest that a defining factor of inhibiting tumourigenic progression is *p16*[INK4a]-activated senescence. This is particularly evident in reference to human serrated CRCs that express Braf mutations.

4.2 Aims

In Chapter 3 it was determined that Braf[V600E] expression induces an initial burst of crypt cell proliferation, a typical characteristic of an oncogene, but this was not sustained. After 2 weeks of Braf[V600E] expression the level of proliferation was returned to the control level. The aims of this chapter were to continue to characterise changes post-*Braf*[V600E] expression in the mouse jejunum, with particular reference to identifying the mechanisms that inhibit the initial pro-proliferative signals.

4.3 Results

4.3.1 Braf[V600E] induces p16[Ink4a] expression in the crypt epithelium

As discussed above $p16^{INK4a}$ is a tumour suppressor gene involved in oncogene induced senescence (OIS). $BRAF^{V600E}$ is an oncogene that has been shown to induce senescence in melanocytes associated within the upregulation of p16[INK4a] activation in melanocytes (Dhomen et al., 2009). To see whether this mechanism affected crypt homeostasis in the gut, $p16^{INK4a}$ mRNA and protein levels were investigated by quantitative/semi-quantitative RT-PCR and IHC. $p16^{INK4a}$ is transcribed from the *Cdkn2a* locus that is spliced to produce mRNA from 3 encoding exons (1α, 2 & 3). Semi-quantitative RT-PCR was performed on 3 alternative time courses for all samples, using primers that amplify a cDNA region across exon 1α and 2 of the $p16^{INK4a}$ gene (Figure 4.3A). Each time course showed a slightly different pattern of expression. Overall, $p16^{INK4a}$ was expressed at very low levels in both controls (Figure 4.3B).

During the *Braf*[V600E]-expressing time course $p16^{INK4A}$ was absent at 3 days. It was then expressed as early as 1 wk p.i. and increased in its expression at the later time points. The most predominant expression was at the 2 wk p.i. time point

qRT-PCR for $p16^{INK4a}$ was performed using the Universal Probe Library (UPL) method because previous attempts using standard (Sybr Green) qPCR had shown $p16^{INK4a}$ was of relatively low abundance in the SI. UPL primers for qPCR were designed to amplify across exons 1α and 2 with the forward primer sequence directly across the exon 1α and 2 intron boundaries (Figure 4.4A). A probe was

Figure 4.3 *p16^{INK4a}* mRNA is induced at late time points following *Braf^{V600E}* expression. (A) The *Cdkn2a* locus comprises the *p19^{ARf}* and *p16^{INK4a}* genes. For *p16^{INK4a}* RT-PCR primers were designed to amplify a region containing sequences from exons 1α and 2. The primers are shown by black arrows. (B) RT-PCR on three alternative time courses. cDNA was transcribed from RNA isolated from the SI of WT, Cre and the *Braf^{V600E}*-expressing time course of 3 days p.i. to 11wks p.i. RT-PCR was performed for *p16^{INK4a}* and *Calnexin* as a control. Levels of *p16^{INK4a}* are elevated at variable time points but are consistently increased at later time points compared to the controls.
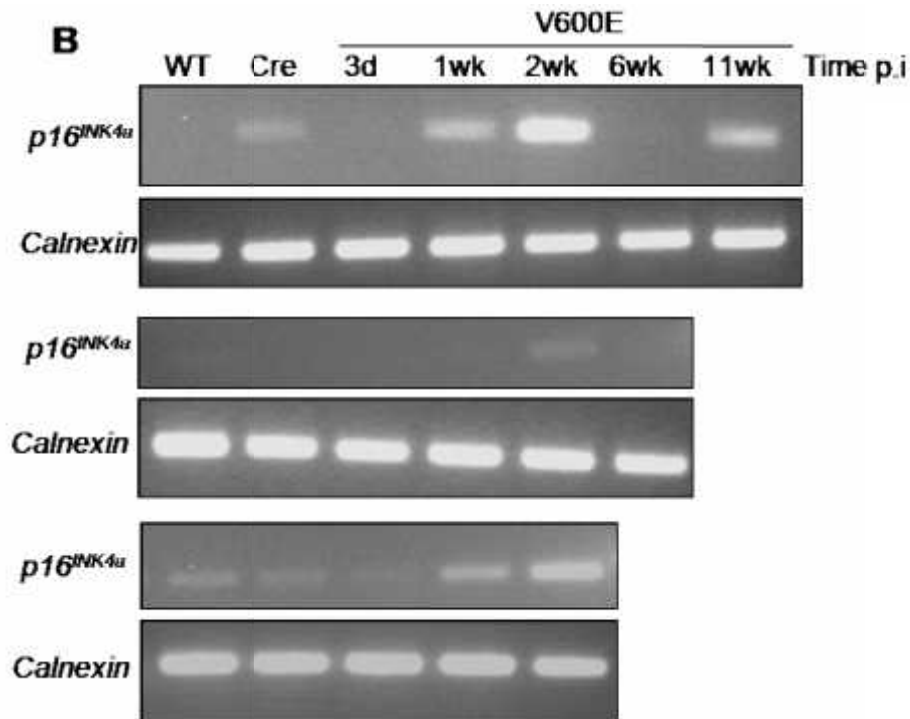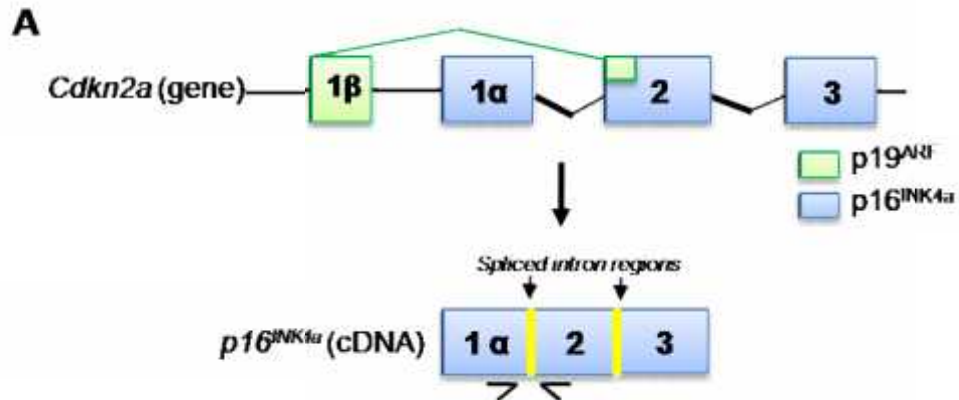
Figure 4.4 qRT-PCR of *p16[INK4a]* post [V600E]*Braf*-expression. qPCR for *p16[INK4a]* was performed using primers and a probed designed for the specific gene by the Universal Probe Library (UPL). (A) *p16[INK4a]* gene locus and cDNA transcript, the primer annealing points are shown by the arrows. (B) qPCR analysis on a single time course (n=1). *p16[INK4a]* expression peaks at 2wks p.i.
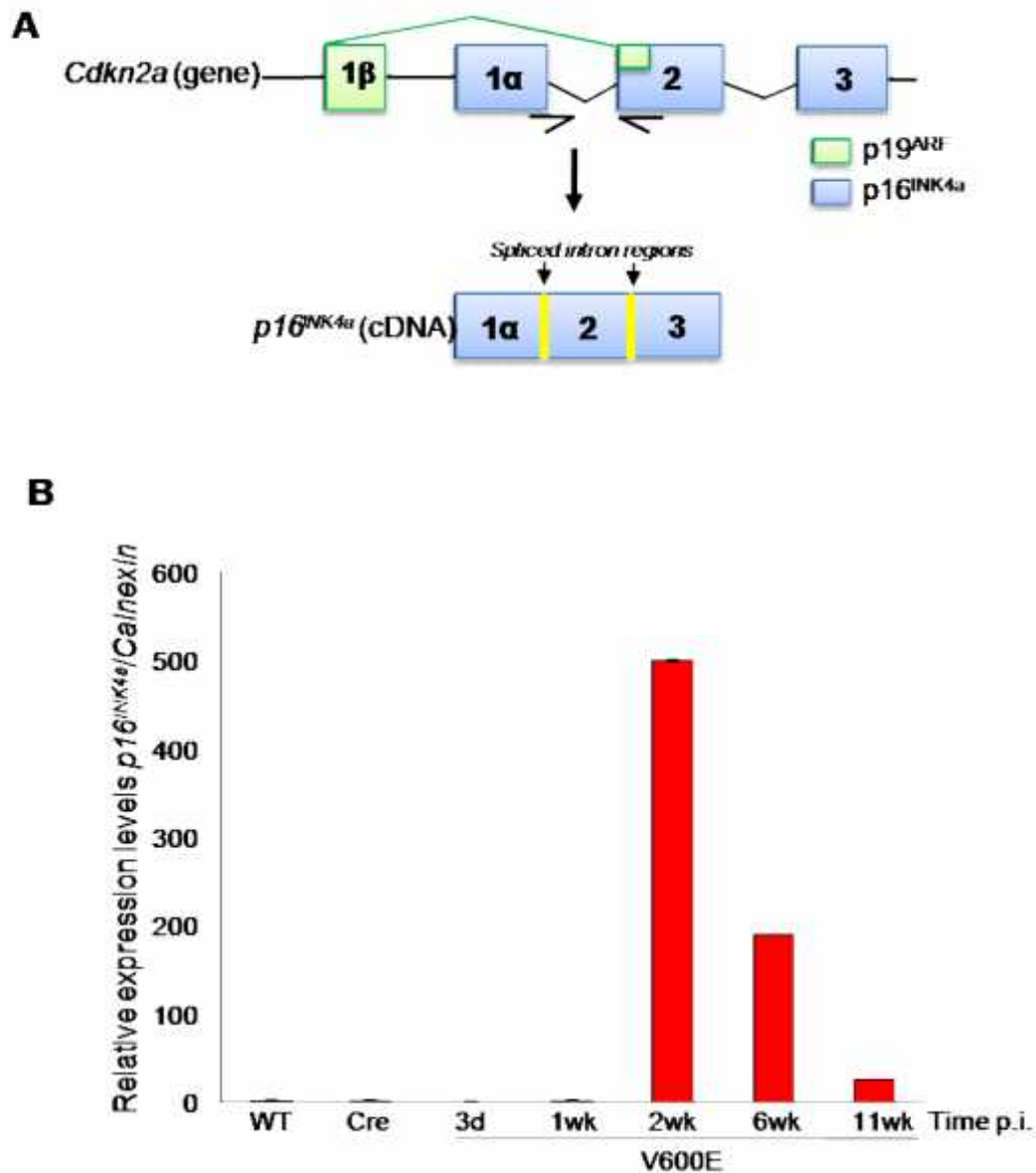
designed that was complementary to a region of the sequence amplified by the PCR primers; this increased the sensitivity of the reaction. In experimental terms, every new strand of DNA produces a fluorescent flare and each replication is therefore identified in the PCR. *p16^INK4a* mRNA levels by qPCR were very low/absent in the control samples. In the experimental samples, *p16^INK4a* was significantly increased at 2 wks post-VE expression and was also elevated at 6 and 11 wks p.i, but at lower levels (Figure 4.4B). This is similar to the standard RT-PCR results (Figure 4.3B).

Immunohistochemistry for p16^INK4a was performed on small intestine jejunum sections for both controls and over the experimental time course. Nuclear expression of p16^INK4a was identified in crypt cells at 2, 6 and 10 wks p.i, most predominantly at the later two time points (6 & 10 wks) (Figure 4.5). Thus, the rise in *p16^INK4a* mRNA levels occurs prior to protein nuclear expression.

Both qPCR and immunohistochemistry results provide strong evidence that *p16^INK4a* is expressed in the SI beginning from ~1wk p.i.. This expression pattern corresponds with the loss of proliferation and Erk phosphorylation at these time points, suggesting *Braf^V600E*-induced senescence occurs in the crypt cells after the initial burst of proliferation, through induction of *p16^INK4a*.

4.3.2 p19^ARF is not expressed in response to Braf^V600E expression

p19^ARF is a cell cycle regulator encoded from the *Cdkn2a* locus along with p16^INK4A. p19^ARF is involved in inducing cell cycle arrest in association with p53. In mouse

Figure 4.5 p16^INK4a^ expression is induced in the V600E-expressing gut. p16^INK4a^ IHC on mouse jejunum SI sections from WT and *Braf*^V600f^-expressing 2, 6 and 10 wk time points. Increased p16^INK4a^ expression is observed in the 6 and 10 wk samples. Scale bars = 50μm.
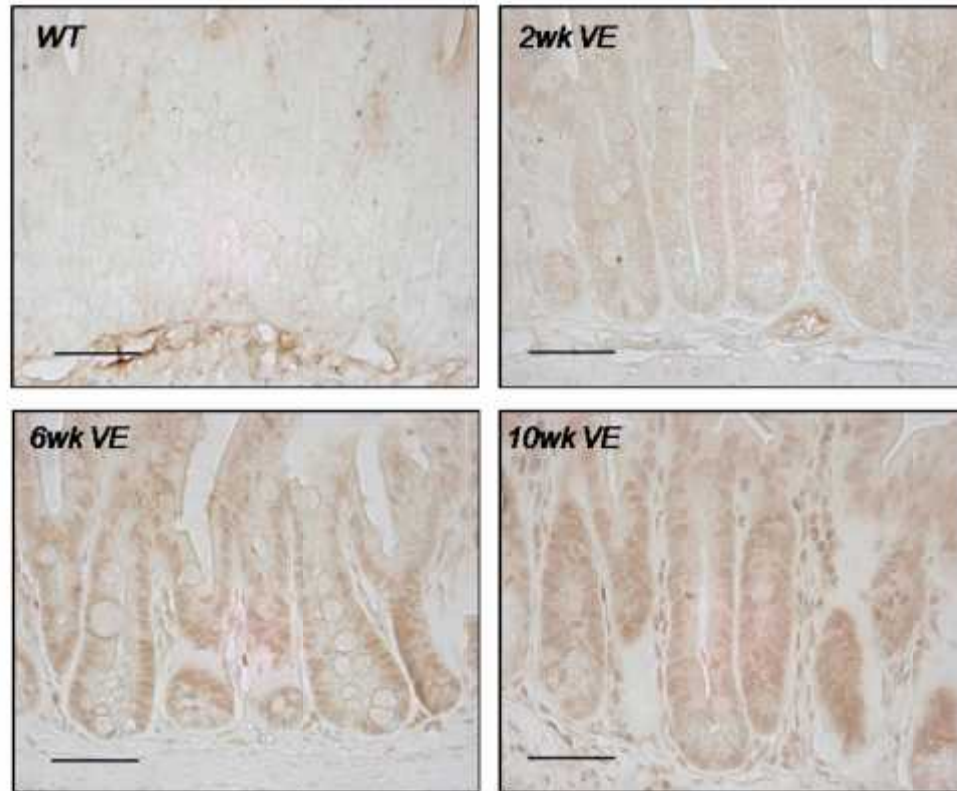
embryonic fibroblasts (MEFs) oncogenic signalling from Ras can induce

$p19^{ARF}$-induced senescence. As a key effector of Ras and a potent oncogene it

was thought that Braf^{V600E} activity could upregulate $p19^{ARF}$ expression, which may

contribute to the senescence observed in the crypts. $p19^{ARF}$ mRNA expression

level was analysed from cDNA over a single time course using semi-quantitative

RT-PCR. Primers were designed to amplify a region of exon 1β and exon 2 (Figure

4.6A). cDNA derived from MEFs was used as a positive control (C) for $p19^{ARF}$

expression. $p19^{ARF}$ was not present in any of the samples except the positive

control, suggesting $p19^{ARF}$ is not expressed in the mouse small intestine in the

presence/absence of oncogenic *Braf^{V600E}* (Figure 4.6B).

4.3.3 $p15^{INK4b}$ is expressed in the Braf^{V600E}-expressing jejunum

The $p15^{INK4b}$ gene contains two exons and is coded for by the *Cdkn2b,* which lies

upstream of the *Cdkn2a* locus. It has a similar function to the $p16^{INK4a}$ gene,

inducing cell cycle arrest at the G1 phase. For this reason, $p15^{INK4b}$ levels were

analysed by qRT-PCR to determine if $p15^{INK4b}$ levels were upregulated in response

to *Braf^{V600E},* in a similar way to $p16^{INK4a}$. Analysis was performed on 3 alternative

time courses, except for the 10 wk+ sample, which represents a 10 wk and 11 wk

sample combined (n=2) (Figure 4.7). $p15^{INK4b}$ levels were significantly increased in

all samples except at the 2 wkVE time point (P=0.3), but most significantly in the 1

wkVE time point. This provides evidence that $p15^{INK4b}$ mRNA levels are increased

upon *Braf^{V600E}* expression and may support a role for this tumour suppressor in

activating senescence in the crypt epithelium.

Figure 4.6 p19^ARF^ is not expressed in the mouse SI. RT-PCR was performed on cDNA reverse transcribed from RNA isolated from MEFs (C) and the SI of WT, Cre and the Braf^V600E^-expressing time course of 3 days to 6 wks p.i. MEFs were used as a positive control for expression. (A) Representation of the *Cdkn2a* locus and the primer pair location used to amplify the cDNA. (B) RT-PCR agarose gel. *p19^Arf^* is not expressed in the WT or *Braf*^V600E^-expressing mouse SI. Amplification of *Gapdh* was used as a control.
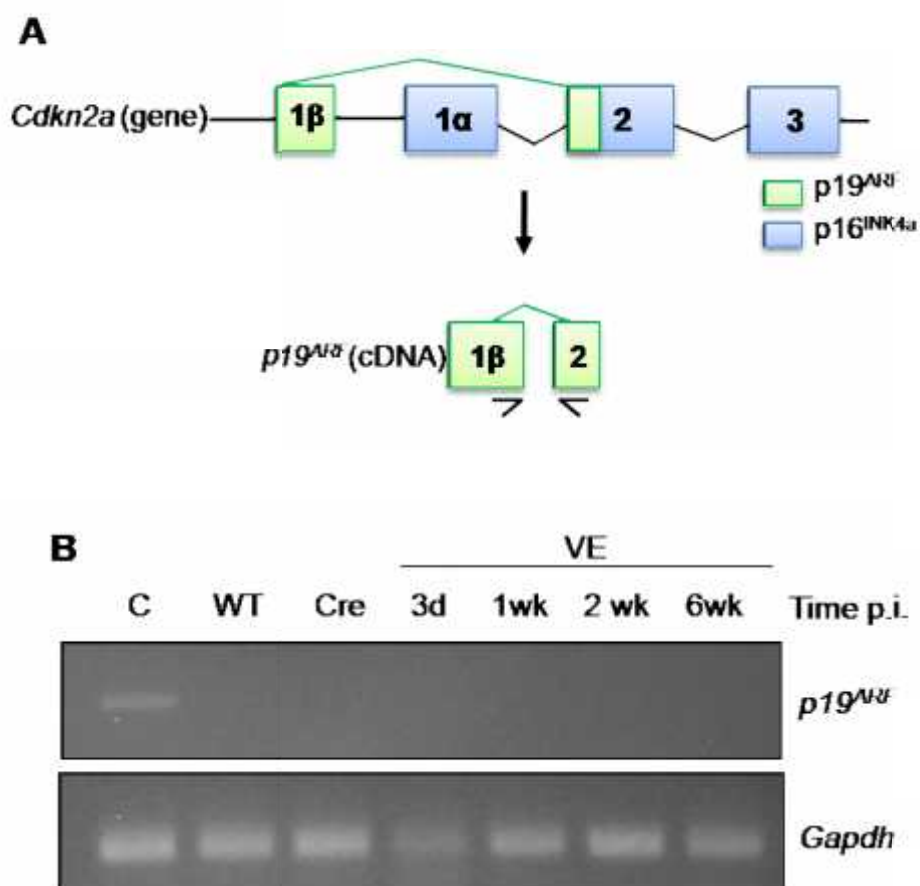
Figure 4.7 p15[INK4b] gene expression is induced by Braf[V600E]. qRT-PCR of the mouse SI using cDNA reverse transcribed from mRNA isolated from SI from WT, Cre and the Braf[V600E] expressing time course of 3 days to 10wks+ using primers for p15[INK4b]. Each bar represents the average expression of 3 samples with the exception of 10 wk+, which represents a 10wk and 11wk p.i. VE samples combined (n=2). Error bars represent standard deviation. Calculated P values give statistically significant increases in p15[INK4b] mRNA expression at 3 days (P=0.007), 1wk (P=0.0005), 6wk (P=0.0037) and 10wks+ (P=0.01) post-[V600E] Braf expression, in comparison to the Cre control. There were no statistical differences between the Cre and 2wk VE p.i. Sample (P=0.36). Asterisks (*) represent statistical significance *= P<0.05, **=P<0.005, ***=P<0.0005.
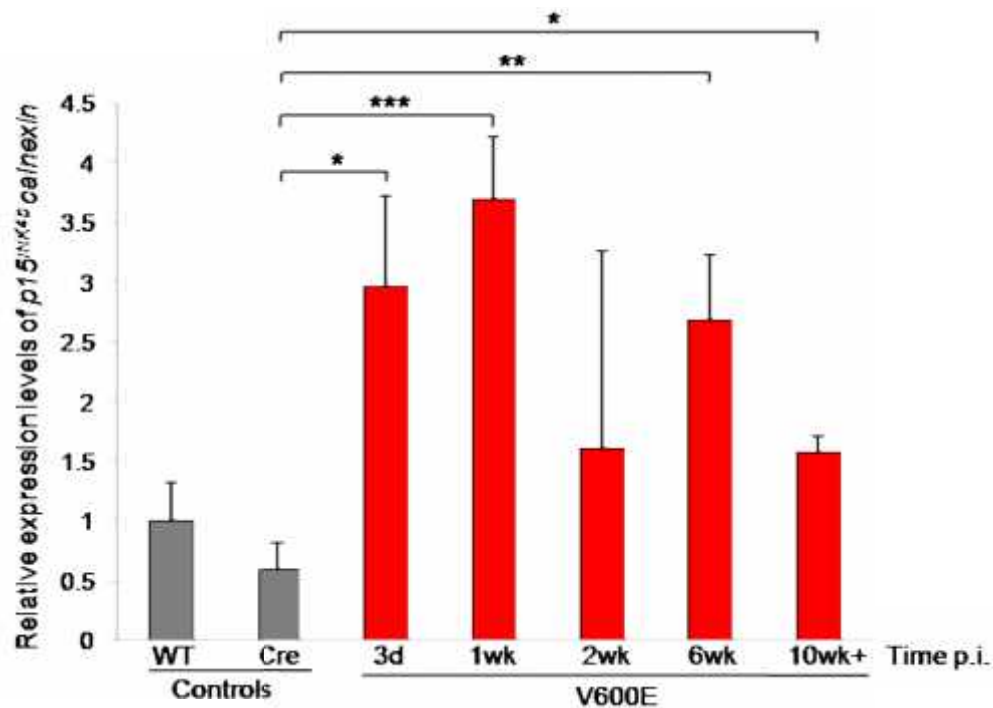
4.3.4 Senescence factor Dec1 is elevated post-Braf^V600E^ expression

Deleted in Oesophageal Cancer 1 is a tumour suppressor gene. The locus that it resides on is often deleted in cancers of developmental tissues such as the oesophagus, head and neck (Leung et al., 2008; Kunimoto et al., 2011). The deletions observed in these tissues have been linked to carcinoma progression. Although little is known about its function it is thought to play a role in senescence. Immunohistochemistry for Dec1 was performed on sections of the jejunum from WT and *Braf*^V600E^ samples at 1, 6 and 10 wks p.i. (Figure 4.8). Dec1 protein expression was absent in WT control crypts but was elevated in all of the Braf^V600E^ time points. The most significant increase was seen in the 6 wk p.i. sample, with both nuclear and cytoplasmic localisations. Dec1 has previously been reported to reside in both the nucleus and cytoplasm using epitope tagging (Leung et al., 2007). This provides support for the onset of senescence with a possible role of Dec1 through Braf^V600E^ activation.

4.3.5 Morphological evidence for Braf^V600E^-induced senescence

In association with the serrated villi observed in Chapter 3, it was observed that the epithelium starts to break down particularly at the tip of the villus, which may reflect the fact that the crypts are in senescence. (Figure 4.9). Normally cells are gradually lost from the tip of the villus into the gut lumen during normal heamostasis. It is possible that senescent cells are not lost from the tip of the villus, and this may results in 'stagnant' villi which are then more prone to extensive mechanical breakdown (Figure 4.9).

92

Figure 4.8 The tumour-suppressor protein Deleted in Oesophageal Cancer 1 (Dec1) shows an altered expression pattern during the early and late stages post-Braf^{V600E} induction. Dec1 IHC on sections of WT, 1wk, 6wk and 10wk p.i. *Braf*^{V600E} SI samples. Levels of Dec1 appear higher from 1wk post-*Braf*^{V600E} induction, most significantly at 6 wks compared to the WT control. These levels are consistent with the observed biochemical changes at these time points. Scale bars = 200µm.
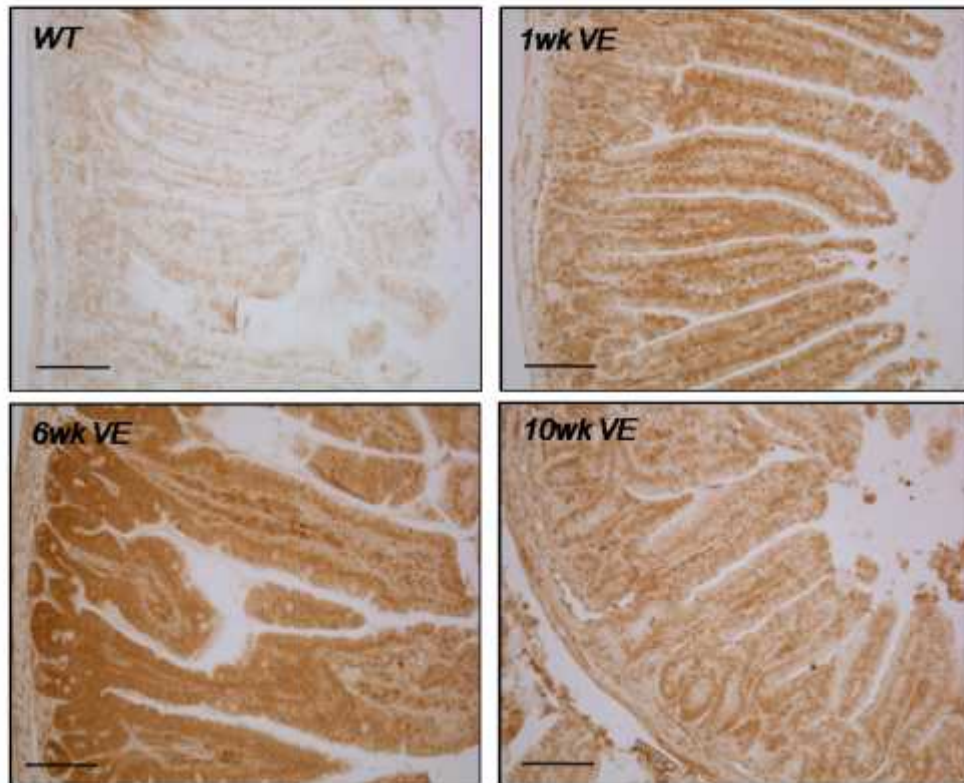
Figure 4.9 Features of senescence coincide with histopathological changes in the SI epithelium. (A) H & E stained sections from the jejunum of a 10wk p.i. VE sample. Increased cell number and senescence resulted in 'ballooning' of the villus and subsequently rupturing of the epithelial lining, denoted by the arrows. Scale bars = 100µm (top) and 50µm (bottom).
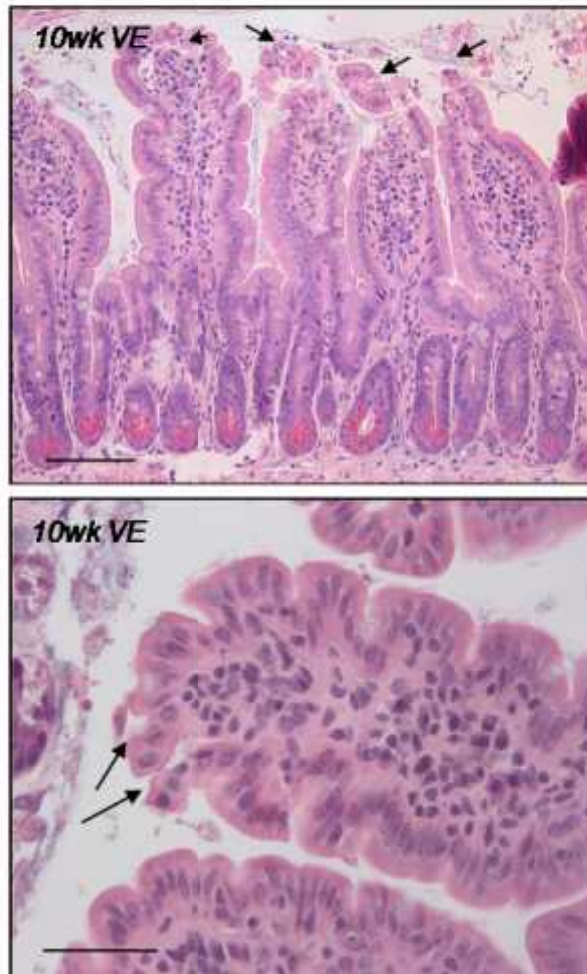
4.3.6 Serrated adenomas develop at 12wks post-Braf[V600E] expression

As previously mentioned, the Ah*Cre*ER[T] strain used in this mouse model results in high levels of *Braf*[V600E] expression in the stomach. Mice survival past 10 wks post induction is reduced due to the stomach hyperplasia. However, a number of mice survived to later stages, up to 12 wks p.i. following Braf[V600E] expression. These mice developed individual tumours that were located throughout the whole length of the small intestine. These were clearly visible by eye under light microscopy; one of the largest tumours was ~1mm in width (Figure 4.10). The number and size of individual tumours varied depending on the section of intestine (1-6). The section that is nearest to the stomach (duodenum) contained more tumours, which were relatively large, in comparison to tumours in the ileum, nearest to the colon. No tumours were identified in the colon.

4.3.7 Tumours are proliferative and lack p16[INK4A] and Dec1 expression

Sections from all segments (1-6) of a 12 wk p.i. small intestine with visible adenomas were stained for Phospho-histone H3 (P-H3), a marker of cell mitosis. As expected all adenomas showed a uniformed pattern of P-H3 expression, suggesting the tumour cells were in mitosis and proliferating (Figure 4.11A). Corresponding serial sections were also stained for p16[INK4A] expression (Figure 4.11B). All visible adenomas were negative for p16[INK4A], with the exception of a few minor pockets of positively stained nuclei. These possibly represent areas of existing senescent crypt epithelium, surrounded by the growth of dysplastic epithelium. In addition to p16[INK4a] a lack of Dec1 staining was observed in the tumour epithelium providing further evidence for a loss of the senescent phenotype

Figure 4.10 Tumours at 12 weeks post-^{V600E}***Braf* induction.** (A) H&E section from a 12wk p.i. VE duodenum SI showing three tumours, denoted by the arrows. Scale bar = 500μm. (B) Enlarged single tumour. Scale bar = 200μm.
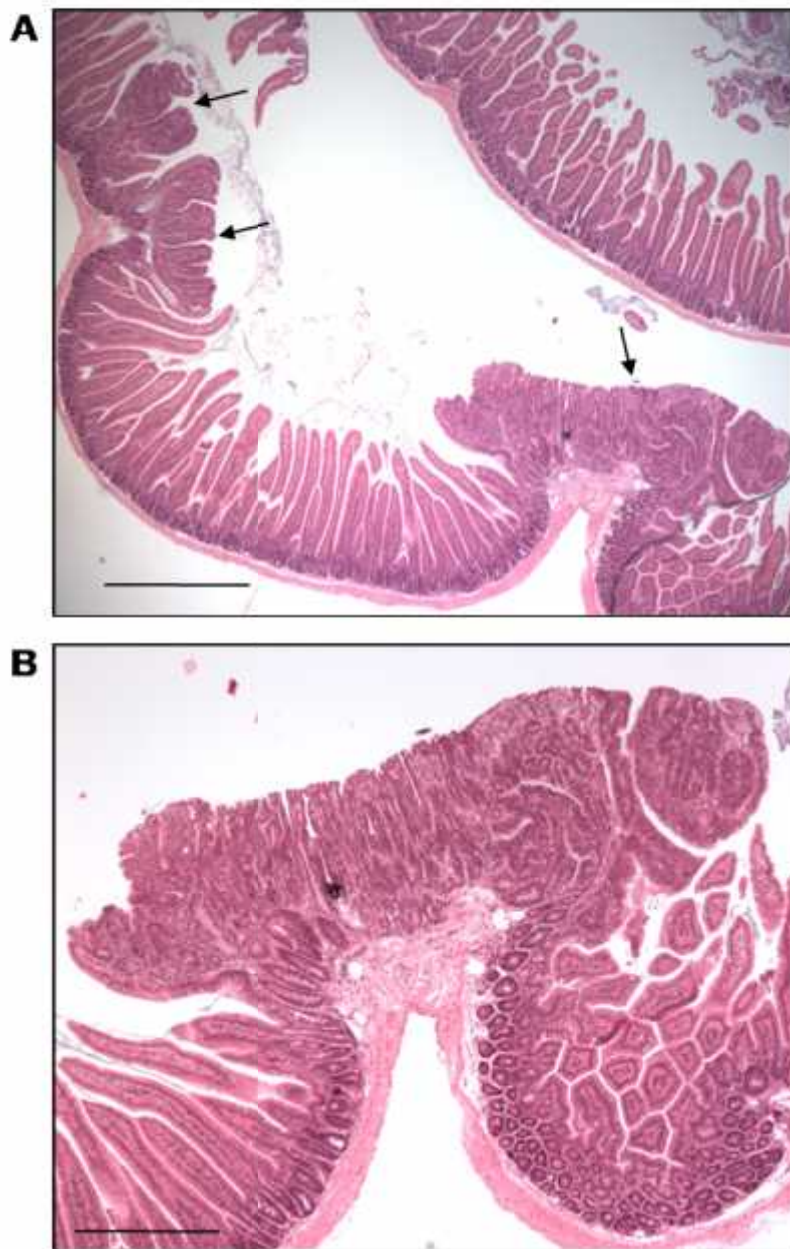
Figure 4.11 Tumours of a 12wk VE from the duodenum show high levels of proliferation and lack p16[INK4a] expression. P-H3 and p16 IHC staining on serial sections of a 12wk p.i. VE tumour. (A) Tumour section stained with P-H3 shows a high level of mitosis by widespread nuclear staining. (B) The same tumour is stained for p16[INK4a] and shows a lack of positive cells. (A/B) A pocket of cells are absent for P-H3 but positive for p16[INK4a] highlighted by dotted line. Scale bar= 50μm. Staining was performed by Susan Giblett. Images taken from Carragher et al., 2010.
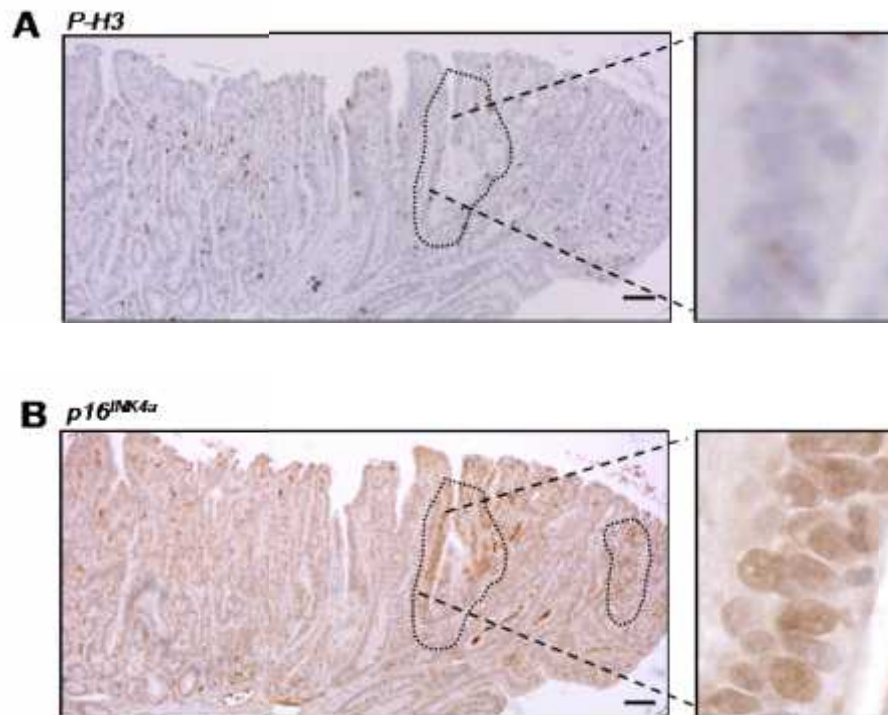
Figure 4.12 Tumours from a 12wk p.i. VE from the duodenum do not express Dec1. (A) Tumour stained with H&E on a section of 12wk Braf^V600E^ expressing SI. Scale bar= 50µm (B) Dec1 IHC staining on the same tumour. A region of the tumour in (A) is enlarged in (B) Scale bar = 100µm.
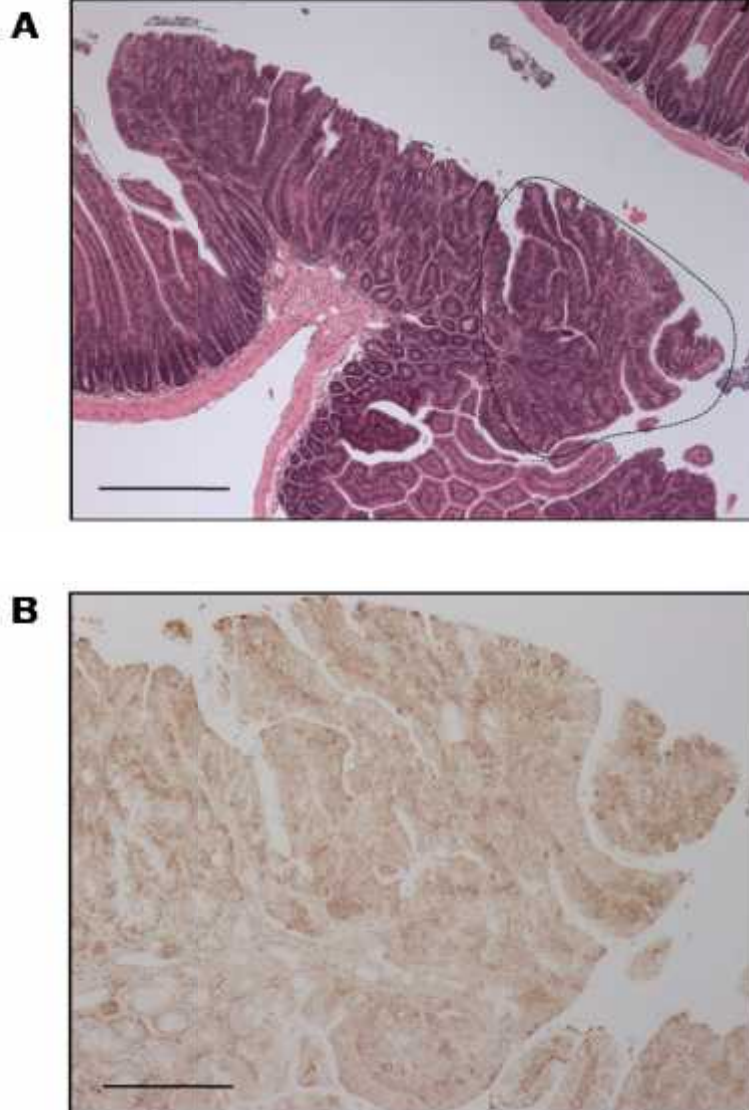
in association with tumour progression (Figure 4.12).

4.4 Discussion

In chapter 3, upregulated crypt cell proliferation was identified in response to *Braf^V600E* expression. However, this was not sustained and at ~6wks-post *Braf^V600E* induction the crypt cell number returned to that of a wild type crypt. The mechanism inhibiting proliferation at this time point was investigated in this chapter.

The most obvious candidate to investigate the loss of signalling was by tumour suppressor gene activation, in relation to senescence. Oncogene-induced senescence (OIS) by *p16^INK4a* is already well documented in melanomas, where the precursor lesions, known as melanocytic nevi, express both *BRAF^V600E* and *p16^INK4a* (Dhomen et al., 2009). *In this chapter, p16^INK4a* mRNA and subsequently the protein expression both increase after as early as ~1 wk of *Braf^V600E* induction and remain expressed up to ~11 wks post-induction. These results suggest *p16^INK4a* is activated in response to *Braf^V600E* in a similar manner to melanocytic nevi. This induction of senescence may correlate with the loss of ppErk and lack of cell proliferation seen at these time points. These results are concordant with a study on human colon tumours that found *p16^INK4a* was expressed in the early neoplastic lesions and its expression inversely correlated with proliferative markers (Dai et al., 2000).

Although *p16^INK4a* and *p19^ARF* are derived from the same locus they have very distinct functions whereas *p15^INK4b* has a similar function to *p16^INK4a* to inhibit

progression of the cell cycle at G1-S phase. The data collected from this model, potentially both *p16*^{INK4a} and *p15*^{INK4b} could be co-activated to induce senescence in response to Braf^{V600E}. Although little has been explored with regard to *p15*^{INK4b} activation and function, *p15*^{INK4b} activation has been shown to occur in response to Ras oncogenic signalling, to a similar level as *p16*^{INK4a} (Malumbres et al., 2000). The loss of the *CDKN2a/b* locus is one of the most common deletions in all tumour types; the significance of this loss is usually attributed to inactivation of *p16*^{INK4a}. However, specific point mutations in *p15*^{INK4b} are also a frequent occurrence in various lymphomas and leukaemias, suggesting it can have a significant TSG role on its own (Ruas and Peters, 1998). In addition, using an *in vivo* mouse model it was shown that deletion of *p16*^{INK4a} and *p15*^{INK4b} together increased the development of skin tumours in comparison to mice solely deficient for *p16*^{INK4a} (Krimpenfort et al., 2007).

In addition to the *Cdkn2a/b* genes the TSG *Dec1* (*Deleted in Esophageal Cancer*), often found over-expressed in developmental tissues, are also associated with Dec1 (Collado et al., 2005) (Dankort et al., 2007). Dec1 protein levels were significantly higher by immunohistochemistry in the jejunum in the nucleus and cytoplasm from 2 to 6 wks *Braf*^{V600E} induction. This correlates with the onset of *p16*^{INK4a} and suggests Dec1 may also have a role in inducing crypt senescence in response to *Braf*^{V600E}. Or alternatively, it may be increased in crypt cells as a consequence of senescence and so represents a marker of the phenotype, rather than an active component, but this remains to be proven.

After 12 wks of *Braf*[V600E]-expression, individual serrated adenomas were present throughout the intestine of a number of mice. They had individual serrated adenomas throughout the whole length of the intestine. These adenomas were highly proliferative and absent for p16[INK4a] protein expression. It seems evident that the progression from Braf[V600E] -induced senescence to adenoma formation is achieved partly through the inactivation of the p16[INK4a] tumour suppressor. *p16[INK4a]* RNA analysis could not be performed on the adenomas due to the nature of their size, which made them undetectable prior to paraffin embedding. In addition to the experimental data supplied in this study, the *Braf*[V600E]-expressing mice were crossed with a *Cdkn2a* homogygous knockout strain, which do not express *p16[INK4a]* but express a truncated form of *p19[ARF]* (Carragher et al., 2010). The survival of these mice was greatly decreased by ~50% compared those with only the *Braf*[V600E] mutation. Both low-grade hyperplastic lesions as well as more advanced dysplastic tumours were identified in the small intestine epithelium of these knockouts, suggesting loss of *p16[INK4a]* has enhanced tumour development. These findings are important when deciphering the role of *p16[INK4a]* in this model. It is possible that adenomas have arisen from a small number of cells that have never been in senescence. However the fact that the *p16[INK4a]* 'knockout' mice develop tumour lesions after ~6 wk p.i. indicates that senescence is a key factor in tumour progression and that *p16[INK4a]* is a key factor in the onset of senescence.

BRAF[V600E] associated OIS in the gut has never been identified before. However, the model for BRAF[V600E]-induced senescence through activated expression of *p16[INK4a]* has been previously defined in melanocytic nevi. p19[ARF] was induced in

the lung (Pollock et al., 2003; Dhomen et al., 2009; Dankort et al., 2007). Expression of both genes has been co-identified in early melanocytic lesions, which remain senescent until additional mutations are acquired.

However, it is not a clear picture as to whether the inactivation of p16^{INK4a} in melanocytic nevi is the key to tumour progression. In one study where *p16^{INK4a}* was deleted in the mice expressing Braf^{V600E} melanocytic nevi, tumour development did not occur when *p16^{INK4a}* was absent (Dhomen et al., 2009). Furthermore, in humans, p16^{INK4a} is detected in malignant melanomas, suggesting the role of p16^{INK4a} is different in alternative tissue types. The adenomas identified in the mouse *Braf^{V600E}*-expressing SI are highly reminiscent of human colorectal 'serrated' adenomas, because they are large, protrude into the lumen and have a serrated and mucinous epithelium (Longacre and Fenoglio-Preiser, 1990). The exact subtype is difficult to determine because of the differences in morphology between the colon and SI. Sessile serrated adenomas typically are mucinous and have dilated crypts that are attached to the sub mucosa, which is suggestive of the adenomas addressed in this study. There were also areas of dysplasia which are a feature of advanced adenoma to carcinoma development (Reviewed in J R Jass, 2007).

Overall these results suggest a model for progression of CRCs with Braf^{V600E} as a founder mutation. Its oncogenic properties induce proliferation in crypt cells, but the activation of the MAPK signalling is not sustained due to the up-regulation of p16^{INK4a} and p15^{INK4b} tumour suppressors. To achieve further progression these

TSGs need to be inactivated. In this chapter it was identified that the growth of adenomas was accompanied by loss of $p16^{INK4a}$ expression. Due to experimental restraints on analysing the adenoma tissue and the lack of sufficient $p15^{INK4b}$ antibodies it was not possible to determine whether this TSG was also inactivated. Data also revealed there was no role for $p19^{ARF}$ in both senescence and Braf^{V600E}-driven tumour development in this model.

Human studies of CRC also show some evidence for loss of $p16^{INK4a}$ expression, one study of 902 CRC cases showed loss of $p16^{INK4a}$ occurred in 25% of cases (Shima et al., 2011). In another study that specifically analysed the serrated CRC subtypes, the expression of $p16^{INK4a}$ followed by the loss of expression correlated with increased neoplastic progression (Kriegl et al., 2011). Low-grade tumours exhibited $p16^{INK4a}$ expression that was also seen in late stage tumours, although expression was increasingly heterogeneous. All late stage malignant lesions (adenocarcinomas) were absent of any $p16^{INK4a}$ expression (Kriegl et al., 2011). These studies support the hypothesis that loss of $p16^{INK4a}$ is has a significant role in malignant transformation of serrated CRC lesions.

5. Investigating *p16^INK4a* inactivation post-*Braf^V600E* expression

5.1 Introduction

5.1.1 DNA methylation and CpG island methylation

In eukaryotic organisms methylation occurs by the addition of a methyl (CH_3) group from *S*-adenosyl-L-methionine to the C-5 position on a cytosine nucleotide. Methylation occurs on cytosines that are directly followed by a guanine nucleotide and are known as CpG dinucleotides. This mechanism is important in mammalian development because it regulates key processes including genome stability, chromosome imprinting and transcriptional regulation of genes (Li et al., 2002).

CpG dinucleotides are found randomly, spread throughout the genome and represent 1% of DNA content (Bird, A. 2002). These are usually single, isolated CpGs, which are located in repetitive, noncoding sequences and are generally always methylated. However, CpGs are also found densely populated in gene-coding regions and about 50% are located in the promoters of genes. These are known as CpG islands, which are generally unmethylated. However in some circumstances, these CpG islands become methylated, which results in loss of gene expression. This epigenetic mechanism is not widely understood but its importance in gene expression has become increasing publicised since CpG hypermethylation has been identified to some extent in almost all human cancers. This is mainly due to hypermethylation of CpG islands within gene promoters and encoding exons. Interestingly, it was revealed that cancer cell lines exhibited global CpG hypomethylation of CpGs in non-coding sequences, whilst also exhibiting

hypermethylation promoter CpG islands (Herman and Baylin, 2003). Furthermore, analysis on genes targeted for DNA methylation revealed that two or more genes were often methylated in the same tumour types. This phenomenon is known as the CpG methylation phenotype (CIMP) and was initially described in colon cancer but has also been described in breast cancer cell lines (Toyota et al., 1999; Roll et al., 2008).

5.1.2 The DNMT family of DNA methyltransferase

A number of *DNA methyltransferase* (*DNMT*) genes have been identified these being; *DNMT1, DNMT2, DNMT3* and *DNMTL*, although it is only the DNMT1 and DNMT3 methyltransferases that are known to have functional methyltransferases activity. Both genes have been shown to target alternative DNA sequences (Okano et al., 1998a/b). DNMT1 has a preference for hemimethylated DNA, whereas DNMT3 are *de novo* methyltransferases, meaning they target previously unmethylated DNA. This is most likely due to their distinct alternative N-terminal domains, which is thought to determine nuclear localisation and target sequences.

The DNMT1 methyltransferase was the first to be identified. It acts as a maintanence methyltransferases and is the most prominently expressed in somatic tissues (Bestor et al, 1988; Lei et al., 1992; Pradhan et al., 1999). A key role of this protein is to provide heritable DNA methylation patterns on replicated DNA sequences. Alternatively, as previously mentioned, DNMT3 methyltransferases target *de novo* DNA (Okano et al., 1999). There are two *DNMT3* genes *DNMT3A* and *DNMT3B* that occur through alternative splicing of the *DNMT3* gene; they have similar expression

patterns and functions and are essential for mammalian development (Chen et al., 2002). They are both expressed in embryonic stem (ES) cells at high levels but are down-regulated in somatic adult tissues (Okano et al., 1998). There are also two isoforms of DNMT3A; 3A and 3A2, which are produced from alternative promoters (Chen et al., 2002). DNMT3A is expressed ubiquitously and is thought to target nuclear heterochromatin, whereas DNMT3A2 is expressed at higher levels and has been shown to localise to euchromatin. *DNMT3A2* expression is up-regulated in various ovarian and breast cancer cell lines, this is interesting because euchromatin encode single copy genes, which are known to be hypermethylated in cancer, although its presence has not been shown to induce hypermethylation as such (Chen et al., 2002).

The *DNMT3B* gene gives rise to up to eight isoforms (*3B1-3B8*) through splicing of exons 11, 22 and/or 23 in both the human and mouse genomes (Weisenberger et al., 2004). The DNMT3B C-terminus contains highly conserved motifs that are important in catalysing methylation. Splicing at exons 22 and 23 are thought to interrupt the catalytic domain functioning and for this reason it was thought that only DNMT3B1 and DNMT3B2 were capable of direct DNA methylation (Roberson et al., 1999). However, although the DNMT3B3 lacks an important motif in its catalytic domain its capacity to methyl transfer has been shown in human cells, although the murine Dnmt3b3 isoform is not thought to have this capability (Soejima et al., 2003; Chen et al, 2003; Aoki et al., 2001). The splice variant DNMT3B7 has also been linked to gene expression changes and CpG island DNA methylation (Ostler et al., 2007). Identifying the functions of DNMT3B isoforms is ongoing, in particular

understanding the role of those that have truncated C-termini and therefore are not able to directly methylate DNA. It is thought that these may still have a role through co-operating with activate DNMT3B variants.

5.1.3 Aberrant DNMT3B induced DNA methylation in cancer

Overexpression of DNMT3B has been identified in many cancers. The role of DNMT3B in tumourigenesis is thought to be its ability to co-operate in hypermethylation of CpG islands. This has been identified most significantly in cancers of the breast and colon (Roll et la., 2008; Nosho et al., 2009). Evidence that supports this has also been determined *in vivo* using an *APC* mutant mouse model. The *Dnmt3b1* isoform was overexpressed in the intestinal epithelium and subsequently induced a rapid increase in tumour growth in relation to methylation of TSGs (Linhart et al., 2007). In an earlier study, using gene targeting to 'knockout' total *Dnmt3b* expression in intestine cells, early tumour development was not initially inhibited but further progression to larger, macroadenomas was greatly reduced in the absence of DNMT3B (Lin et al., 2006).

Whether DNMT3B has a specific role in carcinogenesis or if its expression is a direct consequence is still debatable. It seems possible to suggest that the importance of DNMT3B presence in various cancers is tissue dependable, with a particularly significant role in colon cancers.

5.2 Aims

The progression from a normal epithelium to adenocarcinoma in human colorectal cancers occurs by the acquirement of multiple genetic mutations or epigenetic modifications and chromosomal anomalies. In chapter 4, $p16^{INK4a}$ mRNA and protein levels were shown to be elevated post $Braf^{V600E}$ expression in the crypt cells. This was followed by the growth of serrated adenomas that developed with the loss of $p16^{INK4a}$ expression. The aim of this chapter was to determine the mechanism/s involved in inactivating $p16^{INK4a}$, with particular reference to DNA methylation.

5.3 Results

5.3.1 Dnmt3b transcription increases post-^{V600E}Braf expression

The *Dnmt3b* mouse gene has 24 exons and exons 11, 22 and/or 23 can be differentially spliced (Figure 5.1A). It has been reported that splicing at these regions can give up to 8 alternative *Dnmt3b* transcripts (*3b1-8*) (Figure 5.1B) (Chen *et al.,* 2002; Weisenberg et al., 2004; Salle and Trasler 2006). To determine *Dnmt3b* expression levels in the *Braf^{V600E}*-expressing mouse gut, RT-PCR was performed. Two sets of PCR primers were developed to exploit the regions across the two possible splice sites. Primers were designed across exon 11, with the forward primer annealing within exon 10 and the reverse in exon 12. Either a 200bp or 150bp was produced depending on whether exon 11 was present or absent, respectively. Similarly primers were designed to amplify across exons 21 to 24; this would determine the level of splicing at exons 22 and 23 by the presence of 4 alternative sized products (261, 190, 142 or 72 base pairs). *Dnmt3b* is highly expressed in mouse ES cells and are essential to mammalian development (Chen et al., 2002).

Figure 5.1 *Dnmt3b* gene expression analysis in the mouse SI by RT-PCR. (A) The *Dnmt3b* mouse gene has 24 exons and can be differentially spliced in two regions of the gene; between exons 10-12 and exons 21-24. Primers were designed against the two regions; exons 10-12 = A & B, exons 21-24 = C & D, to distinguish alternative splice variants. The sizes of these products are shown in base pair (bp) (B) The alternative isoforms are denoted as 3b1 - 8 depending on the composed exons. Nomenclature taken from Salle and Trasler, 2006.
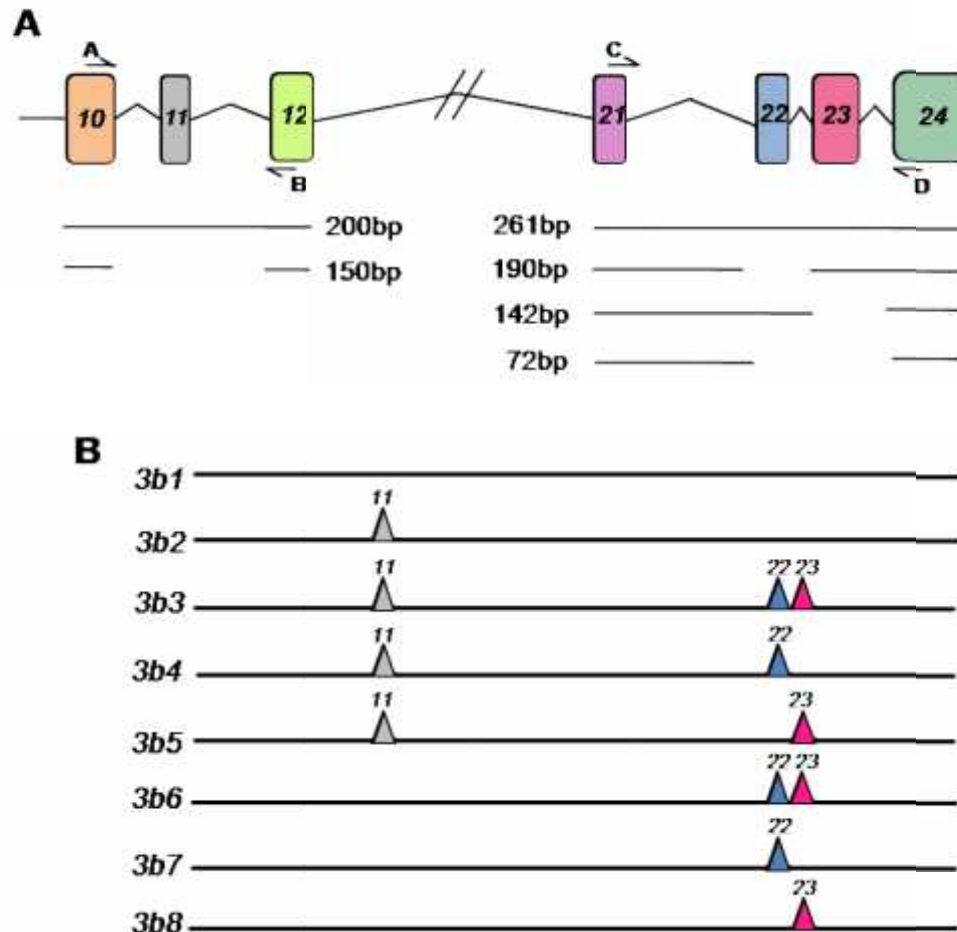
RNA/cDNA from mouse ES cells was used as a positive control for *Dnmt3b* expression; the cells were a gift from Dr Emma Stringer (Biochemistry Department, The University of Leicester).

cDNA used for analysis was made from RNA isolated from the duodenum. Successful amplification of both target regions was shown by *Dnmt3b* expression in the positive control (ES cell) (Figure 5.2). These cells were found to express full length *Dnmt3b1* and to a lower extent, the *3b6* transcript that does not contain exons 22 and 23 (Figure 5.2A). The wild-type and *Braf^V600E* experimental time course gut did not express the *3b1* transcript because only the 150bp PCR product was produced with primers A and B (Figure 5.2B). Instead they expressed the 3 transcripts that were identified as; *3b2, 3b3* and *3b4*. The splicing pattern did not change across the Braf^V600E time course. However, the levels of *Dnmt3b* transcripts were elevated across the *Braf^V600E*-expressing time course in comparison to the WT control, particularly at 1wk post-*Braf^V600E* induction. The most prominently expressed transcript was *3b3* and to a lower extent *3b2*. These are the two known transcripts identified in human cell lines (Weisenberger et al., 2004). It was originally presumed that *3b3* was an inactive form because it does not have a functional catalytic domain due to the absence of exons 22 and 23 (Aoki et al., 2001; Chen et al., 2003). However, one study has shown it is associated with hypermethylation of DNMT3B targets and DNA binding (Weisenberger et al., 2004).

5.3.2 Dnmt3b protein levels are elevated post-*Braf^V600E* expression

Dnmt3b protein expression was determined by western blotting and IHC. Protein

Figure 5.2 *Dnmt3b* gene expression in the mouse SI by RT-PCR. PCRs were set up using the primers in Figure 5.1 on cDNA reverse transcribed from RNA of WT mouse embryonic stem (ES) cells, WT SI and over the ^V600E*Braf* -expressing time course of 3 days - 10wks. ES cells were used as a positive control for *Dnmt3b* expression. (A) RT-PCR on cDNA from an ES cell and a 3dVE SI sample using primers for differential splicing in exons 10-12 (left) or exons 21-23 (right). (B) RT-PCR on SI cDNA from WT and the VE time course from 3days to 10wks. The presence of ^V600E*Braf* does not affect splicing at either region, but *Dnmt3b* has an increased expression in the ^V600E*Braf*-expressing SI time course compared to the WT. *Gapdh* PCR was used as a control.
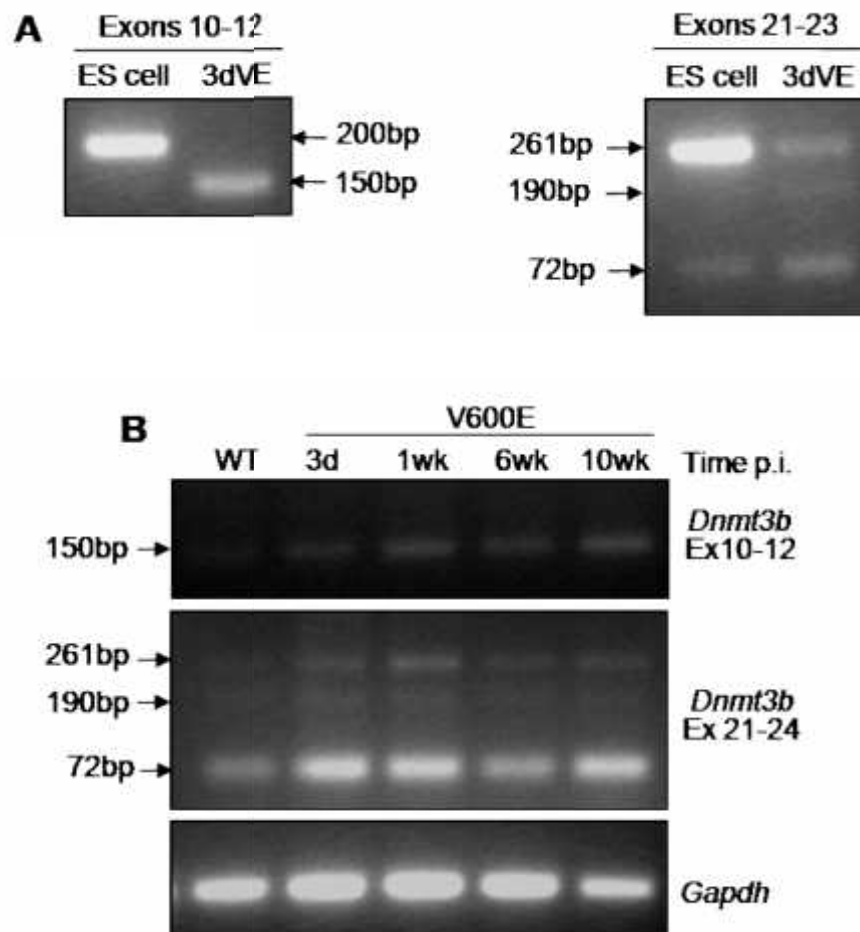
isolated from both wild-type (WT) and Dnmt3b homologous knockout (-/-) ES cells were used as positive and negative controls. Both sets of ES cells were provided by Christine Armstrong, (Department of Genetics, University of Leicester). Protein made from MEFs after 48 and 72hrs post-*Braf^V600E*-expression (using *Cre* expression) were also analysed as positive controls; these lysates were a gift from Maria Aguilar Hernandez, (Biochemistry Department, University of Leicester). All three positive controls produced the expected band at ~100kDa whereas the Dnmt3b^-/- negative control cells did not produce a band at any size (Figure 5.3). Smaller band sizes were also observed and these were lost in the Dnmt3b cells, but the origin of these smaller bands is not known as they are too small to be represented by any of the Dnmt3b splice variants.

Western blots were performed on two *Braf^V600E* small intestine experimental time courses (Figure 5.4). Protein lysates were made from SI tissue taken from the top end of the duodenum. As with the mRNA, three Dnmt3b bands were produced that seemed to represent the three Dnmt3b isoforms identified by RT-PCR (Figure 5.2A&B). Expression in the both controls (WT and Cre) was very low, as expected for differentiated, somatic tissue (Chen et al., 2002). Levels increased across the whole *Braf^V600E* time course from 3 days to 10 wks, with the exception of the 6 wk samples when Dnmt3b was reduced. The predominant band was at 88kDa whereas isoforms expressed at lower levels were at 90kDa and 92kDa. It is assumed that p88 corresponds to the 3b3 transcript, p90 to the 3b4 isoform and p92 by the 3b2 isoform.

Figure 5.3 Western blot analysis of Dnmt3b protein expression. Lysates were prepared from; Dnmt3b WT and homozygous knockout (-/-) mouse ES cells and mouse embryonic fibroblast cells (MEFs) after 48 and 72hrs of ^V600E *Braf* induction. ES cells & MEFs were used as positive controls to determine the specificity of the antibody. Western blots were analysed with an antibody for Dnmt3b and Erk2.
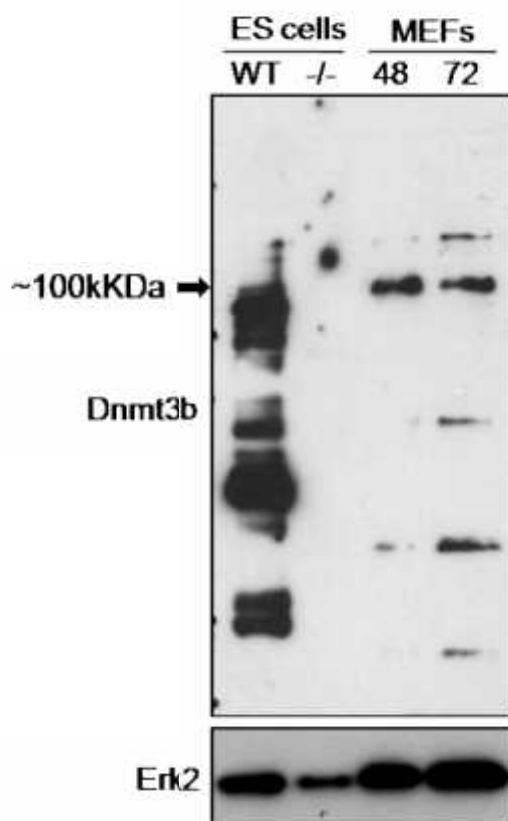
Figure 5.4 Western blot analysis of Dnmt3b protein expression over the ^{V600E}Braf - expressing time course. Lysates were prepared from the mouse SI over two alternative time courses and western blotted for Dnmt3b and Erk2. (A&B) All samples produced the three bands suggested to be the equivalent proteins to the mRNA products, these being 95kDa, 92kDa and 88kDa. Dnmt3b protein level is increased in the ^{V600E}Braf samples, partcularly at 3 days and 2wks. Expression of Dnmt3b is low in the Cre and WT samples suggesting up-regulation is a consequence of ^{V600E}Braf expression. The different band represent the predominant alternative splice variants.
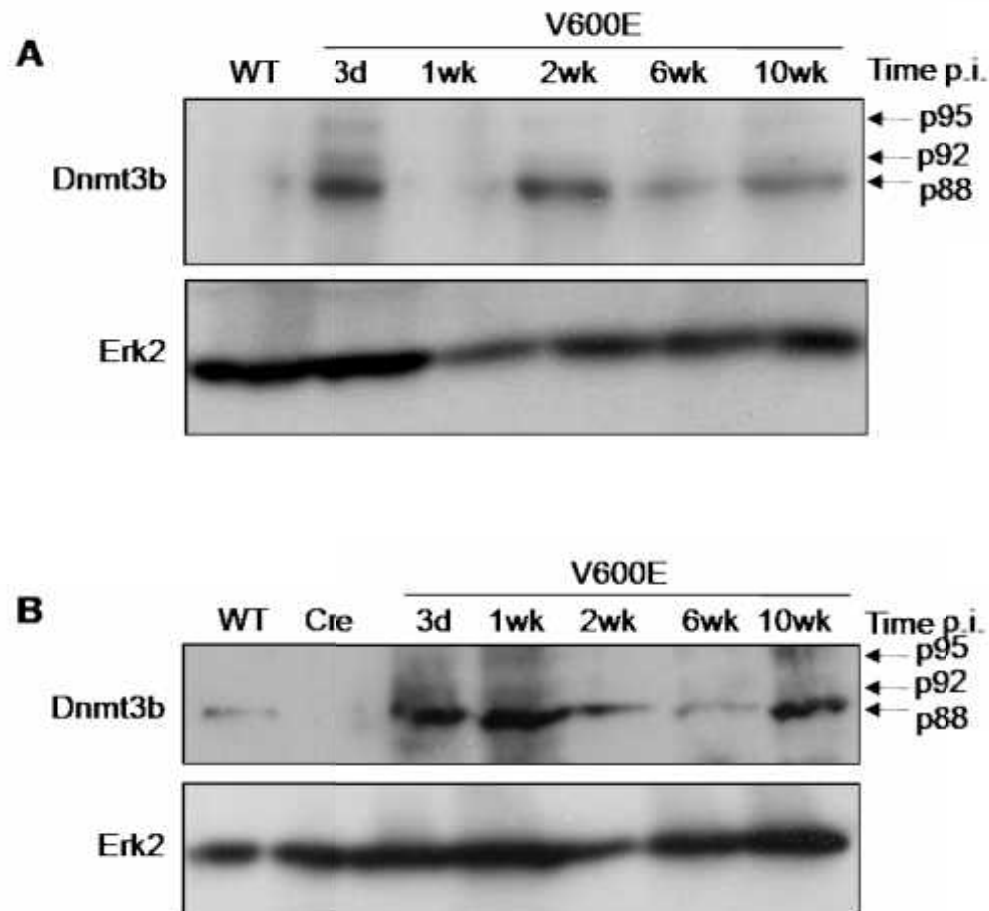
Immunohistochemistry was also performed on sections of the jejunum from both the controls and over the *Braf^V600E*-expressing time course (Figure 5.5). The pattern of Dnmt3b staining was similar to that of the western; it was highly expressed over the time course, most significantly at 3 days and 2 wks post- *Braf^V600E* expression but was low at 1 wk p.i. It was localised in the nucleus, as expected of a DNA methyltransferase.

Dnmt3b protein levels were also determined in the adenomas of the 12 wk *Braf^V600E* expressing small intestine by immunohistochemistry (Figure 5.6A&B). Nuclear expression was observed throughout the whole tumour epithelium and in the surrounding normal crypts. Adenomas from each section of the gut, the duodenum through to the ileum, were stained for Dnmt3b. All tumours showed strong, nuclear expression of Dnmt3b. In areas of high dysplasia, Dnmt3b was particularly strong in the nuclei.

As previously mentioned, due to the size of the adenomas both RNA and protein could not be isolated for further analysis by RT-PCR or western blot analysis.

5.3.3 The increase in Dnmt3b expression is Mek-dependent

To determine if Dnmt3b expression is regulated by the Mek/Erk pathway in the gut, Dnmt3b protein levels were analysed using 3 day Braf^V600E-expressing samples that were also treated with the MEK inhibitor PD184352. The regime of treatment is shown in Figure 5.7A. Protein expression was significantly reduced in the three Mek inhibited samples compared to the 3dayVE control (Figure 5.7B), suggesting

Figure 5.5 Dnmt3b immunohistochemistry (IHC) on mouse SI sections. Mouse jejunum sections from WT and the [V600E]*Braf*-expressing time course from 3 days - 10wks were stained with Dnmt3b and visualised under light microscopy. Bar = 100µm. Dnmt3b expression is increased in the [V600E]Braf samples, particularly at 3 days and 2wks. This follows the similar expression pattern as show in the western blot analysis.
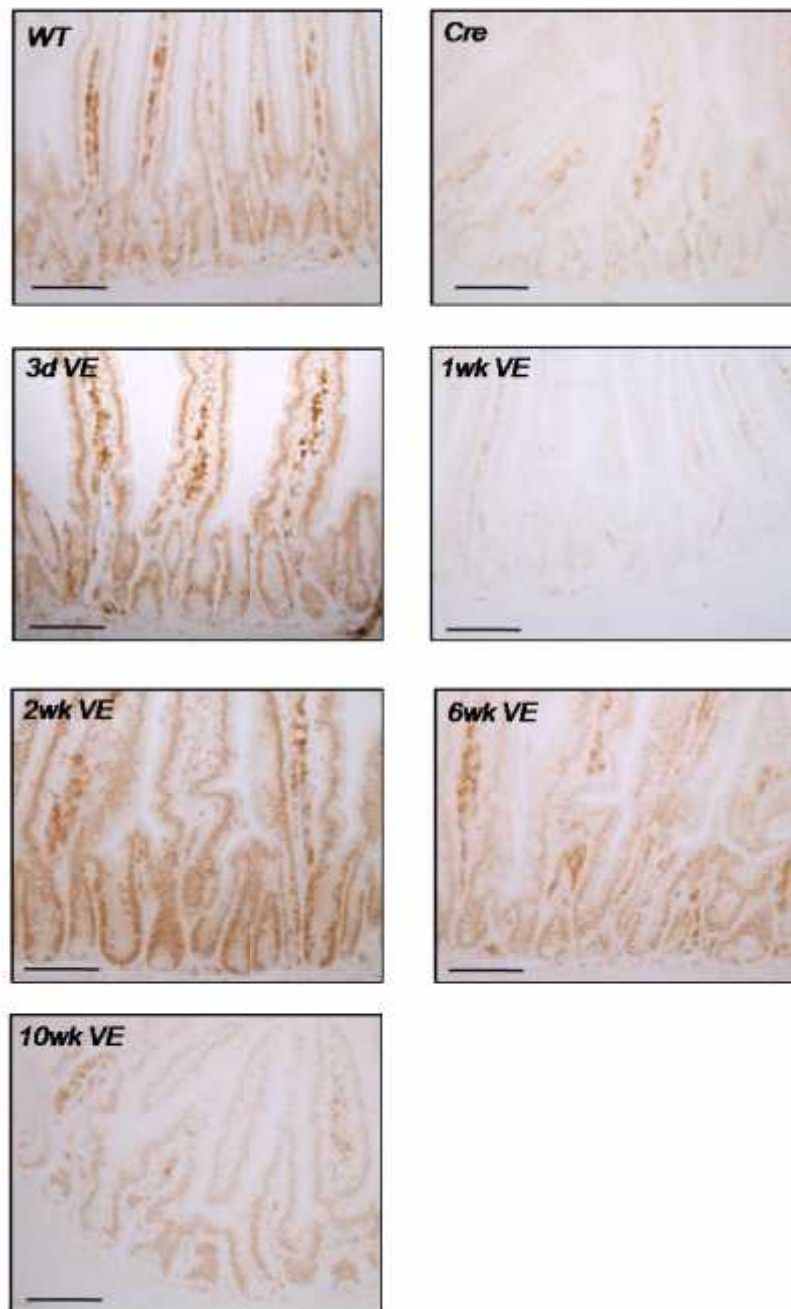
Figure 5.6 Dnmt3b is highly expressed in tumours from 12wk [V600E]***Braf*-expressing SI.** (A) H&E and Dnmt3b stained sections of a single tumour from a 12wk VE SI. The tumour is shown at increasing magnifications. Strong nuclear staining is evident. Scale bars; Top - H&E & Dnmt3b =200µm Bottom (left) Dnmt3b= 100µm, (right) Dnmt3b=50µm. (B) The 12wk VE SI has multiple tumours throughout the whole of its length. Tumours from sections 5, 4, 3 and 2 were stained for Dnmt3b. These all stained positively for Dnmt3b. Regions with particularly strong nuclear staining are highlighted with either arrows or a dotted line. Scale bars= 100µm.
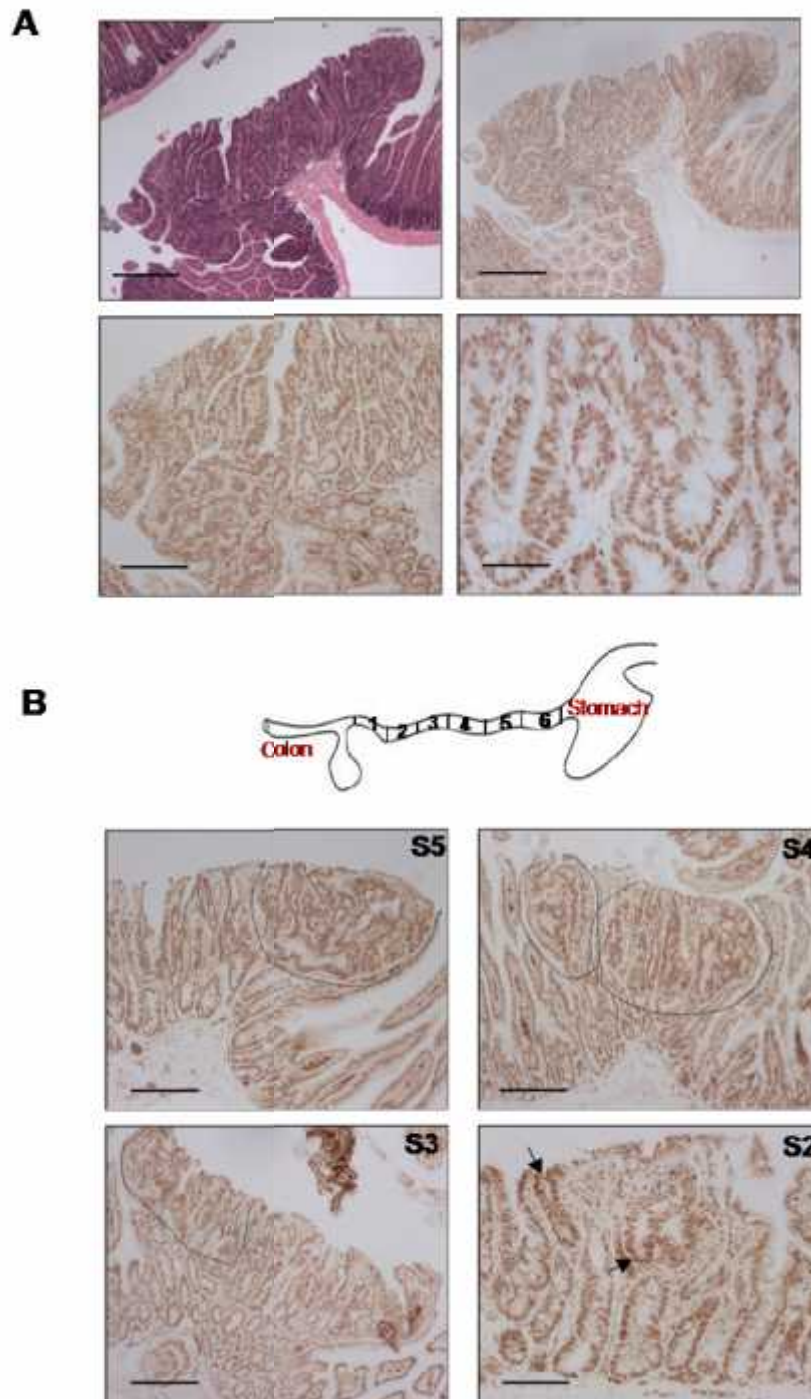
Figure 5.7 MEK inhibition reduces Dnmt3b expression at the protein level. (A) Mice expressing ^{V600K}Braf at 3 days were subjected to the MEK inhibitor PD184352 over a 3 day period. The regime of treatment is shown. (B) Levels of Dnmt3b were considerably reduced compared to the 3 day VE sample. The band size of the Dnmt3b protein in the PD184352 sample was also shifted slightly higher than that of the untreated 3day VE sample. Erk2 was used as a loading control. Protein lysates were provided by Dr Linda Carragher.

A

β-NF   β-NF+TM

0   1d   2d   3d

Time p.i

PD184352
200mg/kg/day

Harvest SI

B

3day V600E

PD   −   +

Dnmt3b

Erk2

118
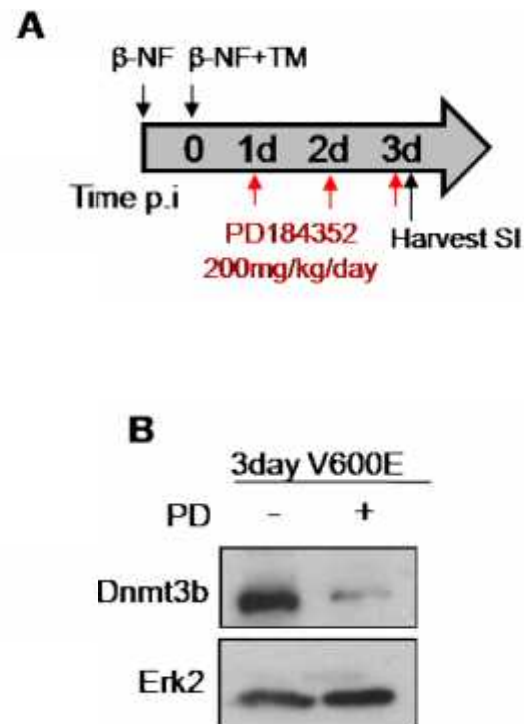
Dnmt3b expression is Braf*^{V600E}*-Mek-dependent.

5.3.4 Dnmt3a expression does not change post-Braf*^{V600E}* expression

Dnmt3a is an alternative DNA methyltransferase, because Dnmt3b was shown to be highly expressed in the *Braf^{V600E}* intestine the level of Dnmt3b was also investigated. The *Dnmt3a* gene can be differentially spliced, to give two alternative splice variants *3a* and *3a2* (Chen et al., 2002). Due to the up-regulation of *Dnmt3b* seen over the *Braf^{V600E}* expressing time course, the expression of *3a* and *3a2* were also determined (Figures 5.8 and 5.9). RT-PCR was chosen to analyse 3 alternative time courses for each transcript. Two forward primers were used to amplify the transcripts. One primer was designed to anneal to exon 6 of *3a*, which is not present in the *3a2* transcript (Figure 5.8A). Another forward primer was also designed to anneal to the *3a2* unique exon; this is within intron 6 of the *Dnmt3a* gene. Both PCRs used the reverse primer set in exon 8 of *Dnmt3a* (Figures 5.9A). Calnexin was used as a PCR control for total cDNA input. Both *3a* and *3a2* levels were found to be expressed over the control and experimental time points (Figures 5.8B and 5.9B). The average expression level for each control/time point was determined using ImageJ quantification of the RT-PCR data (Figures 5.8C and 5.9C). The data revealed that both *Dnmt3a* and *3a2* mRNA expression levels are consistently expressed over the experimental time course in comparison to the WT and Cre controls.

5.3.5 CpG islands in the Cdkn2a locus

The *Cdkn2a* locus is located on chromosome 4 in the M*us musculus* genome. It

119

Figure 5.8 *Dnmt3a* levels do not change in the mouse SI following [V600E]***Braf*-expression.** (A) Representation of the *Dnmt3a* gene with intron (gaps) and exons (boxes). Primers were designed to span an intron, as taken from Chen *et al*, 2002. (B) RT-PCR on cDNA reverse transcribed from RNA of the SI of WT, Cre and the [V600E]*Braf*-expressing time course over 3 days -11wks. One time course ran on a 1.8% agarose gel is shown. RT-PCR for *Calnexin* was used as a control for total cDNA input. (C) Image J quantification of RT-PCRs. Each sample n=3 expect for the 2wk VE where n=2 and 11wk where n=1. Each sample was normalised to *Calnexin* and the mean values were calculated and are represented in a bar graph. Standard deviations are shown as error bars. No statistically differences were seen between the controls and [V600E]*Braf*-expressing samples (3d P=0.35, 1wk P=0.62, 2wk P=0.88, 6wk P=0.82).
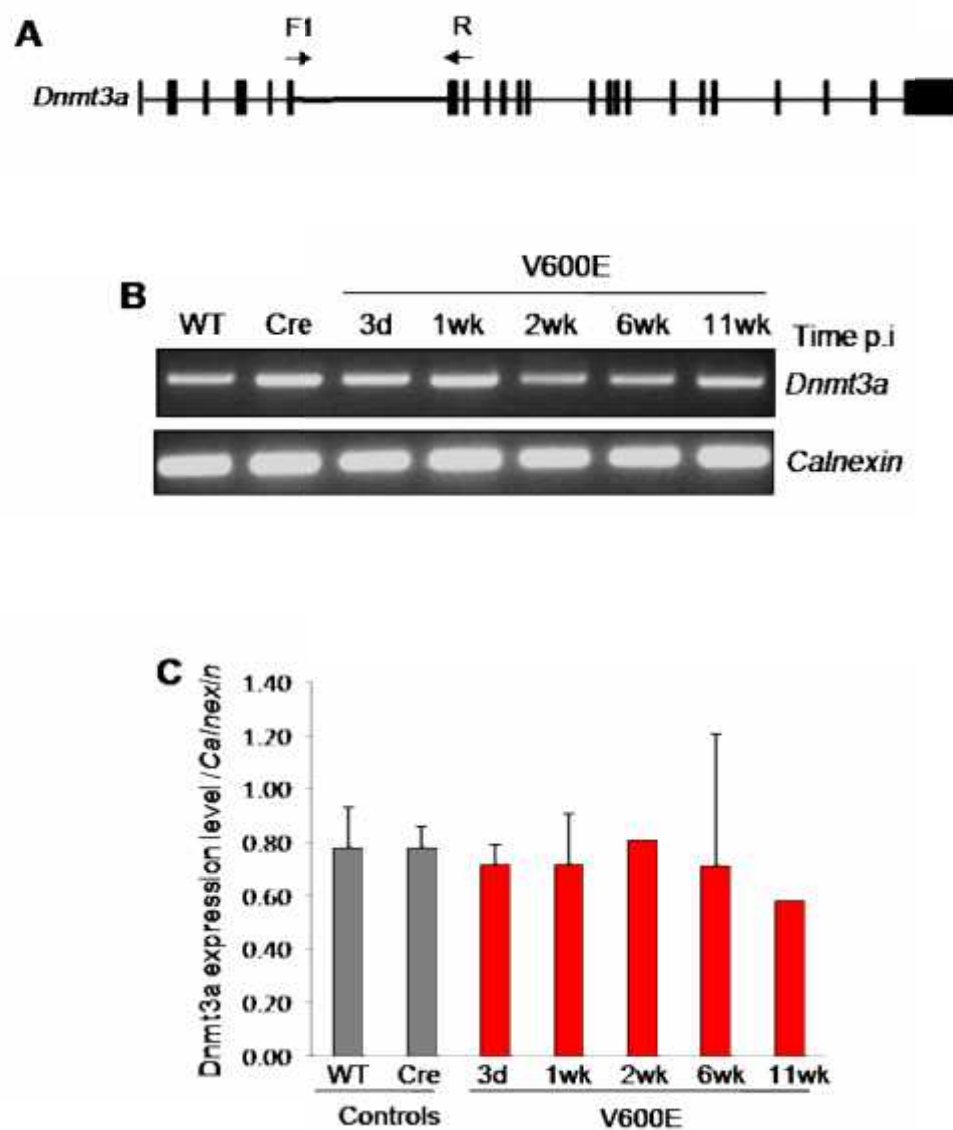
Figure 5.9 *Dnmt3a* alternative splice variant *Dnmt3a2* gene expression in the mouse SI by RT-PCR. (A) Representation of the *Dnmt3a* and *Dnmt3a2* gene differences. A forward primer was designed in an alternative exon (red) not present in the *Dnmt3a* gene. (B) RT-PCR on cDNA reverse transcribed from RNA of the SI of WT, Cre and the *[V600E]Braf*-expressing time course over 3 days –11 wks. A single time course is shown. *Calnexin* was used as a control for total cDNA input. (C) Image J quantification of RT-PCRs. Each bar represents the average of 3 samples (n=3) except for the 2wkVE where n=2 and 11wk where n=1. Each sample was normalised to *Calnexin* and the mean values were calculated and are represented as a bar graph. Standard deviations are shown as error bars. No statistical difference was seen between the controls and *[V600E]Braf*-expressing samples (3d P=0.26, 1wk P=0.38, 2wk P=0.23, 6wk P=0.13).
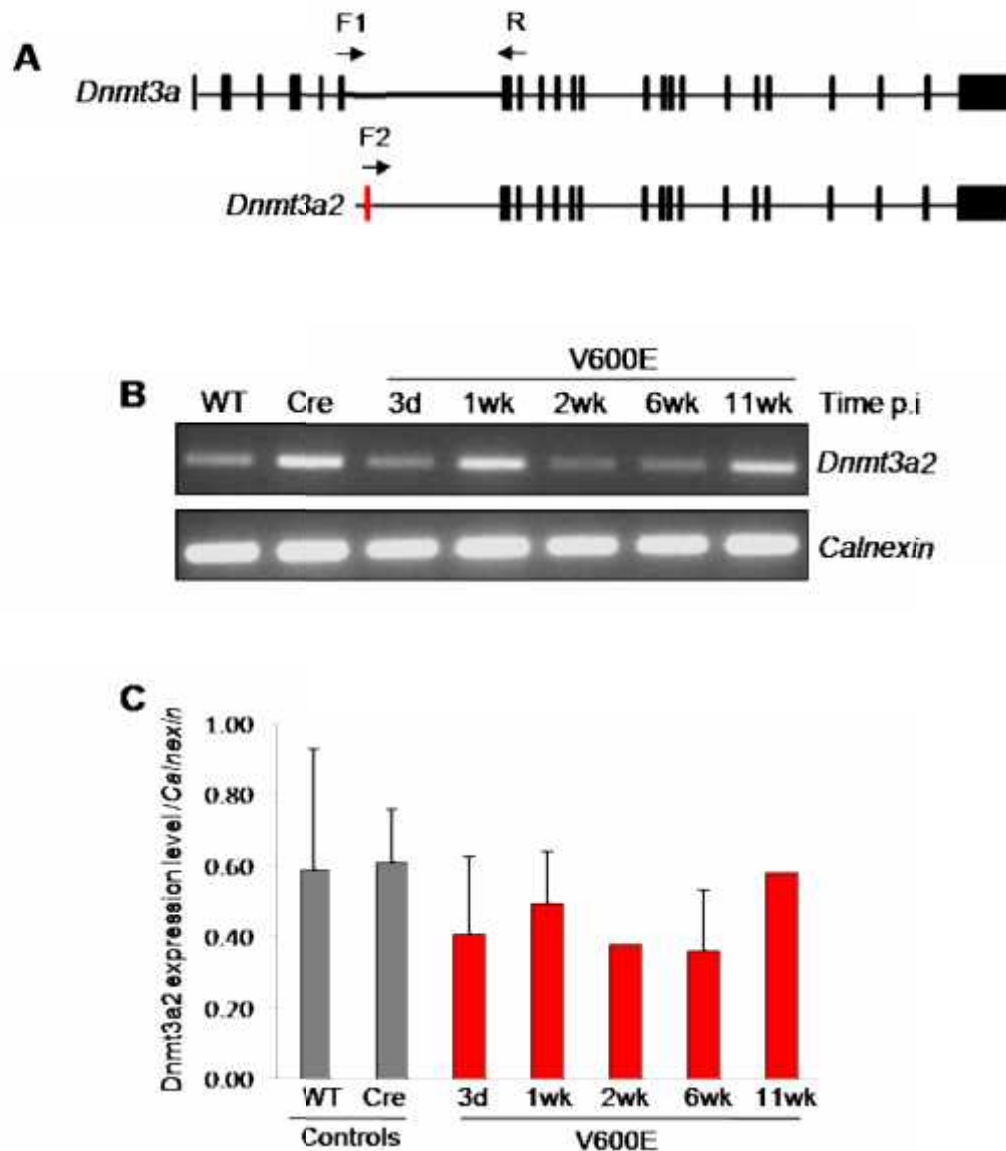
Figure 5.10 Representation of the *Cdkn2a* mouse locus that contains three CpG islands. The *Cdkn2a* locus encodes two genes *p19^ARF* (green) and *p16^INK4a* (blue) and each gene has its own promoter. *p16^INK4a* is comprised of exons; 1α, 2 and 3, whereas *p19^ARF* consists of exon 1β and also shares part of *p16^INK4a* exon 2. The *Cdkn2a* locus contains 3 CpG islands located in exons 1β, (purple) 1α (red) and 2 (orange).
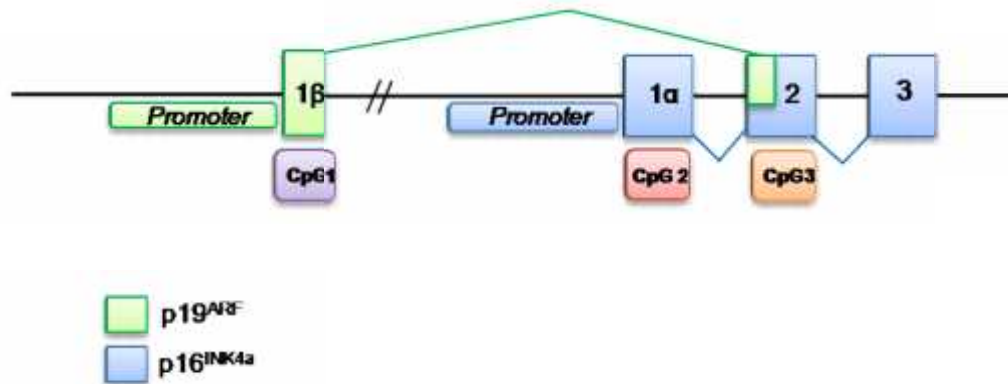
encodes two genes; *p16^INK4a* and *p19^ARF* (Figure 5.10). The *p19^ARF* gene contains exon 1β and shares a coding sequence in exon 2 of *p16^INK4a*, which has three encoding exons 1α, 2 and 3. Both genes are transcribed from separate promoters upstream of their corresponding 1st exons. Three CpG islands were identified in the mouse *Cdkn2a* locus; in exons 1β (CpG1), 1α (CpG2) and 2 (CpG3) using the CpG plot program from the European Molecular Biology Open Software Suite (EMBOSS) (http://www.ebi.ac.uk/Tools/emboss/cpgplot/).

5.3.6 Cdkn2a CpG2 and the p16^INK4a promoter methylation analysis

The loss of *p16^INK4a* expression was observed in the serrated adenomas arising in the Braf^V600E mice. Gene expression can be silenced by DNA methylation of regulatory CpG islands within genes. The silencing of tumour suppressor genes such as *p16^INK4a* is a common feature in the progression of cancers, typically by methylation of CpG islands in their promoters. Results from the Dnmt3b analysis has suggested a role for DNA methylation in this model of serrated CRC. In humans, the *p16^INK4a* CpG island 2 (CpG2) spans a region across the promoter and exon 1α of the gene, whereas in the mouse this CpG-rich region only spans across exon 1α. The methylation status of CpG2 of the mouse *p16^INK4a* gene was determined.

The initial route for methylation analysis utilised the methylation sensitivity of DNA restriction endonucleases. A number of restriction endonucleases have a cytosine next to a guanine (CG) in their recognition sequence. Digestion does not occur at these sequences when a 5-methyl group is present on the cytosine of the CpG. Several of these enzymes were found to have recognition sites in the *p16^INK4a* region

Figure 5.11 Analysis of the methylation status of 7 CpG dinucleotides within the promoter and exon 1α of the *p16^{INK4a}* gene using PCR and enzyme restriction digestion. (A) The promoter/exon 1α region has enzyme restriction sites for *Hhal* (purple), *Hpall* (blue), *Aval* (red) *and BstUI* (grey). The positions of these sites are shown by the coloured arrows. Post-digestion, DNA was amplified by PCR using primers (black arrows) that span across the promoter/exon 1α sequence as indicated. A 741bp product was produced when digestion was inhibited. (B) Genomic DNA from the epithelial lining of the mouse SI of WT, Cre and the ^{V600E}*Braf*-expressing time course of 3d - 6wk was digested with *EcoRI* with or without *Hhal, Hpall, Aval* and *BstUI* and then PCR amplified as described in A. (C) Levels of each PCR band were quantified using ImageJ and normalised against the value for the *EcoRI* digested sample. The WT sample was standardised to 1. Data is represented as a bar chart for one experiment.
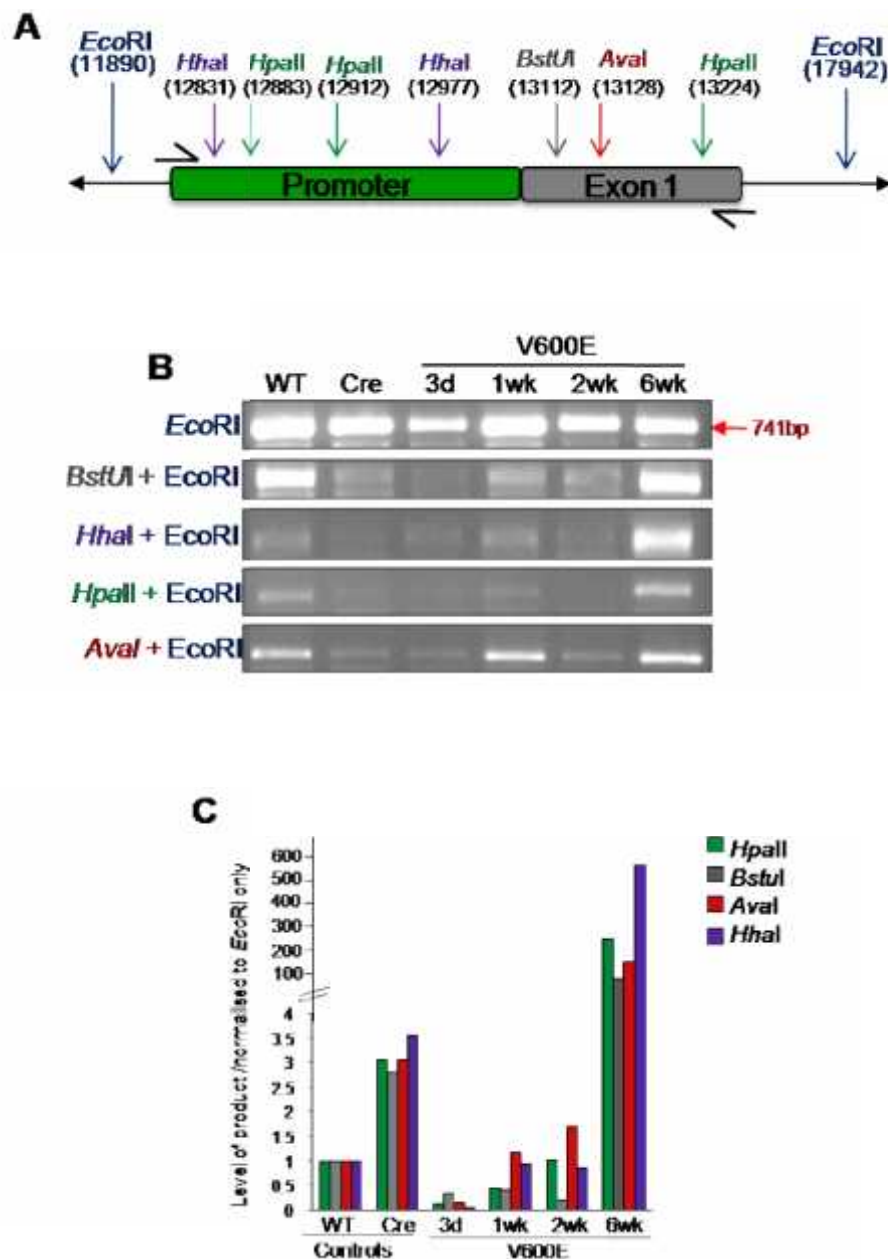
of interest; *HpaII* (3 sites), *AvaI* (1 site), *BstUI* (1 site) and *HhaI* (2 sites) (Figure 5.11A).

Genomic DNA was isolated from cells of the epithelial layer of the whole small intestine from both the controls (WT & Cre) and over the *Braf^{V600E}* experimental time course of 3 days - 6 wks. *EcoRI* sites were identified at 11890kb and 17942kb around the *Cdkn2a* locus; these co-ordinates surround a 6052bp region of the promoter and exon 1α of the gene (Figure 5.11A). The DNA was first subjected to *EcoRI* digestion to produce the 6052bp DNA fragment. The DNA was then re-digested using the methylation sensitive enzymes (*HpaII*, *AvaI*, *BstUI* & *HhaI*) (Figure 5.11B). Primers were designed to amplify the region containing the 9 enzyme restriction sites, which would produce a band of 741bp if the *EcoRI* digested DNA fragment was intact. Alternatively if CG sites were unmethylated, the DNA would be sliced and the 741bp would not be product would be visible.

Primary *EcoRI* digested DNA was amplified as a loading control for total input DNA. When ImageJ quantification was performed, the levels of the methylation endonuclease digested-DNA were normalised to the level of amplification from the *EcoRI* (single-digested) input level. The WT levels were set at 1.0 and fold-differences in other samples were normalised to this value.

At 3 days post-VE induction expression, DNA was greatly reduced for all the enzymes compared to the control suggesting there was a lack of methylation present at the CpG sites. The level of DNA was highest in the 6wk VE digested

samples, suggesting methylation was beginning to occur at the CpG sites within this region, particularly at the two *HhaI* CpGs.

These results do not entirely confer with what would be predicted, since at 3 days crypt cell proliferation is occurring and expression of p16^{INK4a} is low and therefore DNA methylation of the *p16^{INK4a}* would be expected to be low. Also, at 6 wks p.i. when *p16^{INK4a}* levels are elevated, DNA methylation at this locus would not be expected to be present. The silencing of genes is a complex process and involves methylation of histones as well as DNA. In addition, the number of CpG dinucleotides analysed by this method is low and only 3 of these reside in the recognized CpG island in exon 1α. Only 7 out of a total 46 CpGs within CpG 2 were analysed here and 2 out of the 4 enzymes chosen had more than one restriction site in close proximity. This meant their products could not be distinguished because they would be of similar size and therefore methylation at none or both sites could only be determined.

5.3.7 Bisulphite Conversion and sequencing of CpG2

Methylation analysis by the restriction endonuclease method did not prove to be sufficient or sensitive enough to gain a clear view on the status of *p16^{INK4a}* methylation. For this reason an alternative approach was taken using bisulphite conversion and sequencing, which allows for the analysis of the methylation status of each individual CpG dinucleotide. Bisulphite conversion is the chemical removal of all unmethylated cytosines in a DNA sequence followed by the replacement with uracil nucleotides, leaving all methylated cytosines unchanged. This allows for the

detection of methylation differences between DNA strands, by altering the DNA sequence.

DNA from the epithelial lining of the small intestine for both controls and over the experimental *Braf^{V600E}* time course of 3 days to 6 wks was bisulphite converted. For analysis of 12 wk VE adenoma DNA, fresh tissue was not available. Instead, the tumour epithelium from 4 separate adenomas was microdissected from paraffin-embedded sections. DNA was extracted from the scrapings and bisulphite converted. Colon sections from the same mouse were also processed alongside the tumours as a control for endogenous methylation levels because *Braf^{V600E}* expression is low in the colon using the inducible Ah*Cre*ER^{T} strain.

PCR using a high quality *Taq Polymerase* was used to amplify the DNA using primers specific for bisulphite converted DNA; these were designed by MethPrimer software (Li and Dahiya, 2002). The PCR products from the tumours were often re-amplified by PCR, using the same primers, to obtain a higher concentration of products for sequencing. The PCR products were sent for sequencing by the Protein Nucleic Acid Chemistry Laboratory (PNACL) at University of Leicester (http://www.le.ac.uk/mrctox/pnacl/). Sequencing results were given in the format of chromatograms. These represent the amplified sequences of PCR products formatted so that the DNA base sequences can be revealed, which are indicated by peaks for each separate base. A typical chromatogram is shown in Figure 5.12. Based on the level of each peak, the level of methylation was defined as being unmethylated or methylated to a low, medium or high level.

Figure 5.12 Definition of the levels of CpG methylation following bisulphite sequencing of exon 1α (CpG2). DNA sequencing chromatograms from a 46bp coding region of exon 1α (CpG2) from a Cre and microdissected tumour from a 12wk VE sample. Methylation is partial, with the presence of both a red thymidine (unmethylated) peak and a blue cytosine (methylated) peak. The level of methylation (height of blue peak) varies at each CpG compared to the unmethylated peak. To define the status of methylation for each CpG a colour code was used; Orange = Height of C peak is less than T peak. Red = Height of C peak is equal to the T peak. Black = Height of C peak is greater than T peak. For both samples 7 CpGs are shown and the level of methylation is represented by the colour.
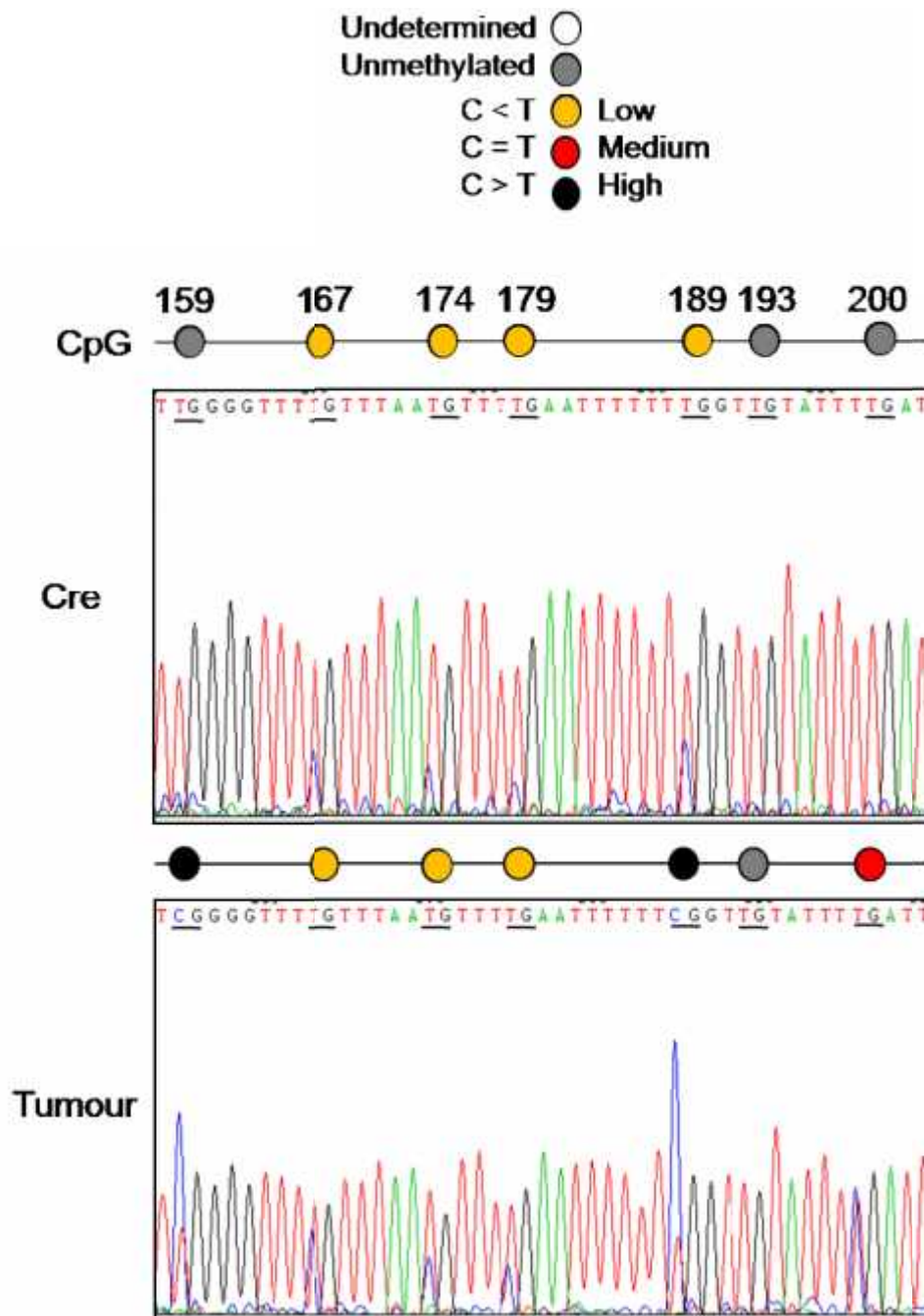
Bisulphite sequencing was performed using primers against the CpG island in exon 1α of *p16^INK4a*. The methylation status of a number of CpGs was changed between the controls and the *Braf^V600E*-experimental samples, but in particularly for the 12 wk tumour DNA (Figure 5.13). The methylation levels seen at most CpG sites was heterogeneous, because two peaks were present; one for cytosine (C) and one for thymidine (T). However the size of peaks and therefore the level of methylation varied. For this reason a staging system was produced to identify the level of methylation at each CpG position (Figure 5.12). If the thymidine peak was larger than the cytosine the methylation was classed as low (yellow). If the cytosine peak was the same size as the thymidine then this was classed as medium (red) and if the cytosine was greater than the thymidine this was classed as high (black).

Both controls and *Braf^V600E* expressing DNA at 3 days – 2 wks contained CpGs with only a low level of methylation (yellow). Interestingly the *Braf^V600E* samples at early time points post-induction (3 days - 2 wks) lost methylation at several CpGs close to the transcription start site (TSS) when compared to the controls. The 2 wk VE time point had the least number of CpG methylated sites, this corresponds to the time point when *p16^INK4a* expression is high. Two CpGs were methylated to a much greater extent in the 6 wk VE compared to the early time course samples. This suggests hypermethylation of *p16^INK4a* CpG2 is initiated around 6 wks of *Braf^V600E* expression, supporting the restriction digestion data. Even more evident was the high levels of methylation identified at a number of CpGs in the tumour samples compared to the controls and time course samples. Up to four CpGs highly

Figure 5.13 Bisulphite sequencing results for the *p16*[INK4a] CpG island 2. (A) Diagram of the *p16*[INK4a] gene and its relevant CpG islands. The transcription start site is shown by the arrow. (B) Genomic DNA from the epithelial lining of the mouse SI of WT, Cre and the [V600E] *Braf*-expressing time course of 3d - 6wk was bisulphite converted and sequenced. For the 12wk VE sample, DNA was extracted from paraffin-embedded sections from; the colon, normal region as well as micro-dissected tumours T1 – T4. Exon 1α contains 20 CpG dinucleotides. Using the sequence chromatograms and based on the coding system from Figure 5.12 the methylation status of each CpG was determined.
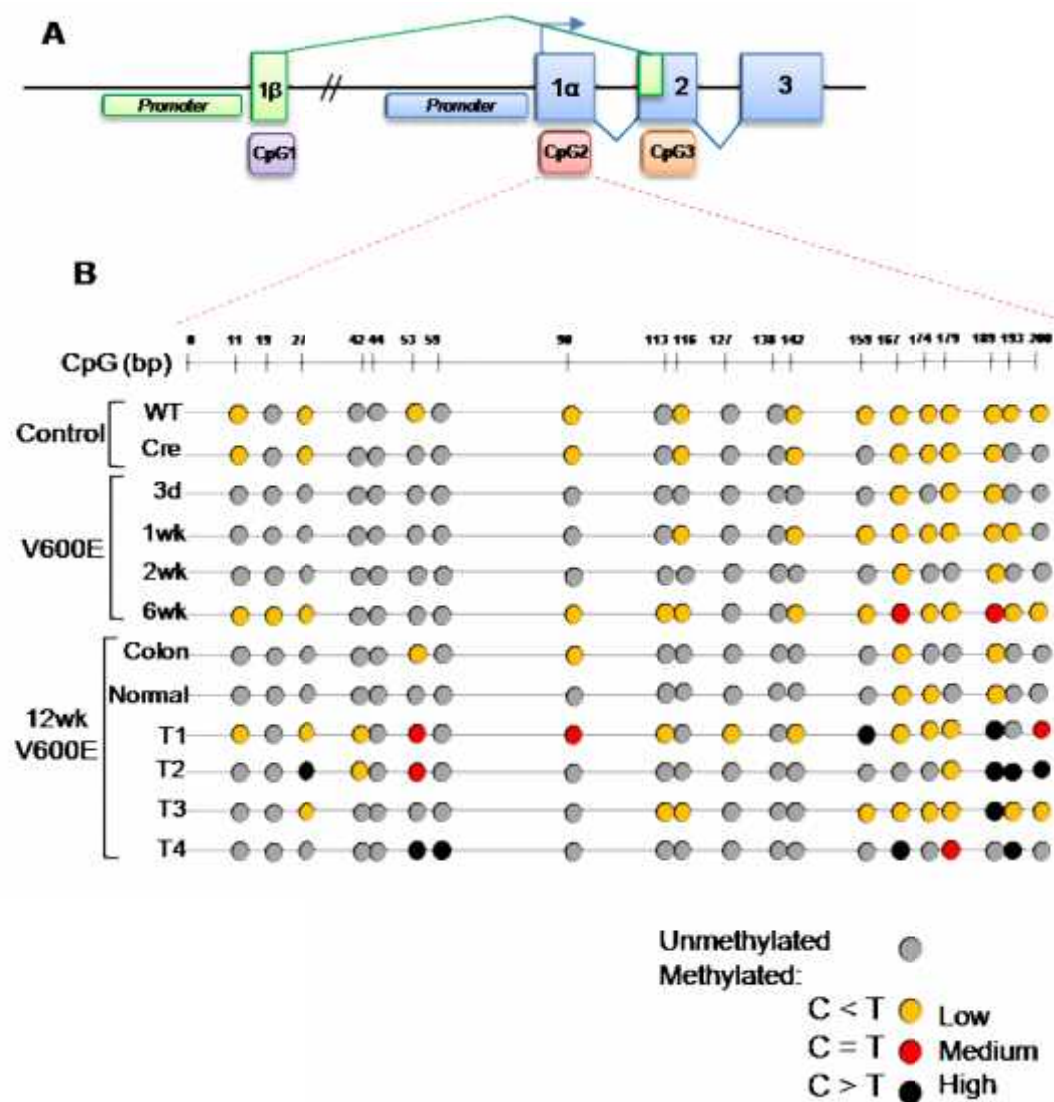
methylated compared to only low levels in the controls.

5.3.8 Bisulphite Conversion and sequencing of p16^INK4a^ promoter CpGs

Although not identified as a CpG island, the promoter region of *p16^INK4a* contains some CpGs. Therefore the methylation status of these CpGs were also identified.

Initially one set of primers was attempted to amplify the promoter region as a whole. However, a product could not be obtained. Instead several sets of primers were used to amplify the promoter in smaller fragments. Of the 26 CpGs in the promoter region, the methylation status of between 13 - 18 CpGs was determined for all the samples (Figure 5.14), of these all the CpGs were found to be unmethylated by the presence of a Thymidine (T) peak that was in place of the original unmethylated cytosine (C). The tumour DNA samples had the least number of CpGs successfully sequenced (13/26).   Overall, the *p16^INK4a* promoter does not become hypermethylated in the *Braf^V600E*-expressing small intestine epithelium, even in the presence of adenoma development, when *p16^INK4a* expression is absent.   However, a complete analysis of all CpGs in the promoter region could not be identified. This is because of a problem with both amplifying the regions as well as the sequencing. Multiple primers, PCR reagents and cycling changes were made but successful sequencing could not be obtained for the remaining CpGs.

5.3.9 Genetic analysis of the p16^INK4a^ gene

Genetic DNA point mutations are involved in the progression of human cancers, such as mutation of the *APC* and *KRAS* genes in CRC. For this reason the promoter

Figure 5.14 Bisulphite sequencing results of the *p16*[INK4a] promoter.
(A) Representation of the *Cdkn2a* locus. The relevant CpG islands are denoted as CpG1, 2 and 3. (B) Genomic DNA from the epithelial lining of the mouse SI of WT, Cre and the [V600E]*Braf*-expressing time course of 3d - 6wk was bisulphite converted and amplified using primers against the promoter region. For the 12wk VE sample, DNA was extracted from paraffin - embedded sections from the colon and micro-dissected tumours; T1 – T5 and processed for sequencing. The *p16*[INK4a] promoter has 26 CpG dinucleotides. Using the sequence chromatograms and based on the numbering system from Figure 5.12 the methylation status of each CpG was determined.
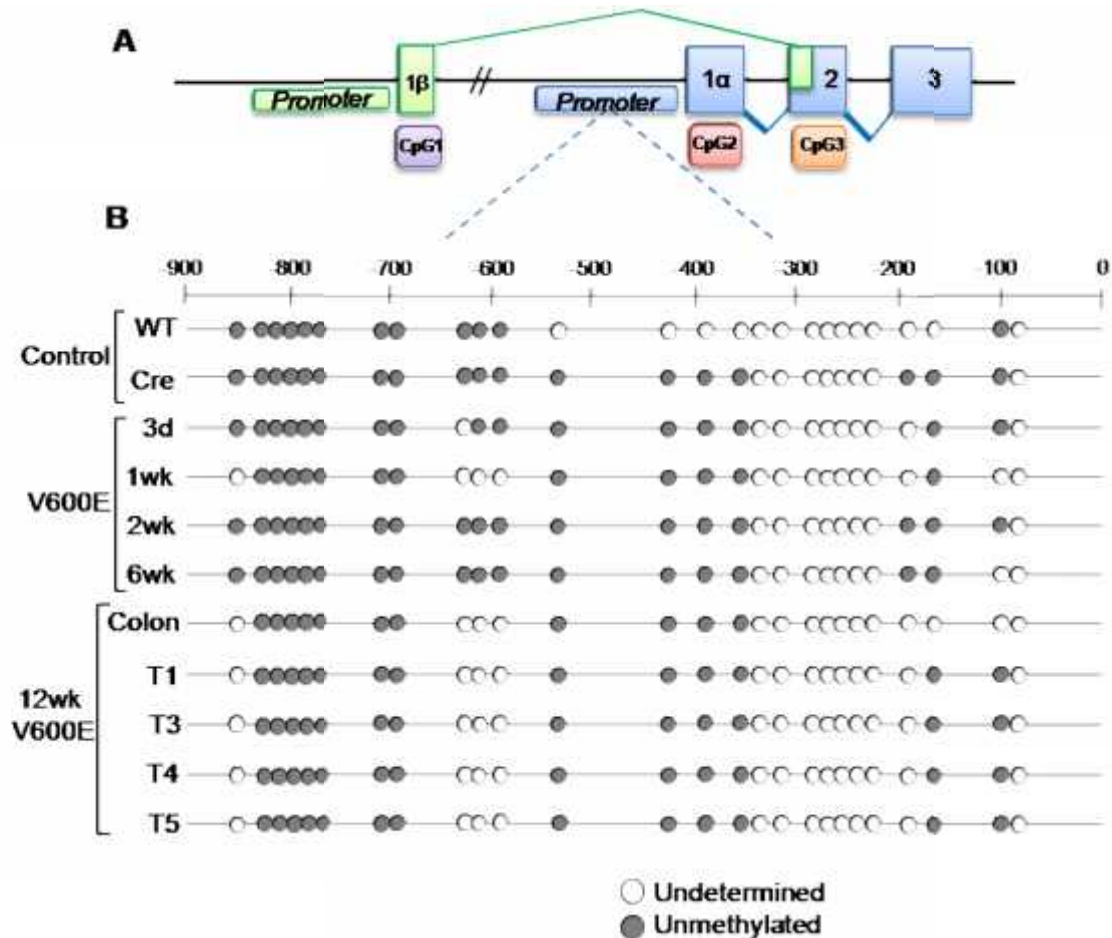
and 3 encoding exons of $p16^{INK4a}$ were sequenced to determine whether any such

mutations corresponded to the absence of $p16^{INK4a}$ expression and growth of the

adenomas at 12 wks p.i.

DNA was extracted from paraffin-embedded SI tissue sections from WT and 12 wk

VE sections containing adenomas. PCR was performed using primers designed to

amplify the promoter and exons 1α, 2 and 3 of the $p16^{INK4a}$ gene. The products were

then isolated and sequenced.

Two single nucleotide changes were identified in the promoter and exon 1α in the

12wkVE sample (data not shown). To confirm whether this genetic mutation was

induced post-$Braf^{V600E}$ expression, DNA from the liver that does not express

$Braf^{V600E}$ and sections of normal SI epithelium, from the 12wkVE were also analysed

by PCR and sequencing. DNA from both tissues contained both nucleotide changes,

suggesting these are not mutations corresponding to adenoma growth but

polymorphisms in this particular mouse. Overall, no genetic mutations were

specifically detected in the tumours.

5.3 Discussion

RT-PCR was revealed as a sound method to determine the expression of different

Dnmt3b splice variants. The presence of both *Dnmt3b1* and *3b6* spliced variants in

ES cells has previously been demonstrated (Chen et al., 2002). These transcripts were not expressed in the mouse small intestine; instead *3b2*, *3b3* and *3b4* spliced variants were identified, which supports previous data on mouse somatic tissue expression (Weisenberger et al. 2004). Of the expressed isoforms identified, only *3b2* has an intact catalytic domain giving it enzymatic activity and the ability to directly methylate DNA. The *3b3* and *3b4* are thought to act as co-regulators of DNA methylation (Okano et al., 1999; Aoki et al., 2001). The *3b3* transcript was the most prominently expressed transcript in the small intestine and was up-regulated by Braf[V600E]. The potential consequences of high expression of this catalytically inert form of Dnmt3b, is unclear because this isoform is not thought to have the required catalytic domain to induce DNA methylation but is instead thought to be an active accessory to the process. The human *DNMT3b3* isoform has been identified as the predominant isoform in normal fibroblasts and bladder cancer cell lines and its expression corresponds with methylation of DNMT3B target sequences (Wiesenburger et al., 2004). The Mek-inhibition data suggests Dnmt3b activation is Mek-dependent and previous studies have shown Dnmt transcription is induced by Mek-Erk signallying so these data would be consistent with this.

In addition to this, protein expression by both western blotting and immunohistochemistry revealed similar results to the RT-PCR. Levels were high in the early Braf[V600E] time points followed by a reduction at 6 wks p.i. Although interestingly, Dnmt3b expression was much greater by protein analysis compared to the mRNA levels detected. This has previously been documented in a study on

colon tumours, where 54% of tumours analysed showed an increase in DNMT3B

expression at the protein levels, only. This suggest post-transcriptional regulation of

DNMT3B could be key to its methylation properties in this form of cancer (Huidobro

et al., 2012). The previous chapter discussed the onset of $p16^{INK4a}$-induced

senescence over the time course from as early as 1wk post-$Braf^{V600E}$ expression.

This raises questions of how senescence and methylation can co-exist. The link

between senescence, high $p16^{INK4a}$ expression and yet high Dnmt3b expression is

not an obvious one. It has been shown that methylation of unmethylated CpG island

such as in the $p16^{INK4a}$ gene, can be rapidly induced by the addition of *SssI*

methyltransferase enzyme (Fatemi et al., 2005). When taking into consideration

most CpG islands in somatic cells are unmethylated even in the presence of

DNMTs, this suggests there is a mechanism through which DNMTs are controlled

and targeted to specific loci. In this model it would seem there are two possibilities as

to how this could occur. Firstly, *Dnmt3b* is immediately up-regulated post-$Braf^{V600E}$

(3days) when proliferation is occurring. This may represent a pro-proliferation role

that relates to its primitive role in ES cells when it is targeted to methylate genes

involved in tumour suppressor pathways. At ~2-6wks when crypt senescence is

peaking, levels of Dnmt3b are also high, which correlates with a loss of proliferation

and senescent induction. This would suggest Dnmt3b is not targeted to the DNA to

mediate *de novo* methylation.   Secondly, at the $p16^{Ink4a}$ locus Dnmt3b is activated

through protein-protein interactions such as with the Polycomb repressor complexes

(PRC) 1 and 2. The PRC2 complex has a catalytic protein component known as

Ezh2, that is thought to recruit Dnmt3b to DNA for methylation. It is possible these

factors are not up-regulated in the crypt cells at the senescent time points and

therefore Dnmt3b is elevated but not actively methylating DNA.

A rise in Dnmt3b at 10wks post-VE induction is observed and levels remain high in the adenomas. At this stage Dnmt3b could be targeted to suppress senescent regulators such as *p16^INK4a*, aiding in proliferation. This is consistent with previous reports showing Dnmts are transcriptional targets of the Erk pathway.

A restriction endonuclease PCR method was a starting point for investigating DNA methylation of the *p16^INK4a* gene. Initial results suggested the promoter/exon 1α was unmethylated, although results were based on analysis of only 7 out of 46 unmethylated CpGs. However further investigations using bisulphite sequencing revealed hypermethylation at exon 1α but not in the promoter in CpG2 , from as early as 6wks post-*Braf^V600E* expression but most significantly in the 12 wk VE adenomas (Figure 5.14). The CpG methylation status of CpG2 was identified for four adenomas. Each of these showed a different pattern and level of methylation at each CpG, which might correspond to the different stages of tumour development, i.e. the percentage of mutant cells in the tumour cell population. Alternatively, those with fully methylated CpGs might have *p16^INK4a* methylation on both alleles. The majority of methylated CpGs were located at the start of the exon near to the TSS. Although ~5-7 of CpGs were identified as being hypermethylated, low levels of CpG methylation are capable of altering gene expression (Cassandra et al., 2008).

The mouse *p16^INK4a* promoter region was not identified as a CpG island by the CpG

plot in EMBOSS. However in the human *Cdkn2a* locus the CpG island in exon 1α extends ~500bp into the promoter. For this reason the methylation status of the CpGs in the promoter were determined. Difficulty in determining the methylation status of several CpGs was found for the promoter region in all samples and more often with the tumour DNA. One particular region, ~600kb from the transcription start site (TSS), contained 3 CpGs that could not be sequenced using the tumour DNA. This is most likely due to the processes by which the tumours were microdissected, since the scraping process could have caused shearing of the DNA. Also the amount of DNA isolated was very small following both DNA extraction and bisulphite conversion. In addition, PCR products were often lost during the Qiagen clean-up stage and following repeated PCR cycles. Interestingly an even larger region, ~200-350kb from the TSS could not be sequenced for any of the samples. This region contained 8 CpGs that were in close proximity to one another. A number of primer sets were used to amplify this region that were unsuccessful at either producing a product or were not suitable for sequencing, for unknown reasons.

In conclusion, DNA methylation is up-regulated in the CpG island of exon 1α of $p16^{INK4a}$ particularly in tumours arising in mice at 12 wks following $Braf^{V600E}$ expression. This epigenetic alteration appears to be the key mechanism for loss of $p16^{INK4a}$ expression and adenoma progression, as opposed to the acquisition of any genetic mutations. The next stage is to determine the regulatory mechanisms involved in the silencing of $p16^{INK4a}$ in these tumours.

6. Gene regulation at the *Cdkn2a/b* loci post-*Braf*^{V600E} expression

6.1 Introduction

6.1.1 Histone modifications in epigenetic gene regulation

Similar to DNA methylation, histone modification is also an epigenetic mechanism that controls gene expression. DNA within the cell nucleus is tightly condensed into chromosomes. The chromatin itself is made up of nucleosomes; which are histone cores wrapped in ~200bp of DNA (Figure 6.1). These histone cores contain eight histone (H) proteins of which there are four types; H2A, H2B, H3 and H4 (Wolffe. A., 1998). The histones H1 and H5 also exist but are not found in the histone core instead they link the histone core to the DNA, in order to control the amount of DNA linked to each histone. Each histone protein has an N-terminal 'tail' of amino acids that is targeted for covalent modification such as; methylation, acetylation, phosphorylation, poly(ADP)-ribosylation and ubiquitination (Sparmann and Lohuizen., 2006). These modifications each have diverse effects on chromatin structure. Although the control of gene expression by chromatin remodelling is not well understood, the effects of some specific histone modifications have been characterised. For instance, on histone H3, both tri-methylation of lysine 4 (H3K4me) and acetylation of lysine 14 (H3K14ac) represent regions of active gene expression, whereas tri-methylation on lysine 9 (H3K9me3) and tri-methylation on lysine 27 (H3k27me3) are associated with repressed chromatin and gene silencing (Hublitz et al., 2009). Depending on the histone/histone modification, the chromatin structure is altered to inhibit or allow proteins access to the DNA, which is a key factor in influencing gene expression patterns.

Figure 6.1 Histone modification in eukaryotic cells. (A) Nucleosomes, are structures consisting of a histone core and coiled DNA. The histone core contains 8 histones and around 200bps of DNA coiled around the core. There are 4 alternative core histones; 2A, 2B, 3 or 4. The DNA is linked to the histone core by histone 'linkers'. There are 5 alternative histone modifications; methylation (Me), acetylation (Ac), phosphorylation (P), poly(ADP)–ribosylation (Po) and ubiquitination (Ubi). Their roles allow for the activation or repression of genes within their associated DNA. (B) DNA is packaged into Nucleosomes that are then tightly compacted together as chromatin, which then further coils on itself to form nuclear chromosomes.
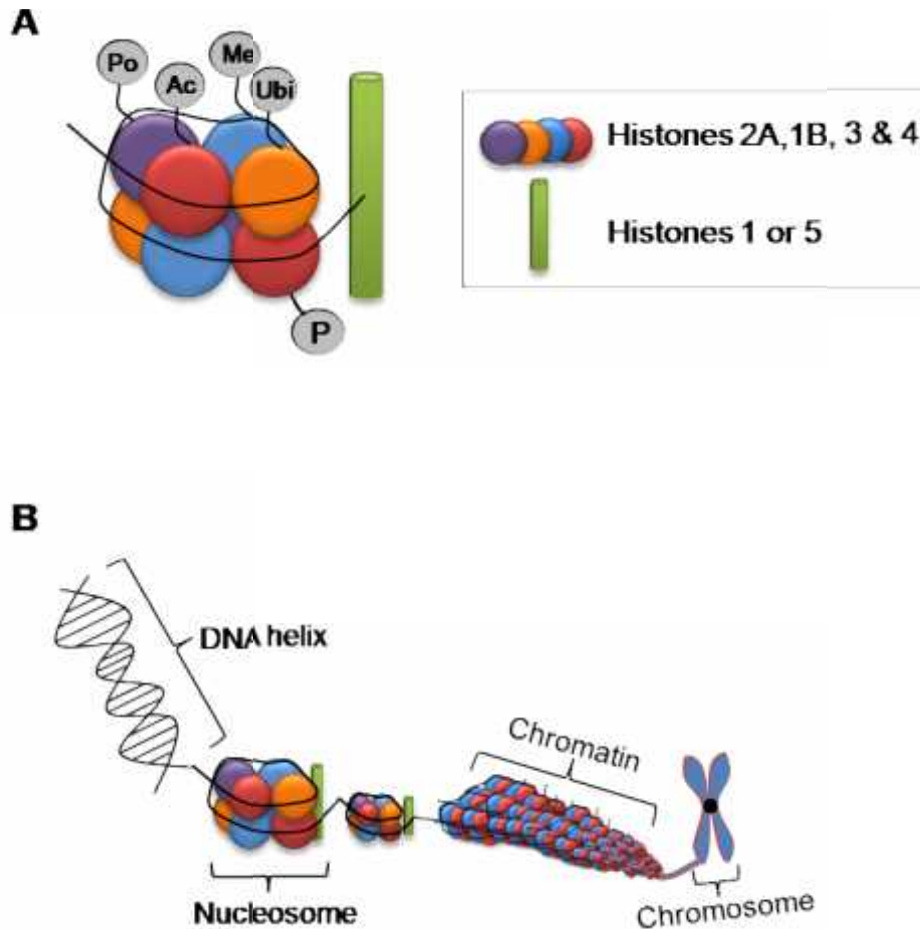
6.1.2 Polycomb group protein (PcG) complexes

Regulation of histone modifications is extremely important in gene expression during developmental processes in both prokaryotes and eukaryotes. As mentioned above these mechanisms have evolved to either repress or allow gene expression. One particular class of proteins has been identified that is involved in regulating repression of chromatin and these are known as the Polycomb group proteins (PcG) proteins. Their role was first established through studies on *Drosophilia melanogaster* in the repression of key developmental genes (Brock and van Lohuizen, 2001). It was soon established that the proteins could be divided into two groups by their association with one another into complexes. These are known as Polycomb group complex 1 and 2 (PRC1 & PRC2). The PRC1 complex is quite diverse in its isoform content, although the core proteins are defined as; Polycomb (Pc), Polyhomeotic (PH) Posterior sex comb (Psc) and Sex combs extra (Sce). In mammalian genomes there are multiple alternative homologues to these proteins including, Chromobox (CBX) and B-cell specific Moloney murine leukaemia virus intergration site 1 (BMI1) (Figure 6.2) (Ringrose and Paro., 2004).

The PRC2 complex is composed of four main core proteins; Enhancer of zeste (Ez), Suppressor of zeste 12 (Suz12), Extra sex combs (Esc) and the Nucleosome remodelling factor 55kDa subunit (Nurf55) (Cao and Zhang, 2004). Again, multiple alternative isoforms of these proteins have been established in mammalian cells, including the Enhancer of zeste homologue 2 (Ezh2) (Figure 6.2) (Kuzmichev et al., 2004). EZH2 is the key catalytic protein in the PRC2

Figure 6.2 Histone modification in eukaryotic cells. The Polycomb group protein complexes 1 and 2 (PRC1 & PRC2) are highly conserved from prokaryotes to eukaryotes, all though they have slightly alternative homologues. (A) The table contains the names of alternative mammalian homologues that relate to each *Drosophilia melanogaster* protein. (B) There are multiple possible constituents of the PRC1 and 2 complexes in mammals. Shown in the circles are a few of the most common proteins. Some of these proteins have been up-regulated in human malignancies, which are labelled around the corresponding protein.

A

Drosophilia	Mammalian
Pc	CBX2,4,7,8
Ph	PH1, 2
Psc	BMI1, MEL-18
Sce	RING1b, RING1a

Drosophilia	Mammalian
Ez	EZH2
Esc	EED,EED2
Suz12	SUZ12
Nurf55	RbAp46

B

PRC1

RING1B   HPH1
BMI1   CBX2

Breast
Leukaemia
Lymphoma

Gastric

PRC2

EZH2
Eed   Suz12

Breast, prostate, colon & lung

Colon, breast
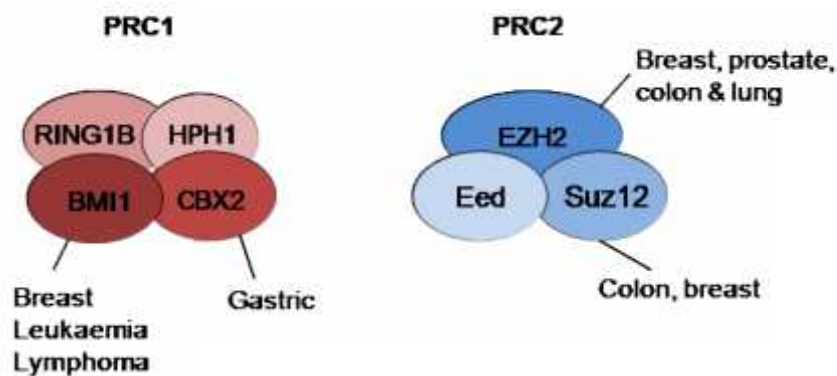
complex and can methylate histone H3 on both lysine 9 (H3K9) and lysine 27 (H3K27) (Muller et al., 2002; Czermin et al., 2002). In association with this the PRC1 complex recognises the H3K27me3 histone marks catalysed by the PRC2 complex and aids in histone methylation alongside the PRC2 complex (Henandez-Munzo et al., 2005).

6.1.3 Histone methylation at the Cdkn2a/Cdkn2b locus

A number of *in vitro* studies have provided corresponding evidence for PRC1 and PRC2 regulation of the *CDKN2a/b* expression in both human and mouse cells (Figure 6.3). In Mouse embryonic fibroblasts (MEFs) Ezh2 and H3K27me3 were located across the whole *Cdkn2a/b* locus, these were then lost from the gene loci when *p16*[INK4a] expression and senescence ensued (Bracken et al., 2009). In association with this, RAS-induced senescence through activated *p16*[INK4a] expression in human fibroblasts, was accompanied with the loss of H3K27me3 and Ezh2 at the *p16*[INK4a] locus (Barradas et al., 2009). In the same study it was identified that the loss of H3K27me3 was attributed to up-regulation of the histone H3K27 demethylase *JMJD3*. This was also substantiated in another study that ectopically expressed using MEFs oncogenic Braf, which induced rapid expression of *Jmjd3* followed by *p16*[INK4a] expression and a decrease in Ezh2 levels (Agger et al., 2009). These studies suggest oncogenic signalling through excessive MAPK signalling can invoke expression of a key histone demethylase *Jmjd3,* to reverse *p16*[INK4a] repression and down-regulate the associated histone methylase, Ezh2.

Figure 6.3 Regulation of *Cdkn2a* gene expression by Histone H3 lysine methylation. The mouse *Cdkn2a* locus encodes two transcripts; *p19^Arf* and *p16^INK4a*. These genes share 3 CpG islands in exon 1β, 1α and 2. Transcription of the genes can be silenced through DNA and histone methylation. At this locus histone methylation occurs by the addition of tri-methylation of lysine 27 on Histone H3 (H3k27me3). This mark is added by the actions of two protein complexes named Polycomb Repressor Complexes 1 and 2 (PRC1/PRC2). The Enhancer Zeste Homologue 2 (Ezh2) PRC2 component is thought to be the key instigator in this event. In addition, the DNA methyltransferases (DNMTs) are also brought to the DNA by the PRC2 complex to simultaneously induce DNA methylation. Histone methylation can be removed by histone demethylases. At the locus, the H3K27me3 mark is removed by the histone demethylase Jumonji-domain 3 (Jmjd3).
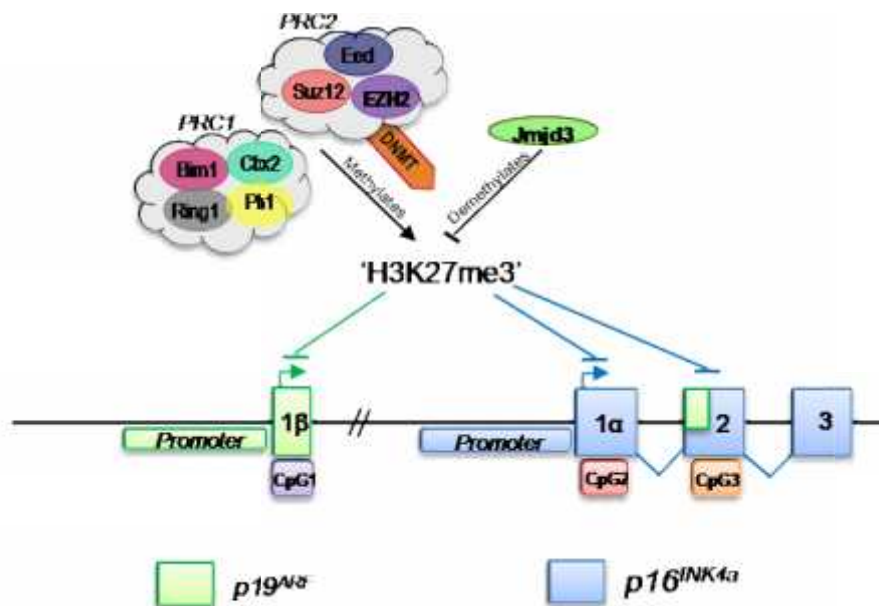
6.1.4 Polycomb group protein aberrations in cancer

Research into the roles of PcG proteins has become increasingly important since aberrant histone modifications have been described in human malignancies. Of the PRC1 group, aberrant expression of the Psc homologue, BMI1, is the most commonly described in cancers, such as lymphoma, leukaemia and breast (van Kemenade et al., 2001; Sawa et al., 2005; Pietersen et al., 2008). As well as EZH2, BMI1 is also associated with repression at the *CDKN2a/b* locus and in addition BMI1 over expression has been linked to silencing of this locus (Jacobs et al., 1999; O'Carroll et al., 2001). The link between over expression of other PRC1 components is still being investigated, but CBX proteins are suggested to have oncoprotein potential in gastric cancer and leukaemia (Zhang et al., 2010; Tan et al., 2011).

The role of the PRC1 complex is thought to be redundant in histone methylation without the initial actions of the PRC2 catalyst, EZH2 protein (Raaphorest et al., 2003). Evidence suggests EZH2 is an Oncogene. Ectopic expression of Ezh2 provides a proliferative advantage to MEFs, also *EZH2* has been shown to be specifically amplified in almost all forms of cancer (Bracken et al., 2007) (Reviewed in Simon and Lange 2008). EZH2 over expression is particularly evident in breast cancers and is associated with metastasis and low survival (Collett et al., 2006; Kleer et al., 2003). Up-regulation of this gene can be linked to activation of multiple proliferative pathways such as the MAPK cascade, because it contains at least 2 binding sites for E2F and is therefore suggestive as an pRb-E2F target (Muller et al., 2001). In addition, up-regulation of *SUZ12* also occurs in breast, ovarian and colon cancers (Kirmizis et al., 2003; Li et al.,

144

2012). Both PRC1 and 2 constituents that are associated with tumourigenesis, are now being treated as substantial therapeutic targets.

6.2 Aims

The aims of this chapter were to find evidence to further support the role of $p16^{INK4a}$ inactivation in the progression of serrated CRC. The main focus was to investigate hypermethylation and gene silencing at the $p16^{INK4a}$ locus, with particular reference to addressing the expression levels of key regulatory factors that have previously been linked to the regulation of DNA methylation.

6.3 Results

6.3.1 Jmjd3 expression is up-regulated in response to Braf^{V600E} expression

The expression of $p16^{INK4a}$ is increased in response to Braf^{V600E} signalling in the intestine epithelium. Dnmt3b levels are also increased but this does not allow for the immediate methylation of the $p16^{INK4a}$ Exon 1α CpG island. To determine what instigates the expression of this gene, the levels of the of histone lysine demethylase *Jmjd3* were first investigated in the *Braf*^{V600E}-expressing small intestine.

RNA/cDNA isolated from tissue of the duodenum was analysed by qPCR. *Jmjd3* is located on chromosome 11 of the mouse genome and has 23 exons. Primers were designed to anneal to exon 20 (forward) and exon 21 (reverse) across intron 20. Three alternative time courses, including both controls were analysed and the average expression levels were determined (Figure 6.4). Positive *Jmjd3* expression was found in the normal SI. Statistically significant

Figure 6.4 *Jmjd3* mRNA expression increases post *Braf*[V600E]induction but is reduced at later time points. Graph results from qPCR analysis for Jmjd3 expression. cDNA was transcribed from mRNA isolated from mouse SI tissue from WT, Cre and the *Braf*[V600E] -expressing time course. Each bar represents the average expression of 3 samples with the exception of the 10'wk where n=2. The 10'wk sample represents the combined results from 10wk & 11wk VE samples. All samples were normalised to *Calnexin* and quantified relative to the WT (WT=1). Error bars correspond to standard deviation. Calculated P values give statistically significant increases at 3 days, 1wk & 6wks but not quite at 2wks (p=0.06). These values are in comparison to the Cre control. Asterisks (*) represent statistical significance *=<0.05 **=<0.005, ***=<0.0005.
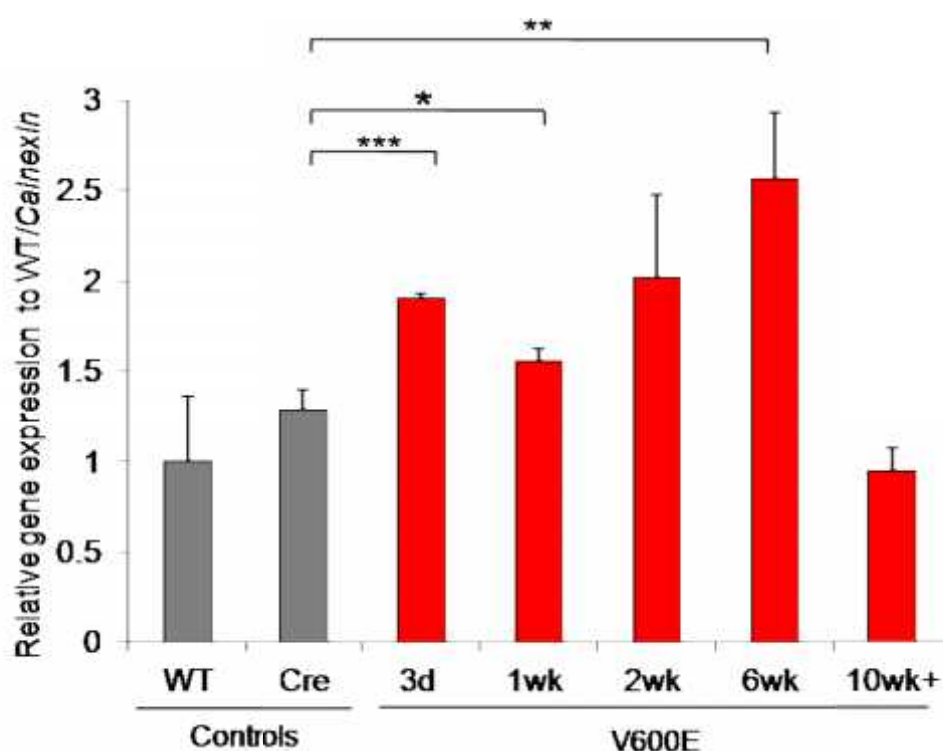
increases were identified at 3 days, 1 wk and 6 wk post-*Braf*^{V600E} induction but not at 2 wks. A statistically significant decrease was also identified at the 10+wk VE time point. The most significant increases were seen at 3 days and 6 wks p.i. and this was also seen in results gained from RNA analysed by microarray analysis by Dr Linda Carragher, University of Leicester. In both samples, a 1.5-fold increase was seen above the wild type. These results correspond to previous reports that *Jmjd3* has an Erk binding site in its promoter and is immediately elevated in response to both oncogenic Ras and Braf induced-MAPK signalling (Barradas et al., 2009) (Agger et al., 2009).

6.3.2 Jmjd3 protein levels increase after Braf^{V600E} expression

To determine whether the increase in *Jmjd3* was also evident at the protein level, IHC was performed on sections of mouse SI for the controls and over the *Braf*^{V600E}-expressing time course. IHC was attempted using two alternative antibodies from Aviva and Abcam. The Aviva antibody had previously been published in a study using mouse skin (Barradas et al., 2008). This proved to be the more specific of the two and consistent with the mRNA data, crypt cells stained positively at 3 days and 6 wks post-*Braf*^{V600E} expression (Figure 6.5). Protein expression of Jmjd3 was also evident at low levels in the tumours, although staining was consistently mosaic across all tumours (Figure 6.6).

6.3.3 Ezh2 is expressed in the mouse SI

Ezh2 is the key catalyst for the activation of DNA and histone methylation in mammalian genes. Ezh2 has been shown to induce methylation and gene silencing at the *Cdkn2a* locus (Bracken et al., 2009). To determine whether

Figure 6.5 Jmjd3 protein levels increase post *Braf*^V600E^ induction but are reduced at later time points. IHC for Jmjd3 using an Aviva antibody, on SI sections of WT, Cre and over the *Braf*^V600E^-expressing time course of 3days to 10wks. Both controls show low levels of Jmjd3 staining. Nuclear staining can be seen in the 3dayVE and 6wkVE crypts. Staining is absent at 2wks and 10wk post-VE-expression. Scale bar = 50µm.
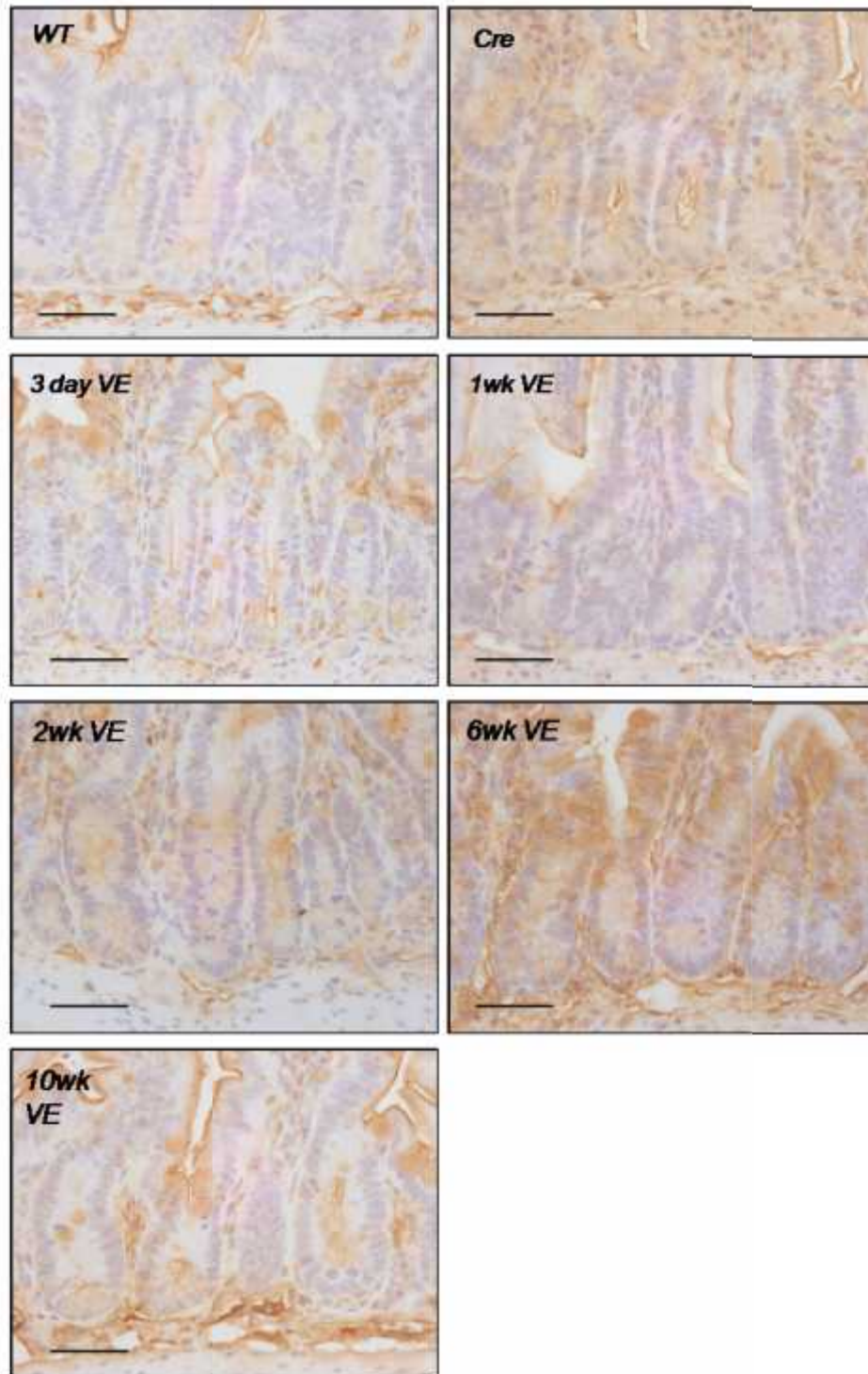
Figure 6.6 Jmjd3 protein levels are high in tumours from a 12wk Braf[V600E]-expressing SI. IHC for Jmjd3 on an SI sections of a 12wk *Braf*[V600E]-expressing mouse. (A) Shown on the left is a 12wkVE tumour stained using an Aviva Ab. Scale bar = 200µm. To the right is an enlarged region of the tumour. Scale bar = 50µm. Staining shows presence of Jmjd3 in the cell nuclei of the tumours, although this is mosaic and not present in every cell.
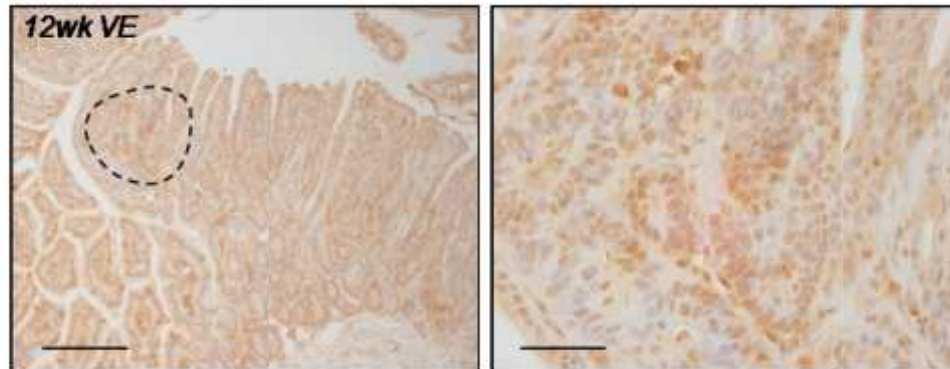
Ezh2 was altered in response to Braf^{V600E} and involved in adenoma progression, *Ezh2* expression levels were investigated by qPCR.

RNA/cDNA isolated from tissue of the duodenum was analysed by qPCR. Ezh2 is located on exon 6 of the mouse genome and has 20 exons. Primers were designed to anneal in exon 16 (forward) and the sequence spanning the end of exon 16 to the start of exon 17 (reverse), across intron 16. qPCR was performed on two alternative time courses including both controls and the average expressions were determined (Figure 6.7B). An initial RT-PCR was performed that identified *Ezh2* was expressed in the mouse SI in all samples including the controls (Figure 6.7A). qPCR was then performed. Results confirmed Ezh2 expression and revealed there were no significant *Ezh2* expression changes in the SI in response to Braf^{V600E}.

6.3.4 Ezh2 protein is highly expressed at 10wks post Braf^{V600E-}expression

The protein level of Ezh2 was also determined for the control and experimental time course samples. A western blot was performed for Ezh2 on lysates made from the duodenum tissue of the SI (Figure 6.8). Protein from HeLa cells that are known to express high levels of Ezh2, was used as a positive control. A single band at the expected 91kDa size was produced. Protein expression of Ezh2 was not present in the control or the 3 day VE and 6 wk VE samples. However, it was expressed at 2 wks and even more evidently at 10 wks post-*Braf*^{V600E} induction. Two extra alternative 10 wk VE samples were also analysed and confirmed the high expression occurred at the 10 wk time point.

Figure 6.7 *Ezh2* **mRNA expression remains stable post** *Braf*^V600E **induction by RT-PCR & qPCR.** cDNA was transcribed from mRNA isolated from mouse SI tissue from WT, Cre and the *Braf*^V600E - expressing time course. (A) RT-PCR for *Ezh2, Calnexin* was used as a control. (B) qRT-PCR for *Ezh2. Calnexin* was used as a control. Each bar represents the average expression of 2 samples (n=2). All samples were normalised to *Calnexin* and quantified relative to WT.
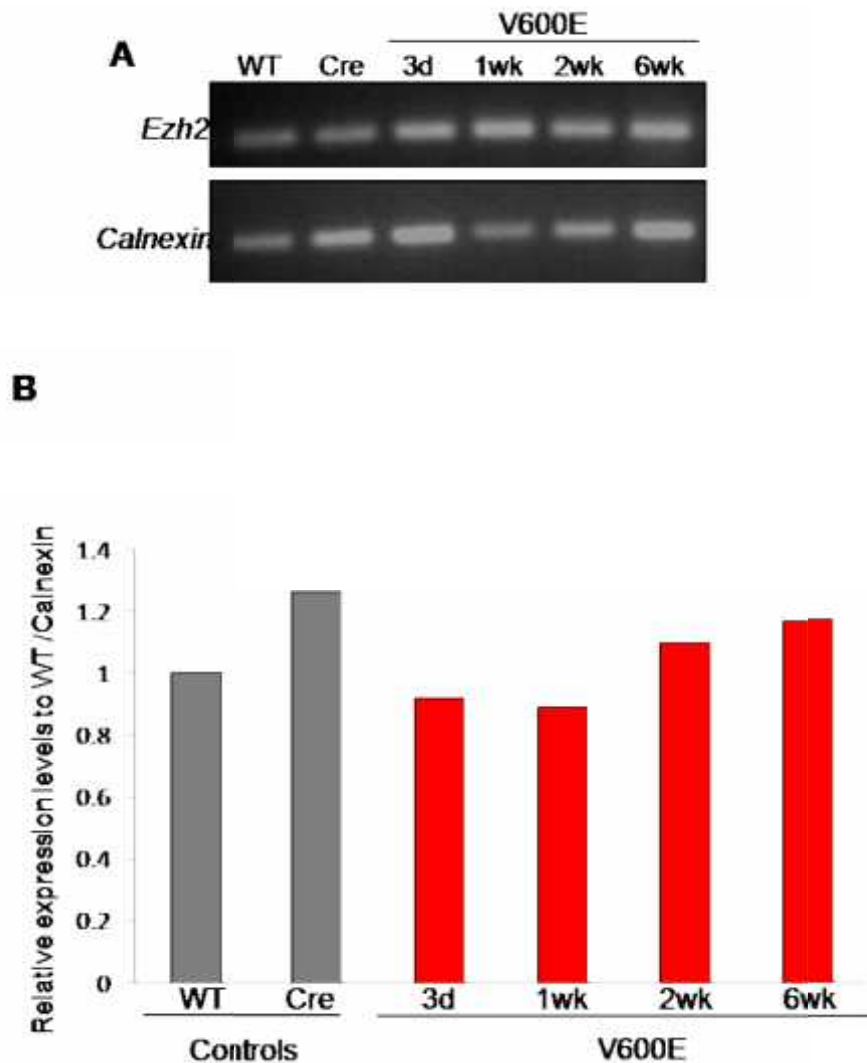
Figure 6.8 Ezh2 protein levels are elevated after 10wks of *Braf*[V600E] expression. Western blotting on mouse SI lysates from WT, Cre and the *Braf*[V600E]-expressing time course of 3days to 10wks. Lysates were western blotted and analysed with antibodies for Ezh2 and Erk. Ezh2 protein is absent in the controls and over most of the VE-expressing samples until 10wks where is it highly expressed in 3 alternative samples. It is also slightly elevated at 2wks.
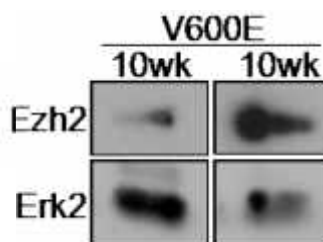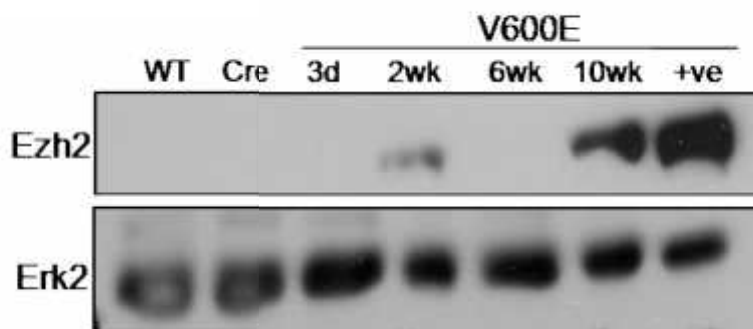
6.3.5 Ezh2 protein levels are elevated in adenomas of the SI

Fresh tumour tissue was not available for either mRNA or protein analysis because of the size of the adenomas. To investigate Ezh2 levels in the tumour epithelium, protein analysis was performed by IHC.

Tumours from 2 sections of the duodenum (5 and 6) were stained for Ezh2 (Figure 6.9). All tumours present in the sections stained positively for Ezh2. Ezh2 was located only in the cell nuclei and strong staining was particularly evident in dysplastic areas of the adenomas. A very small number of crypts showed a lack of Ezh2 staining. One explanation for this is that the crypts are still in the senescent phase of tumourigenesis. The high expression of Ezh2 in the tumours correlates with adenoma progression and supports a possible role in the progression of serrated CRC.

6.3.6 Investigation of H3K27me3 levels at the Cdkn2a/b locus by ChIP

To further determine the roles of Jmjd3 and Ezh2 and to establish whether DNA/histone methylation was present, the level of H3k27 tri-methylation at the *Cdkn2a/b* locus was investigated. Chromatin immunoprecipitation (ChIP) was the chosen method because it identifies the type of histone mark/proteins binding at a specific locus and also provides relative quantification for the level of modification as assayed using qPCR. Analysis was performed on both controls and the experimental *Braf*^{V600E} time course of 3 days to 6 wks. Fresh tissue was not available from mice at the 10 wk/11 wk time points. ChIP was performed at the London Institute of Cancer Research UK at Lincoln Fields Inn, within the laboratory of Dr Gordon Peters.

Figure 6.9 Tumours from 12wk *Braf*[V600E]-expressing SI show a high level of Ezh2 staining. Immunohistochemistry was performed on tumours from 12wk VE-expressing SI using an antibody for Ezh2. All tumours show positive staining for Ezh2. (A) A large tumour is stained positively for Ezh2. Scale bar = 200µm. The dashed region of the tumour is enlarged to the right, which shows strong nuclear localisation. Scale bar = 50µm (B) A second tumour is stained positively for Ezh2. Scale bar = 200µm. On the right and below are the same region magnified. Scale bar = 200µm (top left),100µm (top right) and 50 µm (bottom). Highlighted in the dashed region is a crypt stained negative for Ezh2. Such crypts might exhibit senescent features whilst the surrounding epithelium becomes dysplastic.
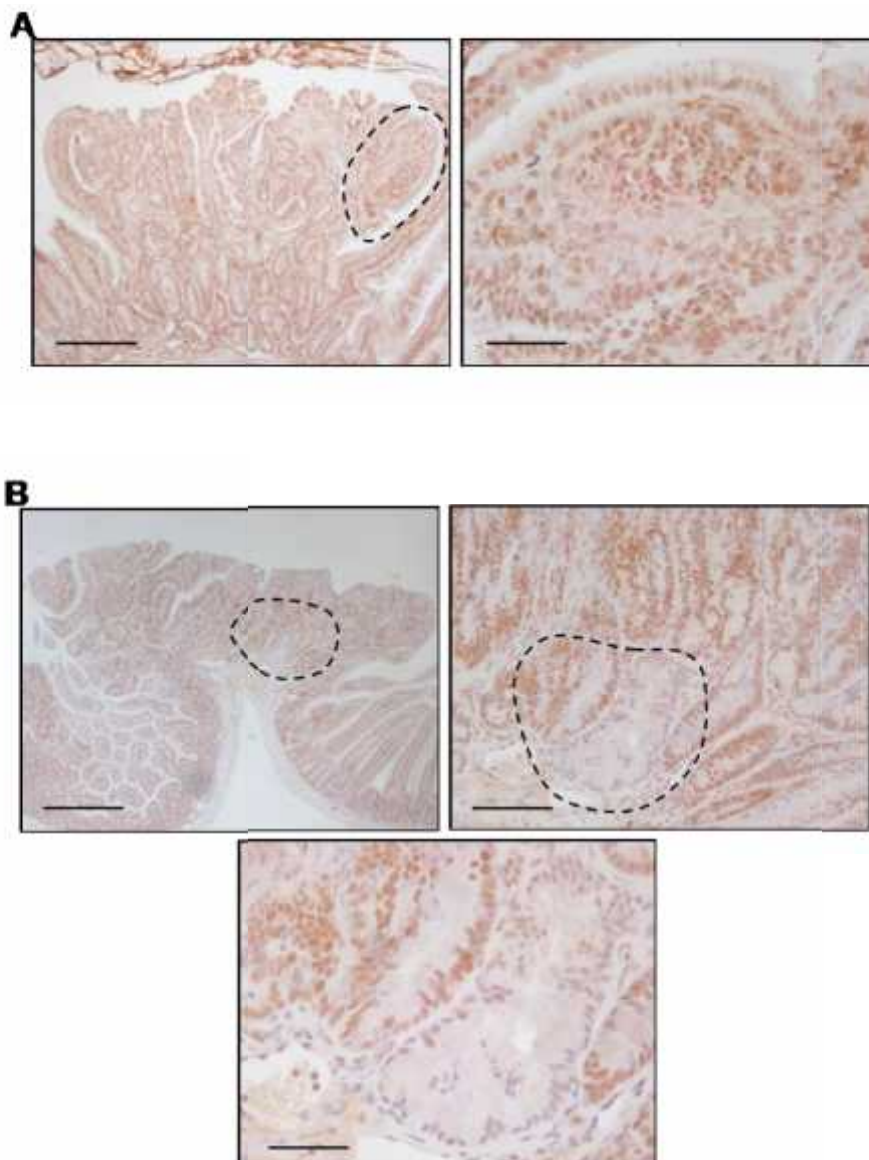
Chromatin was processed and isolated from cells from the epithelial layer of the whole SI (duodenum to ileum). Immunoprecipitation was performed using an antibody for H3K27me3. Each chromatin sample was also immunoprecipitated for mouse/rabbit IgG as a control for the level of nonspecific binding. Immunoprecipitated chromatin was analysed by qPCR using five sets of primers. 1) Exon 2 of *p15*^INK4b^, 2) Exon 1β of *p19*^ARF^ and 3) in three different sets in exons 1α and 2 of *p16*^INK4a^ (Figure 6.10). Primers had previously been published but sequences were revised since publication (Barradas et al., 2009). Samples were duplicated per qPCR and the PCR was then repeated (n=4) and the average % of H3K27me3 per total input of chromatin was calculated.

A dramatic drop in H3k27me3 was seen across the whole *Cdkn2a/b* locus in the 1 wk VE sample. Statistical significant differences were calculated against the Cre control for Ps1, 2, 4, 5 & 7. Ps5 was not statistically different from the Cre (P=0.13), perhaps because the Cre sample had a large standard error bar.

These results suggest, overall, H3k27me3 is lost at this time-point. In addition, to this an increase of H3k27me3 occurred at 2 wks p.i. at Ps2 that relates to the *p19*^ARF^ region. The Ps5 and Ps7 results were not quite statistically significant when compared to the Cre sample (P=0.52 and P=0.08, respectively at 2 wks). These relate to the *p16*^INK4a^ exons 1α and 2 regions, suggesting H3k27me3 may increase around this 2 wk p.i. The IgG non-specific PCRs were extremely low for all samples (<0.005). At other time points there were no significant differences. At the 6 wk time point there were no statistically significant differences compared to controls.

Figure 6.10 Chromatin Immuno-precipitation (ChIP) for tri-methylation on lysine-27 of histone H3 (H3K27me3) across regions of the *Cdkn2a/b* locus across the VE timecourse. ChIP was performed for H3k27me3 on chromatin prepared from cells of the epithelial SI lining of both controls and over the *Braf*[V600E]-expressing time course of 3 days to 6wks. qPCRs were run using 5 primer pairs (Ps1-7) flanking regions of *p15*[Ink4b] (exon 2), *p19*[Arf] (exon 1β) and *p16*[Ink4a] (exon 1α & exon 2). These regions are indicated by the red arrows. The results are shown in a bar graph; each control and experimental time point was grouped and labelled by colour. Samples were duplicated per PCR and duplicate qPCRs were analysed (n=4). Each bar represents the average % of H3K27me3 per total input of chromatin. Error bars equal standard deviation. Statistical analysis was performed using an unpaired t-test. Asterisks (*) represents statistical significance compared to the Cre control,*=<0.05, ** =<0.005, ***=<0.0005.
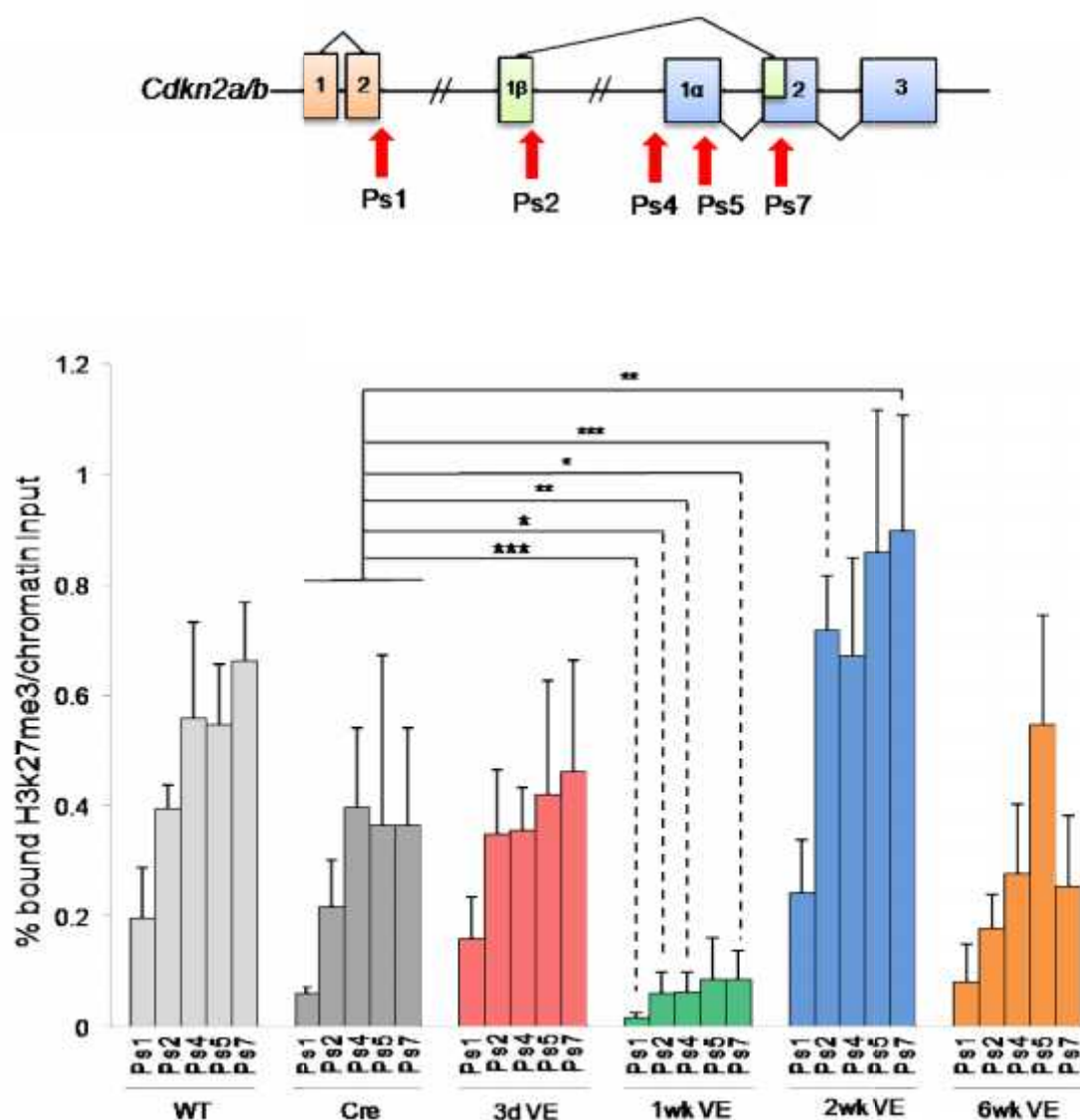
6.4 Discussion

In the last chapter it was determined that hypermethylation of the CpG island in exon 1α of $p16^{INK4a}$ was linked to the growth of adenomas in the $Braf^{V600E}$-expressing SI epithelium. The *de novo* methyltransferase Dnmt3b was also found to be highly expressed over the $Braf^{V600E}$ time course and in the tumours suggesting a role for DNA methylation in this model. As well as DNA methylation, histone methylation is a key factor in the repression of gene expression. This chapter focused on investigating the PcG proteins that regulate DNA and histone methylation, as well as the histone demethylation enzyme Jmjd3, which counteracts the effects of PcGs.

Expression of the histone demethylase *Jmjd3* has been shown to be up-regulated in response to oncogenic MAPK signalling and is associated with removal of the H3K27me3 mark at the *Cdkn2a* locus (Xiang et al., 2007). In this chapter the level of *Jmjd3* increased at the mRNA level by both qRT-PCR and microarray analysis, at both the 3day/6wk VE time points. Protein levels of Jmjd3 were also elevated at these time points. The data suggests *Jmjd3* is up-regulated in response to Braf^V600E^ signalling in the epithelial crypt cells, which correlates with an increase in $p16^{INK4a}$ expression, during the senescence phase. $p16^{INK4a}$ is a known target for histone de-methylation by Jmjd3 particularly in response to oncogenic signalling by Ras and Braf in both human and mouse cells. In this model the onset of *Jmjd3* expression coincides with $p16^{INK4a}$ expression. This supports the hypothesis that crypt cell expression of oncogenic Braf^V600E^ induces Jmjd3 up-regulation, which targets the $p16^{INK4a}$ locus for histone de-methylation and expression as a tumour suppressive

response.

Unexpectedly, the adenomas were also found to be positive for Jmjd3, although the staining was not as widely coherent and prominent as Ezh2. It is possible the loss of senescence and re-intervention of proliferation induces a second burst of *Jmjd3* expression, but in the presence of the PRC1/2 complexes and in particular the Ezh2 catalyst inhabiting the *Cdkn2a* locus, Jmjd3 is not active. Overall whether *p16*[INK4a] is expressed or not is likely to be related to the relevant expression of Jmjd3 and Ezh2.

The levels of histone methyltransferase Ezh2 were determined because this is the main catalyst for DNA and histone methylation and has been shown to bring DNMTs to gene loci to mediate methylation events. An initial increase of Ezh2 protein expression was identified at 2 wks p.i. but more predominantly it was highly expressed in multiple 10 wk VE samples. However, changes in *Ezh2* mRNA levels were not seen. Ezh2 has been shown to be a direct target of the E2F transcription factor, which in turn is a MAP kinase pathway target (Muller et al., 2001). Also, using experiments on Braf[V600E]-expressing melanoma cells, it was shown that 'knockdown' of *Braf*[V600E] expression significantly reduced the levels of Ezh2 (Hou et al., 2012). However, in this study Ezh2 was found to be expressed at the protein but not at the mRNA level, indicating stabilisation of the protein translation could be a defining factor rather than gene expression up-regulation.

Ezh2 protein levels correlated with the time points when p16[INK4a] expression

was lost, which was prior to tumour formation. Following, this strong nuclear staining was present throughout the tumour epithelium of the 12 wk VE SI. Interestingly, IHC staining for Jmjd3 was also identified in the corresponding tumours. However, *p16^{INK4a}* is not expressed in the 12 wk tumours and a key CpG island in the gene becomes hypermethylated in these lesions, suggesting Ezh2 is active at the locus and can counteract the effects, if any, of Jmjd3.

To determine whether the expression changes of Jmjd3 and Ezh2 were functional, the levels of H3K27me3 were analysed by ChIP across the *Cdkn2a/b* locus including *p15^{INK4b}*, *p19^{ARF}* and *p16^{INK4a}*. In this model, striking loss of H3K27me3 levels was established at the 1 wk VE p.i. across the whole Cdkn2a/b locus. This corresponds to earlier data (Chapter 4) where *p16^{INK4a}* expression was identified as early as 1 wk VE expression. The levels of *p15^{INK4b}* were also significantly increased at this experimental time point. CpG sequencing at exon 1α of *p16^{INK4a}* also revealed loss of DNA methylation at several CpGs between the 3 days to 2 wk time points. Interestingly at 1 wk p.i. H3K27me3 was also lost at the *p19^{ARF}* locus. Induction of senescence in MEFs appears to be regulated mostly by *p19^{ARF}* and regulation of *p19^{ARF}* in the mouse genome has been shown to be strongly associated with PcG proteins. However, we determined *p19^{ARF}* was not expressed in the normal mouse SI (Chapter 4) or in response to Braf^{V600E}. The loss of H3k27me3 at the *p19^{ARF}* locus is most likely a response to down-regulation of Ezh2 across the whole locus, but changes in *p19^{ARF}* expression were clearly not affected by this.

Statistically significant increases for H3K27me3 levels were identified at the 2

wk time point for exons 1α and 2 of *p16*[INK4a]. These results at the 2 wk time point seem to correlate with the short lived initial expression of Ezh2 at this time point. The reason for this is not entirely clear but throughout our studies the 2 wk time point has been a slightly anomalous time point. Senescence was initially observed at 1 wk p.i. followed by a reduction at 2 wks and then re-established at 6 wks. A possible reason for this is that the gut epithelium is responding to adjust to senescence at this time point.

The control of Ezh2 protein expression is unknown but clearly it could be associated with hyperplastic progression in this model. Hypoxia-associated DNA damage has been linked to Ezh2 expression in cancers as well as other model systems (Chang et al., 2011). Indeed, preliminary IHC data (not shown) on 12 wk VE tumours is suggestive of activation of DNA damage pathways, whereby phosphorylation of the H2AX (γ-H2AX) was observed using IHC. The presence of γ-H2AX has been shown to be a primary response to DNA damage in prokaryotes and eukaryotes and is thought to recruit DNA repair proteins to DNA damage regions (Rogakou et al., 1999; Downs et al., 2004; Shroff et al., 2004).

To confirm the H3k27me3 levels across the *Braf*[V600E] time course, the ChIP experiments would require repeating on alternative time courses. Also, performing Ezh2 and Jmjd3 ChIP over the Braf[V600E] time course would determine Ezh2 and Jmjd3 activities on the *Cdkn2a* locus. Ezh2 ChIP was previously attempted, but this was unsuccessful due to possible problems with cross–linking and available antibodies. Also, antibodies for Jmjd3 ChIP are not

highly regarded. Therefore more technical developments need to be made before this can be done.

Overall the data collected in this chapter suggest *p16*^{INK4a} and possibly *p15*^{INK4a} expression is linked to up-regulation of *Jmjd3* expression. This could directly result in the loss of methylated CpGs in exon 1α of *p16*^{INK4a} and associated H3k27me3. Ezh2 expression was induced in-relation to tumour growth and remained highly expressed in the adenomas. It is possible that this is required for ensuring Dnmt3b is brought to the *Cdkn2a* locus to down regulate the expression of *p16*^{INK4a} and *p15*^{INK4b}. However, this remains to be proven, possibly by performing 'knockout' experiments of *Ezh2* on a *Braf*^{V600E} background. Control of Ezh2 protein expression also needs to be investigated to determine whether this relates to a response to DNA damage signal, possibly due to hypoxia.

7. Summary and Conclusion

7.1 Project background

Over the last decade research into an alternative pathway to human CRC has provided strong evidence against for the existence of a pathway different from the tradition CRC, which includes the inactivation of the tumour suppressors *APC* and *p53*. The alternative pathway is known as the 'Serrated neoplastic pathway' and is thought to develop through a separate pathway of genetic and epigenetic molecular aberrations. In addition, it also has distinct morphological characteristics that were the basis to its initial identification. The most significant correlations with the serrated CRC pathway have been identified as microsatellite instability (MSI), CpG island methylator phenotype (CIMP) and the *BRAF*^{V600E} mutation. Although the exact sequence of these biomolecular changes in serrated CRC is not known, it is thought that *BRAF*^{V600E} is a founder mutation since it has been identified in both early and advanced lesions.

There are three *RAF* homologues; *ARAF*, *CRAF* and *BRAF*. In 2002 mutations in *BRAF* were discovered, in human cancers and the most common BRAF mutation V600E was determined to have oncogenic potential. Until this time most research had been focused on *CRAF* (Davies et al., 2002). Over 40 mis-sense mutations in *BRAF* have since been identified in human cancers, most significantly in melanoma, ovarian, papillary thyroid and colorectal cancers. Since the discovery of mutant *BRAF* genes, the level of research into its role in cancer has heightened, with over ~300 research papers on *BRAF* being published between 2011 to the present day.

162

Mutation of the *RAS* mutant homologue, *KRAS* has been defined as a key initiating factor in traditional CRCs. RAS mutations are found in ~50% of all sporadic CRCs and most significantly in those that progression through the traditional CIN pathway (Barry et al., 2006). However, they are also identified in all lesions of serrated neoplastic pathway in including the earliest precursor lesions, aberrant crypt foci (ACF) (Kambara et al., 2004; Beach et al., 2005). KRAS and BRAF mutations are mutually exclusive in this pathway and it is thought that they represent alternative pathways to development of serrated CRCs (Rajagopalan et al., 2002).

Both RAS and BRAF are key components of the MAPK signalling pathway. The identification of both *KRAS* and *Braf*^{V600E} in the serrated pathway of CRC, provides a strong link between MAPK signalling and CRC tumourigenesis. For this reason a mouse model was developed to conditionally and spatially express the *Braf*^{V600E} mutation in the mouse gastro-intestinal tract using the inducible Ah*Cre*ER^T Cre recombinase strain (Mercer and Pritchard, 2003). The role of *Braf*^{V600E} expression in the intestinal crypt cells and its contribution to serrated CRC was investigated in this study. The aim was to increase our understanding of the mechanistic role of Braf^{V600E} in serrated CRC using this mouse model.

7.2. Overview of project results

7.2.1 *Braf*^{V600E} induces crypt hyperplasia in the mouse SI

Preliminary investigations on the small intestine revealed Braf^{V600E}-induced hyperplasia in the crypts of the mouse ileum (Carragher et al., 2010). In chapter

163

3, these findings were further investigated and confirmed in the jejunum section of the SI. Using morphometric analysis, the number of cells in the Braf^{V600E}-expressing crypts increased at ~3days p.i. and the number of cells remained stably increased up to 2 wks p.i. at ~200 cells per crypt. Biochemical changes within this time frame (3 days-2 wks) also revealed an increase in MAPK signalling through up-regulated ppErk levels and mitosis by an increased number of positive P-H3 cells. In addition the number of cells in the villi of the SI was also elevated in response to the increase in the number of cells in the crypt, but this occurred at the slightly later time point of 1wk p.i. In relation to this serrations were also identified in the villi epithelium, as a consequence of increased cell number.

Although not investigated in this particular study, data from the *Braf^{V600E}* expressing mouse SI also revealed cross talk between Braf^{V600E}-activated MAPK signalling and the Wnt signalling pathway through increased nuclear β-catenin levels in the cells of the crypts (Carragher et al., 2010). The Wnt signalling pathway is the major pathway in crypt cell proliferation and survival. Therefore the activation of β-catenin further indicates the role of Braf^{V600E} as an inducer of crypt cell hyperplasia and more importantly an early initiating mutation in serrated CRC. The mechanism behind this cross talk has yet to be elucidated.

7.2.2 Features of crypt senescence coincide with p16^{INK4a} expression

Following the initial burst of crypt hyperplasia, homeostasis appears to be regained as the number of cells of the crypts at the later time points are reduced

to that of the control groups. MAPK signalling is not sustained, shown by the lack of ppErk staining in the crypt cell nuclei. This is possibly due partly to increased expression of negative feedback regulators of Mek and Erk, such as; DUSPs and Sproutys, although this remains to be shown. Levels of the senescence markers $p16^{INK4a}$ and $p15^{INK4a}$ were shown to increase in the crypts and in addition to this data from the ileum of this mouse model, identified the presence of crypt senescence at this stage using the SA β–galactosidase assay (Carragher et al., 2010). This is the first time senescence has been shown in the gut.

Since time studies using mice and on human CRC samples have provided support for the role of senescence in this pathway. In one study, expression of *Kras* in the mice intestinal epithelium induced p16^{INK4a} expression and SA β–galactosidase. Silmilar to the Braf^{V600E} model, loss of *Cdkn2a* increased the number of tumours in these mice (Bennecke et al., 2010). Studies in human CRC samples have also confirmed the expression of p16^{INK4a} in CRC lesions and that the expression is lost in late stage malignancies (Shima et al., 2011; Kriegl et al., 2011).

These studies shed light on the early developments of CRC but the reasons behind the switch from proliferation to senescence remain unclear.

7.2.3 Braf^{V600E} cells escape p16^{INK4a} OIS with the growth of adenomas

After ~12wk post *Braf^{V600E}*-expression crypt senescence was evaded by the growth of individual tumours along the whole length of the SI and these

displayed the morphological features of serrated adenomas, including serrated and mucinous epithelium. The adenomas were highly proliferative, by the presence of widespread P-H3 positive cells throughout the epithelium and all tumours were absent of $p16^{INK4a}$ expression. This suggested inactivation of $p16^{INK4A}$ was a likely target for tumour progression. In support of this, $Braf^{V600E}$/AhCreER$^{T+/o}$ expressing mice were cross bred with $Cdkn2a$ mutant mice and the loss of the $Cdkn2a$ locus with Braf^{V600E} expression resulted in extensive crypt hyperplasia, with no features of senescence and reduced survival of mice from 12 to 6 weeks p.i. (Serrano et al., 1996; Carragher et al., 2010).

This $Cdkn2a$ knockout results in loss of both $p19^{ARF}$ and $p16^{INK4a}$ expression and as such using this model, loss of senescent features cannot be solely attributed to inactive $p16^{INK4a}$. However in the present study expression of $p19^{ARF}$ was not identified in the wildtype or $Braf^{V600E}$ small intestine. In addition, protein expression analysis for p53, p21^{CIP} and p19^{ARF} on the $Braf^{V600E}$ intestine (performed on the ileum) provided evidence that these alternative pathways to senescence were not induced in response to $Braf^{V600E}$ and in fact p21^{CIP} appeared to be reduced in its presence (Carragher et al,. 2010). This provides evidence that it is $Braf^{V600E}$ related senescence is established though $p16^{INK4a}$ expression.

It has been identified that mutations are required to target the stem crypt cells rather than the differentiating transit amplifying cells to drive intestinal cancer (Barker et al., 2009). The progression of tumour development and the

presence of Braf^{V600E} in the mice aged up to 12wks p.i. suggest it is targeted to the stem cells in this model. Crypt stem cells constitutively divide to provide progenitor cell lineages. In doing so they drive crypt cell replenishment every ~3-5 days, if *Braf^{V600E}* was not recombined/activated in the crypt stem cells it would be lost ~1wk p.i. which is not the case because *Braf^{V600E}* expression is present by PCR across the whole time course of 3 days to 12 wks p.i. (Figure 7.1).

7.2.4 Inactivation of p16^{INK4A} occurs through methylation of exon 1α

The method of *p16^{INK4A}* inactivation was investigated in chapter 5. Levels of the DNA methyltransferase Dnmt3b but not Dnmt3a isoforms, were up-regulated in immediate response to Braf^{V600E} and remained elevated over the time course and in the tumours. The up-regulation of Dnmt3b was also shown to be Mek-dependent. This suggested a role of DNA methylation in this mouse model, which corresponds to the association of *Braf^{V600E}* and CIMP-H in serrated CRCs.

The strong link between serrated CRCs and CIMP-H suggested that epigenetics could be attributed to the loss of *p16^{INK4a}*. Three CpG islands were determined in the *Cdkn2a* locus. These were located in exon 1β of *p19^{ARF}*, exon 1α and 2 of *p16^{INK4A}*. Although the promoter region was not defined as a CpG island in the mouse, the CpG Island in exon 1α in humans also extends into the promoter region. For this reason the promoter region (~1kb) was investigated. Overall the promoter was found to be unmethylated over the *Braf^{V600E}* time course (3days-6wks) and in the tumours. Not all CpGs were determined due to

Figure 7.1 Illustration to demonstrate the consequences of Braf^{V600E} expression in the crypt stem cells. The cells of the crypt are maintained by the stems cell that give rise to a pool of daughter progenitor cells, which in-turn divide and differentiate into the functional cells of the crypt and villi. The cells of the crypt are replenished every 3-5 days. (A) If the transit amplifying cells (TA) but not the crypt stems expressed Braf^{V600E} then after ~1-2wks these cells would be lost into the villi and crypt homeostasis would be regained. (B) If the crypt stems cells expressed Braf^{V600E}, all progenitor daughter cells and TA cells would express Braf^{V600E} from 1wk+ p.i and indefinitely. Recombination and Braf^{V600E} expression is observed in mice up to 12wks p.i.
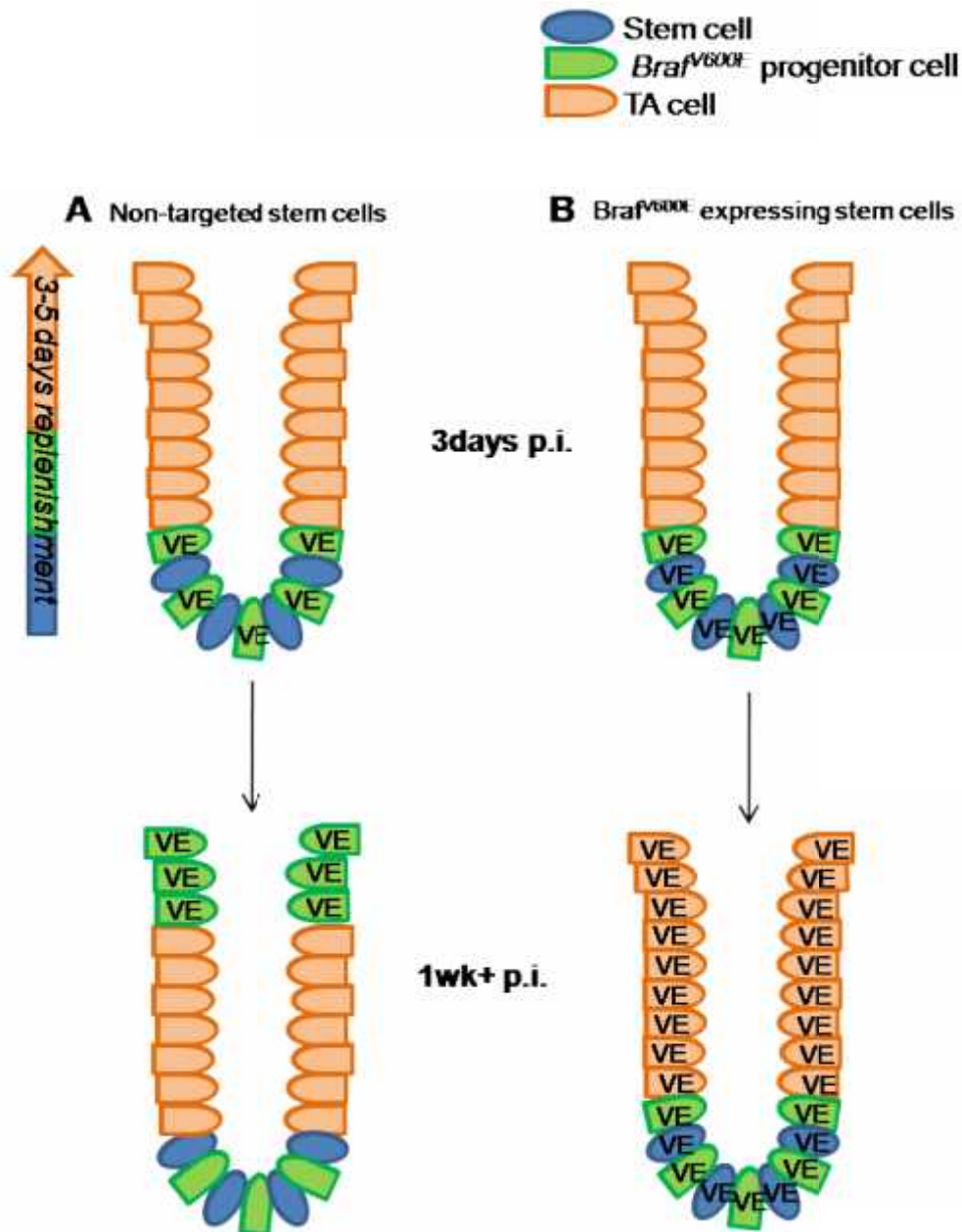
unsuccessful PCR and sequencing problems. The methylation status of the CpG Island in exon 1α was successfully determined. Hypomethylation was observed over the $Braf^{V600E}$ time course from 3 days to 2 wks. This reflects the onset of $p16^{INK4a}$ expression. However, hypermethylation of exon 1α occurred from 6wks p.i. but was much higher in the tumour samples. This data provides strong evidence for a role of methylation in tumour progression

In chapter 4, RT-PCR for $p19^{ARF}$ revealed it was not expressed in the $Braf^{V600E}$-expressing SI and so the methylation status of the CpG Island of exon 1β was not investigated. Primers designed for methylation analysis of the CpG Island in exon 2 were unsuccessful and as such methylation status of this CpG Island was not determined.

7.2.5 Changes in gene expression regulators occur at the Cdkn2a/b locus
In chapter 4 and 5, the growth of $Braf^{V600E}$-induced tumours occurred with the loss of $p16^{INK4a}$ expression, which was linked to alterations in CpG Island methylation. Changes in histone methylation by the removal and addition of the H3K27me3 mark was also observed at the Cdkn2a/b locus. Widespread loss of H3K27me3 occurred at ~1wk p.i. and was associated with up-regulated expression of the histone demethylase $Jmjd3$. At the later stages of $Braf^{V600E}$ expression, protein expression of the PcG protein Ezh2, which catalyses the addition of H3K27me3 at the $Cdkn2a$/b locus was elevated in the crypts. This occurred prior to tumour development and remained highly expressed in the tumours. DNA damage may to be a trigger for Ezh2 expression and analysis of the $γ-H_2AX$ DNA damage marker revealed positive cells throughout the tumour

epithelium. Analysis of H3k27me3 levels could not be performed directly on the tumour cells because of the size of the tumours, due to the lack of fresh tissue.

7.3 Future work

The results in the first two chapters provide strong evidence for $Braf^{V600E}$ induced hyperplasia, followed by OIS. This occurred in relation to $p16^{INK4a}$ expression and subsequent down-regulation in the tumours. The levels of p15^{INK4b} were also up-regulated after $Braf^{V600E}$ expression but whether this had a role in the senescent phenotype could not be determined because analysis of $p15^{INK4b}$ levels in the tumours could not be performed. An alternative approach could be taken by determining the methylation status of the $p15^{INK4a}$ promoter and encoding exons by bisulphite sequencing, extensive ChIP for H3K27me3 and by combing a conditional knockout $p15^{INK4b}$ with the $Braf^{V600E}$ mice. It would also be useful to determine the methylation status of exon 2 of $p16^{INK4a}$, the levels of H3K27me3 were altered at this region over the $Braf^{V600E}$ time course in a similar manner to exon 1α.

ChIP should also be performed on alternative $Braf^{V600E}$-expressing time courses, to confirm the loss and gain of H3K27me3 in relation to $p16^{INK4a}$ expression.

Overall the number of tumours analysed by bisulphite sequencing in chapter 5 should be increased because the number of CpGs and the level of methylation was varied between the tumours. This may provide an explanation for the variation that could possibly correlate to either the size of the tumour i.e. stage

and/or the area of the SI which could correlate to *Cre/Braf^{V600E}* expression, as hypothesised.

Hyperplastic lesions can be seen in the *Braf^{V600E}*-expressing SI epithelium from as early as 10wks p.i. along with the loss of *p16^{INK4a}* expression. It would be informative to analyse the *Braf^{V600E}* time course in greater depth between the 9-12 weeks time points when the 'switch' between senescence and tumour progression occurs. Possibly by breaking down this time-frame into smaller periods and observing the expression changes of *Jmjd3, Ezh2, H3K27me3* and *P-H$_2$AX,* this would provide additional mechanistic insights.

The Ah*Cre*ER^T Cre strain targets gene expression to the gastrointestinal tract under the CYP1A1 promoter in a mosaic and sporadic pattern, in an ascending gradient from the duodenum to the ileum and with little expression in the colon (Kemp et al., 2004). Using the ROSA26R Cre reporter strain, *Braf^{V600E}* expression in the intestine was shown to be mosaic and up to 70%, using the ROSA26R Cre reporter strain (Carrager et al., 2010). This made analysis of the *Braf^{V600E}* expressing intestine difficult to determine because not every crypt was recombined and the positive crypts were unidentifiable. To overcome this issue an alternative Cre stain should be crossed with the *Braf$^{LSL/+}$* mice. The obvious choice would be the Tamoxifen inducible Villin-Cre transgenic mouse strain, whereby Cre expression is targeted to the enterocyte cells of the crypt and villi. Gene expression using this system has been shown to have high levels of recombination throughout the entire intestinal epithelium including in the colon (el Marjou et al., 2004; Wakeman et al., 2012).

To progress this study further and to confirm the role of Ezh2 in the development of serrated adenomas, $Braf^{LSL-V600E}$/Villin-Cre mice could be crossed to Ezh2 'knockout' mice. This will determine if the hypothesis from this study is correct, that activation and expression of Ezh2 is a key factor in the progression from senescence epithelium to serrated adenoma development.

7.4 Conclusion

This data from this mouse model has provided insight into the role of $Braf^{V600E}$ in serrated colorectal cancer. The epithelial crypt cells expressing $Braf^{V600E}$ exhibit multiple changes to gene and protein expression over a 12wk time course, this is summarised in Figure 7.2. Briefly, sporadic expression of $Braf^{V600E}$ in the crypts of the SI results in crypt hyperplasia through enhanced activation of the MAPK signalling pathway. This however is short lived and OIS occurs through activation of the TSG $p16^{INK4A}$. OIS is overcome by the growth of sporadic individual serrated adenomas, which are absent of $p16^{INK4A}$ expression. DNA methylation of a key CpG Island in $p16^{INK4a}$ is associated with loss of expression of this gene. Levels of the histone methylation mark H3K27me3 were also significantly reduced upon $p16^{INK4a}$ expression and this was related to the up-regulated expression of the de methylase $Jmjd3$, which is known to act at the $Cdkn2a$ locus. Tumour progression was associated with activation of the protein expression of the Ezh2 that was elevated in the crypts prior to tumour development and was highly expressed in the serrated tumours (Figure 7.3). The cause of elevated Ezh2 was not identified in this study, however recent data has suggested that Ezh2 is up-regulated in by DNA damage possibly as a consequence of hypoxia (Chang et al., 2011). To confirm

172

Figure 7.2 Hypothesis for transcriptional regulation of *p16^INK4a* exon 1α after *Braf^V600E*-expression in crypt cells of the mouse SI. A) In wildtype cells, exon 1α of the *Cdkn2a* locus shows some level of histone and DNA methylation by the presence of both H3k27me3 and 5-methylcytosine. p16^INK4A expression is low/absent. B) After ~3days-1wk post-*Braf^V600E* expression, levels of the histone demethylase *Jmjd3* are up-regulated and both H3k27me3 and 5-methylcytosine are down-regulated leading to expression of *p16^INK4A* and senescence. Dnmt3b levels remain high but are not active at the *Cdkn2a* locus possibly because Ezh2 is not present. (C) p16^INK4A expression is repressed when expression of Ezh2 is increased. Ezh2 could be increased due to a DNA damage response induced by hypoxia.
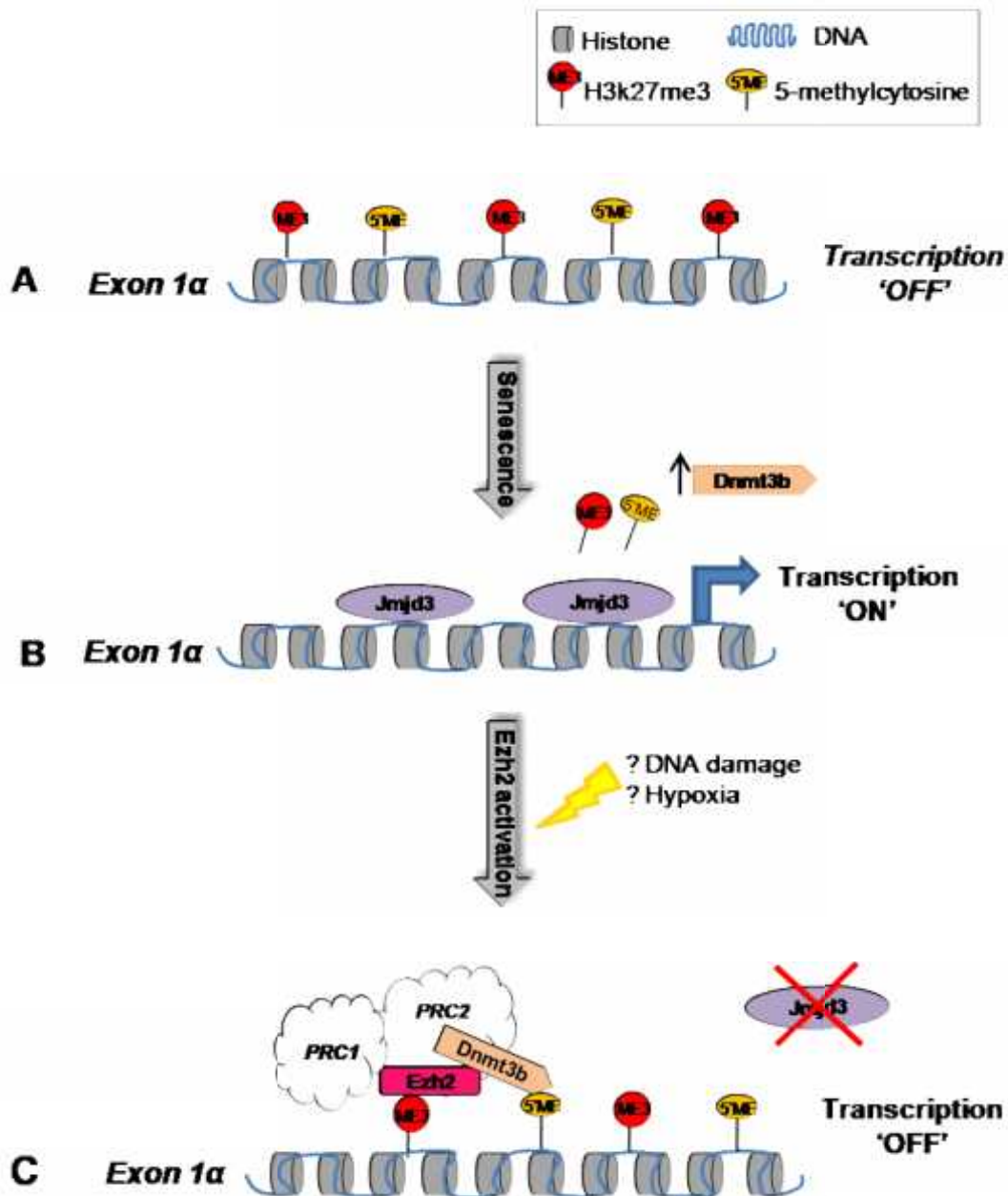
this further analysis needs to be performed focusing on the expression and activity of *Ezh2* using an *Ezh2* knockout mouse strain.

The results from this study confirm *Braf*^{V600E} is a founder mutation in serrated CRCs and that *Braf*^{V600E}-induced OIS is a significant factor in this pathway, similar to the activities of *Braf*^{V600E} in melanoma progression. It also provides evidence for the association of *Braf*^{V600E} and CIMP-H in this form of CRC and supports the need for clear identification of early CRC polyps/adenomas to provide tailored treatment plans.

Figure 7.3 Diagram to illustrate the morphological and gene/protein expression changes in the mouse gut over the *Braf*^V600E expressing time course. The time course analysed was over 3 days to 12wks post-*Braf*^V600E expression. Braf^V600E expression induced crypt cell hyperproliferation, this was followed by oncogene induced senescence (OIS), with the up-regulation of *p16*^INK4a and *p15*^INK4b TSGs. Up-regulated expression of a key histone demethylase, Jmjd3 was also seen at this time. This suggesting a role for histone demethylation in this model. Proliferation was then regained in the epithelium along with the growth of adenomas, which occurred with an increase in the key histone methylation regulator, Ezh2. Increased expression of genes/proteins is shown at the corresponding time point by the coloured lines.
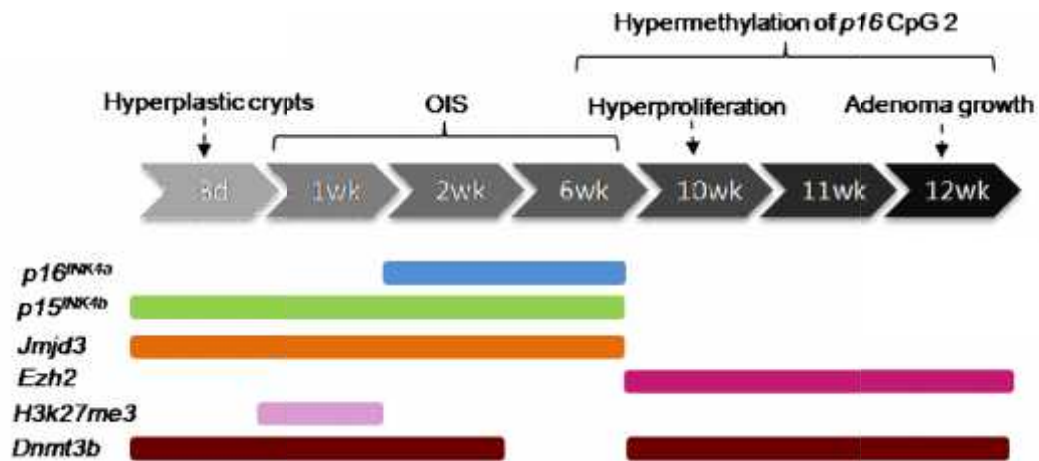
The following published article is not available in the electronic version of this thesis due to copyright restrictions:

Carragher, L.A.S.; Snell, K.R. et al. (2010) ^{V600E}Braf induces gastrointestinal crypt senescence and promotes tumour progression through enhanced CpG methylation of $p16^{INK4a}$. EMBO Molecular Medicine, 2 (11), pp. 458-471. http://dx.doi.org/10.1002/emmm.201000099.

The full version can be consulted at the University of Leicester Library.

References

Abraham D, Podar K, Pacher M, Kubicek M, Welzel N, Hemmings BA, Dilworth SM, Mischak H, Kolch W, Baccarini M. 2000. Raf-1-associated protein phosphatase 2A as a positive regulator of kinase activation. *J Biol Chem.* Jul 21;275(29):22300-4.

Agger, K., Cloos, P.A., Rudkjaer, L., Williams, K., Andersen, G., Christensen, J. & Helin, K. 2009, "The H3K27me3 demethylase JMJD3 contributes to the activation of the INK4A-ARF locus in response to oncogene- and stress-induced senescence", *Genes & development,* vol. 23, no. 10, pp. 1171-1176.

Ahnen, D.J. 1991, "Genetics of colon cancer", *The Western journal of medicine,* vol. 154, no. 6, pp. 700-705.

Aoki, A., Suetake, I., Miyagawa, J., Fujio, T., Chijiwa, T., Sasaki, H. & Tajima, S. 2001, "Enzymatic properties of de novo-type mouse DNA (cytosine-5) methyltransferases", *Nucleic acids research,* vol. 29, no. 17, pp. 3506-3512.

Assoian, R.K. 1997, "Control of the G1 phase cyclin-dependent kinases by mitogenic growth factors and the extracellular matrix", *Cytokine & growth factor reviews,* vol. 8, no. 3, pp. 165-170.

Avruch, J., Khokhlatchev, A., Kyriakis, J.M., Luo, Z., Tzivion, G., Vavvas, D. & Zhang, X.F. 2001, "Ras activation of the Raf kinase: tyrosine kinase recruitment of the MAP kinase cascade", *Recent progress in hormone research,* vol. 56, pp. 127-155.

Baker, S.J., Fearon, E.R., Nigro, J.M., Hamilton, S.R., Preisinger, A.C., Jessup, J.M., vanTuinen, P., Ledbetter, D.H., Barker, D.F., Nakamura, Y., White, R. & Vogelstein, B. 1989, "Chromosome 17 deletions and p53 gene mutations in colorectal carcinomas", *Science (New York, N.Y.),* vol. 244, no. 4901, pp. 217-221.

Barnier JV, Papin C, Eychène A, Lecoq O, Calothy G. 1995. The mouse B-raf gene encodes multiple protein isoforms with tissue-specific expression. *J Biol Chem.* Oct 6;270(40):23381-9

Barradas, M., Anderton, E., Acosta, J.C., Li, S., Banito, A., Rodriguez-Niedenfuhr, M., Maertens, G., Banck, M., Zhou, M.M., Walsh, M.J., Peters, G. & Gil, J. 2009, "Histone demethylase JMJD3 contributes to epigenetic control of INK4a/ARF by oncogenic RAS", *Genes & development,* vol. 23, no. 10, pp. 1177-1182.

Barry, E.L., Baron, J.A., Grau, M.V., Wallace, K. & Haile, R.W. 2006, "K-ras mutations in incident sporadic colorectal adenomas", *Cancer,* vol. 106, no. 5, pp. 1036-1040.

Bartkova, J., Rezaei, N., Liontos, M., Karakaidos, P., Kletsas, D., Issaeva, N., Vassiliou, L.V., Kolettas, E., Niforou, K., Zoumpourlis, V.C., Takaoka, M., Nakagawa, H., Tort, F., Fugger, K., Johansson, F., Sehested, M., Andersen, C.L., Dyrskjot, L., Orntoft, T., Lukas, J., Kittas, C., Helleday, T., Halazonetis, T.D., Bartek, J. & Gorgoulis, V.G. 2006, "Oncogene-induced senescence is part of the tumorigenesis barrier imposed by DNA damage checkpoints", *Nature,* vol. 444, no. 7119, pp. 633-637.

Batlle, E., Henderson, J.T., Beghtel, H., van den Born, M.M., Sancho, E., Huls, G., Meeldijk, J., Robertson, J., van de Wetering, M., Pawson, T. & Clevers, H. 2002, "Beta-catenin and TCF mediate cell positioning in the intestinal epithelium by controlling the expression of EphB/ephrinB", *Cell,* vol. 111, no. 2, pp. 251-263.

Beach, R., Chan, A.O., Wu, T.T., White, J.A., Morris, J.S., Lunagomez, S., Broaddus, R.R., Issa, J.P., Hamilton, S.R. & Rashid, A. 2005, "BRAF mutations in aberrant crypt foci and hyperplastic polyposis", *The American journal of pathology,* vol. 166, no. 4, pp. 1069-1075.

Bennecke, M., Kriegl, L., Bajbouj, M., Retzlaff, K., Robine, S., Jung, A., Arkan, M.C., Kirchner, T. & Greten, F.R. 2010, "Ink4a/Arf and oncogene-induced senescence prevent tumor progression during alternative colorectal tumorigenesis", *Cancer cell,* vol. 18, no. 2, pp. 135-146.

Bestor, T., Laudano, A., Mattaliano, R. & Ingram, V. 1988, "Cloning and sequencing of a cDNA encoding DNA methyltransferase of mouse cells. The carboxyl-terminal domain of the mammalian enzymes is related to bacterial restriction methyltransferases", *Journal of Molecular Biology,* vol. 203, no. 4, pp. 971-983.

Bhatt, K.V., Spofford, L.S., Aram, G., McMullen, M., Pumiglia, K. & Aplin, A.E. 2005, "Adhesion control of cyclin D1 and p27Kip1 levels is deregulated in melanoma cells through BRAF-MEK-ERK signaling", *Oncogene,* vol. 24, no. 21, pp. 3459-3471.

Bird, A. 2001, "Molecular biology. Methylation talk between histones and DNA", *Science (New York, N.Y.),* vol. 294, no. 5549, pp. 2113-2115.

Bodmer WF, Bailey CJ, Bodmer J, Bussey HJ, Ellis A, Gorman P, Lucibello FC, Murday VA, Rider SH, Scambler P. 1987. Localization of the gene for familial adenomatous polyposis on chromosome 5. *Nature.* Aug 13-19;328(6131):614-6.

Bodnar, R.J., Romero, M.T. & Kramer, E. 1988, "Organismic variables and pain inhibition: roles of gender and aging", *Brain research bulletin,* vol. 21, no. 6, pp. 947-953.

Boland, C.R., Sato, J., Saito, K., Carethers, J.M., Marra, G., Laghi, L. & Chauhan, D.P. 1998, "Genetic instability and chromosomal aberrations in colorectal cancer: a review of the current models", *Cancer detection and prevention,* vol. 22, no. 5, pp. 377-382.

Booth, C., Brady, G. & Potten, C.S. 2002, "Crowd control in the crypt", *Nature medicine,* vol. 8, no. 12, pp. 1360-1361.

Bos, J.L., Fearon, E.R., Hamilton, S.R., Verlaan-de Vries, M., van Boom, J.H., van der Eb, A.J. & Vogelstein, B. 1987, "Prevalence of ras gene mutations in human colorectal cancers", *Nature,* vol. 327, no. 6120, pp. 293-297.

Bracken, A.P., Pasini, D., Capra, M., Prosperini, E., Colli, E. & Helin, K. 2003, "EZH2 is downstream of the pRB-E2F pathway, essential for proliferation and amplified in cancer", *The EMBO journal,* vol. 22, no. 20, pp. 5323-5335.

Bracken A.P, Kleine-Kohlbrecher D, Dietrich N, Pasini D, Gargiulo G, Beekman C, Theilgaard-Monch K, Minucci S, Porse BT, Marine JC, et al (2007). The polycomb group proteins bind throughout the INK4A-ARF locus and are disassociated in senescent cells. Genes Dev 21: 525-530.

Brock, H.W. & van Lohuizen, M. 2001, "The Polycomb group--no longer an exclusive club?", *Current opinion in genetics & development,* vol. 11, no. 2, pp. 175-181.

Busca, R., Abbe, P., Mantoux, F., Aberdam, E., Peyssonnaux, C., Eychene, A., Ortonne, J.P. & Ballotti, R. 2000, "Ras mediates the cAMP-dependent activation of extracellular signal-regulated kinases (ERKs) in melanocytes", *The EMBO journal,* vol. 19, no. 12, pp. 2900-2910.

Campisi, J. 2005, "Senescent cells, tumor suppression, and organismal aging: good citizens, bad neighbors", *Cell,* vol. 120, no. 4, pp. 513-522.

Cao, R. & Zhang, Y. 2004, "SUZ12 is required for both the histone methyltransferase activity and the silencing function of the EED-EZH2 complex", *Molecular cell,* vol. 15, no. 1, pp. 57-67.

Chan, T.L., Zhao, W., Leung, S.Y., Yuen, S.T. & Cancer Genome Project 2003, "BRAF and KRAS mutations in colorectal hyperplastic polyps and serrated adenomas", *Cancer research,* vol. 63, no. 16, pp. 4878-4881.

Chang., L & Karin., M. 2001, Mammalian MAP kinase signalling cascades. *Nature.*,1;410 (6824) pp.37-40.

Chang, C.J., Yang, J.Y., Xia, W., Chen, C.T., Xie, X., Chao, C.H., Woodward, W.A., Hsu, J.M., Hortobagyi, G.N. & Hung, M.C. 2011, "EZH2 promotes expansion of breast tumor initiating cells through activation of RAF1-beta-catenin signaling", *Cancer cell,* vol. 19, no. 1, pp. 86-100.

Chen Z, Seimiya H, Naito M, Mashima T, Kizaki A, Dan S, Imaizumi M, Ichijo H, Miyazono K, Tsuruo T. 1999, "ASK1 mediates apoptotic cell death induced by genotoxic stress", *Oncogene,* Jan 7;18 (1) pp.173-80.

Chen, T., Ueda, Y., Dodge, J.E., Wang, Z. & Li, E. 2003, "Establishment and maintenance of genomic methylation patterns in mouse embryonic stem cells by Dnmt3a and Dnmt3b", *Molecular and cellular biology,* vol. 23, no. 16, pp. 5594-5605.

Chen, T., Ueda, Y., Xie, S. & Li, E. 2002, "A novel Dnmt3a isoform produced from an alternative promoter localizes to euchromatin and its expression correlates with active de novo methylation", *The Journal of biological chemistry,* vol. 277, no. 41, pp. 38746-38754.

Chong H, Lee J, Guan KL. 2001. Positive and negative regulation of Raf kinase activity and function by phosphorylation. *EMBO J.* Jul 16;20(14):3716-27

Clark R, Wong G, Arnheim N, Nitecki D, McCormick F.1985. Antibodies specific for amino acid 12 of the ras oncogene product inhibit GTP binding. *Proc Natl Acad Sci USA.* Aug;82(16):5280-4.

Collado, M., Gil, J., Efeyan, A., Guerra, C., Schuhmacher, A.J., Barradas, M., Benguria, A., Zaballos, A., Flores, J.M., Barbacid, M., Beach, D. & Serrano, M. 2005, "Tumour biology: senescence in premalignant tumours", *Nature,* vol. 436, no. 7051, pp. 642.

Collado, M. & Serrano, M. 2006, "The power and the promise of oncogene-induced senescence markers", *Nature reviews.Cancer,* vol. 6, no. 6, pp. 472-476.

Collett, K., Eide, G.E., Arnes, J., Stefansson, I.M., Eide, J., Braaten, A., Aas, T., Otte, A.P. & Akslen, L.A. 2006, "Expression of enhancer of zeste homologue 2 is significantly associated with increased tumor cell proliferation and is a marker of aggressive breast cancer", *Clinical cancer research : an official journal of the American Association for Cancer Research,* vol. 12, no. 4, pp. 1168-1174.

Czermin, B., Melfi, R., McCabe, D., Seitz, V., Imhof, A. & Pirrotta, V. 2002, "Drosophila enhancer of Zeste/ESC complexes have a histone H3 methyltransferase activity that marks chromosomal Polycomb sites", *Cell,* vol. 111, no. 2, pp. 185-196.

Dai, C.Y., Furth, E.E., Mick, R., Koh, J., Takayama, T., Niitsu, Y. & Enders, G.H. 2000, "p16(INK4a) expression begins early in human colon neoplasia and correlates inversely with markers of cell proliferation", *Gastroenterology,* vol. 119, no. 4, pp. 929-942.

Dankort, D., Filenova, E., Collado, M., Serrano, M., Jones, K. & McMahon, M. 2007, "A new mouse model to explore the initiation, progression, and therapy of BRAFV600E-induced lung tumors", *Genes & development,* vol. 21, no. 4, pp. 379-384.

Davies, H., Bignell, G.R., Cox, C., Stephens, P., Edkins, S., Clegg, S., Teague, J., Woffendin, H., Garnett, M.J., Bottomley, W., Davis, N., Dicks, E., Ewing, R., Floyd, Y., Gray, K., Hall, S., Hawes, R., Hughes, J., Kosmidou, V., Menzies, A., Mould, C., Parker, A., Stevens, C., Watt, S., Hooper, S., Wilson, R., Jayatilake, H., Gusterson, B.A., Cooper, C., Shipley, J., Hargrave, D., Pritchard-Jones, K., Maitland, N., Chenevix-Trench, G., Riggins, G.J., Bigner, D.D., Palmieri, G., Cossu, A., Flanagan, A., Nicholson, A., Ho, J.W., Leung, S.Y., Yuen, S.T., Weber, B.L., Seigler, H.F., Darrow, T.L., Paterson, H., Marais, R., Marshall, C.J., Wooster, R., Stratton, M.R. & Futreal, P.A. 2002, "Mutations of the BRAF gene in human cancer", *Nature,* vol. 417, no. 6892, pp. 949-954.

Dérijard.,B, Hibi., M, Wu.,IH, Barrett.,T, Su,.B, Deng.,T, Karin.,M, Davis. 1994, "JNK1: A protein kinase stimulated by UV light and Ha-Ras that binds and phosphorylates the c-Jun activation domain" Cell: Vol. 76, 6. 1025-1037.

Dhillon, A.S., Hagan, S., Rath, O. & Kolch, W. 2007, "MAP kinase signalling pathways in cancer", *Oncogene,* vol. 26, no. 22, pp. 3279-3290.

Dhomen N, Reis-Filho JS, da Rocha Dias S, Hayward R, Savage K, Delmas V, Larue L, Pritchard C, Marais R (2009) Oncogenic Braf induces melanocyte senescence and melanoma in mice. Cancer Cell 15: 294-303.

Downs, J.A., Allard, S., Jobin-Robitaille, O., Javaheri, A., Auger, A., Bouchard, N., Kron, S.J., Jackson, S.P. & Cote, J. 2004, "Binding of chromatin-modifying activities to phosphorylated histone H2A at DNA damage sites", *Molecular cell,* vol. 16, no. 6, pp. 979-990.

Emuss, V., Garnett, M., Mason, C. & Marais, R. 2005, "Mutations of C-RAF are rare in human cancer because C-RAF has a low basal kinase activity compared with B-RAF", *Cancer research,* vol. 65, no. 21, pp. 9719-9726.

Ettarh, R.R. & Carr, K.E. 1996, "Morphometric analysis of the small intestinal epithelium in the indomethacin-treated mouse", *Journal of anatomy,* vol. 189 (Pt 1), no. Pt 1, pp. 51-56.

Fatemi, M., Pao, M.M., Jeong, S., Gal-Yam, E.N., Egger, G., Weisenberger, D.J. & Jones, P.A. 2005, "Footprinting of mammalian promoters: use of a CpG DNA methyltransferase revealing nucleosome positions at a single molecule level", *Nucleic acids research,* vol. 33, no. 20, pp. e176.

Fearon, E.R. & Vogelstein, B. 1990, "A genetic model for colorectal tumorigenesis", *Cell,* vol. 61, no. 5, pp. 759-767.

Fodde, R., Edelmann, W., Yang, K., van Leeuwen, C., Carlson, C., Renault, B., Breukel, C., Alt, E., Lipkin, M. & Khan, P.M. 1994, "A targeted chain-termination mutation in the mouse Apc gene results in multiple intestinal tumors", *Proceedings of the National Academy of Sciences of the United States of America,* vol. 91, no. 19, pp. 8969-8973.

Garnett MJ, Rana S, Paterson H, Barford D, Marais R. 2005, "Wild-type and mutant B-RAF activate C-RAF through distinct mechanisms involving heterodimerization", *Mol Cell*, 22;20(6) pp.963-9.

Gibson, S.L., Boquoi, A., Chen, T., Sharpless, N.E., Brensinger, C. & Enders, G.H. 2005, "p16(Ink4a) inhibits histologic progression and angiogenic signaling in min colon tumors", *Cancer biology & therapy,* vol. 4, no. 12, pp. 1389-1394.

Groden, J., Thliveris, A., Samowitz, W., Carlson, M., Gelbert, L., Albertsen, H., Joslyn, G., Stevens, J., Spirio, L. & Robertson, M. 1991, "Identification and characterization of the familial adenomatous polyposis coli gene", *Cell,* vol. 66, no. 3, pp. 589-600.

Halaban, R. 2000, "The regulation of normal melanocyte proliferation", *Pigment Cell Research / sponsored by the European Society for Pigment Cell Research and the International Pigment Cell Society,* vol. 13, no. 1, pp. 4-14.

Halilovic E, FAU - Solit, D.B. & Solit DB "Therapeutic strategies for inhibiting oncogenic BRAF signaling.", *- Curr Opin Pharmacol.2008 Aug;8(4):419-26.Epub 2008 Aug 3.,* , no. 1471-4892 (Print).

Hanahan, D. & Weinberg, R.A. 2000, "The hallmarks of cancer", *Cell,* vol. 100, no. 1, pp. 57-70.

Hawkins NJ, FAU - Bariol, C., Bariol C, FAU - Ward, R.L. & Ward RL "The serrated neoplasia pathway.", *- Pathology.2002 Dec;34(6):548-55.,* , no. 0031-3025.

Hayashi, T., Yatani, R., Apostol, J. & Stemmermann, G.N. 1974, "Pathogenesis of hyperplastic polyps of the colon: a hypothesis based on ultrastructure and in vitro cell kinetics", *Gastroenterology,* vol. 66, no. 3, pp. 347-356.

Hayflick, L. & Moorhead, P.S. 1961, "The serial cultivation of human diploid cell strains", *Experimental cell research,* vol. 25, pp. 585-621.

Hekman M, Wiese S, Metz R, Albert S, Troppmair J, Nickel J, Sendtner M, Rapp UR. Dynamic changes in C-Raf phosphorylation and 14-3-3 protein binding in response to growth factor stimulation: differential roles of 14-3-3 protein binding sites.

Herman, J.G. & Baylin, S.B. 2003, "Gene silencing in cancer in association with promoter hypermethylation", *The New England journal of medicine,* vol. 349, no. 21, pp. 2042-2054.

Hernandez-Munoz, I., Taghavi, P., Kuijl, C., Neefjes, J. & van Lohuizen, M. 2005, "Association of BMI1 with polycomb bodies is dynamic and requires PRC2/EZH2 and the maintenance DNA methyltransferase DNMT1", *Molecular and cellular biology,* vol. 25, no. 24, pp. 11047-11058.

Hmitou I, Druillennec S, Valluet A, Peyssonnaux C, Eychène A. 2007. Differential regulation of B-raf isoforms by phosphorylation and autoinhibitory mechanisms. Jan;27(1):31-43. Epub 2006 Oct 30.

Hocker, M. & Wiedenmann, B. 1998, "Molecular mechanisms of enteroendocrine differentiation", *Annals of the New York Academy of Sciences,* vol. 859, pp. 160-174.

Hoshino, R., Chatani, Y., Yamori, T., Tsuruo, T., Oka, H., Yoshida, O., Shimada, Y., Ari-i, S., Wada, H., Fujimoto, J. & Kohno, M. 1999, "Constitutive activation of the 41-/43-kDa mitogen-activated protein kinase signaling pathway in human tumors", *Oncogene,* vol. 18, no. 3, pp. 813-822.

Hou, P., Liu, D., Dong, J. & Xing, M. 2012, "The BRAF(V600E) causes widespread alterations in gene methylation in the genome of melanoma cells", *Cell cycle (Georgetown, Tex.),* vol. 11, no. 2, pp. 286-295.

Hoyle, P.E., Moye, P.W., Steelman, L.S., Blalock, W.L., Franklin, R.A., Pearce, M., Cherwinski, H., Bosch, E., McMahon, M. & McCubrey, J.A. 2000, "Differential abilities of the Raf family of protein kinases to abrogate cytokine dependency and prevent apoptosis in murine hematopoietic cells by a MEK1-dependent mechanism", *Leukemia : official journal of the Leukemia Society of America, Leukemia Research Fund, U.K,* vol. 14, no. 4, pp. 642-656.

Hublitz, P., Albert, M. & Peters, A.H. 2009, "Mechanisms of transcriptional repression by histone lysine methylation", *The International journal of developmental biology,* vol. 53, no. 2-3, pp. 335-354.

Huidobro, C., Urdinguio, R.G., Rodriguez, R.M., Mangas, C., Calvanese, V., Martinez-Camblor, P., Ferrero, C., Parra-Blanco, A., Rodrigo, L., Obaya, A.J., Suarez-Fernandez, L., Astudillo, A., Hernando, H., Ballestar, E., Fernandez, A.F. & Fraga, M.F. 2012, "A DNA methylation signature associated with aberrant promoter DNA hypermethylation of DNMT3B in human colorectal

cancer", *European journal of cancer (Oxford, England : 1990),* vol. 48, no. 14, pp. 2270-2281.

Huleihel M, Goldsborough M, Cleveland J, Gunnell M, Bonner T, Rapp UR. 1986, Characterization of murine A-raf, a new oncogene related to the v-raf oncogene. *Mol Cell Biol.* July; 6(7) 2655-62.

Hüser M, Luckett J, Chiloeches A, Mercer K, Iwobi M, Giblett S, Sun XM, Brown J, Marais R, Pritchard C. 2001. MEK kinase activity is not necessary for Raf-1 function. *EMBO J.* Apr 17;20(8):1940-51.

Hutchison M, Berman KS, Cobb MH. Isolation of TAO1, a protein kinase that activates MEKs in stress-activated protein kinase cascades.1998. *J Biol Chem.* Oct 30;273(44):28625-32.

Iino H, Simms L, Young J, Arnold J, Winship IM, Webb SI, Furlong KL, Leggett B, Jass JR. 2000. DNA microsatellite instability and mismatch repair protein loss in adenomas presenting in hereditary non-polyposis colorectal cancer. Jul;47(1):37-42.

Issa, J.P. 2004, "CpG island methylator phenotype in cancer", *Nature reviews.Cancer,* vol. 4, no. 12, pp. 988-993.

Jacobs, J.J., Kieboom, K., Marino, S., DePinho, R.A. & van Lohuizen, M. 1999, "The oncogene and Polycomb-group gene bmi-1 regulates cell proliferation and senescence through the ink4a locus", *Nature,* vol. 397, no. 6715, pp. 164-168.

Jass, J.R. 1999, "Towards a molecular classification of colorectal cancer", *International journal of colorectal disease,* vol. 14, no. 4-5, pp. 194-200.

Jass JR. Pathology. 2002. Progress in gastrointestinal pathology in the genetic era. Dec;34(6):493.

Jass JR (2007) Classification of colorectal cancer based on correlation of clinical, morphological and molecular features. Histopathology 50: 113-130.

Jo, Y.S., Li, S., Song, J.H., Kwon, K.H., Lee, J.C., Rha, S.Y., Lee, H.J., Sul, J.Y., Kweon, G.R., Ro, H.K., Kim, J.M. & Shong, M. 2006, "Influence of the BRAF V600E mutation on expression of vascular endothelial growth factor in papillary thyroid cancer", *The Journal of clinical endocrinology and metabolism,* vol. 91, no. 9, pp. 3667-3670.

Kambara, T., Simms, L.A., Whitehall, V.L., Spring, K.J., Wynter, C.V., Walsh, M.D., Barker, M.A., Arnold, S., McGivern, A., Matsubara, N., Tanaka, N., Higuchi, T., Young, J., Jass, J.R. & Leggett, B.A. 2004, "BRAF mutation is associated with DNA methylation in serrated polyps and cancers of the colorectum", *Gut,* vol. 53, no. 8, pp. 1137-1144.

Karasarides, M., Chiloeches, A., Hayward, R., Niculescu-Duvaz, D., Scanlon, I., Friedlos, F., Ogilvie, L., Hedley, D., Martin, J., Marshall, C.J., Springer, C.J. & Marais, R. 2004, "B-RAF is a therapeutic target in melanoma", *Oncogene,* vol. 23, no. 37, pp. 6292-6298.

Kato Y, Kravchenko VV, Tapping RI, Han J, Ulevitch RJ, Lee JD. 1997. BMK1/ERK5 regulates serum-induced early gene expression through transcription factor MEF2C. *EMBO J.* Dec 1;16(23):7054-66.

Kato Y, Tapping RI, Huang S, Watson MH, Ulevitch RJ, Lee JD. 1998. Bmk1/Erk5 is required for cell proliferation induced by epidermal growth factor. *Nature.* Oct 15;395(6703):713-6.

Kemp R, FAU - Ireland, H., Ireland H, FAU - Clayton, E., Clayton E, FAU - Houghton, C., Houghton C, FAU - Howard, L., Howard L, FAU - Winton, D.J. & Winton DJ "Elimination of background recombination: somatic induction of Cre by combined transcriptional regulation and hormone binding affinity.", - *Nucleic Acids Res.2004 Jul 1;32(11):e92.Print 2004.,* , no. 1362-4962 (Electronic).

King AJ, Sun H, Diaz B, Barnard D, Miao W, Bagrodia S, Marshall MS. 1998. The protein kinase Pak3 positively regulates Raf-1 activity through phosphorylation of serine 338. *Nature.* Nov 12;396(6707):180-3.

Kinzler, K.W. & Vogelstein, B. 1996, "Lessons from hereditary colorectal cancer", *Cell,* vol. 87, no. 2, pp. 159-170.

Kirmizis, A., Bartley, S.M. & Farnham, P.J. 2003, "Identification of the polycomb group protein SU(Z)12 as a potential molecular target for human cancer therapy", *Molecular cancer therapeutics,* vol. 2, no. 1, pp. 113-121.

Kleer, C.G., Cao, Q., Varambally, S., Shen, R., Ota, I., Tomlins, S.A., Ghosh, D., Sewalt, R.G., Otte, A.P., Hayes, D.F., Sabel, M.S., Livant, D., Weiss, S.J., Rubin, M.A. & Chinnaiyan, A.M. 2003, "EZH2 is a marker of aggressive breast cancer and promotes neoplastic transformation of breast epithelial cells", *Proceedings of the National Academy of Sciences of the United States of America,* vol. 100, no. 20, pp. 11606-11611.

Koinuma, K., Shitoh, K., Miyakura, Y., Furukawa, T., Yamashita, Y., Ota, J., Ohki, R., Choi, Y.L., Wada, T., Konishi, F., Nagai, H. & Mano, H. 2004, "Mutations of BRAF are associated with extensive hMLH1 promoter methylation in sporadic colorectal carcinomas", *International journal of cancer.Journal international du cancer,* vol. 108, no. 2, pp. 237-242.

Kolch.,W. 2000, Meaningful relationships: the regulation of the Ras/Raf/MEK/ERK pathway by protein interactions, *Biochem J,*15;351 Pt 2:289-305.

Konishi K, Yamochi T, Makino R, Kaneko K, Yamamoto T, Nozawa H, Katagiri A, Ito H, Nakayama K, Ota H, Mitamura K, Imawari M. Clin Cancer Res. 2004. Molecular differences between sporadic serrated and conventional colorectal adenomas. May 1;10(9):3082-90.

Kriegl, L., Neumann, J., Vieth, M., Greten, F.R., Reu, S., Jung, A. & Kirchner, T. 2011, "Up and downregulation of p16(Ink4a) expression in BRAF-mutated polyps/adenomas indicates a senescence barrier in the serrated route to colon cancer", *Modern pathology : an official journal of the United States and Canadian Academy of Pathology, Inc,* vol. 24, no. 7, pp. 1015-1022.

Krimpenfort, P., Ijpenberg, A., Song, J.Y., van der Valk, M., Nawijn, M., Zevenhoven, J. & Berns, A. 2007, "p15Ink4b is a critical tumour suppressor in the absence of p16Ink4a", *Nature,* vol. 448, no. 7156, pp. 943-946.

Kunimoto, Y., Nakano, S., Kataoka, H., Shimada, Y., Oshimura, M. & Kitano, H. 2011, "Deleted in Esophageal Cancer 1(DEC1) is down-regulated and contributes to migration in head and neck squamous cell carcinoma cell lines", *ORL; journal for oto-rhino-laryngology and its related specialties,* vol. 73, no. 1, pp. 17-23.

Kuzmichev, A., Jenuwein, T., Tempst, P. & Reinberg, D. 2004, "Different EZH2-containing complexes target methylation of histone H1 or nucleosomal histone H3", *Molecular cell,* vol. 14, no. 2, pp. 183-193.

Kyriakis.,JM, App., H, Zhang., XF, P, Banerjee.,P, David L. Brautigan, Ulf R. Rapp & Avruch., J. 1992, Raf-1 activates MAP kinase-kinase, *Nature* 358, 417 - 421.

La Salle, S. & Trasler, J.M. 2006, "Dynamic expression of DNMT3a and DNMT3b isoforms during male germ cell development in the mouse", *Developmental biology,* vol. 296, no. 1, pp. 71-82.

Leslie A, Carey FA, Pratt NR, Steele RJ. 2002. The colorectal adenoma-carcinoma sequence. *Br J Surg.* Jul;89(7):845-60.

Leung, A.C., Wong, V.C., Yang, L.C., Chan, P.L., Daigo, Y., Nakamura, Y., Qi, R.Z., Miller, L.D., Liu, E.T., Wang, L.D., Li, J.L., Law, S., Tsao, S.W. & Lung, M.L. 2008, "Frequent decreased expression of candidate tumor suppressor gene, DEC1, and its anchorage-independent growth properties and impact on global gene expression in esophageal carcinoma", *International journal of cancer.Journal international du cancer,* vol. 122, no. 3, pp. 587-594.

Li, L.C. & Dahiya, R. 2002, "MethPrimer: designing primers for methylation PCRs", *Bioinformatics (Oxford, England),* vol. 18, no. 11, pp. 1427-1431.

Light Y, Paterson H, Marais R. 2002. 14-3-3 antagonizes Ras-mediated Raf-1 recruitment to the plasma membrane to maintain signaling fidelity. *Mol Cell Biol.* Jul;22(14):4984-96.

Lin, H., Yamada, Y., Nguyen, S., Linhart, H., Jackson-Grusby, L., Meissner, A., Meletis, K., Lo, G. & Jaenisch, R. 2006, "Suppression of intestinal neoplasia by deletion of Dnmt3b", *Molecular and cellular biology,* vol. 26, no. 8, pp. 2976-2983.

Linhart, H.G., Lin, H., Yamada, Y., Moran, E., Steine, E.J., Gokhale, S., Lo, G., Cantu, E., Ehrich, M., He, T., Meissner, A. & Jaenisch, R. 2007, "Dnmt3b promotes tumorigenesis in vivo by gene-specific de novo methylation and transcriptional silencing", *Genes & development,* vol. 21, no. 23, pp. 3110-3122.

Liu, W., Kelly, J.W., Trivett, M., Murray, W.K., Dowling, J.P., Wolfe, R., Mason, G., Magee, J., Angel, C., Dobrovic, A. & McArthur, G.A. 2007, "Distinct clinical and pathological features are associated with the BRAF(T1799A(V600E)) mutation in primary melanoma", *The Journal of investigative dermatology,* vol. 127, no. 4, pp. 900-905.

Longacre, T.A., Fenoglio-Preiser, C,M. 1990, Mixed hyperplastic adenomatous polyps/serrated adenomas. A distinct form of colorectal neoplasia. *Am J Surg Pathol.* 14(6):524-37.

Loonstra, A., Vooijs, M., Beverloo, H.B., Allak, B.A., van Drunen, E., Kanaar, R., Berns, A. & Jonkers, J. 2001, "Growth inhibition and DNA damage induced by Cre recombinase in mammalian cells", *Proceedings of the National Academy of Sciences of the United States of America,* vol. 98, no. 16, pp. 9209-9214.

Lowenstein EJ, Daly RJ, Batzer AG, Li W, Margolis B, Lammers R, Ullrich A, Skolnik EY, Bar-Sagi D, Schlessinger J. 1992. Cell. Aug 7;70(3):431-42.

MacDonald, J.L., Gin, C.S. & Roskams, A.J. 2005, "Stage-specific induction of DNA methyltransferases in olfactory receptor neuron development", *Developmental biology,* vol. 288, no. 2, pp. 461-473.

Makinen MJ "Colorectal serrated adenocarcinoma.", *- Histopathology.2007 Jan;50(1):131-50.,* , no. 0309-0167 (Print).

Malumbres, M., Perez De Castro, I., Hernandez, M.I., Jimenez, M., Corral, T. & Pellicer, A. 2000, "Cellular response to oncogenic ras involves induction of the Cdk4 and Cdk6 inhibitor p15(INK4b)", *Molecular and cellular biology,* vol. 20, no. 8, pp. 2915-2925.

Marais, R., Light, Y., Paterson, H.F., Mason, C.S. & Marshall, C.J. 1997, "Differential regulation of Raf-1, A-Raf, and B-Raf by oncogenic ras and

tyrosine kinases", *The Journal of biological chemistry,* vol. 272, no. 7, pp. 4378-4383.

Marais R, Marshall CJ. 1996. Control of the ERK MAP kinase cascade by Ras and Raf, *Cancer Surv.*, 27:101-25.

Marais R, Light Y, Paterson HF, Marshall CJ. 1995. *EMBO J.* Ras recruits Raf-1 to the plasma membrane for activation by tyrosine phosphorylation. Jul 3;14(13):3136-45.

Marais.,R, Wynne.,J, Treisman.,R. 1993. "The SRF accessory protein Elk-1 contains a growth factor-regulated transcriptional activation domain", *Cell,* volume 73 issue 2 pp.381 – 393.

Markowitz S, Wang J, Myeroff L, Parsons R, Sun L, Lutterbaugh J, Fan RS, Zborowska E, Kinzler KW, Vogelstein B. **1995.** Inactivation of the type II TGF-beta receptor in colon cancer cells with microsatellite instability. *Science.* Jun 2;268(5215):1336-8

Marshman, E., Ottewell, P.D., Potten, C.S. & Watson, A.J. 2001, "Caspase activation during spontaneous and radiation-induced apoptosis in the murine intestine", *The Journal of pathology,* vol. 195, no. 3, pp. 285-292.

Mason, C.S., Springer, C.J., Cooper, R.G., Superti-Furga, G., Marshall, C.J. & Marais, R. 1999, "Serine and tyrosine phosphorylations cooperate in Raf-1, but not B-Raf activation", *The EMBO journal,* vol. 18, no. 8, pp. 2137-2148.

Mercer, K., Giblett, S., Green, S., Lloyd, D., DaRocha Dias, S., Plumb, M., Marais, R. & Pritchard, C. 2005, "Expression of endogenous oncogenic V600EB-raf induces proliferation and developmental defects in mice and transformation of primary fibroblasts", *Cancer research,* vol. 65, no. 24, pp. 11493-11500.

Mercer, K.E. & Pritchard, C.A. 2003, "Raf proteins and cancer: B-Raf is identified as a mutational target", *Biochimica et Biophysica Acta (BBA) - Reviews on Cancer,* vol. 1653, no. 1, pp. 25-40.

Michaloglou, C., Vredeveld, L.C., Soengas, M.S., Denoyelle, C., Kuilman, T., van der Horst, C.M., Majoor, D.M., Shay, J.W., Mooi, W.J. & Peeper, D.S. 2005, "BRAFE600-associated senescence-like cell cycle arrest of human naevi", *Nature,* vol. 436, no. 7051, pp. 720-724.

Minoo, P. & Jass, J.R. 2006, "Senescence and serration: a new twist to an old tale", *The Journal of pathology,* vol. 210, no. 2, pp. 137-140.

Minoo, P., Moyer, M.P. & Jass, J.R. 2007, "Role of BRAF-V600E in the serrated pathway of colorectal tumourigenesis", *The Journal of pathology,* vol. 212, no. 2, pp. 124-133.

Miyaki M, Konishi M, Kikuchi-Yanoshita R, Enomoto M, Igari T, Tanaka K, Muraoka M, Takahashi H, Amada Y, Fukayama M. 1994. Characteristics of somatic mutation of the adenomatous polyposis coli gene in colorectal tumors. *Cancer Res*. Jun 1;54(11):3011-20.

Muller, H., Bracken, A.P., Vernell, R., Moroni, M.C., Christians, F., Grassilli, E., Prosperini, E., Vigo, E., Oliner, J.D. & Helin, K. 2001, "E2Fs regulate the expression of genes involved in differentiation, development, proliferation, and apoptosis", *Genes & development,* vol. 15, no. 3, pp. 267-285.

Muller, J., Hart, C.M., Francis, N.J., Vargas, M.L., Sengupta, A., Wild, B., Miller, E.L., O'Connor, M.B., Kingston, R.E. & Simon, J.A. 2002, "Histone methyltransferase activity of a Drosophila Polycomb group repressor complex", *Cell,* vol. 111, no. 2, pp. 197-208.

Nikiforova, M.N., Kimura, E.T., Gandhi, M., Biddinger, P.W., Knauf, J.A., Basolo, F., Zhu, Z., Giannini, R., Salvatore, G., Fusco, A., Santoro, M., Fagin, J.A. & Nikiforov, Y.E. 2003, "BRAF mutations in thyroid tumors are restricted to papillary carcinomas and anaplastic or poorly differentiated carcinomas arising from papillary carcinomas", *The Journal of clinical endocrinology and metabolism,* vol. 88, no. 11, pp. 5399-5404.

Noffsinger, A.E. 2009, "Serrated polyps and colorectal cancer: new pathway to malignancy", *Annual review of pathology,* vol. 4, pp. 343-364.

Nosho, K., Shima, K., Irahara, N., Kure, S., Baba, Y., Kirkner, G.J., Chen, L., Gokhale, S., Hazra, A., Spiegelman, D., Giovannucci, E.L., Jaenisch, R., Fuchs, C.S. & Ogino, S. 2009, "DNMT3B expression might contribute to CpG island methylator phenotype in colorectal cancer", *Clinical cancer research : an official journal of the American Association for Cancer Research,* vol. 15, no. 11, pp. 3663-3671.

O'Carroll, D., Erhardt, S., Pagani, M., Barton, S.C., Surani, M.A. & Jenuwein, T. 2001, "The polycomb-group gene Ezh2 is required for early mouse development", *Molecular and cellular biology,* vol. 21, no. 13, pp. 4330-4336.

Okano, M., Takebayashi, S., Okumura, K. & Li, E. 1999, "Assignment of cytosine-5 DNA methyltransferases Dnmt3a and Dnmt3b to mouse chromosome bands 12A2-A3 and 2H1 by in situ hybridization", *Cytogenetics and cell genetics,* vol. 86, no. 3-4, pp. 333-334.

Okano, M., Xie, S. & Li, E. 1998, "Cloning and characterization of a family of novel mammalian DNA (cytosine-5) methyltransferases", *Nature genetics,* vol. 19, no. 3, pp. 219-220.

Oliveira C, Velho S, Moutinho C, Ferreira A, Preto A, Domingo E, Capelinha AF, Duval A, Hamelin R, Machado JC, Schwartz S Jr, Carneiro F, Seruca R.

2007 "KRAS and BRAF oncogenic mutations in MSS colorectal carcinoma progression",Oncogene. 4;26(1):158-63.

Orlow, I., Begg, C.B., Cotignola, J., Roy, P., Hummer, A.J., Clas, B.A., Mujumdar, U., Canchola, R., Armstrong, B.K., Kricker, A., Marrett, L.D., Millikan, R.C., Gruber, S.B., Anton-Culver, H., Zanetti, R., Gallagher, R.P., Dwyer, T., Rebbeck, T.R., Kanetsky, P.A., Wilcox, H., Busam, K., From, L., Berwick, M. & GEM Study Group 2007, "CDKN2A germline mutations in individuals with cutaneous malignant melanoma", *The Journal of investigative dermatology,* vol. 127, no. 5, pp. 1234-1243.

Ortega, S., Malumbres, M. & Barbacid, M. 2002, "Cyclin D-dependent kinases, INK4 inhibitors and cancer", *Biochimica et biophysica acta,* vol. 1602, no. 1, pp. 73-87.

Ory S, Zhou M, Conrads TP, Veenstra TD, Morrison DK. 2003. Protein phosphatase 2A positively regulates Ras signaling by dephosphorylating KSR1 and Raf-1 on critical 14-3-3 binding sites. *Curr Biol.* Aug 19;13(16):1356-64

Ostler, K.R., Davis, E.M., Payne, S.L., Gosalia, B.B., Exposito-Cespedes, J., Le Beau, M.M. & Godley, L.A. 2007, "Cancer cells express aberrant DNMT3B transcripts encoding truncated proteins", *Oncogene,* vol. 26, no. 38, pp. 5553-5563.

Peters G. 2008 An INKlination for epigenetic control of senescence. Nat Structural & Mol Bio 15: 1133-1134.

Peyssonnaux, C. & Eychene, A. 2001, "The Raf/MEK/ERK pathway: new concepts of activation", *Biology of the cell / under the auspices of the European Cell Biology Organization,* vol. 93, no. 1-2, pp. 53-62.

Pietersen, A.M., Horlings, H.M., Hauptmann, M., Langerod, A., Ajouaou, A., Cornelissen-Steijger, P., Wessels, L.F., Jonkers, J., van de Vijver, M.J. & van Lohuizen, M. 2008, "EZH2 and BMI1 inversely correlate with prognosis and TP53 mutation in breast cancer", *Breast cancer research : BCR,* vol. 10, no. 6, pp. R109.

Pinto D, FAU - Clevers, H. & Clevers H "Wnt, stem cells and cancer in the intestine.", *- Biol Cell.2005 Mar;97(3):185-96.,* , no. 0248-4900 (Print).

Pollock, P.M., Harper, U.L., Hansen, K.S., Yudt, L.M., Stark, M., Robbins, C.M., Moses, T.Y., Hostetter, G., Wagner, U., Kakareka, J., Salem, G., Pohida, T., Heenan, P., Duray, P., Kallioniemi, O., Hayward, N.K., Trent, J.M. & Meltzer, P.S. 2003, "High frequency of BRAF mutations in nevi", *Nature genetics,* vol. 33, no. 1, pp. 19-20.

Pradhan, S., Bacolla, A., Wells, R.D. & Roberts, R.J. 1999, "Recombinant human DNA (cytosine-5) methyltransferase. I. Expression, purification, and comparison of de novo and maintenance methylation", *The Journal of biological chemistry,* vol. 274, no. 46, pp. 33002-33010.

Pratilas CA, FAU - Solit, D.B. & Solit DB "Therapeutic strategies for targeting BRAF in human cancer.", *- Rev Recent Clin Trials.2007 May;2(2):121-34.,* , no. 1574-8871 (Print).

Pritchard C, FAU - Carragher, L., Carragher L, FAU - Aldridge, V., Aldridge V, FAU - Giblett, S., Giblett S, FAU - Jin, H., Jin H, FAU - Foster, C., Foster C, FAU - Andreadi, C., Andreadi C, FAU - Kamata, T. & Kamata T "Mouse models for BRAF-induced cancers.", *- Biochem Soc Trans.2007 Nov;35(Pt 5):1329-33.,* , no. 0300-5127 (Print).

Qian, Y., Zhang, J., Yan, B. & Chen, X. 2008, "DEC1, a basic helix-loop-helix transcription factor and a novel target gene of the p53 family, mediates p53-dependent premature senescence", *The Journal of biological chemistry,* vol. 283, no. 5, pp. 2896-2905.

Raaphorst, F.M., Meijer, C.J., Fieret, E., Blokzijl, T., Mommers, E., Buerger, H., Packeisen, J., Sewalt, R.A., Otte, A.P. & van Diest, P.J. 2003, "Poorly differentiated breast carcinoma is associated with increased expression of the human polycomb group EZH2 gene", *Neoplasia (New York, N.Y.),* vol. 5, no. 6, pp. 481-488.

Radtke, F. & Clevers, H. 2005, "Self-renewal and cancer of the gut: two sides of a coin", *Science (New York, N.Y.),* vol. 307, no. 5717, pp. 1904-1909.

Rajagopalan, H., Bardelli, A., Lengauer, C., Kinzler, K.W., Vogelstein, B. & Velculescu, V.E. 2002, "Tumorigenesis: RAF/RAS oncogenes and mismatch-repair status", *Nature,* vol. 418, no. 6901, pp. 934.

Rapp, U.R., Goldsborough, M.D., Mark, G.E., Bonner, T.I., Groffen, J., Reynolds, F.H.,Jr & Stephenson, J.R. 1983, "Structure and biological activity of v-raf, a unique oncogene transduced by a retrovirus", *Proceedings of the National Academy of Sciences of the United States of America,* vol. 80, no. 14, pp. 4218-4222.

Razidlo GL, Kortum RL, Haferbier JL, Lewis RE. 2004. Phosphorylation regulates KSR1 stability, ERK activation, and cell proliferation. *J Biol Chem.* Nov 12;279(46):47808-14.

Reed, K.R., Meniel, V.S., Marsh, V., Cole, A., Sansom, O.J. & Clarke, A.R. 2008, "A limited role for p53 in modulating the immediate phenotype of Apc loss in the intestine", *BMC cancer,* vol. 8, pp. 162-2407-8-162.

Reynolds PA, Sigaroudinia M, Zardo G, Wilson MB, Benton GM, Miller CJ, Hong C, Fridlyand J, Costello JF, Tlsty TD. (2006) Tumor Suppressor p16INK4A Regulates Polycomb-mediated DNA Hypermethylation in Human Mammary Epithelial Cells. J Bio Chem 281 : 24790-24802.

Ringrose, L. & Paro, R. 2004, "Epigenetic regulation of cellular memory by the Polycomb and Trithorax group proteins", *Annual Review of Genetics,* vol. 38, pp. 413-443.

Robertson, K.D., Uzvolgyi, E., Liang, G., Talmadge, C., Sumegi, J., Gonzales, F.A. & Jones, P.A. 1999, "The human DNA methyltransferases (DNMTs) 1, 3a and 3b: coordinate mRNA expression in normal tissues and overexpression in tumors", *Nucleic acids research,* vol. 27, no. 11, pp. 2291-2298.

Rogakou, E.P., Boon, C., Redon, C. & Bonner, W.M. 1999, "Megabase chromatin domains involved in DNA double-strand breaks in vivo", *The Journal of cell biology,* vol. 146, no. 5, pp. 905-916.

Roll, J.D., Rivenbark, A.G., Jones, W.D. & Coleman, W.B. 2008, "DNMT3b overexpression contributes to a hypermethylator phenotype in human breast cancer cell lines", *Molecular cancer,* vol. 7, pp. 15-4598-7-15.

Rosenberg, D.W., Yang, S., Pleau, D.C., Greenspan, E.J., Stevens, R.G., Rajan, T.V., Heinen, C.D., Levine, J., Zhou, Y. & O'Brien, M.J. 2007, "Mutations in BRAF and KRAS differentially distinguish serrated versus non-serrated hyperplastic aberrant crypt foci in humans", *Cancer research,* vol. 67, no. 8, pp. 3551-3554.

Russell, J.L., Weaks, R.L., Berton, T.R. & Johnson, D.G. 2006, "E2F1 suppresses skin carcinogenesis via the ARF-p53 pathway", *Oncogene,* vol. 25, no. 6, pp. 867-876.

Sancho, E., Batlle, E. & Clevers, H. 2004, "Signaling pathways in intestinal development and cancer", *Annual Review of Cell and Developmental Biology,* vol. 20, pp. 695-723.

Sancho, E., Batlle, E. & Clevers, H. 2003, "Live and let die in the intestinal epithelium", *Current opinion in cell biology,* vol. 15, no. 6, pp. 763-770.

Sansom, O.J., Meniel, V.S., Muncan, V., Phesse, T.J., Wilkins, J.A., Reed, K.R., Vass, J.K., Athineos, D., Clevers, H. & Clarke, A.R. 2007, "Myc deletion rescues Apc deficiency in the small intestine", *Nature,* vol. 446, no. 7136, pp. 676-679.

Sansom, O.J., Reed, K.R., Hayes, A.J., Ireland, H., Brinkmann, H., Newton, I.P., Batlle, E., Simon-Assmann, P., Clevers, H., Nathke, I.S., Clarke, A.R. & Winton, D.J. 2004, "Loss of Apc in vivo immediately perturbs Wnt signaling,

differentiation, and migration", *Genes & development,* vol. 18, no. 12, pp. 1385-1390.

Sawa, M., Yamamoto, K., Yokozawa, T., Kiyoi, H., Hishida, A., Kajiguchi, T., Seto, M., Kohno, A., Kitamura, K., Itoh, Y., Asou, N., Hamajima, N., Emi, N. & Naoe, T. 2005, "BMI-1 is highly expressed in M0-subtype acute myeloid leukemia", *International journal of hematology,* vol. 82, no. 1, pp. 42-47.

Sawyer, E.J., Cerar, A., Hanby, A.M., Gorman, P., Arends, M., Talbot, I.C. & Tomlinson, I.P. 2002, "Molecular characteristics of serrated adenomas of the colorectum", *Gut,* vol. 51, no. 2, pp. 200-206.

Serrano, M. 1997, "The tumor suppressor protein p16INK4a", *Experimental cell research,* vol. 237, no. 1, pp. 7-13.

Serrano, M., Hannon, G.J. & Beach, D. 1993, "A new regulatory motif in cell-cycle control causing specific inhibition of cyclin D/CDK4", *Nature,* vol. 366, no. 6456, pp. 704-707.

Sharma, A., Trivedi, N.R., Zimmerman, M.A., Tuveson, D.A., Smith, C.D. & Robertson, G.P. 2005, "Mutant V599EB-Raf regulates growth and vascular development of malignant melanoma tumors", *Cancer research,* vol. 65, no. 6, pp. 2412-2421.

Shen, L., Toyota, M., Kondo, Y., Lin, E., Zhang, L., Guo, Y., Hernandez, N.S., Chen, X., Ahmed, S., Konishi, K., Hamilton, S.R. & Issa, J.P. 2007, "Integrated genetic and epigenetic analysis identifies three different subclasses of colon cancer", *Proceedings of the National Academy of Sciences of the United States of America,* vol. 104, no. 47, pp. 18654-18659.

Shima, K., Nosho, K., Baba, Y., Cantor, M., Meyerhardt, J.A., Giovannucci, E.L., Fuchs, C.S. & Ogino, S. 2011, "Prognostic significance of CDKN2A (p16) promoter methylation and loss of expression in 902 colorectal cancers: Cohort study and literature review", *International journal of cancer.Journal international du cancer,* vol. 128, no. 5, pp. 1080-1094.

Shroff, R., Arbel-Eden, A., Pilch, D., Ira, G., Bonner, W.M., Petrini, J.H., Haber, J.E. & Lichten, M. 2004, "Distribution and dynamics of chromatin modification induced by a defined DNA double-strand break", *Current biology : CB,* vol. 14, no. 19, pp. 1703-1711.

Simon, J.A. & Lange, C.A. 2008, "Roles of the EZH2 histone methyltransferase in cancer epigenetics", *Mutation research,* vol. 647, no. 1-2, pp. 21-29.

Soejima, K., Fang, W. & Rollins, B.J. 2003, "DNA methyltransferase 3b contributes to oncogenic transformation induced by SV40T antigen and activated Ras", *Oncogene,* vol. 22, no. 30, pp. 4723-4733.

Souza RF, Appel R, Yin J, Wang S, Smolinski KN, Abraham JM, Zou TT, Shi YQ, Lei J, Cottrell J, Cymes K, Biden K, Simms L, Leggett B, Lynch PM, Frazier M, Powell SM, Harpaz N, Sugimura H, Young J, Meltzer SJ. 1996. Microsatellite instability in the insulin-like growth factor II receptor gene in gastrointestinal tumours. *Nat Genet.* Nov;14(3):255-7.

Sparks AB, Morin PJ, Vogelstein B, Kinzler KW. 1998. Mutational analysis of the APC/beta-catenin/Tcf pathway in colorectal cancer. *Cancer Res.* Mar 15;58(6):1130-4.

Sparmann, A. & van Lohuizen, M. 2006, "Polycomb silencers control cell fate, development and cancer", *Nature reviews.Cancer,* vol. 6, no. 11, pp. 846-856.

Storm SM, Cleveland JL, Rapp UR. 1990. Expression of raf family proto-oncogenes in normal mouse tissues. *Oncogene.* Mar;5(3):345-51.

Sutrave P, Bonner TI, Rapp UR, Jansen HW, Patschinsky T, Bister K. 1984, Nucleotide sequence of avian retroviral oncogene v-mil: homologue of murine retroviral oncogene v-raf. *Nature.* May 3-9;309 (5963):85-8.

Takaku, K., Oshima, M., Miyoshi, H., Matsui, M., Seldin, M.F. & Taketo, M.M. 1998, "Intestinal tumorigenesis in compound mutant mice of both Dpc4 (Smad4) and Apc genes", *Cell,* vol. 92, no. 5, pp. 645-656.

Takayama T, Miyanishi K, Hayashi T, Sato Y, Niitsu Y. 2006. Colorectal cancer: genetics of development and metastasis. *J.Gastroenterol.* Mar;41(3):185-92.

Toyota, M., Ahuja, N., Suzuki, H., Itoh, F., Ohe-Toyota, M., Imai, K., Baylin, S.B. & Issa, J.P. 1999, "Aberrant methylation in gastric cancer associated with the CpG island methylator phenotype", *Cancer research,* vol. 59, no. 21, pp. 5438-5442.

Toyota, M., Ohe-Toyota, M., Ahuja, N. & Issa, J.P. 2000, "Distinct genetic profiles in colorectal tumors with or without the CpG island methylator phenotype", *Proceedings of the National Academy of Sciences of the United States of America,* vol. 97, no. 2, pp. 710-715.

Treisman., R, Alberts., AS, Sahai., E. 1999. "Regulation of SRF activity by Rho family GTPases". *Cold Spring Harb Symp Quant Biol.* 63, pp. 643-51

Van Kemenade, F.J., Raaphorst, F.M., Blokzijl, T., Fieret, E., Hamer, K.M., Satijn, D.P., Otte, A.P. & Meijer, C.J. 2001, "Coexpression of BMI-1 and EZH2 polycomb-group proteins is associated with cycling cells and degree of malignancy in B-cell non-Hodgkin lymphoma", *Blood,* vol. 97, no. 12, pp. 3896-3901.

Viré E, Brenner C, Deplus R, Blanchon L, Fraga M, Didelot C, Morey L, Van Eynde A, Bernard D, Vanderwinden JM, Bollen M, Esteller M, Di Croce L, de Launoit Y, Fuks F (2006) The Polycomb group protein EZH2 directly controls DNA methylation. Nature 439: 871-874.

Vogelstein, B., Fearon, E.R., Hamilton, S.R., Kern, S.E., Preisinger, A.C., Leppert, M., Nakamura, Y., White, R., Smits, A.M. & Bos, J.L. 1988, "Genetic alterations during colorectal-tumor development", *The New England journal of medicine,* vol. 319, no. 9, pp. 525-532.

Vojtek AB, Hollenberg SM, Cooper JA. 1993. Mammalian Ras interacts directly with the serine/threonine kinase Raf. *Cell.* Jul 16;74(1):205-14.

Wan, P.T., Garnett, M.J., Roe, S.M., Lee, S., Niculescu-Duvaz, D., Good, V.M., Jones, C.M., Marshall, C.J., Springer, C.J., Barford, D., Marais, R. & Cancer Genome Project 2004, "Mechanism of activation of the RAF-ERK signaling pathway by oncogenic mutations of B-RAF", *Cell,* vol. 116, no. 6, pp. 855-867.

Wang J, Vantus T, Merlevede W, Vandenheede JR. 1997, "Identification and characterization of an auto-activating MEK kinase from bovine brain: Phosphorylation of serine-298 in the proline-rich domain of the mammalian MEKs*", The International Journal of Biochemistry; Cell Biology*, Volume 29, Issues 8–9, pp. 1071-1083

Weber, C.K., Slupsky, J.R., Herrmann, C., Schuler, M., Rapp, U.R. & Block, C. 2000, "Mitogenic signaling of Ras is regulated by differential interaction with Raf isozymes", *Oncogene,* vol. 19, no. 2, pp. 169-176.

Weisenberger, D.J., Siegmund, K.D., Campan, M., Young, J., Long, T.I., Faasse, M.A., Kang, G.H., Widschwendter, M., Weener, D., Buchanan, D., Koh, H., Simms, L., Barker, M., Leggett, B., Levine, J., Kim, M., French, A.J., Thibodeau, S.N., Jass, J., Haile, R. & Laird, P.W. 2006, "CpG island methylator phenotype underlies sporadic microsatellite instability and is tightly associated with BRAF mutation in colorectal cancer", *Nature genetics,* vol. 38, no. 7, pp. 787-793.

Weisenberger, D.J., Velicescu, M., Cheng, J.C., Gonzales, F.A., Liang, G. & Jones, P.A. 2004, "Role of the DNA methyltransferase variant DNMT3b3 in DNA methylation", *Molecular cancer research : MCR,* vol. 2, no. 1, pp. 62-72.

Wellbrock, C., Karasarides, M. & Marais, R. 2004, "The RAF proteins take centre stage", *Nature reviews.Molecular cell biology,* vol. 5, no. 11, pp. 875-885.

Wellbrock, C., Ogilvie, L., Hedley, D., Karasarides, M., Martin, J., Niculescu-Duvaz, D., Springer, C.J. & Marais, R. 2004, "V599EB-RAF is an oncogene in melanocytes", *Cancer research,* vol. 64, no. 7, pp. 2338-2342.

Wojnowski, L., Zimmer, A.M., Beck, T.W., Hahn, H., Bernal, R., Rapp, U.R. & Zimmer, A. 1997, "Endothelial apoptosis in Braf-deficient mice", *Nature genetics,* vol. 16, no. 3, pp. 293-297.

Wolffe, A.P. 1998, "Packaging principle: how DNA methylation and histone acetylation control the transcriptional activity of chromatin", *The Journal of experimental zoology,* vol. 282, no. 1-2, pp. 239-244.

Xiang, Y., Zhu, Z., Han, G., Lin, H., Xu, L. & Chen, C.D. 2007, "JMJD3 is a histone H3K27 demethylase", *Cell research,* vol. 17, no. 10, pp. 850-857.

Xie ZH, Zhang J, Siraganian RP. 2000. Positive regulation of c-Jun N-terminal kinase and TNF-alpha production but not histamine release by SHP-1 in RBL-2H3 mast cells. *J Immunol.* 1;164(3):1521-8.

Xing, M., Westra, W.H., Tufano, R.P., Cohen, Y., Rosenbaum, E., Rhoden, K.J., Carson, K.A., Vasko, V., Larin, A., Tallini, G., Tolaney, S., Holt, E.H., Hui, P., Umbricht, C.B., Basaria, S., Ewertz, M., Tufaro, A.P., Califano, J.A., Ringel, M.D., Zeiger, M.A., Sidransky, D. & Ladenson, P.W. 2005, "BRAF mutation predicts a poorer clinical prognosis for papillary thyroid cancer", *The Journal of clinical endocrinology and metabolism,* vol. 90, no. 12, pp. 6373-6379.

Yang, S., Farraye, F.A., Mack, C., Posnik, O. & O'Brien, M.J. 2004, "BRAF and KRAS Mutations in hyperplastic polyps and serrated adenomas of the colorectum: relationship to histology and CpG island methylation status", *The American Journal of Surgical Pathology,* vol. 28, no. 11, pp. 1452-1459.

Yang,. SH, Sharrocks., AD, Whitmarsh.,AJ. 2003. "Transcriptional regulation by the MAP kinase signaling cascades", Gene, Volume 320, Pages 3-2.

Zhu J, Woods D, McMahon M, Bishop JM. 1998. Senescence of human fibroblasts induced by oncogenic Raf. *Genes Dev.* Oct 1;12(19):2997-3007.

Yoon, S. & Seger, R. 2006, "The extracellular signal-regulated kinase: multiple substrates regulate diverse cellular functions", *Growth factors (Chur, Switzerland),* vol. 24, no. 1, pp. 21-44.

Zhang, B.H. & Guan, K.L. 2000, "Activation of B-Raf kinase requires phosphorylation of the conserved residues Thr598 and Ser601", *The EMBO journal,* vol. 19, no. 20, pp. 5429-5439.